

Titre: Seismic Behaviour, Numerical Modelling and Displacement-Based
Title: Design of Steel Storage Rack Structures for Canadian Applications

Auteur: Emily Jacobsen
Author:

Date: 2017

Type: Mémoire ou thèse / Dissertation or Thesis

Référence: Jacobsen, E. (2017). Seismic Behaviour, Numerical Modelling and Displacement-Based Design of Steel Storage Rack Structures for Canadian Applications
Citation: [Mémoire de maîtrise, École Polytechnique de Montréal]. PolyPublie.
<https://publications.polymtl.ca/2550/>

 **Document en libre accès dans PolyPublie**
Open Access document in PolyPublie

URL de PolyPublie: <https://publications.polymtl.ca/2550/>
PolyPublie URL:

Directeurs de recherche: Robert Tremblay
Advisors:

Programme: Génie civil
Program:

UNIVERSITÉ DE MONTRÉAL

SEISMIC BEHAVIOUR, NUMERICAL MODELLING AND DISPLACEMENT-BASED
DESIGN OF STEEL STORAGE RACK STRUCTURES FOR CANADIAN APPLICATIONS

EMILY JACOBSEN

DÉPARTEMENT DES GÉNIES CIVIL, GÉOLOGIQUES ET DES MINES
ÉCOLE POLYTECHNIQUE DE MONTRÉAL

MÉMOIRE PRÉSENTÉ EN VUE DE L'OBTENTION
DU DIPLÔME DE MAÎTRISE ÈS SCIENCES APPLIQUÉES
(GÉNIE CIVIL)
JANVIER 2017

UNIVERSITÉ DE MONTRÉAL

ÉCOLE POLYTECHNIQUE DE MONTRÉAL

Ce mémoire intitulé :

SEISMIC BEHAVIOUR, NUMERICAL MODELLING AND DISPLACEMENT-BASED
DESIGN OF STEEL STORAGE RACK STRUCTURES FOR CANADIAN APPLICATIONS

présenté par : JACOBSEN Emily

en vue de l'obtention du diplôme de : Maîtrise ès sciences appliquées

a été dûment accepté par le jury d'examen constitué de :

M. LÉGER Pierre, Ph. D., président

M. TREMBLAY Robert, Ph. D., membre et directeur de recherche

M. HIGGINS Peter, M.Sc., membre

DEDICATION

Pour Léo

ACKNOWLEDGEMENTS

Professor Robert Tremblay for patience, criticism, encouragement and generosity with time and guidance. Thank you for suggesting this gem of a project.

Poulad Daneshvar for advice, the selection and scaling of accelerograms and investigations of pallet sliding and cooperation on analysis of time history results in CHAPTER 4 .

Peter Higgins B.Sc., M.Sc, M.E.Sc. P.Eng and Prof. Pierre Leger for having accepted to sit as members of the jury.

Ihor Koval on whose undergraduate project this masters project expanded and who aided during the physical tests.

Martin Leclerc and Romain Sigieur for the design of the physical testing apparatuses and procedures, direction of test setup and operation of instrumentation and laboratory equipment. Émile Lord and Aziz El Meskini for their participation in test set-up and the other members of the GRS laboratory staff.

The members of the S16 Rack Annex sub-committee for their advice and review of designs, as well as materials for physical tests and testing data for connections.

Financial support for this project was generously provided by NSERC Discovery and Engage grant programs.

RÉSUMÉ

Les étagères industrielles en acier, fabriquées des profilés formés à froid ou laminés à chaud sont mise en œuvre dans une panoplie de contextes tels que des centres de distribution ou des centres commerciaux où l'on charge avec des pallets de marchandises souvent accessibles au grand public. Ces étagères sont habituellement composées des cadres contreventés dans l'une des directions et des cadres semi-rigides dans la direction orthogonale. Les cadres sont semi-rigides en raison des connecteurs poutres-colonnes qui se doivent d'être faciles à reconfigurer afin de s'adapter aux besoins du propriétaire. Ce projet vise la caractérisation de la réponse sismique de ces cadres semi-rigides et le développement d'un modèle robuste de ces derniers ainsi que la validation des provisions, actuellement en état de développement, à l'Annexe du Code canadien sur le calcul des charpentes d'acier.

Onze essais physiques sur des spécimens d'un étage formés à froid ont été effectués à Polytechnique Montréal. Cette configuration simple a pour but l'isolation de la réponse des connecteurs poutres-colonnes, des plaques de base et du glissement des pallets, réduisant le problème à l'essentiel afin de produire un modèle précis de son comportement. Parmi les essais étaient trois du type quasi statique, deux essais vibrations libres et six essais sur la table vibrante. Les essais quasi statiques comportaient trois configurations d'étagère : rotulé à la base avec des connecteurs aux accroches, rotulés au niveau des poutres avec des plaques de base conventionnelles, et connecteurs aux accroches avec des plaques de base. Les deux essais vibrations libres comportaient un spécimen avec plaques de base et l'autre avec rotules, les deux avec connecteurs aux accroches. Les six essais restants étaient divisés de façon égale entre des spécimens rotulés à leur base et des spécimens avec des plaques de base. Ces spécimens subissaient des tremblements de terre de l'est et de l'ouest du Canada.

La réponse sismique des étagères était gouvernée par la plastification des connecteurs poutres-colonnes, par la plastification des plaques de base et par la dissipation d'énergie due au glissement des pallets. Les poutres et les colonnes demeuraient élastiques à l'exception de la surface des colonnes où se faisait l'interface avec les connecteurs. Le modèle aux éléments finis, fruit des essais quasi statiques et de vibrations libres était modifié suite aux essais sismiques pour prendre en compte l'action des palets. Le modèle final emploie une gamme de matériels dans les ressorts concentrés, avec des lois de comportement multilinéaires, intégrant de la dégradation,

afin de reproduire l'action des connecteurs, plaques de base et palets. En combinaison avec des colonnes et des poutres élastiques, le modèle parvient à reproduire les déplacements et les accélérations des essais physiques.

Les essais quasi statiques menés à Polytechnique se concordent avec des tests indépendants sur les connecteurs. En conjonction avec le constat que la réponse globale est dictée par la plastification de ces connecteurs (et plaques de base), le modèle peut être généralisé à d'autres combinaisons de poutres, de colonnes, de connecteurs et de plaques de base en se servant d'autres données disponibles pour les connecteurs. Le modèle est généralisé encore plus en incluant des colonnes de fibre, des poutres à plasticité concentrée et des plaques de base sensibles au niveau de compression appliquée. Ces derniers permettent l'analyse d'autres configurations d'étagère. Ces dernières modifications assurent que l'hypothèse de poutres et colonnes linéaires n'est pas dépassée de façon inaperçue.

Pour aider avec la validation des provisions sismiques, quatre étagères (de 3 à 6 étages et 6-baies) conçues selon la pratique actuelle ont été analysées suivant l'Annexe N. Ensuite, ces étagères ont été reconçues pour les conditions de site de Vancouver et Montréal sites C & E avec le plus petit de marge de sécurité possible par rapport aux provisions de l'Annexe. Les méthodes par déplacements et par force ont été suivies. Les provisions pour la conception par force ont conduit à des membrures et connecteurs irréalistes. Les étagères conçues selon la méthode par déplacements ont été raisonnables. Par la suite, ces étagères prototypes ont été assujetties à une suite de séismes représentatifs de l'est et de l'ouest du Canada. Ces analyses constituent le repère pour des analyses multiparamétriques à venir. Les étagères ont réagi tel que prévue sauf quelques exceptions importantes – les étagères très flexibles sont susceptibles l'effondrement malgré le fait qu'elles rencontrent les critères de déformation et de résistance latérale stipulés dans l'Annexe N.

ABSTRACT

Rack shelving structures, made of cold-formed or hot-rolled members, are used in a variety of contexts, in storage and distribution centres and in publicly accessible warehouse type stores stacked with merchandise on pallets. Racks are typically composed of braced-frames in the “cross-aisle” direction and semi-rigid moment-frames in the “down-aisle” direction. The moment-frames are semi-rigid due to their clip-in or bolt-on beam-column connections which allow easy assembly and geometric modifications according to user needs. This project aims to characterise the seismic response of these semi-rigid moment frames, develop a robust model and test the proposed seismic design provisions currently under development as an annex to the CSA S16 – Design of steel structures.

Eleven physical tests were carried out on 1-bay, 1-level cold-form specimens at Polytechnique Montréal. This simple configuration was chosen to isolate the response of beam-column connections, base-plates and pallet sliding and facilitate accurate modelling of their behaviour. The tests included quasi-static tests, free-vibration tests and six-seismic tests. Quasi-static tests were performed on three different configurations: pinned-base with clip-in beam-column connections, fix-base with pinned beam-column connections and fix-base with clip-in connections. Two free vibration tests were conducted on pin-based and fix-based specimens both with clip-in beam column connections. The remaining six uni-directional seismic tests were equally divided between pin-base and fix-base specimens subjected to eastern and western Canadian quakes.

Seismic response of the racks was governed by yielding of the beam-column connections, yielding of the base-plates and energy dissipation due to sliding of the pallets. Beams and columns remained elastic except where the connectors clip-in to the columns. The finite element model developed during the quasi-static and free-vibration test stages was modified following the seismic tests to include the action of pallet sliding. This model uses an assortment of materials with multi-linear rules and various types degradation in zero-length springs to reproduce accurately the non-linear action of the beam-column connectors, base-plates and pallets. Combined with elastic beams and columns, the model succeeds in reproducing displacements and accelerations observed in the seismic tests.

The quasi-static tests performed at Polytechnique Montreal compared favorably to independent testing of the beam-column connections. Combined with the fact that overall response is dictated by the yielding of these connectors (and base-plates), this allowed generalization of the finite element model to other configurations of beams, columns, connectors and base-plates using test data available for the connections. The model was expanded to include in-plane buckling of the column elements, yielding of beams at their junction with the non-linear connector elements and base-plate assemblies able to accommodate changes in strength and stiffness with increased compression. This ensures that many combinations of beams, columns, connectors and base-plates may be analyzed in multi-bay, multi-level configurations while validating the hypothesis that beams and column remain elastic.

To aide the validation of the seismic provisions of the proposed annex, four racks (3 to 6 levels and 6-bays) designed according to current industry practice were analyzed according to guidelines set out in the Annex. These racks were then redesigned to give as close as possible match to the guidelines and to accommodate seismic conditions in Vancouver and Montreal sites C & E. Design procedures following a displacement-based method and a force-based method of analysis were followed. The guidelines for the force-based method resulted in unrealistic designs and are currently under revision. Racks designed according to the displacement-based method were subjected to non-linear time history analysis with a representative number of quakes for eastern and western Canada. These analyses constitute the base-line series, in a planned series of multi-parameter analyses. These racks performed as expected with some exceptions, notably very flexible racks were susceptible to collapse despite having met both the deformation and minimum lateral resistance stipulations of Annex N.

TABLE OF CONTENTS

DEDICATION	III
ACKNOWLEDGEMENTS	IV
RÉSUMÉ.....	V
ABSTRACT	VII
TABLE OF CONTENTS	IX
LIST OF TABLES	XIII
LIST FO FIGURES	XV
LIST OF SYMBOLS AND ABBREVIATIONS	XXIII
LIST OF APPENDICES	XXIX
CHAPTER 1 INTRODUCTION.....	1
1.1 Problem Under Study	1
1.2 Goals of Study	3
1.3 Methodology	4
1.4 Organisation	5
CHAPTER 2 LITERATURE REVIEW	6
2.1 Seismic response of rack moment frames	6
2.2 Existing standards on rack seismic design	7
2.2.1 Canada.....	7
2.2.2 USA.....	8
2.2.3 Europe	10
2.2.4 New Zealand	12
2.3 Existing applications of DBD to racks.....	12
2.4 Design quandaries	14
2.4.1 Lateral stiffness	14

2.4.2	Base plate stiffness and energy dissipation capacity.....	14
2.4.3	Pallet sliding, sloshing & shedding.....	15
2.4.4	Scaling of spectra for damping.....	17
2.4.5	P-delta.....	17
2.4.6	Higher mode participation.....	18
CHAPTER 3 ARTICLE 1: SHAKE-TABLE TESTING AND NUMERICAL MODELING OF INELASTIC SEISMIC RESPONSE OF SEMI-RIGID COLD-FORMED RACK MOMENT FRAMES		19
3.1	Introduction	19
3.2	Testing Program	23
3.2.1	Test Setup.....	23
3.2.2	Test matrix and loading protocols.....	26
3.2.3	Results from Quasi-Static Cyclic Tests.....	30
3.3	Numerical Modelling	36
3.3.1	Base-plates	37
3.3.2	Beam-column connectors.....	38
3.3.3	Base-plate and connector in combination	41
3.4	Results from Pull-back Tests.....	42
3.5	Results from Seismic Tests	46
3.5.1	Pinned-base specimens.....	46
3.5.2	Fixed-based specimens.....	48
3.5.3	Sliding of pallets.....	50
3.5.4	Numerical modelling of pallet sliding.....	51
3.5.5	Effect of damping modelling on response prediction	52
3.5.6	Numerical prediction of hysteretic response	52

3.5.7	Evaluating equivalent damping by two methods	55
3.6	Numerical Seismic Response of Multi-level, Multi-bay Racks	57
3.6.1	Structures studied	57
3.6.2	Seismic effects on column axial loads	59
3.6.3	Displacement profiles.....	59
3.6.4	Pallet sliding.....	60
3.6.5	Drift-rotation relationship	61
3.6.6	Influence of added viscous damping	62
3.6.7	Influence of base plate flexural strength	63
3.7	Conclusions and Recommendations.....	64
3.8	Acknowledgements	66
CHAPTER 4	DISPLACEMENT-BASED DESIGN OF RACKS ACCORDING TO ANNEX N AND COMPARISON WITH NON-LINEAR TIME HISTORY ANALYSIS	73
4.1	Introduction	73
4.2	A proposed displacement-based design method for racks	73
4.3	Design according to proposed Annex N provisions.....	79
4.3.1	Properties, dimensions and loads	79
4.3.2	Design of 3-level, 6-bay rack in Vancouver site C	84
4.3.3	Design of 6-level, 6-bay rack in Montreal site E	95
4.4	Summary of design of prototype racks	103
4.5	Summary of force-based designs	106
4.6	Discussion of preliminary results of NLTH trials.....	106
4.6.1	FEM model.....	107
4.6.2	Displacement profiles.....	107
4.6.3	Summary of results DBD vs. NLTH.....	111

4.6.4 Collapse Case	115
CHAPTER 5 GENERAL DISCUSSION.....	128
CHAPTER 6 CONCLUSIONS AND RECOMMENDATIONS.....	130
6.1 Conclusions	130
6.2 Recommendations	132
6.2.1 Modelling	132
6.2.2 Design.....	132
6.2.3 Further reasearch	133
BIBLIOGRAPHY	134
APPENDICES	148

LIST OF TABLES

Table 3-1: Testing Program.....	27
Table 3-2: Sliding accelerations and distances in seismic tests.	51
Table 3-3: Summary of peak drifts from physical tests compared with drift from two models. Test to model prediction ratio in brackets.	52
Table 3-4: Equivalent damping properties	56
Table 3-5: Strength adjustment factors for different base-plate thickness and compression level	58
Table 3-6: Average peak connector rotations and top drifts of multi-level racks without sliding subject to Q1 ground motion at SF = 1.0	62
Table 4-1: Connectors and product loads for prototype racks.	79
Table 4-2: Material properties.....	83
Table 4-3 : Spectral values for Montreal and Vancouver Sites C & E from NBCC 2015.....	84
Table 4-4: Finding the generalised displacement coordinate.....	89
Table 4-5: Column Design Moments	92
Table 4-6: Column gravity loads.....	93
Table 4-7: Calculation of minimum lateral resistance.	94
Table 4-8: Finding the generalised displacement coordinante of a 6-level rack.....	98
Table 4-9: Column Design Moments.....	100
Table 4-10: Column gravity loads.....	100
Table 4-11 : Minimum lateral resistance.....	102
Table 4-12: Sections and section inertias (I_b & I_c), material yield limits (F_{yb} & F_{yc}), connectors, scaling factors (SF_c) and base-plate thickness (t_p).	103
Table 4-13: Deformation limits (θ_{lim} & Δ_{lim}), design deformations (θ_d & Δ_d) and corresponding connector and base-plate and secant stiffness (k_c & k_{bpl}) and energy dissipated by cycle (EDC_c & EDC_{bpl}).....	104

Table 4-14: Iterations to converge on displacement of 3-level rack in Montreal Site C.	105
Table 4-15: Effective period (T_{eff}) and lateral stiffness (k_{eff}) of the structure of the substitute SDOF structure, reduced lateral stiffness ($k_{eff,red.}$) and augmented natural period ($T_{eff,aug.}$) to account for P-delta, effective damping (β_{eff}), spectral reduction coefficient for damping (R_β), spectral displacement of the substitute SDOF at 5% and at β ($S_{d5\%}$ & $S_{d\beta}$), design displacement of the SDOF and design displacement of the real structure (δ_d & δ_{tot}).	105
Table 4-16: Summary of expected and calculated connector rotations.	114
Table C-1: Distribution of equivalent static forces	166
Table C-2: Inelastic drift	166
Table C-3: Notional loads	167
Table C-4: U2 factors	168
Table C-5: Connector moments under gravity and lateral loads.....	168
Table C-6: Connector moments under gravity and lateral loads	169
Table C-7: Amplified connector moments: $U2*ME + MD$	169
Table C-8: Notional Loads.....	171
Table C-9: Inelastic drift	171
Table C-10: U2 factor	171
Table C-11: Connector moments under lateral loads ($F_x + N_x$).....	171
Table C-12: Connector moments under gravity and lateral loads.....	172
Table C-13: P-delta amplified forces induced by lateral loads + gravity loads: $U2ME + MD$...	172
Table C-14: P-delta amplified forces induced by lateral loads + gravity loads: $U2ME + MD$...	173
Table C-15: Calculation of U2 factors.....	174
Table C-16: Connector moments under lateral loads ($F_x + N_x$).....	175
Table C-17: P-delta amplified forces induced by lateral loads plus gravity loads.....	175

LIST OF FIGURES

Figure 1-1: Typical storage rack [7].....	1
Figure 1-2: A non-exhaustive sample of available beam-column connections: Clockwise from top-left a bolt-on connector attached to a hot-rolled beam [8], a cold-form column with “tear-drop” clip-in connection [9], a similar cold-form column with another model of connector [10], “redi-rack” type columns and connectors with rolled-beams [11], cold-form and rolled-beams connected to rolled-column via a bolt-on connector [12], HSS columns with bolt-on connectors attached to channel beams [13].	2
Figure 2-1: Base-plate testing assembly as recommended by the FEM and discussed in [32].....	15
Figure 2-2: Accounting for P-delta according to [43].....	17
Figure 3-1: Test setup (all dimensions in mm): a) Elevation view; b) Side view.	24
Figure 3-2 : Loading and instrumentation: a) Linear-pot assembly to measure rotations at beam-column joints; b) instrumentation schematic showing measurement locations; c) Cable and position of load cell during static tests.	25
Figure 3-3 : Beam-column connection (all dimensions in mm): a) Photo (taken after testing) and figure of the beam-column connection and section of the column and beam; b) Modified “pinned” beam-column connection in Test F1.	26
Figure 3-4: Displacement protocols in: a) Quasi-static tests; and b) Pull-back tests.	28
Figure 3-5: Test ground motions and corresponding 5% damped displacement spectra.	29
Figure 3-6: a) Base-shear vs. average drift measured in test P1; b) Average moment-rotation of a single connector in test P1 compared with RMI cruciform unit test of the same type of connector.	31
Figure 3-7: Progression of connector damage in test P1: a) at 0.03 rad little damage; b) at 0.08 rad yielding and buckling begins; c) at 0.1 rad shearing and plate buckling worsens; d) at 0.14 rad connector twists and disengages from column; e) at 0.14 rad weld damage; and f) post-test.	32
Figure 3-8: Behavior of the specimen F1 as governed by yielding of the base-plate: a) Front view at $\Delta_{avg} = 0.2$; b) side view at $\Delta_{avg} = 0.2$; c) & d) yield-line model parameters on front and	

side view; e) top view of yield lines; f) top view base-plate at $\Delta_{avg} = 0.2$; g) base-shear vs. average drift measured in test F1.	33
Figure 3-9: Base-plate moment-rotation hysteresis: Experimental, analytical and FEM: a) Each material present in FEM model of the base-plate shown individually; b) Comparison between complete FEM model of base-plate and experimental data with select features A & B from yield line model discussion. OpenSees material parameters in SI units; see [41] and [42] for definitions of each parameter.	35
Figure 3-10: Test F2: a) Lateral force-displacement relation from test and numerical model (test results are average of two frames including P-delta); b) Level and measuring tape held across the braced frame emphasizes flexural-torsional buckling of the column at 14% drift.	36
Figure 3-11: 2D OpenSees FEM model of the rack's moment frame.	37
Figure 3-12: Validation of the base-plate model against Test F1 results for: a) Secant stiffness; and b) Energy dissipated per cycle (EDC).	38
Figure 3-13: Response of the beam-to-column connector model, with tables showing the parameters for the Pinching4 material in SI units (see [45] for definitions of each parameter) compared to : a) Test P1; b) RMI test.	39
Figure 3-14: Validation of the beam-column connector modelling against P1 and RMI test results for: a) Secant stiffness; and b) Energy dissipated per cycle (EDC).	40
Figure 3-15: Comparison of test P1 and the numerical model with a small initial stiffness modification: a) Lateral force-load displacement response; and b) Secant stiffness.	41
Figure 3-16: Secant stiffness and EDC comparison for test F2.	42
Figure 3-17: Comparison between measured and OpenSees free vibration responses for pull-back amplitudes at several drift increments (e.g. “PB @ 10% #2” indicates the second pull (and release) to 10% drift): a) Test P2 with 5% added viscous damping; and b) Test F3 with 2% added viscous damping.	43
Figure 3-18: a) Variation of viscous damping calculated at every pair of consecutive peaks over the course of one free vibration test; b) Mean viscous damping calculated from the first four	

peaks of amplitude in Tests P2 and F3 compared to OpenSees models with 2 and 5% damping.....	44
Figure 3-19: Comparison between measured and predicted average natural periods in free vibration Tests P2 and F3.....	45
Figure 3-20: Drift vs. average rotation during Tests P1 and F2.....	45
Figure 3-21: Secant stiffness and EDC values from OpenSees model of Test F1 subjected to displacements from RMI cruciform test protocol.	46
Figure 3-22: Displacement and pallet sliding time history during Tests: a) P3; b) P4; and c) P5.	47
Figure 3-23: Displacement and pallet sliding time histories during Tests: a) F4; and b) F5.	49
Figure 3-24 : Hysteretic seismic response of specimens versus models with and without sliding.	54
Figure 3-25: Influence of equivalent damping on displacement of the equivalent linear model for Tests: a) P3; and b) P5.....	57
Figure 3-26: Effect of strength AF on base-plate hysteresis model, compression load for 3-level rack.	58
Figure 3-27: Variation of the base vertical reaction on interior and exterior columns.	59
Figure 3-28: Drift profiles for multi-level racks subjected to Q1 ground motion at scale factors of 1.0 & 1.5 and $\zeta = 2\%$	60
Figure 3-29: Peak rotations and drifts of multi-level racks without sliding subject to Q1 ground motion at SF = 1.0.....	61
Figure 3-30: Influence of added viscous damping on peak drifts under Q1 ground motion at SF = 1.5.....	63
Figure 3-31: Drift profiles with stiffened base-plates and increasing scale factors on the Q1 signal.	64
Figure 4-1: Calculation of secant stiffness, cycle by cycle, from experimental connector test data.	75

Figure 4-2 : Calculation of energy dissipated, cycle-by-cycle, from experimental connector test data.	76
Figure 4-3: Displacement-based design method for racks.	78
Figure 4-4: Geometry of prototype racks.	79
Figure 4-5: Moment-rotation hysteresis of a single 2-bolt connector AC175.	81
Figure 4-6: Moment-rotation hysteresis of a single 3-bolt connector AC200.	82
Figure 4-7: Base-plate dimensions for prototype racks.	82
Figure 4-8 : Design spectra for Montreal and Vancouver Sites C & E from NBCC 2015.	83
Figure 4-9: Drift vs. rotation relationship issue from non-linear pushover of a 3-level rack.	86
Figure 4-10: Moment rotation behaviour determined from physical unit tests and strength scaled by a factor of 2.36.	87
Figure 4-11: Moment-rotation behaviour as determined from FEM tests.	87
Figure 4-12: 1st pass secant stiffness of AC175 connector strength scaled by a factor of 2.36. ..	88
Figure 4-13: 1st pass secant stiffness of 5.5mm base-plates under compressive load of $C_f = 44$ kN.	88
Figure 4-14: 1 st pass energy dissipation of AC175 connector calculated from physical tests and strength scaled by a factor of 2.36.	88
Figure 4-15: 1 st pass energy dissipation of base-plates 5.5mm base-plates under compressive load of $C_f = 44$ kN.	88
Figure 4-16 : Actions on joints of the rack frame a) Top exterior joint b) Top interior joint, c) Middle or bottom exterior joint d) Middle or bottom interior joint.	92
Figure 4-17: Drift vs. rotation relationship issue from non-linear pushover of a 6-level rack.	96
Figure 4-18: Moment rotation behaviour determined from physical unit tests and strength scaled by a factor of 1.85.	96
Figure 4-19: Moment-rotation behaviour as determined from FEM tests under compressive load of $C_f = 66.7$ kN.	96

Figure 4-20: 1st pass secant stiffness of AC175 connector strength scaled by a factor of 1.85. ..	97
Figure 4-21: 1st pass secant stiffness of 2.7mm base-plates under compressive load of $C_f = 66.7$ kN.	97
Figure 4-22: 1 st pass energy dissipation of AC175 connector calculated from physical tests and strength scaled by a factor of 1.85.	97
Figure 4-23: 1 st pass energy dissipation of base-plates 2.7mm base-plates under compressive load of $C_f = 66.7$ kN.	97
Figure 4-24: Displacement profiles from NLTH for racks located in Vancouver site C.	108
Figure 4-25: Displacement profiles from NLTH for racks located in Vancouver site E.	109
Figure 4-26: Displacement profiles from NLTH for racks located in Montreal site C.	110
Figure 4-27: Displacement profiles from NLTH for racks located in Montreal site E.	111
Figure 4-28: Comparision of level drifts from non-linear time history analysis and displacement-based design for racks which did not collapse in a) Vancouver site C and b) Vancouver site E.	112
Figure 4-29: Comparision of level drifts from non-linear time history analysis and displacement-based design for racks which did not collapse in a) Montreal site C and b) Montreal site E.	112
Figure 4-30: Standard deviation in function of peak level drift.	114
Figure 4-31: VC30 ground motion.	115
Figure 4-32 : Select deformed shapes of the rack during the VC30 ground motion at: a) $t = 160.05$ s; b) $t = 160.7$ s; c) $t = 166.4$ s.	116
Figure 4-33 : Displacement time history of each level of a 5-level collapsed rack.	117
Figure 4-34 : Deformed shape of rack just before collapse during the VC30 acceleration at $t = 179.6$ s and 8 % drift.	117
Figure 4-35 : Rotation time histories of connectors at joints 1 and 2.	118
Figure 4-36 : Moments and equilibrium $M = M_c + M_{above} + M_{below}$ histories around joint 1 & 2, factored moment resistance M_r of the exterior column, moment needed to cause	

yielding $M_f - yield$ (including axial interaction) and the connector moment capacity scaled for design $SF_c \cdot M_c, max$	121
Figure 4-37 : Behavior at below joints 1 & 2: a) & b) Moment-curvature in the exterior column segment below the joints; c) Displacement history of joint 1; d) Time history of interaction equation S16 §13.8.3 (a) (yielding) in the column segments below the joints; e) Column axial load history above and below joint 1; f) Column shear history above and below joint 1; g) & h) connector hysteresis at the joints.....	122
Figure 4-38 : Close-up deformed shape of exterior column at times of interest with forms of moment diagram.....	125
Figure 4-39 : Moment distribution in the column at the instant of yielding: a) Form of moment distribution near joints 1 & 2 at 175.9 s; b) Free-body diagram of deformed column above and below joint 1.	126
Figure B-1 : Over all deformation Test F1.....	155
Figure B-2 : Typical damage to base plate test F1.....	155
Figure B-3 : Typical damage to base-plate test F1.....	155
Figure B-4 : Typical damage to base-plate test F1.....	156
Figure B-5 : Base-plate uplift.....	158
Figure B-6 : Connectors are not visibly damaged.....	156
Figure B-7 : Shearing of bottom interior tab and bending out top exterior tabs (eastern side)...	156
Figure B-8 : Shearing of bottom interior tab and bending out of middle and lower exterior tabs (western side)	159
Figure B-9 : Plastic hinging of base-plate.....	157
Figure B-10 : Lever effect at base-plate.....	157
Figure B-11 : View of the combination of plastic hinging (accompanied by paint flaking) and lever effect	158
Figure B-12 : Complete shearing of interior top tabs.....	158
Figure B-13 : Bearing of sheared interior tabs on connector body	159

Figure B-14 : Level is held against the braced frame to emphasize the lateral torsional buckling	159
Figure B-15 : Lateral torsional buckling of the columns	159
Figure B-16 : Local buckling	162
Figure B-17 : Progression of base-plate plastic hinging	162
Figure B-18 : Beam-connector weld damage as well as progression of tab shearing.....	161
Figure B-19 : Close-up for torn 2nd tab on NE connection	162
Figure B-20 : Twisting of connection	164
Figure B-21 : Twisting	164
Figure B-22 : SW close-up.....	164
Figure B-23 : NE connector close-up showing rupture of 1st tab.....	164
Figure B-25 : Shearing of top tab	165
Figure B-26 : Complete shear first (top) tab	165
Figure B-27 : Close-up for torn 2nd tab on NE connection.....	165
Figure B-28 : Typ. Shearing and/or loss of 1st and 2nd tabs.....	165
Figure B-29 : Close-up of NE weld rupture	165
Figure B-30 : Column damage typ.: deformation is most pronounced around bottom connector hole.....	166
Figure B-31 : Typ. All deformation is taking place in the connection	166
Figure B-32 : Typ. Local buckling on the face of the connector	166
Figure B-33 : Typ. Connector after test	166
Figure B-34 : Full frame after testing	166
Figure C-1 : AC175 connector hysteresis as tested (un-scaled).....	165
Figure C-2 : Finding acceleration from spectra	166
Figure C-3 : AC175 Connector with strength scaled by a factor of 9.75.....	176

Figure C-4 : AC175 Connector scaled by a factor of 6.5, secant stiffness of 280 kNm/rad	180
Figure D-1 : Preliminary FEM model of rack.....	177
Figure D-2 : Final FEM model of rack	179
Figure E-1 : Yield-line model of symmetrical base-plate	181
Figure E-2 : Finite element model of symmetrical base-plate	181
Figure E-3 : Base-plate model subjected to RMI type cyclic loading	182
Figure E-4 : Cyclic loading applied to FEM base-plate models	182
Figure G-1 : Simplification of a rack moment frame.....	211
Figure G-2 : Comparision of two approximate equations for fundamental period with periods issue from eigenvalue analys.....	213
Figure G-3 : Rack with eccentric loads.....	214
Figure G-4 : Fundamental period with eccentric loads.....	214
Figure G-5 : Rack with beam-level masses.....	214
Figure G-6 : Fundamental period with beam-level loads.....	214

LIST OF SYMBOLS AND ABBREVIATIONS

a'	- Base-plate dimension
a	- Base-plate dimension
AF	- Adjustment factor
ANSI	- American National Standards Institute
B	- Damping factor
b	- Column width or column depth
c	- Base-plate dimension
C	- Compressive load
C_d	- Deflection amplification factor
C_f	- Factored compressive load
C_r	- Compressive resistance
CSA	- Canadian Standards Association
CYX	- Quasi-cyclic test X
d	- Column width or depth
D_{\max}	- Maximum displacement demand
DOF	- Degree-of-freedom
E	- Modulus of elasticity
E_c	- Concrete modulus of elasticity
EDC	- Energy dissipated per cycle
EDC_{bpl}	- Energy dissipated per cycle by a base-plate
EDC_c	- Energy dissipated per cycle by a connector
ESF	- Equivalent Static Force (Method)
F	- Force applied by the cable in physical tests

FEMA	- Federal Emergency Management Agency
F_y	- Yield strength
F_{yb}	- Yield strength of the beam
F_{yc}	- Yield strength of the column
h	- Column height
h_x	- Height at level x
I_b	- Moment of inertia of the beam
I_{col}	- Column moment of inertia
I_E	- Importance factor
j	- Number of peaks over which viscous damping is calculated
k_{bpl}	- Base-plate stiffness
k_c	- Connector rotational stiffness
K_e	- Effective stiffness
$k_{eff,rack}$	- Effective lateral stiffness
k_{rack}	- Lateral stiffness of a rack
$k_{rack,red.}$	- Rack's reduced lateral stiffness
k_{sec}	- Secant stiffness
l	- Length
L_b	- Beam length
LDMA	- Large displacement method of analysis
M_b	- Base-plate yield moment
M_c	- Connector moment
$M_{c,max}$	- Connector peak strength
m_{eff}	- Effective mass of an SDOF structure

M_f	- Factored moment
m_i	- Mass at level i
$m_{p,bpl}$	- Plastic moment per length of section
M_r	- Moment resistance
MRF	- Moment resisting frame
MRSA	- Modal response spectrum analysis
μ_s	- Static friction coefficient
$M_{y,bpl}$	- Base-plate yield moment
NBCC	- National Building Code of Canada
N_{bpl}	- Number of base-plates
N_c	- Number of connectors
NEHRP	- National Earthquake Hazards Reduction Program
NLTH	- Non-linear time history
PBX	- Pull-back test X
P_{eff}	- Effective gravity load load
PGA	- Peak Ground Acceleration
q	- Behaviour factor
QX	- Shake table signal X
R_d	- Ductility modification factor
R_F	- Filling grade reduction factor
RMI	- Rack Manufacturer's Institute
R_o	- Strength modification factor
R_β	- Damping reduction factor
S_a	- Spectral Acceleration

S_d	- Displacement spectrum
$S_{d,red}$	- Reduced design acceleration spectrum
$S_{d5\%}$	- The 5% damped spectral displacement
SDOF	- Single degree of freedom
SDOF	- Single Degree of Freedom
$S_{d\beta}$	- Spectral displacement at β % damping
S_e	- Elastic acceleration spectrum
SF	- Scale factor of a ground motion
SF_c	- Strength scaling factor on connector
SFRS	- Seismic force resisting system
S_{M1}	- MCE spectral acceleration at one second taking into account site effects
S_p	- Horizontal force factor
T_1	- First fundamental period of vibration
T_{eff}	- Effective fundamental period
$T_{eff,aug.}$	- Effective augmented fundamental period
T_n	- Fundamental period of vibration
t_p	- Base-plate thickness
u_i	- The i th decrement of amplitude
V_p	- Base-shear of the part or portion
V_r	- Lateral resistance
$V_{r,min}$	- Minimum lateral resistance
W	- Weight of two loaded pallets used in physical tests
W_E	- External work
W_I	- Internal work

W_p	- Weight of the part
\ddot{x}_{beam}	- Beam acceleration
$x_{rel.}$	- Relative displacement of the pallet with respect to the beam
β	- Damping ratio
$\beta_{eff.}$	- Effective or equivalent damping
$\beta_{hyst.}$	- Hysteretic damping
δ	- Displacement
δ_d	- Design (or target) displacement
δ_{gen}	- Generalised drift coordinate
δ_{max}	- Maximum displacement
δ_{top}	- Peak displacement at the top level
Δ	- Drift
Δ_d	- Design (or target) drift
Δ_{lim}	- Drift limit
Δ_{avg}	- Average drift
Δ_{bpl}	- Drift due to deformation of the base-plate
Δ_{col}	- Drift due to deformation of the column
Δ_i	- Drift at level i
Δ_{tot}	- Total drift
θ_b	- Base-plate rotation
θ_{bpl}	- Base-plate rotation
$\theta_{c,max}$	- Maximum rotation capacity of a connector
θ_D	- Rotation due to gravity loads
θ_d	- Design displacement or target displacement

- $\theta_{d,i}$ - Target (or design) displacement at the i th iteration
- θ_E - Rotation due to earthquake loads
- χ - Stiffness degradation factor
- Ω_0 - Over strength factor

LIST OF APPENDICES

APPENDIX A	EXTRACTS FROM ANNEX N ON SEISMIC DESIGN	148
APPENDIX B	LABORATORY TESTS	154
APPENDIX C	FORCE-BASED ANALYSIS AND DESIGN ACCORDING TO ANNEX N Draft	164
APPENDIX D	DESCRIPTION OF FEM MODEL OF RACK	177
APPENDIX E	CYCLIC BASE-PLATE PSEUDO TESTS, FEM BASE-PLATE MODELS AND VERIFICATION BY YIELD-LINE method	181
APPENDIX F	TCL SCRIPTS FOR OPENSEES MODEL	183
APPENDIX G	AN APPROXIMATE EQUATION FOR THE FUNDAMENTAL PERIOD OF A RACK MOMENT Frame.....	211
APPENDIX H	CYCLE BY CYCLE CURVE MATCHING OF NON-LINEAR CONNECTORS AND BASE-PLATES	215
APPENDIX I	GROUND MOTIONS FOR TIME HISTORY ANALYSES	248

CHAPTER 1 INTRODUCTION

1.1 Problem Under Study

Racks are ostensibly simple, economical structures, designed very efficiently to resist the gravity loads of pallets stacked with merchandise. Collapse of racks has been observed in several recent earthquakes: [1], [2], [3], [4], [5], [6]. In selective racks, the most widely used type of rack structure, the “cross-aisle ” direction is commonly composed of braced-frames, while the long rows of the “down-aisle” direction are typically composed of frames with beams that can be clipped into or bolted onto the columns. This allows rapid erection and reconfiguration as well as facilitating swap-out of damaged components.



Figure 1-1: Typical storage rack [7].

By default, the seismic force resisting system (SFRS) in the down-aisle direction is a semi-rigid frame where the beam-column connectors act as the capacitive fuse element, instead of weak beams as would be the case in a building’s rigid moments frames. The principal structural components controlling inelastic seismic response are the beam-column connections and the base-plates. Manufacturers often produce proprietary connectors and base-plates, composed of coldform-sections, channels, HSS, or various combinations of rolled and cold-form sections as shown in Figure 1-2. Their common link is that their cyclic moment-rotation behaviour is ductile and highly non-linear, comprising multiple slopes of stiffness and pronounced pinching.

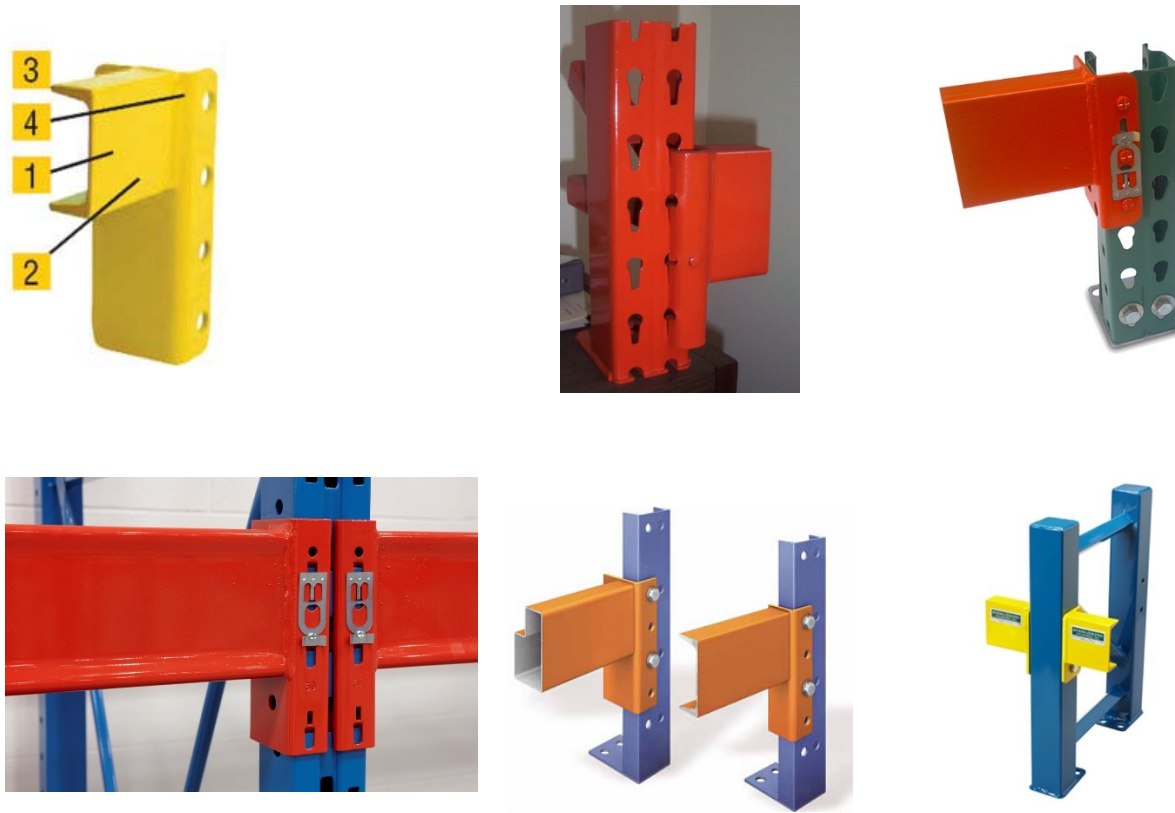


Figure 1-2: A non-exhaustive sample of available beam-column connections: Clockwise from top-left a bolt-on connector attached to a hot-rolled beam [8], a cold-form column with “tear-drop” clip-in connection [9], a similar cold-form column with another model of connector [10], “redi-rack” type columns and connectors with rolled-beams [11], cold-form and rolled-beams connected to rolled-column via a bolt-on connector [12], HSS columns with bolt-on connectors attached to channel beams [13].

Force based methods of seismic design are particularly difficult to apply to racks in part because prescriptive ductility and overstrength factors are a blunt tool considering the variability of rack connectors and more importantly because of the problem of fixing an appropriate stiffness to derive fundamental period and hence spectral accelerations. Initial stiffness is maintained over a small range of the useful rotation range of a connector. Without resorting to some sort of iterative process to find matching strength and stiffness values, strength and stiffness will be incoherent as will be inelastic displacements.

Until recently Canadian codes have provided sparse guidance on the seismic design of racks through the CSA A344-05 (reaffirmed 2011) which references the 1995 edition of the National Building Code of Canada in terms of seismic design. The forthcoming edition of CSA S16-14 will contain Annex N, treating the design of rack structures and specific guidelines for seismic design consistent with the 2015 edition of the NBCC. This annex has adopted ductility modification factors, R_d of 2.0 and 1.5 for rack frames and braced-frames respectively (consistent with findings by [14]) which will result in significantly increased design loads as compared with the A344-05. A displacement-based method for semi-rigid rack moment frames, subject to height limitations in addition to minimum lateral strength requirements, has been proposed in light of several promising studies [15], [16] and a similar method proposed in the American standard FEMA 460 and the European standard NBN EN 16681:2016.

Displacement-based methods promise to adapt well to the unique challenges of designing the semi-rigid moment frame to resist seismic loads by taking into account the stiffness and energy dissipation qualities of specific connectors. However the method as typically applied to rack semi-rigid frames depends on several important assumptions which have yet to face sufficient scrutiny.

Copious and uniformly produced information exists (though is often difficult to obtain) regarding the cyclic behaviour of the beam-column connectors thanks to the RMI qualification procedures to which many manufacturer's subject their products. Since torsion is generally not important in rack response, the semi-rigid frame may be modelled as planar structure. This, in combination with the fact that in a well designed racks the columns and beams remain elastic, makes racks particularly amenable to modelling with a concentrated plasticity model.

1.2 Goals of Study

This project aims to aide in the development and validation of seismic design provisions put forward in the proposed Annex N of the CSA S16. The focus is on the validation of a displacement-based design method but includes investigations comparisons and propositions for the equivalent static force method. In specific, this project aims to:

- Determine whether displacement-based design is a satisfactory method for designing semi-rigid rack moment frames to resist collapse during earthquakes. To this end:

- Produce a robust finite element model capable of predicting the response of racks with a variety connectors and geometries,
- Validate that the finite element model can accurately predict response in comparison to a simple test case,
- Verify the hypotheses underpinning the application of displacement base design to racks through physical tests and numerical tests,
- Test the feasibility of Annex N by designing a series of prototype racks according its provisions,
- Through a series of non-linear time history analysis on prototype racks, evaluate the safety of the code provisions and propose limits and rectifications,
- Develop knowledge on the seismic response of base-plates, beam-column connectors and pallet sliding,
- Compare force-based design and displacement-based design,
- Produce recommendations to amend the seismic design provisions in Annex N and for further studies.

1.3 Methodology

Following the review of relevant literature and identification of hypotheses and conjectures influencing the applicability of displacement-based design, a proposition for a displacement-based design method with direct incorporation of connector unit tests and taking into account P-delta effects was made.

A series of physical tests on 12 specimens of a 1-level, 1-bay cold-formed rack were performed to develop knowledge on the seismic response of racks and generate data for the development and validation of reliable numerical models. The test program included: three quasi-static tests, two pull-back tests and seven seismic tests. The specimens included some with stock base-plates and some with pinned bases. Eastern and western records were scaled to produce a desired level of displacement as predicted by DBD and by preliminary FEM models calibrated from the initial quasi-static and pull-back tests. An attempt was made to induce resonance with a number of specimens following seismic testing.

Finite element models were developed in OpenSees and validated/calibrated against shake table test data and independent qualification tests of the beam-column connectors. These models accounted for yielding in beam-column connectors and base-plates as well as pallet sliding. To generalise the finite element model to take into account the various combinations of hot-rolled and cold-formed members, the model was expanded to incorporate distributed yielding columns allowing for in-plane buckling, concentrated yielding beams, plastic base-plates with compression dependant strength and stiffness.

A number of multi-bay, multi-level prototype racks were designed according to Annex N. The designed racks were subjected to non-linear time history analysis with a large set of representative ground motions for eastern and western Canada. The results of these analyses were used to assess the safety of Annex N provisions for displacement-based seismic design.

1.4 Organisation of the thesis

This thesis is presented in six sections: Chapter 2 gives a review of literature including a general overview of the seismic response of rack moment-frames in §2.1, followed by a summary of world-wide design standards in §2.2, which leads to a detailed review of displacement-based design methods applied to rack moment frames in §2.4 and finishes with summaries of research related to the principal quandaries in rack moment-frame design in §2.4. Chapter 3 reports the results of a series of experiments on a full-scale 1-bay, 1-level rack moment-frame and compares the results with a numerical model developed from these tests. Comparisons of the 1-bay, 1-level configuration are followed by example numerical trials on several multi-level, multi-bay coldform rack models. Chapter 4 presents the application of displacement-based design to a number of multi-level, multi-bay hot-rolled racks containing various connectors and compares their design to non-linear time history analysis. The specifics of the method are outlines in §4.2. In §4.3 several racks are designed and analysed under Annex provisions. The results of the first in a series of non-linear time history analyses are presented in §4.5. Chapter 5 concludes the project and gives a number of recommendations.

CHAPTER 2 LITERATURE REVIEW

2.1 Seismic response of rack moment frames

In 1979 Krawinkler conducted a number static and dynamic tests of rack components and full-size racks [17]. The goal was to determine the governing parameters for rack seismic design which had previously received little study. The ensuing report outlined many of the guiding observations that inform the study and design of racks today, namely:

- seismic response is governed by weak pinched connections between beams and columns and by connections at the base,
- connectors and base-plates can be represented as rotational springs the properties of which should be determined by experimental component tests,
- potential for energy dissipation in the moment frame direction is much greater than in the braced-frame direction,
- columns must be properly designed such that P/P_{cr} ratios are small such that instability is eliminated as a limit state,
- P-delta is very important in the moment frame direction and must be considered in analysis.

This study was closely followed by Chen [18] who conducted shake-table tests on full-scale 3-level, 2-bay racks and compared results to a computer model using elastic beams and columns and a bilinear rule in the beam-column connections. Results from these experiments confirmed Krawinkler's observations. In particular Chen observes that the damping in the moment-frame direction was high (from 3% to 9%) in part do to the loose connection of the beams to columns and early yielding of the connectors and that amplification of story shear due to P-delta was considerable. By adjusting connection stiffness, the computer model used predicted drift well although excursions past the yield point of the connectors were limited. It is suggested that a rack can be adequately modelled by using a linear rotational spring and adjusting damping.

2.2 Existing standards on rack seismic design

2.2.1 Canada

The Canadian standard specific to rack design, the CSA A344.2-05 Standard for the design and construction of steel storage racks, stipulates that racks should be designed to withstand seismic loads §8.2.1 (b) and gives a number of modifications to Part 4 of the NBCC [19] which are largely informed by RMI standards (see 2.2.2):

- Fundamental period should not be determined with the approximate equations given in the NBCC and are limited 4 s in the moment frame direction and 2 s the braced frame direction,
- Design can be carried out following the method for multi-story buildings or by the methods given for parts and portions,
- Ductility and strength modification factor R_d and R_o are left to the discretion of the engineer,
- Seismic weight can be reduced to account for probable loading, load damping up to i.e. sliding (up to 60%), but if this is not to be accounted for the seismic weight is 80% of the maximum design load,
- The concentrated load, F_t , which is typically added to reproduce higher mode effect need not be applied,
- Masses at the first level may be neglected if the beam is less than 300 mm above the floor in seismic weight.

The NBCC does not specifically mention steel storage racks. As such, they may be treated as multi-story buildings or according to §4.1.8.18. Elements of Structures, Non-structural Components and Equipment which gives deflection limits. Non-structural components must be able to accommodate base shear calculated:

$$V_p = 0.3F_a S_a(0.2)I_E S_p W_p \quad (2-1)$$

and deflections caused by this shear. Where S_p is the horizontal force factor for part or portion of a building and its anchorage determined from Table 4.1.8.18. according to the non-structural component considered. Racks would either be considered numbers 21 or 22 - Flexible components with ductile or non-ductile material and connections.

If a rack with hot-rolled sections is to be designed as a multi-story building its seismic design would fall under Chapter 27 of CSA S16-09 which “may be applied to structures provided that the structure includes a clearly defined seismic-force-resisting system and that a level of safety and seismic performance comparable to that required by Clause 27 for building structures” [20]. While the moment frames and braced frames of racking systems appear similar to MRFs and CBFs they have different failure modes and thus their ductility modification factors should not apply. Conventional construction uses $R_d = 1.5$ and $R_o = 1.3$.

Work by Alam & Haque, who derived ductility and overstrength factors in a Canadian context, [14] suggests that these values are conservative. Based on pushover analysis and incremental dynamic analysis of 4, 6, 8 and 10 story racks it is observed that R_d decreases as overall height increases from a high of 2.76 to a low of 1.89. Racks designed using this ductility factor were subjected to non-linear time history analyses and found to have acceptable performance.

Currently an Annex to CSA-S16 is under development. In terms of seismic design, this standard aims to formalize capacity seismic design for racks and includes both provisions for force-based methods and displacement-based methods of design.

2.2.2 USA

The following documents govern the seismic design of racks in the USA:

The NEHRP Recommended Seismic Provisions for New Buildings and Other Structures (racks are designated as Non-Building Structures) gives rack specific force modification factors, over strength factors and deflection modification factors as well as direction as to which loading conditions must be considered and how seismic weight is calculated.

The RMI standards designated ANSI MH16.1- of which the 2012 edition is the latest revision and which are referenced by the NEHRP guidelines gives detailed instruction for testing of beam-column connections, calculation of connection rotation capacity, summarized rack specific design

equations for the calculation of base-shear, distribution of forces and calculation of fundamental period.

FEMA 460 Seismic Considerations for Steel Storage Racks published in 2004 is an extensive design guide based upon RMI standards (up until ANSI MH16.1-2002). It gives not only a historical overview of rack design and research but specific recommendations for force-based and displacement based design of rack moment frames. The RMI standard and FEMA 460 underpin many codes used worldwide.

The equivalent static force method described in FEMA 460 uses an R factor in the moment frame direction of 6 in conjunction with an over strength factor Ω_0 of 3 and a deflection amplification factor, C_d , of 5.5. It is noted that these values are derived loosely from Chen [21] and from NEHRP recommendations for SFRS used in structures similar to buildings and notes that their pertinence as applied to rack structures is debateable. Base-shear is calculated considering 67% of the pallet weight. When distributing base shear as equivalent static forces over the height of the rack, a modified equation is used which accounts for beams placed very close to the floor and for racks with periods longer than 2.5 s. It is noted that NEHRP recommends that at least 5% drift must be assumed for the moment-frame.

Because the stiffness of the rack is dependant on assumed displacement, FEMA 460 recommends an iterative process for determining the fundamental period such that “that when the design base shear is applied to a down-aisle model of the storage rack, the moment determined for the beam-moment connections is consistent with the connection stiffness” [22] or by using a rotational spring constant determined from connection tests outlines in the RMI standard and an analytical equation or other mechanical methods.

Little guidance is given in FEMA 460 on how to account for P-delta effects in force based methods other than to state that they are important in the moment frame direction.

FEMA 460 also proposes a displacement-based method for rack seismic design, but cautions that much of the data needed is still under development. This method is based primarily on [15] which is described in detail in §2.3.

2.2.3 Europe

A wide ranging project entitled SEISRACKS has been undertaken by la Fédération Européenne de la Manutention. The project culminated in a report entitled “Storage Racks in Seismic Areas” which details a number of research projects based around component tests, pallet sliding (see §2.4.3 and this section), full-scale pushover and dynamic tests of multi-level, multi-bay racks and numerical modelling of racks. With recommendations made by the SEISRACKS report, the standard entitled EN 16681: Steel static storage systems - Adjustable pallet racking systems - Principles for seismic design was published in 2016. EN 16681 supports three methods of analysis according to the sensitivity of the rack to interstory drift, θ , and according to which behaviour factor, q , the designer wishes to use. The behaviour factor is used to reduce the elastic acceleration spectrum in recognition of (among other factors) ductility of the structural system. For $q \leq 2$ (low dissipative structures) an equivalent static force method (LFMA) or modal response spectrum analysis (MRSA) is mandated; for $q \geq 2$ (high dissipative structure) when the rack is deemed sensitive to interstory drifts, a non-linear time history analysis is necessary. To design the rack moment frame as a high dissipative structure, the beam-column connectors must adhere to certain energy dissipation criteria characterised by cyclic tests and the effect of connector deformations on the global drift must taken into account by a mandated non-linear analysis method.

The main innovation in EN 16681 brought about by the extensive investigations into the characteristics of pallet sliding (see details in §2.4.3) by the SEISRACKS project is the inclusion of a material and warehouse specific friction coefficient, μ_s , (given in the standard) through the, E_{D1} , factor that is used to calculate reduced design acceleration spectrum, $S_{d,red}(T)$:

$$S_{d,red}(T) = E_{D1}E_{D3}S_d(T) \quad (2-2)$$

where:

$$E_{D1} = \max[0.4; \mu_s/S_e(T_1) + 0.2] \quad (2-3)$$

$S_e(T_1)$ is the ordinate of an elastic acceleration spectrum with 3% viscous damping. The second coefficient, E_{D3} , accounts for “other phenomena typical of the dynamic behaviour of racking structures under seismic actions that are not included in the mathematical approach presented in

[the code], but that are observed on racks that have suffered earthquakes, and from tests performed on shaking tables” [23]:

$$E_{D3} = 1/1.5 = 0.667 \quad (2-4)$$

EN 16681 includes a pallet weight modification factor, E_{D2} , used to reduce the seismic weight for “damping inside the palletized goods” [24]. E_{D2} varies between 0.7 and 1.0 depending on the type of goods to be loaded onto the rack. The SEISRACKS project emitted the following commentary regarding the use of this factor:

“Such a source of energy dissipation would be possible only if the frequencies of the stored goods are tuned on the frequency of the structure. This is very unlikely according to the respective range of frequencies observed during the SEISRACKS project. Natural frequencies of the racks are rather low (between 0.25 and 1 Hz), while the few values of frequencies obtained for merchandise are significantly higher (between 1.5 and 24 Hz). As long as extensive measurements are not performed to assess the actual dynamic behaviour of a wide range of merchandise, it is recommended not to account for any dissipation in the goods and thus to set $E_{D2} = 1.0$ ”

The standard also accounts for a reduction in the seismic weight of the pallets due to the possibility that not all bays may be full via a client provided filling grade reduction factor, $R_F \geq 0.8$ (in the moment-frame direction).

EN 16681 also includes a “Large Displacement” method of analysis for “dissipative structure” where $q > 2$:

When large displacements analysis is performed, the load history shall be defined as follows:

- 1) the target displacement is first calculated; the target displacement is the maximum horizontal displacement in the direction considered, obtained from MRSA multiplied by the behaviour factor q ; the point in which the target displacement is calculated is the target point;
- 2) the pattern of horizontal forces shall be determined using a distribution matching the modal shape of the fundamental mode in each of the two principal directions;
- 3) the vertical loads shall be first applied to the structure, then the horizontal forces shall be incremented until the target point reaches a displacement equal to 1.1.

The nonlinear behaviour of materials and connections shall be taken into account.

2.2.4 New Zealand

Following recent earthquakes, rack collapses have been documented in [4] (Christchurch quake), [5] (Darfield quake), and [6] (Canterbury quake). As a result, the guide for the Seismic Design of High Level Storage Racking Systems with Public Access [25] (which is mainly based on a survey of RMI standards adapted to the New Zealand context) was revised. Most revisions pertained to operation of the racks, but the revision called into question the reduction of seismic weight by the factor of 0.67 for sliding as well as the reduction of seismic weight by 0.8, in the moment frame direction, for the probability that the rack would be fully loaded. The authors found that in the case of commercial systems (where pallets are more closely spaced and fully loaded) these factors were too small [26].

2.3 Existing applications of DBD to racks

The displacement-based method proposed by FEMA 460 was developed in [15] along with an equation for the fundamental period of simple uniform-level, uniform-bay racks. The method supposes that:

- The same connectors are used at each beam-column joint,
- Bay height and width are uniform,
- Equal rotations are experienced by all connectors and base-plates, which are the only elements undergoing inelastic deformation.

Assuming known connector moment-rotation curves, the rack can be transformed, under these hypotheses, into a SDOF.

Since the connectors are the capacitive fuse element to be designed in a rack, the design is said to be adequate when the maximum rotation capacity of the connector (more generally termed the target rotation), $\theta_{c,max}$, is equal to the rotation demand placed on the connector, θ_{demand} . Thus the first step of design is to determine $\theta_{c,max}$ from the experimental moment-rotation curve which can then be used to find the rotational stiffness of the connector, k_c . The fundamental period, T_1 , function of beam and column inertias, pallet mass and connector stiffness is ascertained. To find

θ_{demand} site specific 5% damped spectral acceleration data must be adjusted to account for damping, converted to displacements and then to rotations. Filiatrault uses the following equation from NEHRP provisions with a damping factor, B , issue from the same provisions and dependant on PGA and the viscous damping ratio needed to match the displacement of elastic models to shake table results in [27]:

$$D = \frac{gS_{M1}T_1}{4\pi^2B} \quad (2-5)$$

where g is gravity acceleration, S_{M1} is the MCE spectral acceleration at one second taking into account site effects. The displacement, D , is then augmented to the maximum displacement demand, D_{max} , by applying a factor to account for P-delta, the equation for which is developed in [15]. Finally the displacement, D_{max} , is transformed into rotation using the equal rotations assumption:

$$\theta_{demand} = \frac{D_{max}}{0.72h_{tot}} \quad (2-6)$$

The authors note that experimental beam-column connector data is crucial to determine θ_{max} and k_c .

If, as first noted by Krawinkler and subsequently reiterated by many researchers, damping is largely dependant on the loose connection and yielding of connectors, full-scale shake-table tests would also presumably be necessary to choose appropriate rack/connector specific damping ratios. A method that would obviate the need for these large and expensive tests is proposed in [16] where the energy dissipated (and hence damping) is found by subjecting a numerical model of the frame, with connector elements calibrated from test data to a cyclic protocol. The authors apply displacement-based design in a Canadian context and find that, although non-linear time history analysis gave displacements higher than predictions in some instances, the method is safe. This design was carried-out without consideration of P-delta.

2.4 Design quandaries

2.4.1 Lateral stiffness

Although force-based methods typically rely on elastic stiffness, for racks appropriate connector stiffness must be chosen that takes into account the quick yielding of these components. As mentioned in §2.2.2 the RMI recommends an iterative approach to find values of stiffness coherent with rotation and strength values. [28] performed several shake table tests of a cold-form racks to determine the natural period and connector stiffness and give recommendations of the best ways of testing properties. [29] developed analytical equations for finding displacements and rotations in racks with semi-rigid connections subject to lateral loads and including P-delta, and compared analytical equations and found that correspondence was good with eigenvalue analysis. [30] proposed a way to determine fundamental period by including warping (of cold-formed open-section columns) in the stiffness matrix and finds that the approach proposed by FEMA 460 is unsatisfactory. The authors also proposes a coefficient for second order effects to be included in the calculation of the fundamental period.

2.4.2 Base plate stiffness and energy dissipation capacity

Rack base-plates form semi-rigid connections, are typically welded or bolted to columns and bolted into concrete floors. Some recent studies [31] [32] have explored their influence on response in the braced-frame direction and have explored methods for determining strength and stiffness [33], however much less data is available on the cyclic response of base-plate in the moment-frame, although their important effect on seismic response has been noted [31], [32], [33] & [24]. Consensus has not been reached as to the best method of determining base-plate moment-rotation characteristics whether experimentally or analytically. This is in part due to variation in base-plate design between manufacturers and also to the difficulty of performing small experimental component tests like those widely performed on beam-column connectors. As a result, most tests available are non-cyclic. Response of the base-plate may be function of: yielding of the plate (thickness of the plate, bolt-layout, geometry of the plate, width and depth of the column), interaction with the concrete slab, pull-out of the bolts and applied compression [34].

The FEM recommends the use of the testing procedure outlined in EN 15512 to evaluate cyclic response of base-plates. This method, illustrated in Figure 2-1, has been discussed and modified by Gilbert and Rasmussen to avoid “catastrophic failure” during testing [32].

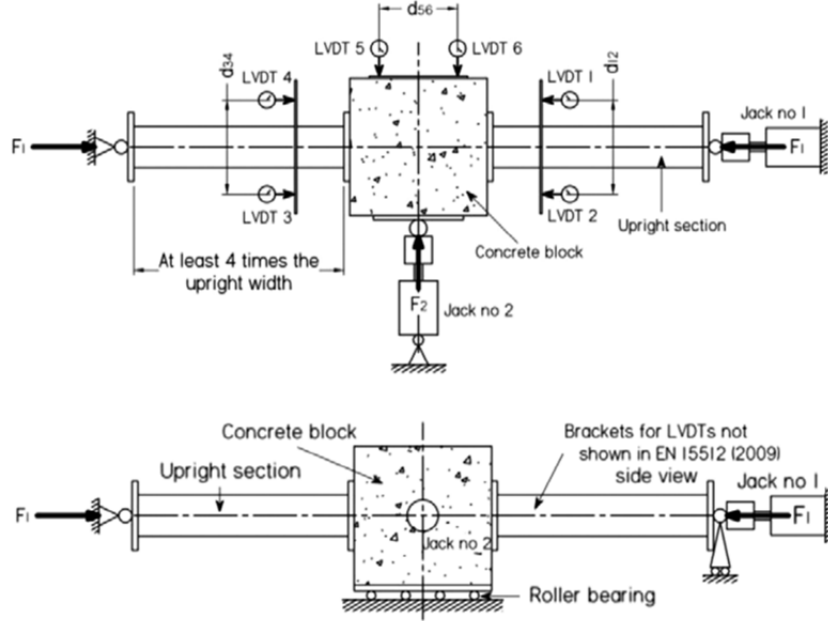


Figure 2-1: Base-plate testing assembly as recommended by the FEM and discussed in [32].

The RMI proposes an analytical approach to determining base-plate stiffness as a function of column width, b , and depth, d , as well as the concrete slab stiffness, E_c :

$$M_b = \frac{1}{12} b d^2 E_c \theta_b \quad (2-7)$$

Modifications to this equation have been proposed by Sarawit in function of the base-plate form [34], who considers four different geometries of base-plate.

2.4.3 Pallet sliding, sloshing & shedding

One important way that racks differ from building structures is that the structural self-weight is negligible in comparison to live load. Live load, composed of pallets and merchandise, is not fixed to beams and can become free to slide on, collide with and fall from racks during earthquakes. This creates difficulties for the application of both force-based and displacement-based methods because the participating mass of the structure can change during an earthquake

and thus also its fundamental period. Mass sliding is often taken into account by reduction of the seismic weight: in [35], [23], [36] and the forth-coming Annex N [20].

The researchers involved in the SEISRACKS project have carried-out the most wide ranging investigation of pallet-beam friction coefficients and pallet-rack-sliding interaction.

- Parameters investigated: pallet and beam material, mass, mass eccentricity, acceleration and frequency,
- For dry pallets μ varies between approx. 0.2 and 0.6 in cross-aisle direction (with plastic pallets being the most slippery) and between 0.1 and 0.6 in the down-aisle direction,
- Applied mass is less influential than other parameters on μ ,
- In cross aisle direction first slippage can occur between 0.15g and 0.35g while in down-aisle direction first slippage occurs around 0.3g to 0.6g. Dynamic slippage depends somewhat on frequency and on materials. Plastic pallets were not investigated in the dynamic portion of testing.

In [37] analytical equations and a finite element friction model is developed. This model was used in conjunction with the experimental results of the SEISRACKS project. In [38] a simple FEM rack with stick-slip pallets is subjected to a single ground motion with peak accelerations around 0.5 g. It is found that inertial forces are reduced by sliding, force decreases in function of μ are presented. The largest pallet sliding displacement is about 50 mm.

Reference [39] also presents the development of equations for the stick, slip, flight, impact of an SDOF pallet by using a series of springs. Analytical equations are followed by a series of numerical tests and experiments using inclined racks with the goal of preventing shedding of merchandise.

In [40] 4-story finite element model of a cross-aisle rack is subject to 10 California ground motions with PGA around 1g. Peak acceleration of the beam-levels is significantly reduced with the use of added damping and sliding pallets. For stiff merchandise sliding effects drastically peak beam-level acceleration, for flexible merchandise less-so.

2.4.4 Scaling of spectra for damping

Acceleration spectra are given by the NBCC for 5% damping. Displacement-based design requires displacement spectra (see 2.3) at many and larger values of damping. Response of a damped structure depends on quake duration, frequency content, site conditions, distance from epicentre and magnitude. An exhaustive survey and comparison of damping scaling factors is given in [41]. The NBCC 2010 does not give recommendations for scaling factors, but the Canadian Bridge design code suggests the following equation:

$$R_\beta = [0.1 / (0.05 + \beta)]^{0.5} \quad (2-8)$$

2.4.5 P-delta

Two main approaches have been proposed to account for P-delta effects during displacement-based design. The first is a general (not rack specific) approach described in [42] which proposes a strength enhancement to lift the force-deformation relationship of a structure analysed with P-delta up to the strength level of a structure analysed without P-delta. The general concept of this approach is illustrated in Figure 2-2.

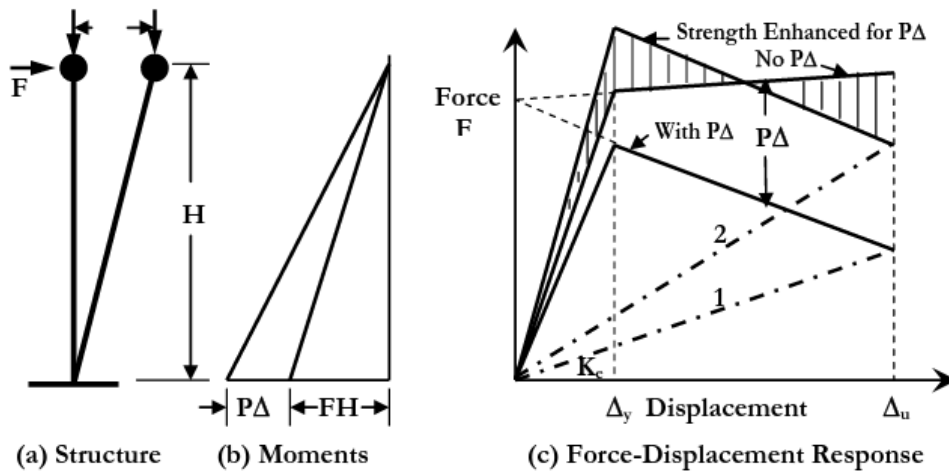


Figure 2-2: Accounting for P-delta according to [43].

In Figure 2-2 (c) the effective stiffness K_e (1) is adjusted to take into account displacements that include P-delta. Strength must be increased to achieve acceptable displacements K_e (2), but strength ought to be increased such that the target displacement matches the displacement without

P-delta. The corresponding increased moment demand is shown in Figure 2-2 (a) & (b) and design equation becomes:

$$M_B = K_e \cdot \Delta_D \cdot h_e + \chi \cdot P \cdot \Delta_D \quad (2-9)$$

where χ depends on the stiffness degradation due to P-delta (rotation of material M- θ curve).

In [15] a rack specific method based on [43] is developed. In this approach the over-turning moment is amplified for P-delta effects. Using the hypothesis of equal rotation in base-plates and beam-connections, the over-turning moment is related to moment demand in the connections and therefore the effect of P-delta on the connections; increased connection moment demand leads to increased connection rotation demand leads to increased lateral displacement of entire building. P-delta is therefore accounted for by increasing displacement demands by a factor.

2.4.6 Higher mode participation

In [15] and [16] displacement based design is performed based on the assumption that the rack responds as a single-degree of freedom. It is unclear under which circumstances (number of levels, level heights, connectors used) this assumption holds true. When the participation of higher modes is important, approaches used for the displacement-based design of irregular bridges [44] or high-rise buildings [45], such as the effective mode shape method described in [46] where the target displacement for each mode is examined individually may prove useful.

CHAPTER 3 ARTICLE 1: SHAKE-TABLE TESTING AND NUMERICAL MODELING OF INELASTIC SEISMIC RESPONSE OF SEMI-RIGID COLD-FORMED RACK MOMENT FRAMES

E. Jacobsen and R. Tremblay

Polytechnique Montreal, Montreal, Canada H3C 3A7

Thin Walled Structures

Abstract

An experimental program consisting of quasi-static cyclic, pull-back and seismic shake table tests was conducted to examine the inelastic seismic response of cold-formed selective rack structures. Hysteretic response of the connectors and base plates are presented. In the seismic tests, racks could sustain up to 10% drifts without collapse. Pallet sliding was observed in the tests. A numerical model is proposed in OpenSees to predict the rack seismic response, including pallet sliding. It is used to study the response of 6-bay racks having 3 to 6 levels. Displacements are sensitive to assumed viscous damping, base plate properties and pallet sliding.

Key words: Rack structure, moment frame, connectors, damping, base plate, global instability, sliding,

3.1 Introduction

Collapse of steel rack structures in recent earthquakes have raised concerns on the ability of steel rack structures to safely withstand seismic effects [1],[2],[3]. Selective steel rack structures are commonly used for storage in commercial and industrial buildings. These structures form semi-rigid moment frames to resist lateral loads in the down aisle direction while braced frames are used for stability and lateral resistance in the cross-aisle direction. For seismic design, most design standards rely on a force-based analysis method wherein design forces determined from anticipated elastic inertia loads reduced to account for the system ductility e.g. [4],[5],[6]. For rack moment frames, ductility is achieved through inelastic rotations in the beam-to-column connectors and column base plates.

Recently, studies have been performed to examine the possibility of using the direct-displacement based design procedure for the seismic design of selective racks structures along their moment

frame direction [7],[8] & [9]. Displacements are evaluated using a linear structural model having a period based on the structure secant lateral stiffness and an equivalent damping ratio reflecting the structure energy dissipation capacity, both properties being determined at peak displacement [10]. In design, the structure properties are modified iteratively until the desired drift is attained. A displacement-based evaluation procedure for racks has been proposed in FEMA 460 [11]. In that procedure, the structure stiffness is based on the secant stiffness of beam-to-column connectors and base plates, as obtained from cyclic test data. All connections are assumed to experience the same rotation and stiffness of base plates can be taken equal to that of the connectors when base plate data is not available. In the RMI Specification [6], seismic design using a displacement-based method is permitted to be used as an alternative to the force based method. In 2016, a displacement-based approach has been introduced in CSA S16 standard for seismic design of rack structures [12]. In view of the relative immaturity of this approach and lack of experimental and numerical validation, the method is limited to racks up to 7.6 m high, stringent drift limits apply, predicted connection rotations are amplified to account for variability and the structure must meet minimum lateral strength and P-delta effects requirements.

Further development of the method requires nonlinear response analysis of representative prototype structures which, in turn, requires robust nonlinear models that can accurately predict the seismic inelastic response of racks including global stability effects. Various such models have been proposed by [13],[14],[15],[16],[17]. Emphasis should be put on the hysteretic response of the beam-to-column connectors and base plates. Limited data, especially cyclic data, is available for the latter and previous experimental and numerical studies e.g. [18], [19], [14], [20], [21], [22], [23], [24], [25] have shown that base plates have a significant influence on lateral response of racks. For the former cyclic tests with non-linear modelling have been carried out by [26], [27], [28]. Sliding of pallets on beams may also affect the seismic response of racks; this has been observed and quantified in [29], [14], [30], [31], [32], [33], [34]. Shake table tests of rack frames have been performed by [35], [36], [19].

This article first presents an experimental program that was performed to generate data on the cyclic inelastic response of beam-to-column connectors and base plates used in typical cold-formed rack structures and develop knowledge on the seismic response of that rack system close to or up to collapse. The test program included quasi-static cyclic, pull-back and shake table seismic tests on one-level, one-bay rack specimens. Ground motions expected in eastern and

western North America were used in the seismic tests and the records were scaled to reach large drifts. Gravity loads were applied on all specimens such that P-delta effects could be examined. One seismic test was conducted up to collapse of the specimen. The test results are then used to develop a detailed model of the racks studied using the OpenSees platform [37]. The model accounts for the nonlinear response of the connectors, including strength degradation. Sliding of pallets is also included to reproduce the sliding behavior observed in the tests. Appropriate viscous damping to match experimental results is also examined. In the last part of the article, the model is used to examine the seismic response of more realistic 6-bay multi-level racks structures to illustrate the capabilities of the proposed model. Effects of ground motion amplitude, viscous damping and pallet sliding on peak displacement profiles and collapse response are briefly examined.

List of symbols:

a – base-plate dimension (see figure 6)

a' – base-plate dimension (see figure 6)

AF – strength adjustment factor of base-plate material model

b – base-plate dimension (see figure 6)

c – base-plate dimension (see figure 6)

C – compressive axial load in a column

d – base-plate dimension (see figure 6)

E – modulus of elasticity

EDC – energy dissipated per cycle

EDC_c – energy dissipated per cycle in a connector

EDC_{bpl} – energy dissipated per cycle in a base-plate

h – rack height

I_{col} – column moment of inertia

j – number of oscillations

k_{rack} – lateral stiffness of a rack

$k_{rack,red.}$ – rack lateral stiffness reduced to account for P-delta

k_{sec} – secant stiffness

f_y – yield strength

F – total applied lateral load

FEM – Finite Element Method

$m_{p,bpl}$ – yield moment per unit length

M_{bpl} – base-plate moment

M_c – connector moment

$M_{y,bpl}$ – base-plate yield moment

RMI – Rack Manufacturer's Institute

SF – ground motion scale factor

t_p – base-plate thickness

T_n – natural period

$u_i - i^{\text{th}}$ decrement of between two successive peaks of displacement amplitude

V – base-shear

W – total weight of the rack

\mathcal{W}_E – external work

\mathcal{W}_I – internal work

$\beta_{hyst.}$ – hysteretic damping

$\beta_{el.}$ – rack damping coming from other sources than hysteretic damping

β_{eff} – equivalent viscous damping

δ – displacement of the rack at beam level

Δ – drift i.e. δ/h

Δ_{avg} – average drift

Δ_{bpl} – drift due to base-plate deformation

Δ_{col} – drift due to deformation of the column

Δ_{top} – drift of the top level of a rack

Δ_{tot} – total drift

θ_{bpl} – base-plate rotation

θ_c – beam-column connector rotation

μ_s – static friction coefficient

μ_k – kinetic friction coefficient

ζ – equivalent viscous damping

$\bar{\zeta}$ – mean viscous damping

3.2 Testing Program

3.2.1 Test Setup

All tests were performed on the 3.5 m x 3.5 m, uniaxial earthquake simulator of the Structural Engineering Laboratory at Polytechnique Montreal. Figure 3-1 shows a 2D view of the single-level, one bay rack specimen. The specimens were built from typical cold-formed uprights and beams (sections shown in Figure 3-4a). Rack specimens with two different base fixities were tested: frames with pins at their bases (series P) as shown in Figure 3-1a, and specimens with 6.4 mm thick base-plates welded to the columns (series F) as shown in Figure 3-1b. Base-plates and pins were bolted to stiff 25.4 mm thick steel plates which sat upon 19.0 mm thick shims all bolted down to the shake table (Figure 3-1a, b & Figure 3-2c). The beams were clipped into the columns such that the height from the base (pin centre or base-plate) to the beam shear centre was always $h = 1708$ mm.

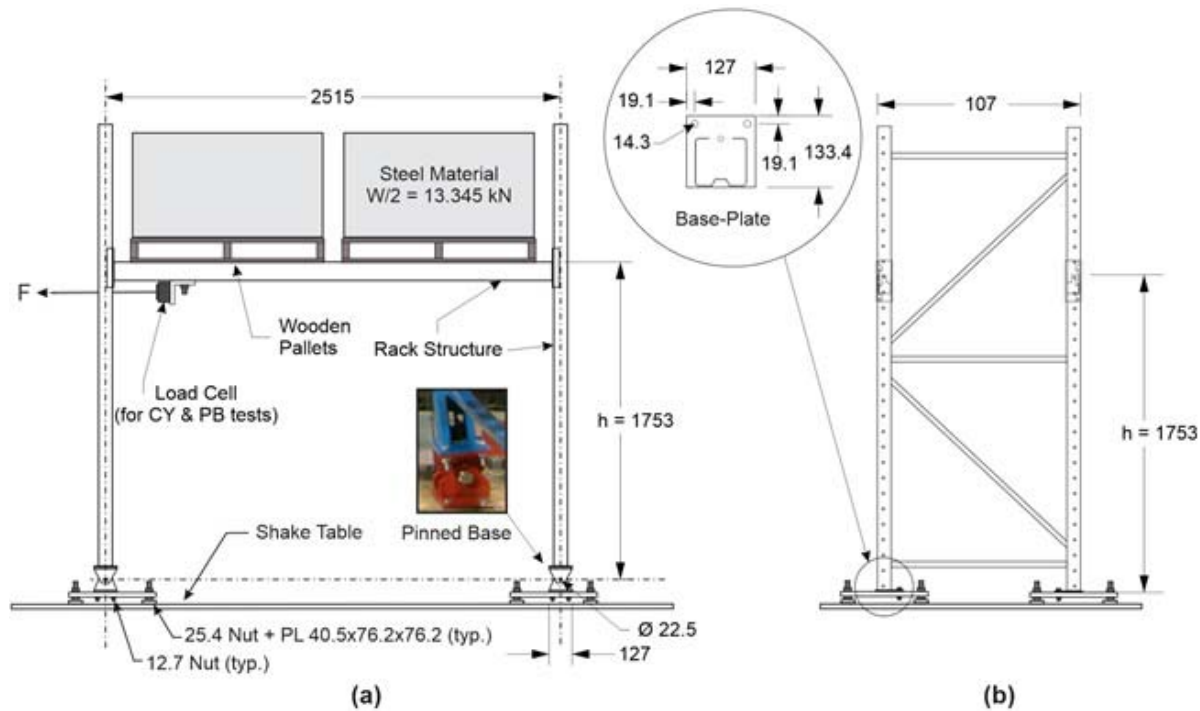


Figure 3-1: Test setup (all dimensions in mm): a) Elevation view; b) Side view.

Two standard wooden pallets measuring 1.02 m wide by 1.22 m deep (40" x 48") holding 13.345 kN each of sundry steel coils in cardboard boxes and shrink-wraps were placed on the beams without attachment preventing sliding nor any surface preparation (Figure 3-1a).

Figure 3-2 shows details of loading and instrumentation: throughout all tests, rotations at the four beam-column joints were captured by two linear pots above and below each connection (Figure 3-2a). Similarly, displacements measured by string pots 152 mm from column bases were used to obtain base-plate rotations (Figure 3-2b). Displacements at beam-level were measured on columns on all four corners of the rack. Initially accelerometers were placed at the centre of the masses and mid-beam during seismic tests; however, beam-level instruments gave overly noisy results due to significant up and down motions and were abandoned in favour of two accelerometers placed on columns at beam-level (see Figure 3-2b).

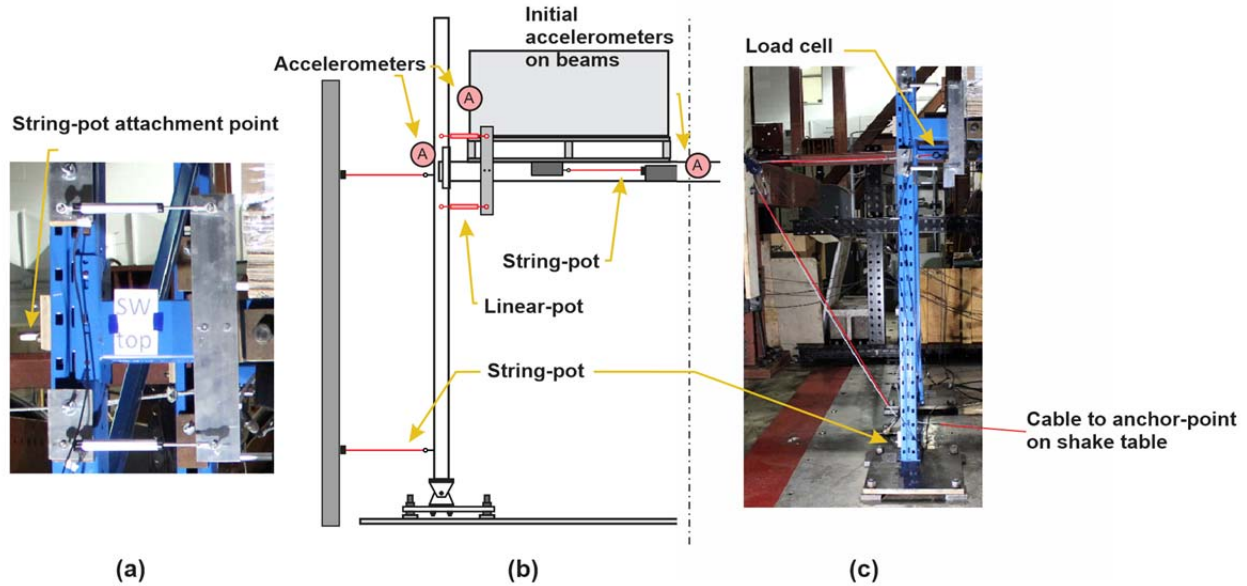


Figure 3-2 : Loading and instrumentation: a) Linear-pot assembly to measure rotations at beam-column joints; b) instrumentation schematic showing measurement locations; c) Cable and position of load cell during static tests.

Sliding of the pallets was measured by four string pots attached to the beams, except for specimen P3 where the pots were placed on the columns above the beams. Figure 3-2c indicates the cable used in quasi-static tests. This cable, attached to a load-cell, fixed to the underside of the beams, was fastened to the shake table which imposed the displacement (see Figure 3-1a Figure 3-2c)

Figure 3-3 shows details of the beam column connection. In Test F1, these connections were modified to create pinned connections between beam and column for isolation of the base plate connection response (Figure 3-3b).

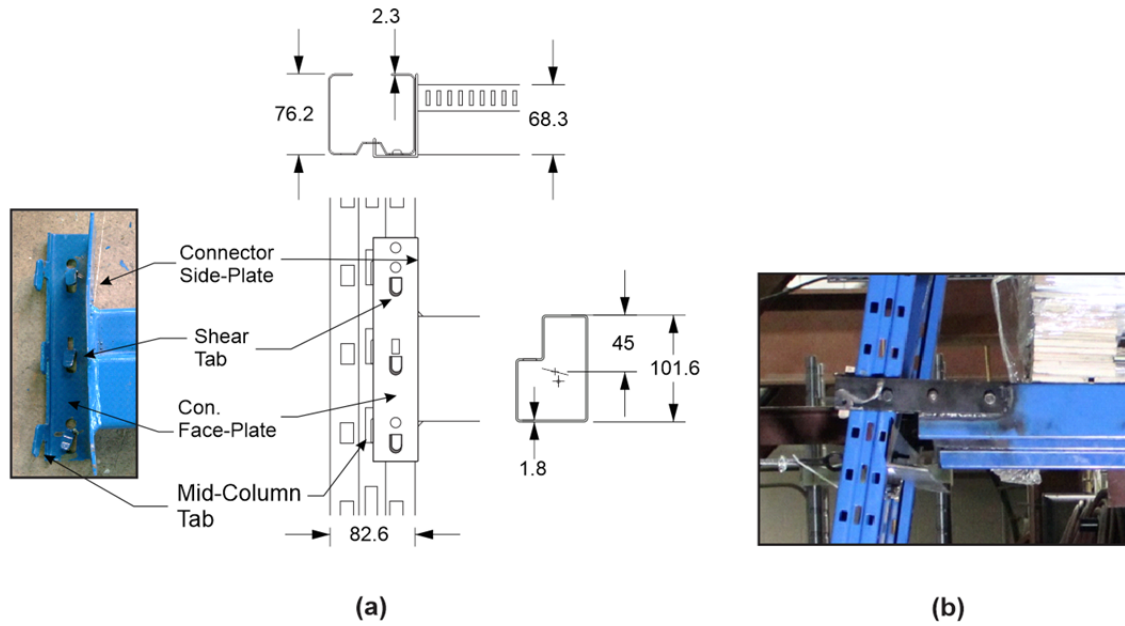


Figure 3-3 : Beam-column connection (all dimensions in mm): a) Photo (taken after testing) and figure of the beam-column connection and section of the column and beam; b) Modified “pinned” beam-column connection in Test F1.

For safety during seismic tests, slack steel cables were attached to column tops to prevent total collapse of the specimens (no photo available).

3.2.2 Test matrix and loading protocols

Figure 3-1 presents the test matrix. Pin-base specimens are identified PX while specimens with base-plates (fixed bases) are identified FX. Five preliminary tests were carried out to determine static and dynamic properties: three quasi-static cyclic (CY) tests and two pull-back (PB) tests. Six seismic tests (Q series) were then performed. A new rack specimen was used for each of the 11 tests. Sine sweeps were performed after some of the seismic tests in an attempt to induce resonance and collapse. However, since displacements were curbed by pallet sliding, attainment of collapse was not possible in these tests and sine-sweep results are not reported in this paper.

Figure 3-4a shows the displacement protocols applied in the quasi-static cyclic tests. They were chosen to progress quickly to large amplitudes and were modified ad hoc to add extra cycles at the end of loading until it was apparent that the full capacity of the connectors/base-plates had been exhausted. The first two cyclic tests aimed to isolate the static behavior of the beam-column

Table 3-1: Testing Program

Specimen	Beam-Column Fixity	Base Fixity	Load Protocol	Scale Factor
P1	pinned	pinned	CY1	-
F1	cold-form	base-plate	CY2	-
F2	cold-form	base-plate	CY3	-
P2	cold-form	pinned	PB	-
F3	cold-form	base-plate	PB	-
P3	cold-form	pinned	Q1	2.45
P4	cold-form	pinned	Q2	0.85
P5	cold-form	pinned	Q3 & Sine Sweep	1.02
F4	cold-form	base-plate	Q1 & Sine Sweep	3.2
F5	cold-form	base-plate	Q3 & Sine Sweep	1.45
F6	cold-form	base-plate	Q2 & Sine Sweep	2.0

and base-plate connectors, respectively. For specimen P1 pins were installed at column bases such that only the beam-to-column connectors resisted induced moments. For specimen F1 pins were created at the beam-column junctions by removing the connectors and welding thick plates to the beams which were then bolted loosely to the columns (see Figure 3-1e).

In pull back tests the top of the rack is pulled to a certain displacement and then abruptly released and allowed to oscillate until movement ceases. These tests generate additional information on the cyclic inelastic frame response and characterize period and damping properties. As shown in Figure 3-4b, the tests were conducted at similar amplitudes to the quasi-static tests but with initial displacement imposed in one direction only. For each displacement amplitude, the PB tests were repeated two or three times.

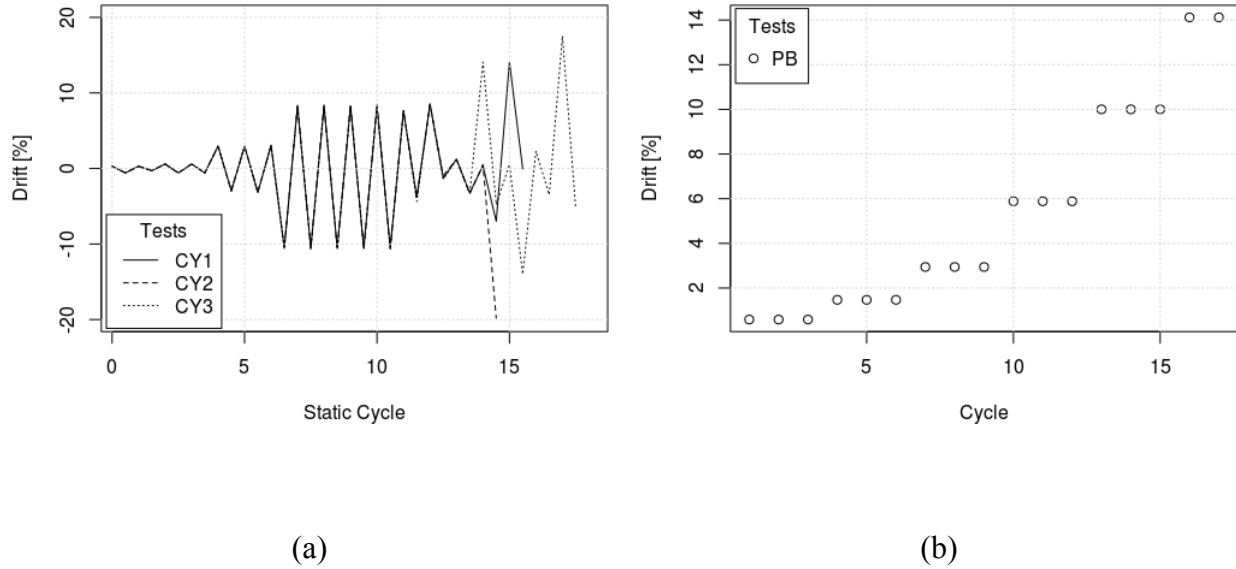


Figure 3-4: Displacement protocols in: a) Quasi-static tests; and b) Pull-back tests.

Representative ground motions for site class C in the two main populated seismic regions of Canada (Montreal, Quebec and Vancouver, British Columbia) were selected for the seismic tests [39]. The accelerograms were scaled to produce drifts between 7 % and 11% as predicted by incremental nonlinear dynamic analysis using preliminary models calibrated from quasi-static and pull-back tests. Target drift amplitude was chosen in order to cause as much damage as possible while safeguarding testing equipment. Scale factors with respect to the uniform hazard spectra of NBCC 2015 at both locations are shown in Table 3-1 [39]. Higher scaling factors were needed in Montreal because it is a lower seismic region compared to Vancouver. The unscaled signals are shown in Figure 3-5. The signals were filtered in order to accommodate the displacement limit of the shake table. Feedback, as measured on the table during physical tests, was used for all numeric comparisons. Displacement spectra of the feedback signals are shown with the natural period of specimens at their target drifts in Figure 3-5.

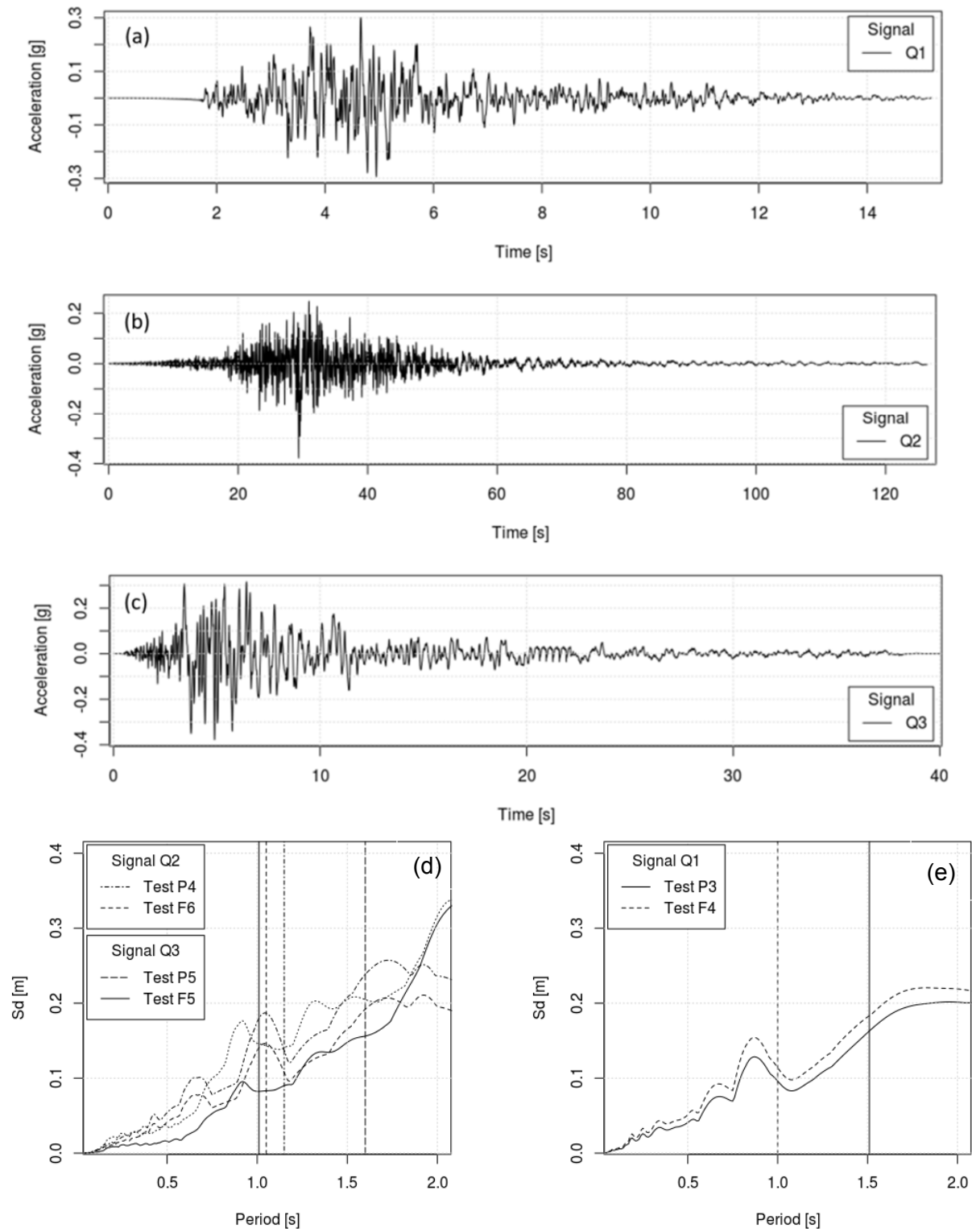


Figure 3-5: Test ground motions and corresponding 5% damped displacement spectra.

3.2.3 Results from Quasi-Static Cyclic Tests

Figure 3-6a shows the lateral load-lateral displacement response of the specimen P1 (pinned base). In the figure, F is the total applied lateral load (see Figure 3-1a) and Δ_{avg} is the average drift of the two frames from measurements at four columns. The specimen is flexible and the frame response is significantly affected by P-delta effects, as can be seen in the cycles with larger amplitudes after pinching has developed in the connector's response. Figure 3-6b shows the moment-rotation hysteresis of a single connector, where θ_c is the connector rotation and M_c is the connection moment. As anticipated, the response was dictated by the beam-column connections; see similarities between Figure 3-6a (force deformation of rack) and Figure 3-6b (moment rotation of connector). Also shown in Figure 3-6b is the single connector response obtained from a cruciform connector test as specified by the RMI in [6]. This type of test is used to design rack connections in both North America [6] and Europe [4]. The unique shape of the hystereses in Figure 3-6 is caused by the many yielding and buckling mechanisms of the connectors. As the connectors are progressively damaged their contact with the column becomes looser which produces more and more pinching with each cycle of loading. Also in Figure 4b, for comparison, is the moment-rotation values from Test P1 averaged among the four connectors; no appreciable difference in their behavior was observed. The connector moment was computed from the lateral load F after removing P-delta effects:

$$M_c = 1/4(F + W \cdot \Delta_{avg}) \cdot h \quad (3-1)$$

The data generated by the static Test P1 fits closely the independently generated data with two principal exceptions: the connectors in Test P1 exhibit higher stiffness in the small amplitude cycles less than 0.02 rad. and slightly lower strength and stiffness under larger rotations. The former difference is attributed to friction in the base pins at the start of Test P1 which reduced frame displacements to give fictitiously higher connector stiffness.

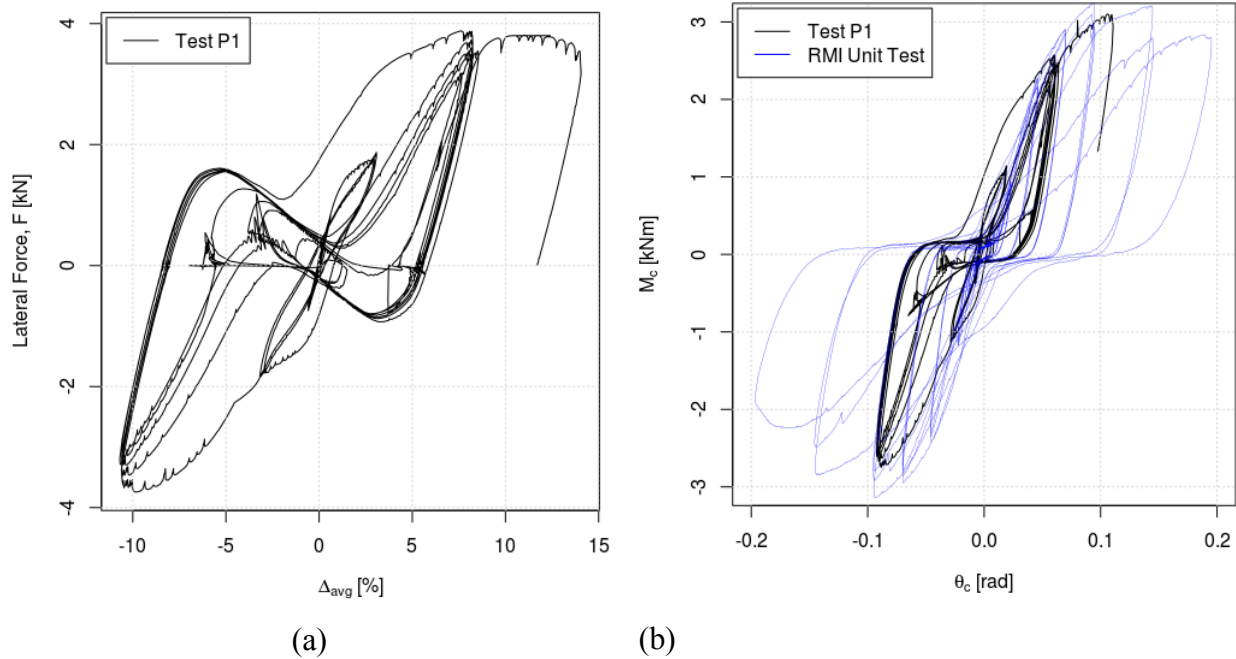


Figure 3-6: a) Base-shear vs. average drift measured in test P1; b) Average moment-rotation of a single connector in test P1 compared with RMI cruciform unit test of the same type of connector.

Figure 3-7 shows the progression of inelastic deformations and damage to the connectors in Test P1: in Figure 3-7a at 0.03 rad minor visible damage to the shear tabs; in Figure 3-7b at 0.08 rad some yielding of the connector shear tabs and local buckling of the connector face-plate begins; in Figure 3-7c at 0.1 rad bending and buckling of the face plate becomes more apparent as well as bending of the mid-column tabs; as the specimen goes through several cycles at 0.1 rad the shear tabs almost completely sheared off; in Figure 3-7d at 0.14 rad, the last cycle, the connector twists out-of-plane disengaging from the column where the connector is in tension, shearing off the mid-column tabs; in Figure 3-7e at 0.14 rad damage to the weld between the connector and the beam is apparent; in Figure 3-7f when the beams are removed damage to the column where the connector was clipped-in is apparent.

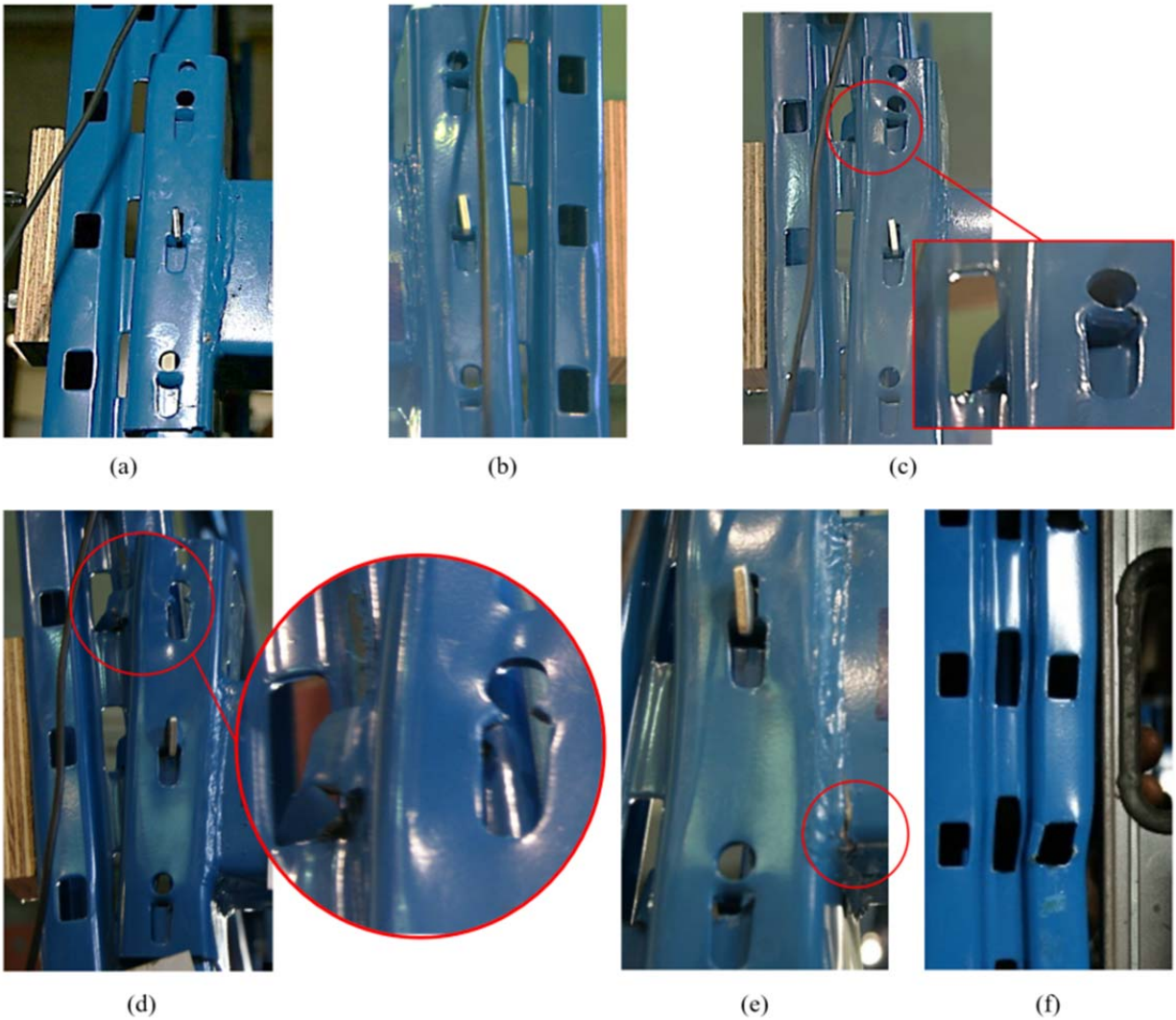


Figure 3-7: Progression of connector damage in test P1: a) at 0.03 rad little damage; b) at 0.08 rad yielding and buckling begins; c) at 0.1 rad shearing and plate buckling worsens; d) at 0.14 rad connector twists and disengages from column; e) at 0.14 rad weld damage; and f) post-test.

The frame response in Test F1 is shown in Figure 3-8. By placing pins at the beam-column junctions, plastic behavior was limited to the base-plates. The lateral strength of specimen F1 is within the same order of magnitude as that of specimen P1 in Figure 3-6a. As opposed to Test P1, however, the yielding of the base plates provided stable lateral resistance, with limited pinching, near the zero deformation position and negative lateral stiffness. P-delta effects are more easily observed upon yielding of the plate. The unsymmetrical placement of the base-plate bolts with respect to the column caused the base-plate to deform both in the lateral and transverse plans. The form by which the base-plates yielded did not vary from cycle to cycle; it is shown at its most

pronounced point in Figure 3-8. Three distinct yield lines are present: along the side of the column (parallel to the plane of bending) a hinge formed which remains bent upwards once deformed, the other two hinges, at the back of the column, are bent and un-bent as the column cycled between positive and negative drifts.

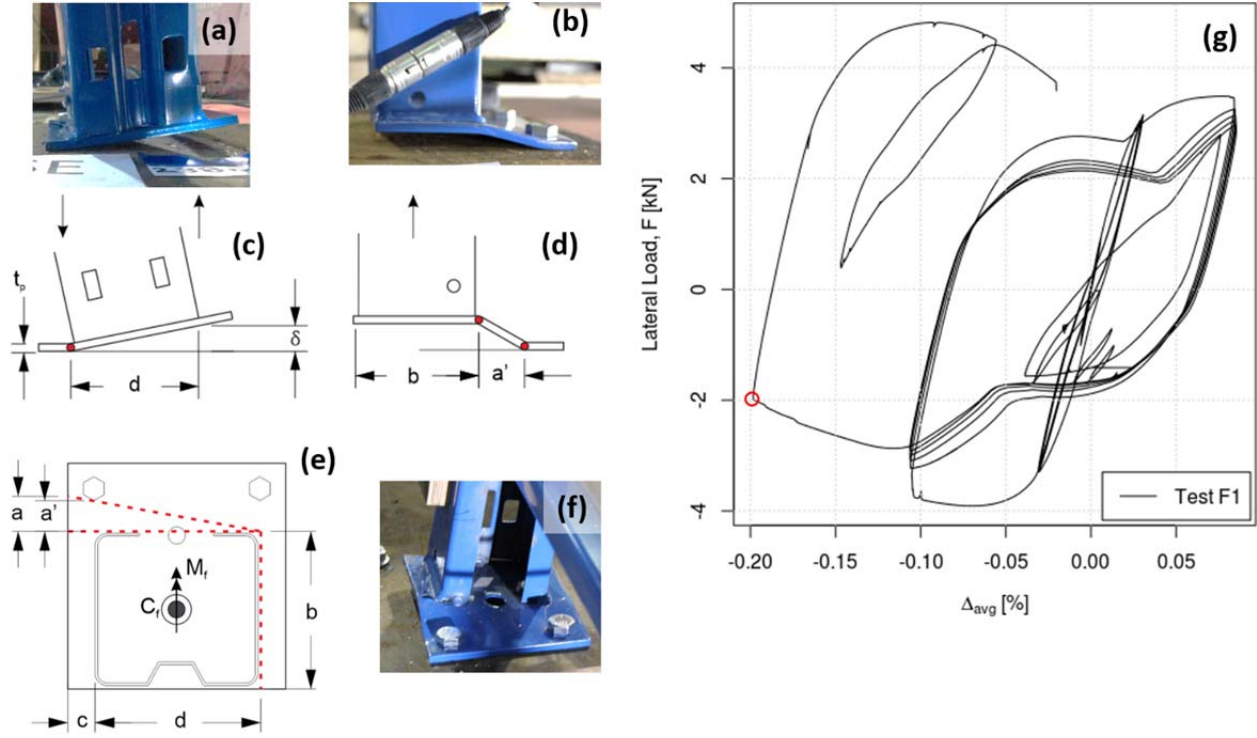


Figure 3-8: Behavior of the specimen F1 as governed by yielding of the base-plate: a) Front view at $\Delta_{avg} = 0.2$; b) side view at $\Delta_{avg} = 0.2$; c) & d) yield-line model parameters on front and side view; e) top view of yield lines; f) top view base-plate at $\Delta_{avg} = 0.2$; g) base-shear vs. average drift measured in test F1.

Figure 3-9 shows the moment-rotation behavior of the base-plate and presents the properties of the numerical model described later in the article. In the figure, the moment M_{bpl} is $F/4h$ while the rotation $\theta_{bpl} = \Delta_{bpl}/h$ is derived from the force-drift record of Figure 3-8 by removing the drift due to flexural deformation of the columns Δ_{col} from the total recorded drift Δ_{tot} :

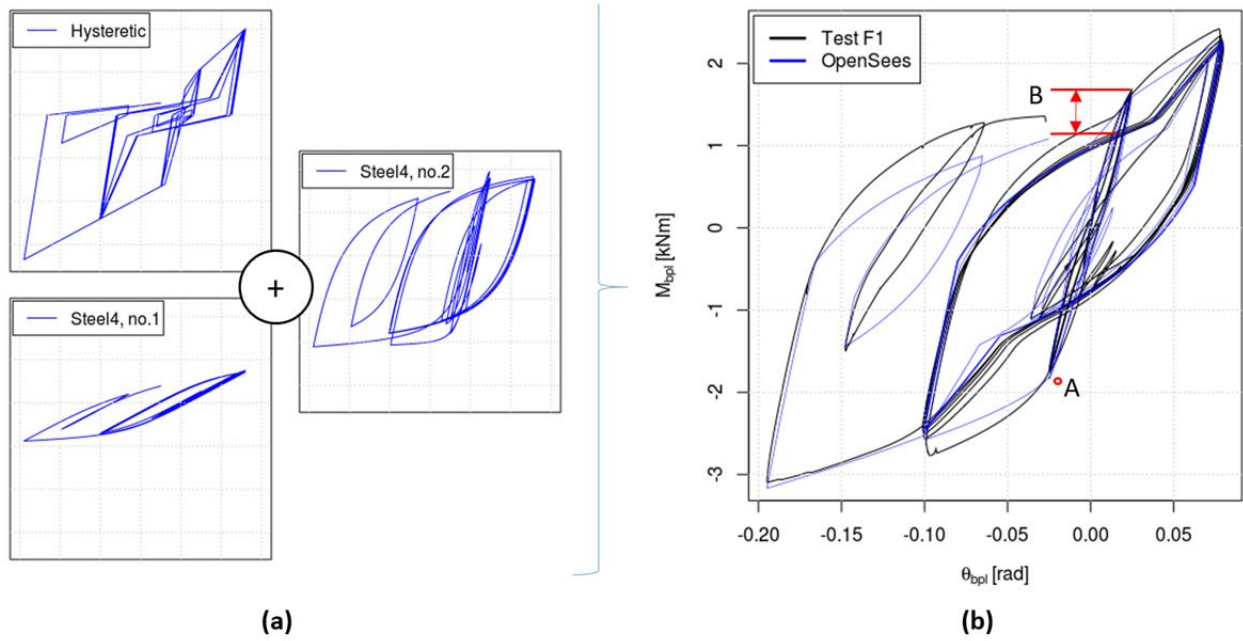
$$\Delta_{bpl} = \Delta_{tot} - \Delta_{col} = \Delta_{tot} - F \frac{h^3}{3E \cdot 4 \cdot I_{col}} \quad (3-2)$$

where I_{col} is the column moment of inertia in the plane of loading. The plot reveals stable plate response up to the maximum rotation imposed in the test (0.19 rad).

From the yielding pattern shown in Figure 3-8, an expression for the base plate yield moment, $M_{y,bpl}$, as a function of the compressive force in the column, C , can be derived from yield line theory [40]:

$$\mathcal{W}_E = \mathcal{W}_I \rightarrow M_{y,bpl} = \left[m_{p,bpl} \cdot \left(\frac{b}{d} + \frac{d+c}{a'} + \frac{\sqrt{a^2 + (d+c)^2}}{a'} \right) + \frac{C}{2} \right] \cdot d \quad (3-3)$$

where \mathcal{W}_I is the internal work of the base-plate and \mathcal{W}_E is the external work. With $t_p = 6.35$ mm and assuming $f_y = 345$ MPa, the plate plastic moment is $m_{p,bpl} = 3.48$ kNm/m. Using dimensions $a = 37.52$ mm, $b = 76.2$ mm, $c = 19.05$ mm, and $d = 82.55$ mm, and an axial load $C = 6.67$ kN, $M_{y,bpl} = 2.52$ kN-m. This is somewhat larger than the moment at initiation of yielding (point A in Figure 3-9) but less than the flexural capacity that develops upon strain hardening of the material, indicating that the moment from eq. (3-3) can be used to estimate the base plate flexural strength. The moment difference marked B in Figure 3-9 corresponds to the yield moment contributed by the yield line along the b dimension in Figure 3-8 ($= m_{p,bpl} \cdot b + C \cdot d/2 = 0.54$ kNm), a flexural capacity that can be mobilized in the first plastic excursion at a given rotation amplitude. This yield line model is used later in the article when evaluating the effect of axial load on the moment capacity of base plates for multi-level rack structures.



- Hysteretic material parameters: $s1p = 300$, $e1p = 0.005$, $s2p = 800$, $e2p = 0.02$, $s3p = 1100$, $e3p = 0.08$, $s1n = -300$, $e1n = -0.005$, $s2n = -500$, $e2n = -0.02$, $s3n = -1000$, $e3n = -0.08$
- Steel4, no.1 material parameters: $f_y = 400$, $E = 5000$, $b_k = 0.08$, $R0 = 15$, $r1 = 0.925$, $r2 = 0.15$, $f_u = 1000$, $R_u = 20$
- Steel4, no.2 material parameters: $f_y = 1000$, $E = 45000$, $b_k = 0.01$, $R0 = 15$, $r1 = 0.925$, $r2 = 0.15$, $f_u = 2200$, $R_u = 20$

Figure 3-9: Base-plate moment-rotation hysteresis: Experimental, analytical and FEM: a) Each material present in FEM model of the base-plate shown individually; b) Comparison between complete FEM model of base-plate and experimental data with select features A & B from yield line model discussion. OpenSees material parameters in SI units; see [41] and [42] for definitions of each parameter.

Figure 3-10a shows the hysteretic response of specimen F2 with fixed base plates and original (non-modified) beam-to-column connections under quasi-static cyclic loading. Yielding was concentrated near both beam-column connections and at base-plates until the last cycle when, at 14 % drift, flexural torsional-buckling of the columns was observed (Figure 3-10b).

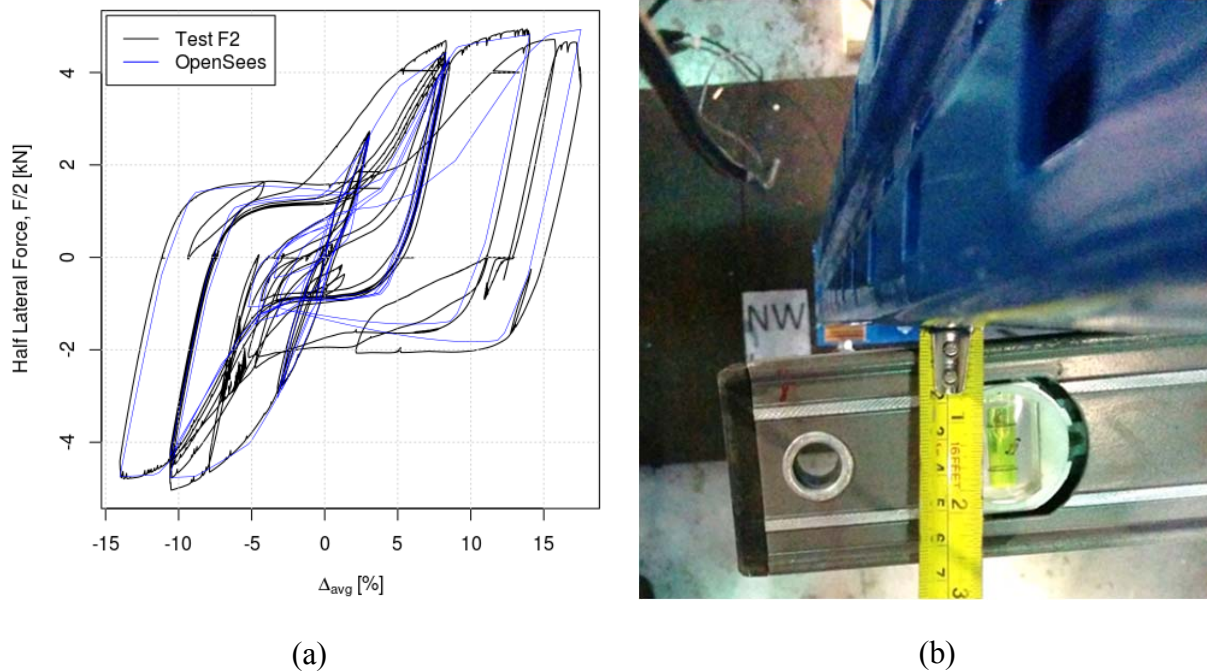


Figure 3-10: Test F2: a) Lateral force-displacement relation from test and numerical model (test results are average of two frames including P-delta); b) Level and measuring tape held across the braced frame emphasizes flexural-torsional buckling of the column at 14% drift.

3.3 Numerical Modelling

A 2D concentrated plasticity model of the rack shown in Figure 3-11 was constructed using the OpenSees software [37] (rev. 6248 32-bit running on Ubuntu 16.04). OpenSees (Open System for Earthquake Engineering) is an opensource finite element framework for the non-linear modeling of seismic response. It offers a plethora of non-linear materials making it ideally suited for modelling the unique behavior of the non-linear rack joints. These joints (beam-column connectors and base-plates) are represented by zero-length rotational springs and calibrated from Tests F1, F2, P1 and the RMI cruciform test. Beams and columns are elastic beam-column elements placed at centre-line dimensions. *Corotational* transformation is applied to the column elements to capture P-delta effects. In the preliminary model (calibrated before seismic tests) beam nodes and nodes representing pallet masses were constrained to move together in all directions. In the final model a horizontal zero-length friction element was inserted between the beam and the mass nodes to simulate pallet sliding. The friction element is discussed in depth in

section 5.4. The full project scripts of the model are available at https://github.com/emjac/rack_moment_frames.

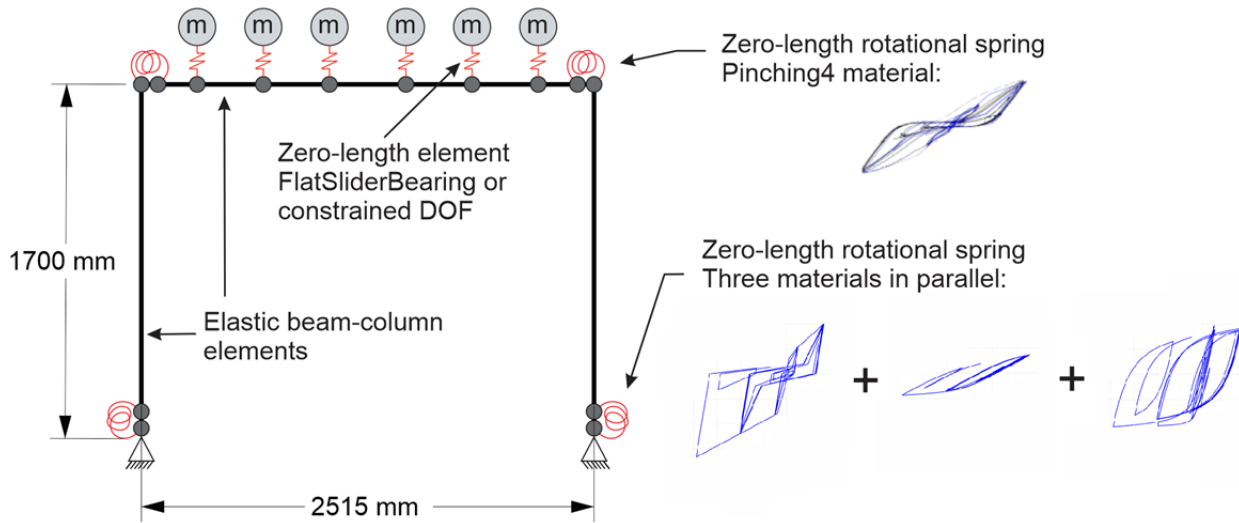


Figure 3-11: 2D OpenSees FEM model of the rack's moment frame.

The materials used for the zero-length rotational springs were calibrated by comparing three response parameters: cycle-by-cycle moment-rotation graphs (form and strength), average peak secant stiffness, k_{sec} (calculated at peak positive and negative moments during a cycle), and energy dissipated per cycle, EDC .

3.3.1 Base-plates

The pinched behavior with smooth transitions between stiffness exhibited by the base-plates was modelled by combining three materials in parallel in one zero-length spring. *Hysteretic* material (defined by three positive and negative strength and deformations points as well as pinching and damage parameters [43]) was used to capture pinching. In parallel to this, two *Steel4* materials (defined by ultimate and yield strength, stiffness, and parameters for kinematic hardening is based on the Menegotto-Pinto material [44]) provided smooth transitions and multiple slopes. Parameters for these materials are found in Figure 3-9.

Figure 3-9 shows that the model can predict well the evolution of strength and stiffness in Test F1. Although the base-plate did present slight strength degradation between the first pass and subsequent passes at the same plastic rotation, the model was judged most accurate without the use of Hysteretic material degradation parameters. In Figure 3-12, the model predicts well the base plate secant stiffness k_{sec} and energy dissipation per cycle (EDC) properties determined in

each cycle of Test F1. The lines shown in these and subsequent similar figures are used to highlight the general trends and ease the comparison between experimental and predicted values.

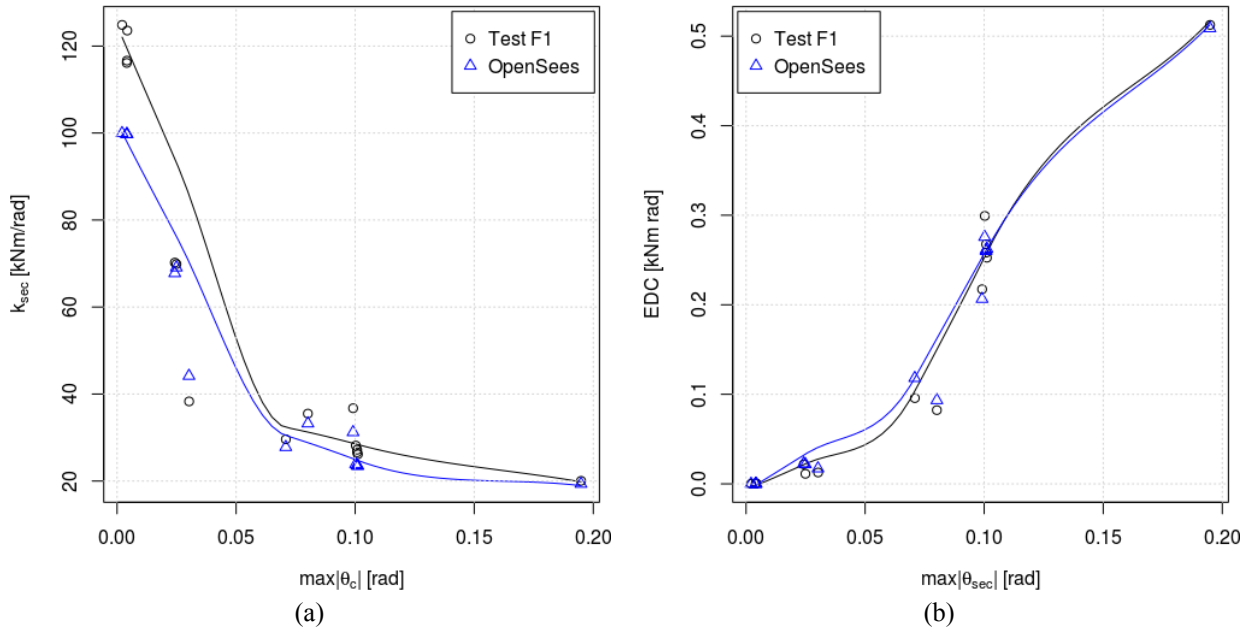
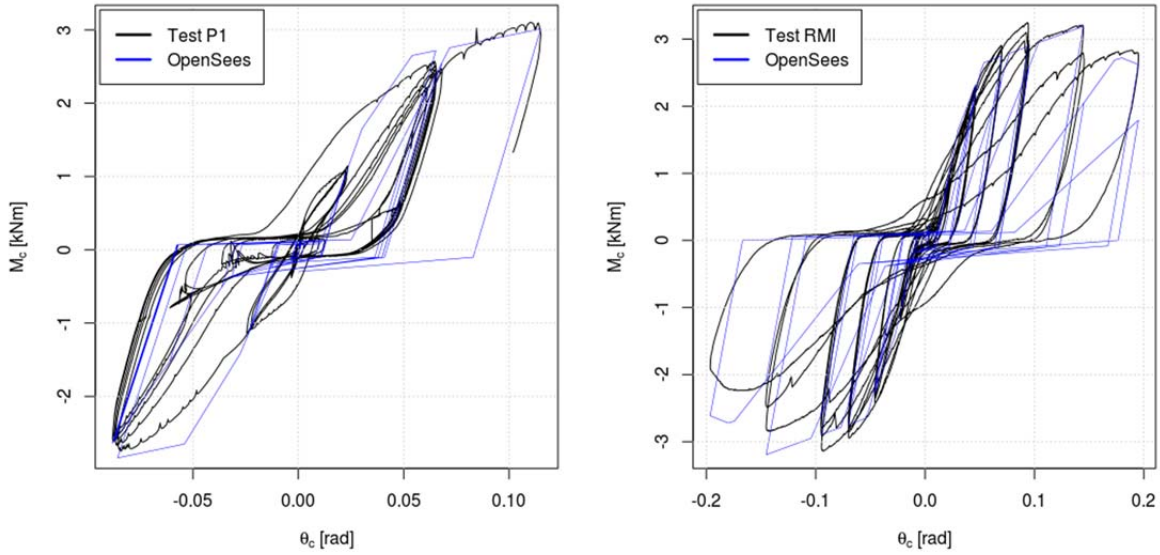


Figure 3-12: Validation of the base-plate model against Test F1 results for: a) Secant stiffness; and b) Energy dissipated per cycle (EDC).

3.3.2 Beam-column connectors

The *Pinching4* material from the OpenSees library was chosen to model the moment rotation behavior of the connectors because the material offers the possibility of introducing multiple slopes, pronounced pinching as well as strength and stiffness degradation. Given that the moment-rotation behavior of the RMI test showed somewhat higher strength than as recorded in Test P1, compromises were necessary to obtain parameters which reflected both data sets. Even with the four distinct slopes available in this material definition, simplifications are apparent when comparing the model to physical tests in Figure 3-13.



- Pinching 4 material parameters : ePd1, eNd1 = 0.023; ePf1, eNf1 = 1000; ePd2, eNd2 = 0.062; ePf2, eNf2 = 2500; ePd3, eNd3 = 0.14; ePf3, eNf3 = 3250; ePd4, eNd4 = 0.4; ePf4, eNf4 = 0; rDispP, rDispN = 0.25; rForceP, rForceN, uForceP, uForceN = 0.01; gK1, gK2, gK3, gK4 = 0; gKLim = -0.9; gD2, gD3, gD4 = 0; gD1, gDLim = 0.2; gF1, gF2, gF3, gF4 = 0; gFLim = 0.1

Figure 3-13: Response of the beam-to-column connector model, with tables showing the parameters for the Pinching4 material in SI units (see [45] for definitions of each parameter) compared to : a) Test P1; b) RMI test.

Figure 3-14 compares the secant stiffness and energy dissipation values from the numerical model to values from test P1 and the RMI connection test. As previously noted, the connectors in test P1 exhibited higher apparent stiffness than the RMI test at rotations below 0.02 rads, which affected the secant stiffness values in Figure 3-14a. Because this stiffness is likely due to friction in the pinned bases, correspondence between the for the secant stiffness from the model and test P1 is poor for small rotations, but the model fits well test P1 measurements at larger rotations and the entire RMI test data.

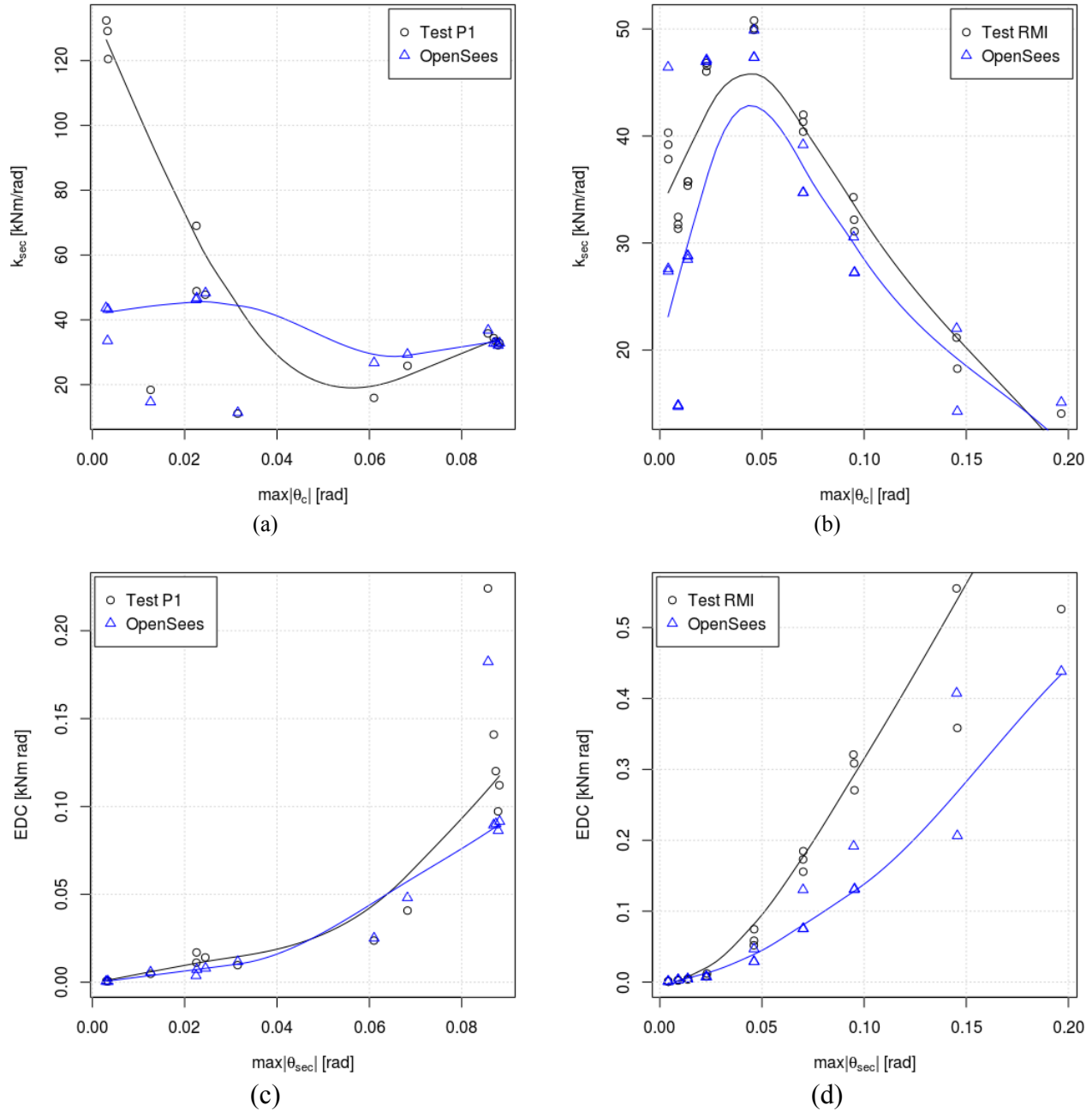


Figure 3-14: Validation of the beam-column connector modelling against P1 and RMI test results for: a) Secant stiffness; and b) Energy dissipated per cycle (EDC).

An elastic *MinMax* material (elastic stiffness of 10 kNm/rad to a limit rotation of ± 0.01 rad after which zero-stiffness) is used in the zero-length base spring to simulate the high initial stiffness (friction) of the pins. The force-drift hysteresis of the model in Figure 3-15 is compared to that of test P1 with correction to remove P-delta effects. With the addition of the *MinMax* material, the secant stiffness of the model (of the whole rack) follows more closely test P1.

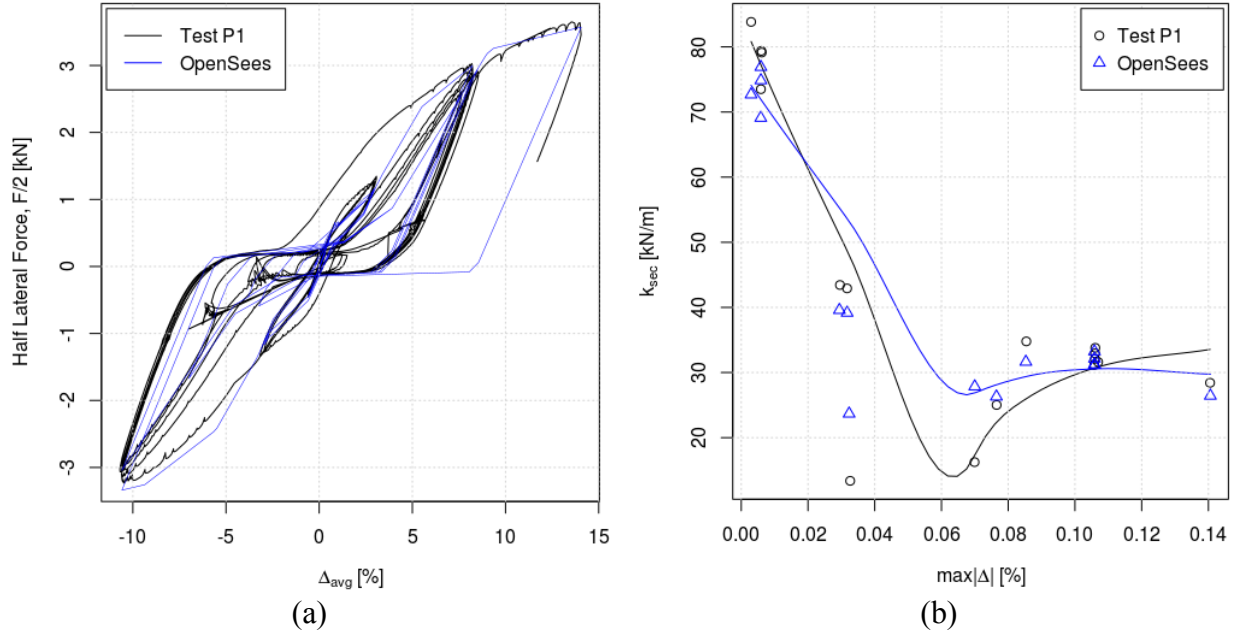


Figure 3-15: Comparison of test P1 and the numerical model with a small initial stiffness modification: a) Lateral force-load displacement response; and b) Secant stiffness.

3.3.3 Base-plate and connector in combination

A comparison with Test F2 was used to verify calibration of the base-plates and beam-column connectors acting together. It was found that using the materials as calibrated above resulted in a model that was slightly stronger than the rack in Test F2. Similarly to Test P1, some friction was likely present in the pinned beam-column connections used in Test F1, meaning that the flexural strength of the base connections was probably overestimated in the model developed from this test. To account for this, the base-plate material strength is scaled by 0.9. With this adjustment applied, in Figure 3-10, Figure 3-16 a & b, agreement between test F2 and the numerical model was satisfactory.

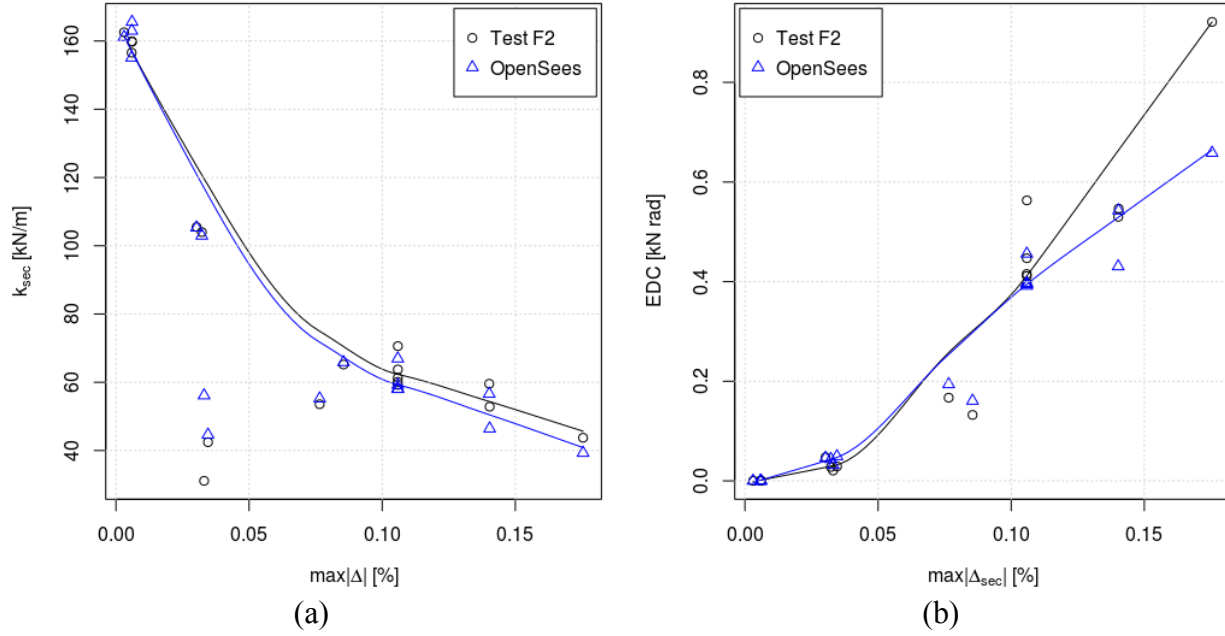


Figure 3-16: Secant stiffness and EDC comparison for test F2.

3.4 Results from Pull-back Tests

Natural periods and damping derived from the pull-back tests P2 and F3 were calculated between peak amplitudes (both maximum and minimum) over the first four cycles of free vibration after pull-back. Examples of free vibration responses and the envelopes used to calculate damping are shown in Figure 3-17. Viscous damping was calculated using the following equation [46] with $j=1$:

$$\zeta = \frac{1}{2\pi j} \ln(u_i) \quad (3-4)$$

Where u_i indicates the i^{th} decrement between two successive peaks of amplitude. Considerable

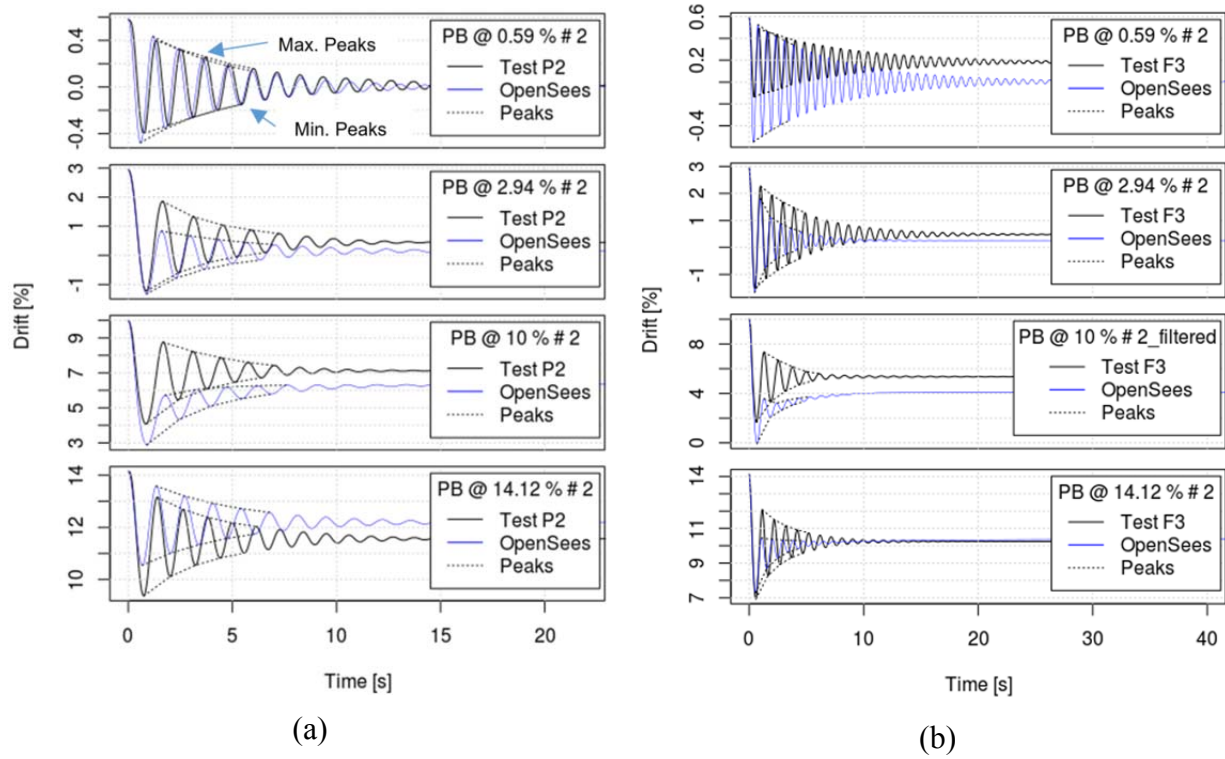


Figure 3-17: Comparison between measured and OpenSees free vibration responses for pull-back amplitudes at several drift increments (e.g. “PB @ 10% #2” indicates the second pull (and release) to 10% drift): a) Test P2 with 5% added viscous damping; and b) Test F3 with 2% added viscous damping.

variation was observed in values calculated from eq. (3-4) between successive peaks. Figure 3-18a shows an example of this variation calculated over the first 9 decrements for Test F3 being pulled to 3% drift for the third time; however, the variation did not follow any set discernible pattern. This is partly due to the role of friction in abating displacement, but also speaks to the imperfect nature of a viscous damping model in this context. Mean viscous damping calculated over the course of the first four decrements of a free vibration test, $\bar{\zeta}$, are plotted in Figure 3-18b. The values vary from values below 2% up to 15% in the pinned-based test (P2) and from 2% up to 8% in the fixed based test (F3). Not shown here: The quickest attenuation of movement occurred between pull-backs to

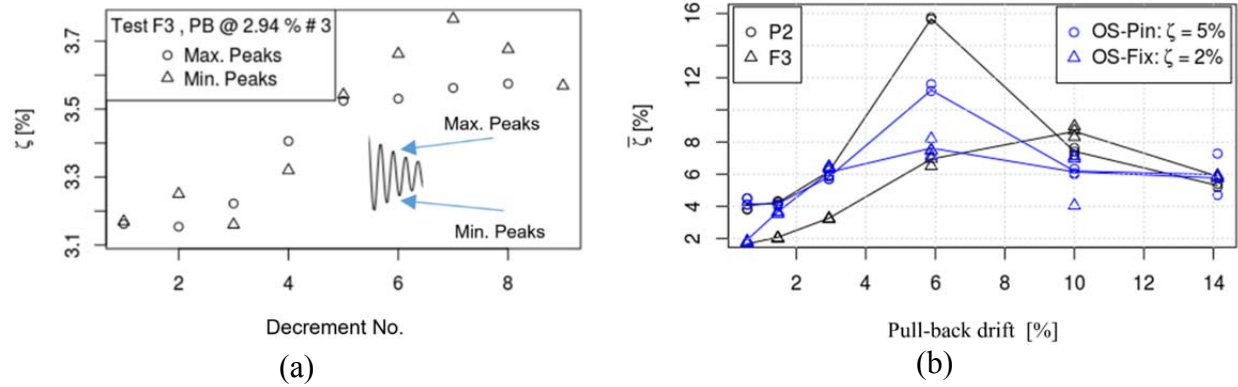


Figure 3-18: a) Variation of viscous damping calculated at every pair of consecutive peaks over the course of one free vibration test; b) Mean viscous damping calculated from the first four peaks of amplitude in Tests P2 and F3 compared to OpenSees models with 2 and 5% damping.

6% and 10% drift in both cases, very little variation was found in mean viscous damping for successive pull-release tests at the same amplitude. In Figure 3-18b, the OpenSees model gives the best overall imitation of decay of movement when 5% Rayleigh damping is applied to the mass in the pinned base configuration and 2 % for fixed base. Comparison of free vibration responses are given in Figure 3-17 when using these two damping values. Damping added to the model was of the same order of magnitude in [14].

Figure 3-19 gives a comparison of fundamental periods from Tests F3 and P2 versus periods from modelled pull-back tests. Periods are calculated, for both the test and the model, by taking the average time elapsed between four peaks of amplitude. In both Tests P2 and F3, the period increases by about 0.4 s when imposing larger initial drifts up to 6% and then gradually decreases for larger initial displacements. Lower fluctuation is reproduced by the model with periods lengthening by approximately 0.2 s up to 6% drift and remaining nearly constant for higher initial drifts. Both pinned and fixed-based models behave more rigidly than the specimens, except the first and last several cycles for the pin-based model.

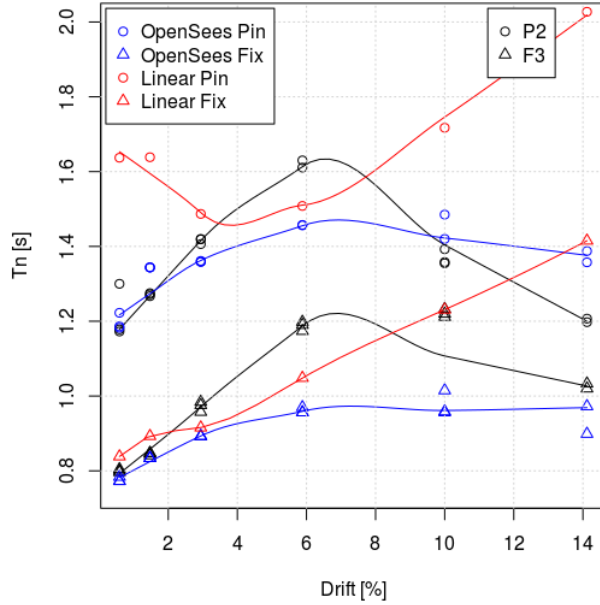


Figure 3-19: Comparison between measured and predicted average natural periods in free vibration Tests P2 and F3.

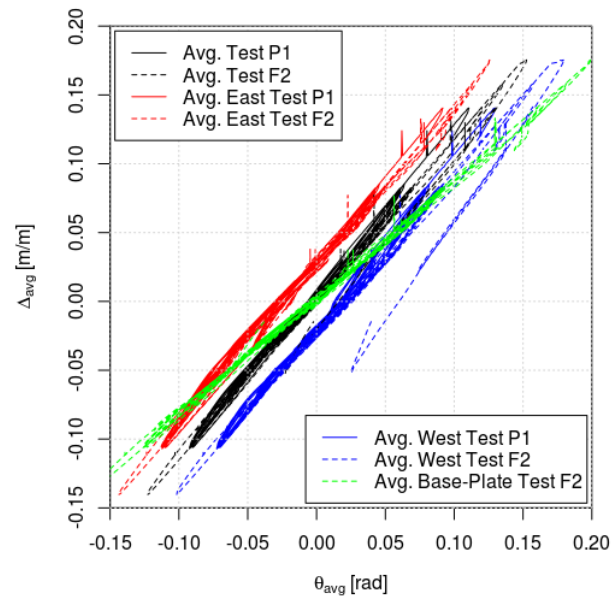


Figure 3-20: Drift vs. average rotation during Tests P1 and F2.

Figure 3-19 also presents a comparison of the natural period of a linear model as computed by eigen-value analysis with the connectors and base-plates at their respective secant stiffness. For this comparison, it is assumed that drifts \approx rotations. On average, this is a relatively good assumption at smaller rotations as shown in

Figure 3-20 from Tests P1 and F2. The secant stiffness of the connector was interpolated from the RMI unit-test of the connector (Figure 3-6). The secant stiffness of the base-plate could not be interpolated from Figure 3-9 because stiffness values presented in this figure are an averaged between unsymmetrical cycles of amplitude. As such, pseudo test data was derived by cycling the element calibrated from Test F1 to the same amplitudes as specified for RMI cruciform tests [6], calculating secant stiffness at peak moments in each cycle and interpolating for intermediate rotations. Results from this pseudo-test are given in Figure 3-21. In Figure 3-19, for the fixed-base model, estimating period with an equivalent linear model is sufficiently accurate up to 10% drift. For the pinned-base model, the estimation is adequate for intermediate drifts but is poorer at smaller and larger rotations.

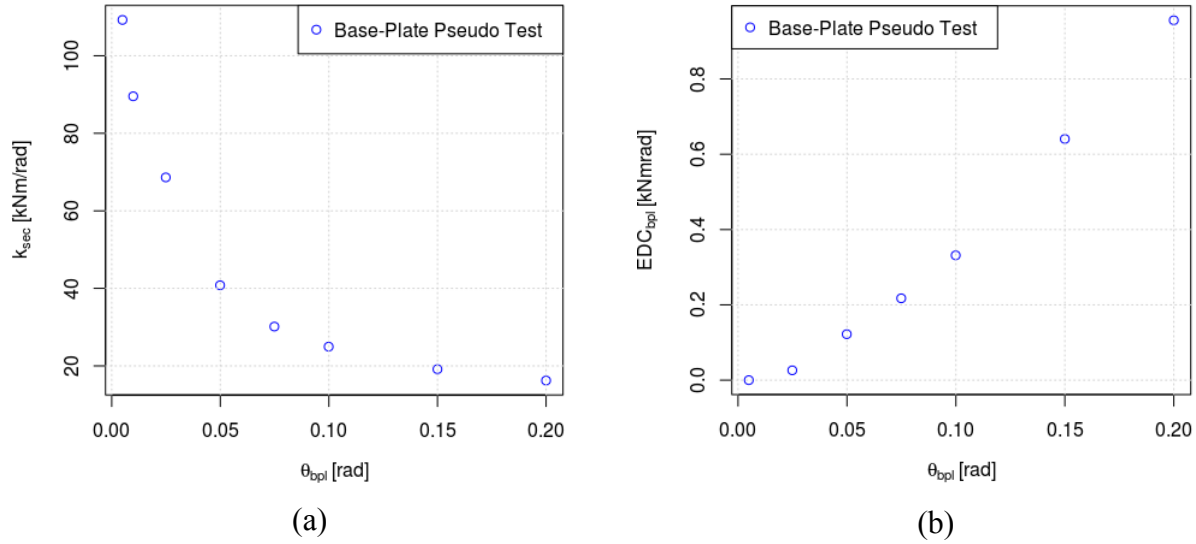


Figure 3-21: Secant stiffness and EDC values from OpenSees model of Test F1 subjected to displacements from RMI cruciform test protocol.

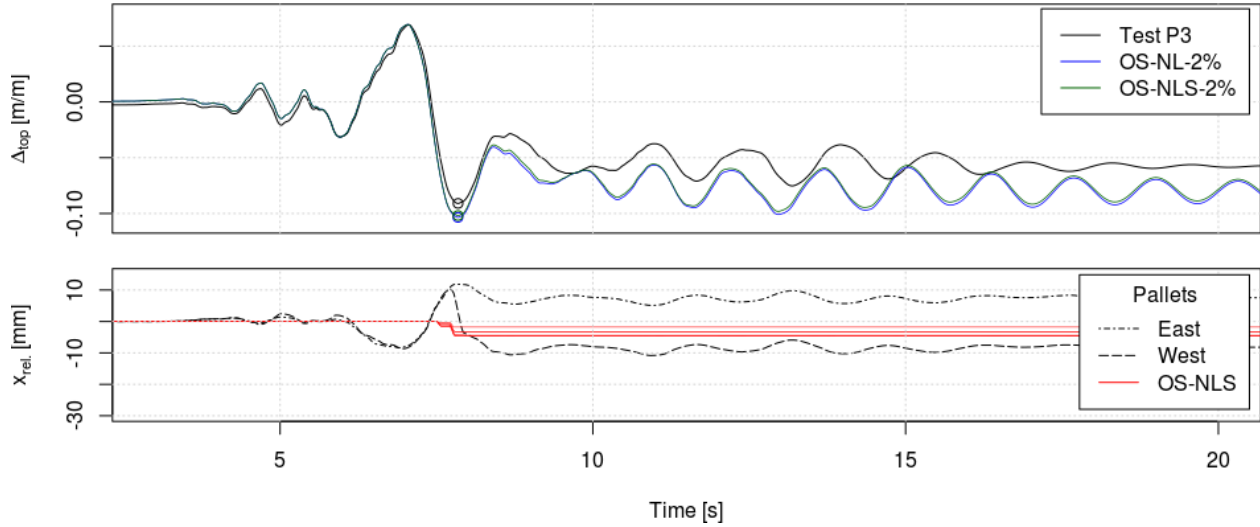
3.5 Results from Seismic Tests

3.5.1 Pinned-base specimens

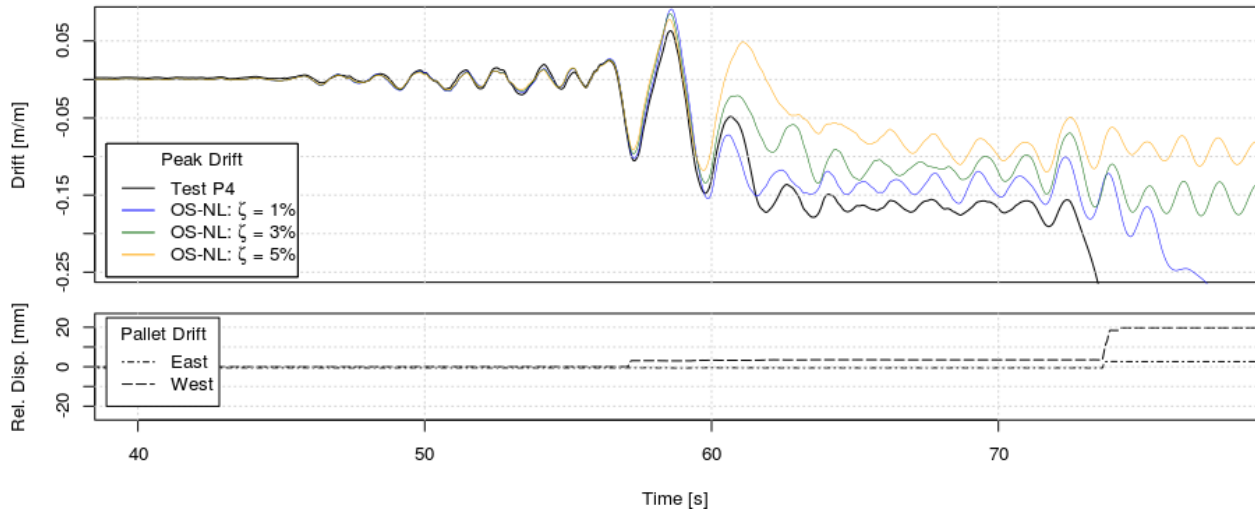
Although specimens were erected straight before loading the pallets onto the beams, small lateral drifts were recorded after the pallets were placed. On the more flexible pin-based specimens, initial drifts were $\pm 0.2\%$. Target drift, as determined by incremental dynamic analysis of the preliminary FEM model with 5% damping (OS-NL-5%), was 8% for Test P3, the first pinned-base seismic test. Measured and predicted time history responses are given in Figure 3-22a. The specimen remained stable during this test but sustained 9.1% peak drift and approximately 5% residual drift. Peak drift was slightly under-predicted by OS-NL-5%. As a result, the target drift was increased for Test P4, to 10%. Drifts were again slightly under-predicted by the model until $t = 60$ s, see Figure 3-22b. At this point the specimen failed to return to zero after an excursion to 10 % drift, shook briefly near 15 % drift and then collapsed. Target drift was subsequently returned to 8% for Test P5. No collapse was observed for that last pinned base specimen (Figure 3-22b).

Significant yielding was observed in all three specimens, confined to the beam-column connections and connection area on columns. Only drift histories for the total rack are presented

in Figure 3-22 because rotation histories of the individual connectors are almost identical both to each other and in form to the overall drift. Residual drift was present in the first and third tests. As shown in Figure 3-22, episodes of pallet sliding occurred in all specimens. In Test P3, the pallet sliding gauge was on the columns above the beam; the data has been corrected to remove the angle introduced by the movement of the column but some parasite oscillations remained; it is clear that sliding has occurred when the two pallet histories diverge.

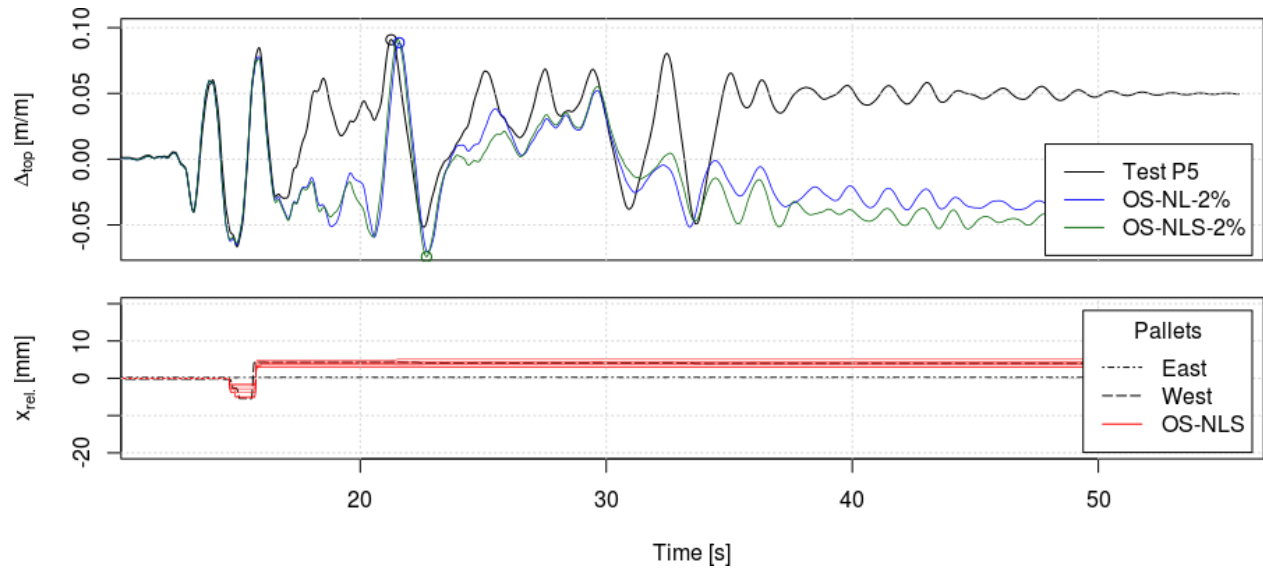


(a)



(b)

Figure 3-22: Displacement and pallet sliding time history during Tests: a) P3; b) P4; and c) P5.



(c)

Figure 3-22 : Suite

3.5.2 Fixed-based specimens

Initial drifts caused by pallet placement on the fixed-based specimens were negligible because of the higher frame lateral stiffness. The measured frame responses in Tests F4 - F6 are shown in **Error! Reference source not found.** Target drift for these tests was set between 6% and 7% but did not exceed 4.5% in the experiments, likely because of the impact of pallet sliding on peak drifts. Although yielding did occur in the beam-column connections and in the base-plates, little damage was apparent to the eye; residual drifts were small and the response remained centered near zero drift.

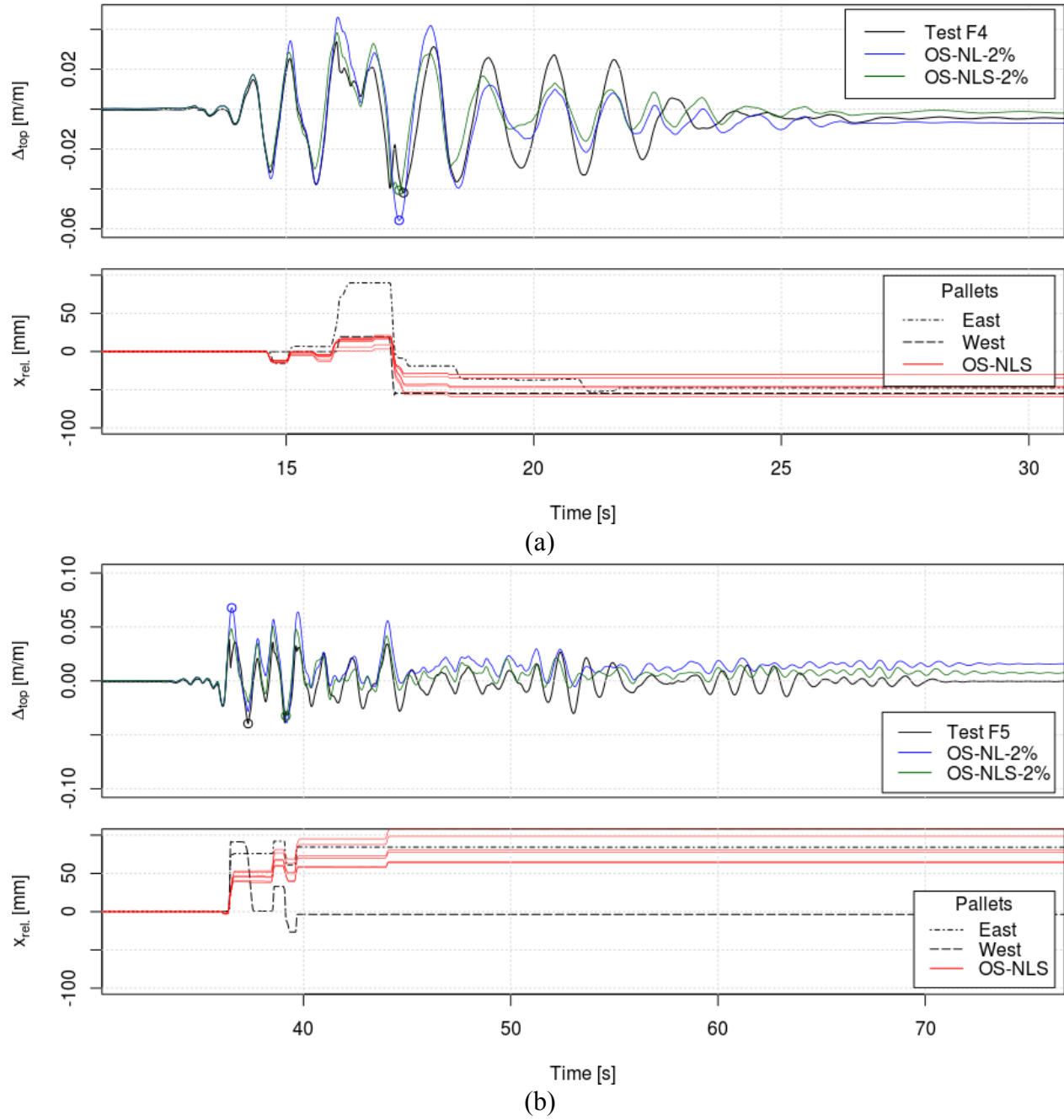


Figure 3-23: Displacement and pallet sliding time histories during Tests: a) F4; and b) F5.

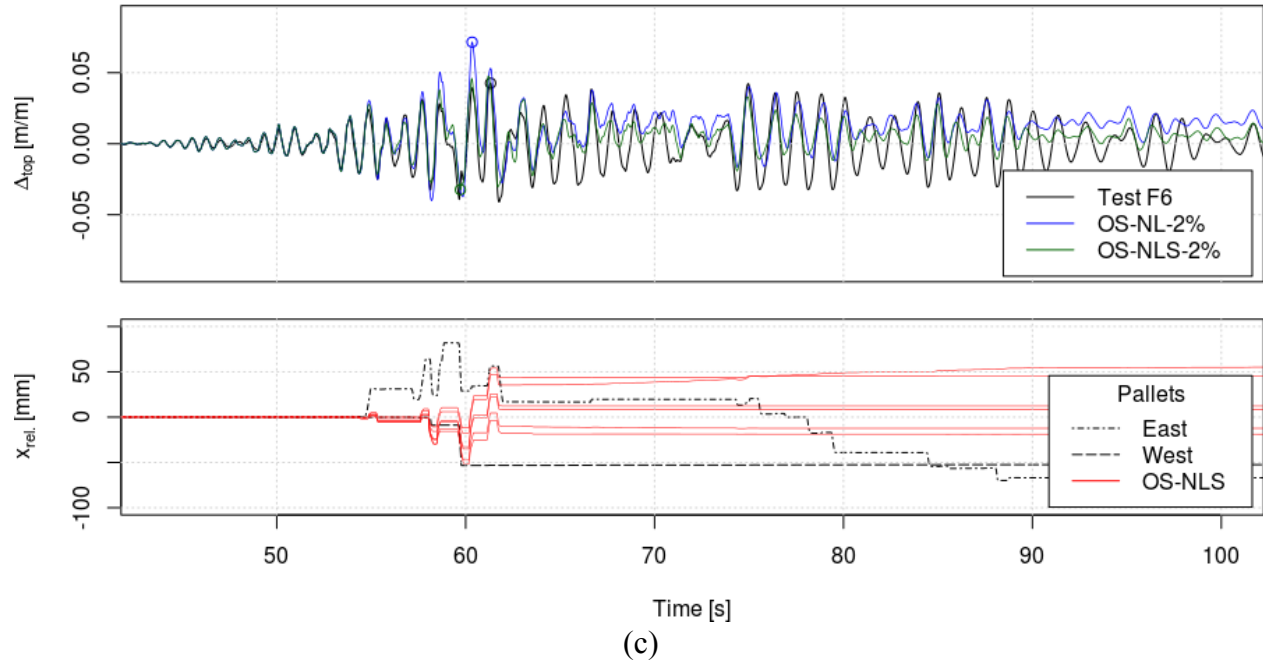


Figure 3-23 : Suite

3.5.3 Sliding of pallets

Limited pallet sliding was observed in the pinned-base tests, except in Test P4 where the collapse response caused significant sliding at the end of the test. Sliding was much more pronounced for the fixed-base tests. The same sliding was never observed for the two pallets; at times one pallet stayed stuck while the other slid and at other times the two slid but to different distances. Measured beam accelerations and relative sliding values are reported in Table 2. The relative slip values in the table are the largest of the two pallets. As shown, sliding was triggered when the beam's acceleration exceeded 0.2 to 0.3 g, which coincides with values obtained in [14].

Table 3-2: Sliding accelerations and distances in seismic tests.

Test	At first episode of sliding		At peak drift	
	\ddot{x}_{beam} g	$x_{rel.}$ mm	\ddot{x}_{beam} g	$x_{rel.}$ mm
P3	-	15	-	15
P4	0.25	3	0.28	0
P5	0.19	5	0.2	0
F4	0.25	10	0.25	80
F5	0.3	80	0.25	80
F6	0.2	30	0.22	20

3.5.4 Numerical modelling of pallet sliding

To model pallet sliding, *FlatSliderBearing* elements [47] were inserted between beam nodes and mass nodes, Figure 3-11b. The sliding surface has a *VelDependent* [48] friction rule with $\mu_s = 0.17$ and a kinetic coefficient of $\mu_k = 0.8$. The static friction coefficient was chosen such that sliding occurred in all tests and was within the order of magnitude of observed sliding. The kinetic coefficient was used to stop sliding and aide in convergence. According to [14], the selected μ_s is at the low end of possible values. Stiffness until sliding initiated was set very large (10^5 kN/m).

Two models are compared with the seismic tests: a model using the non-linear materials (OS-NL- $\zeta\%$) calibrated from Tests P1, F1, and F2 and a model using the same non-linear materials with the addition of a friction element to permit pallet sliding (OS-NLS- $\zeta\%$). The choice of the damping value is discussed in the next section. In Figure 3-22 and **Error! Reference source not found.**, all observed sliding occurrences are predicted with the OS-NLS model. Contrary to the tests, both pallets experience nearly the same slip distance and direction in the numerical models. Notable differences between measured and predicted sliding displacements can be seen although good agreement could be reached in several instances. Such a discrepancies are to be expected in view of the different slip experienced by the two pallets during a same test. Given ostensibly identical pallets, the same model and sliding sensitivity parameters are assumed, but it cannot fit both differently sliding pallets at the same time. At each episode of sliding with model OS-NLS, there is a corresponding reduction in displacement amplitude as compared with model OS-NL.

* Data not available

3.5.5 Effect of damping modelling on response prediction

The level of added viscous damping found during free vibration tests to give the best decay of motion did not necessarily give the most accurate results compared with the seismic tests. For specimen P4 sliding had a negligible effect on displacement since the episode of sliding was very small. The remaining variable effecting response being damping, it can be seen in Figure 3-22b that small variations in added viscous damping can have dramatic effect on the response of the rack - from stability to collapse. Among all tests, peak frame drifts from the model with sliding and 2% viscous damping (OS-NLS-2%) were closest to measured values. The comparison is summarized in Table 3. Unless otherwise specified, all further models are run with 2% viscous damping added.

Table 3-3: Summary of peak drifts from physical tests compared with drift from two models. Test to model prediction ratio in brackets.

	P3	P4	P5	F4	F5	F6
Test	0.091	∞	0.091	0.042	0.04	0.043
OS-NL-2%	0.104	∞	0.089	0.056	0.068	0.072
Ratio	(1.14)		(0.98)	(1.33)	(1.70)	(1.67)
OS-NLS-2%	0.102	∞	0.074	0.041	0.032	0.034
Ratio	(1.12)		(0.82)	(0.97)	(0.81)	(0.78)

3.5.6 Numerical prediction of hysteretic response

Figure 3-24 shows comparisons of the hysteretic response as tested and as modelled during in the time period near peak displacement of the tested specimen. The base-shear, V , shown in Figure 3-24 has been calculated from the average of the two accelerometers placed on the rack at beam-level (see Figure 3-2b) times the mass of the pallets (rack mass is negligible). The signal from the accelerometers has been passed by a butterfield filter to remove frequencies below 15 Hz. Further filtering to smooth results causes unacceptable distortion. In addition to the main horizontal acceleration, the signal contains small components of acceleration in all three directions including vibration of the beam which adds to error in predicting base-shear. Nevertheless, the model and the specimen maintain similar stiffness during different phases of response. This is mostly easily observed on tests P3-P6 where the longer period of the rack causes slower movement and a more

discernible phases of response. Often the slope in stiffness is shifted when a significant error in drift prediction is present e.g. near the end of test P3. The areas covered by the signals are also comparable, indicating that the energy dissipation of the rack is being matched by the model. Models of the fixed-base specimens had somewhat fatter hysteresees which is consistent with the underprediction of drift seen in those cases. The non-linear model without sliding has been plotted for tests P3 and F6 to emphasis the improvement of response prediction when sliding is included. Thus for test P3, where very little sliding was observed little difference is seen between the two models. In opposition, for Test F6 the graph window must be enlarged to include the erroneous part of model NL which wanders away from the observed data and becomes much fatter, while model NLS remains close to the observed response.

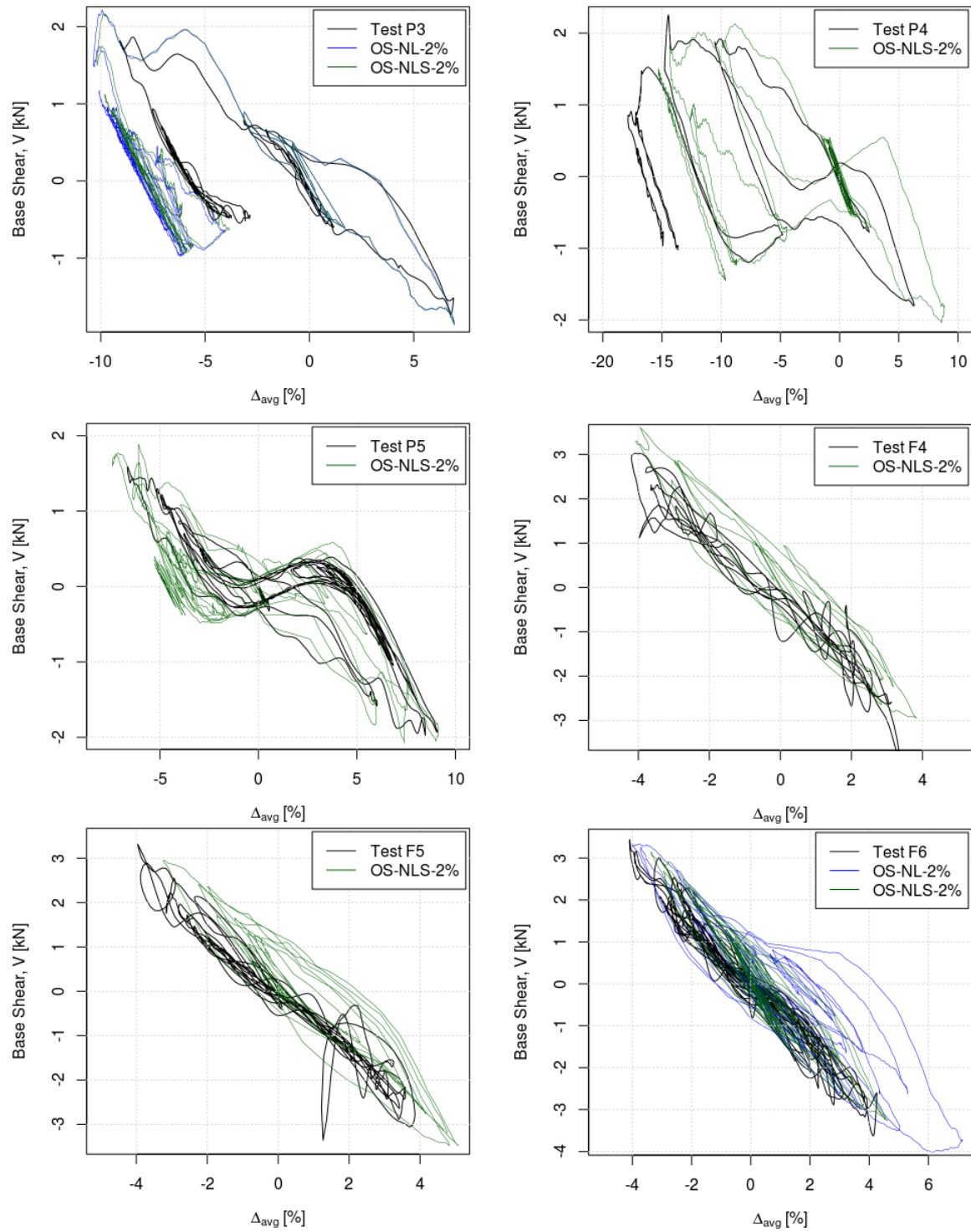


Figure 3-24 : Hysteretic seismic response of specimens versus models with and without sliding.

3.5.7 Evaluating equivalent damping by two methods

In the displacement based analysis method, peak seismic displacement is estimated using an equivalent linear model of the structure that has an effective (secant) lateral stiffness and equivalent viscous damping properties evaluated at peak displacement. Damping of rack structures originates essentially from energy dissipated in the connections and base-plates. This damping, $\beta_{hyst.}$, can be augmented by damping $\beta_{el.}$ reflecting other sources of energy dissipation such as friction in connections and sliding of the pallets to obtain the structure equivalent damping $\beta_{eff} = \beta_{hyst.} + \beta_{el.}$. The results from the test program are used herein to comment the validity of this approach for rack structures.

A 2D equivalent linear model of the test specimens is constructed by choosing the secant stiffness of the connectors and base-plates at the moment of peak displacement. This is estimated by assuming that rotations \approx drifts, as typically done when applying the method [11], and interpolating their secant stiffness from the rotation-stiffness curves in Figure 3-14b & Figure 3-21a. The computed secant stiffness values are then used to determine the lateral stiffness of the rack specimens, k_{rack} .

The hysteretic damping is also estimated at peak displacement by interpolating EDC_c and EDC_{bpl} from Figure 3-14d & Figure 3-21b drift using the same rotations \approx drifts assumption (using real rotations made little difference to the resulting value of $\beta_{hyst.}$). The hysteretic damping is then evaluated from, adapted from [16]:

$$\beta_{hyst.} = \frac{N_{bpl}EDC_{bpl} + N_cEDC_c}{2\pi \cdot k_{rack,red.} \cdot \delta^2} \quad (3-5)$$

where the energy dissipated is multiplied by the number of base-plates N_{bpl} and connectors N_c present, and $k_{rack,red.}$ represents the lateral stiffness of the rack reduced to account for P-delta effects [97]:

$$k_{rack,red.} = k_{rack} - 0.5 \cdot W/h \quad (3-6)$$

For a one-level rack, δ is the peak displacement of the rack at beam level. For Test P4, it is not possible to determine stiffness and energy dissipation properties because the specimen's drift is infinite at collapse and this test is excluded from this comparison.

Table 3-4 shows the period T_n of the model with equivalent secant stiffness properties and the peak displacements measured in the tests. The equivalent damping $\beta_{eff.}$ is calculated by the method of varying damping, i.e. by iteratively modifying viscous damping in the model until the computed peak displacement is same as in the test. The value of $\beta_{hyst.}$ is obtained from eq. (3-5) and $\beta_{el.}$ is the difference between $\beta_{eff.}$ and $\beta_{hyst.}$. The required value of $\beta_{eff.}$ varies considerably from test to test, even between tests with similar base conditions and peak displacement amplitudes (P3 vs P5, and F4 vs F6). Figure 3-25 shows that there is little difference in displacement amplitudes calculated with 25% and 35% viscous damping. In test P4, 25% damping is sufficient to reduce the linear model to the real amplitude, however for Test P5 it is necessary to increase damping to 35% to reduce completely to the measured amplitude. It is unlikely that the quantity of energy dissipated could vary to this level for the same type of rack with very similar peak displacements. The level of hysteretic damping varies little from test to test because the peak response during fixed-base and pinned-based tests is same or similar. Conversely, it is difficult to make sense of the $\beta_{el.}$ values resulting from the tests: for the pinned-base frames, negative damping $\beta_{el.}$ is needed because the hysteretic damping exceeds the values of $\beta_{eff.}$; for the fixed based tests, variations in $\beta_{el.}$ values are not consistent with the observed response. These observations point further to the inadequacy of representing rack response with effective lateral stiffness and equivalent viscous damping properties.

Table 3-4: Equivalent damping properties

Test	T_n	δ_{top}	$\beta_{eff.}$	$\beta_{hyst.}$	$\beta_{el.}$
-	s	m	-	-	-
P3	1.64	0.155	0.11	0.33	-
P5	1.64	0.155	0.05	0.33	-
F4	0.96	0.071	0.35	0.19	0.16
F5	0.95	0.068	0.25	0.19	0.06
F6	0.96	0.073	0.23	0.19	0.04

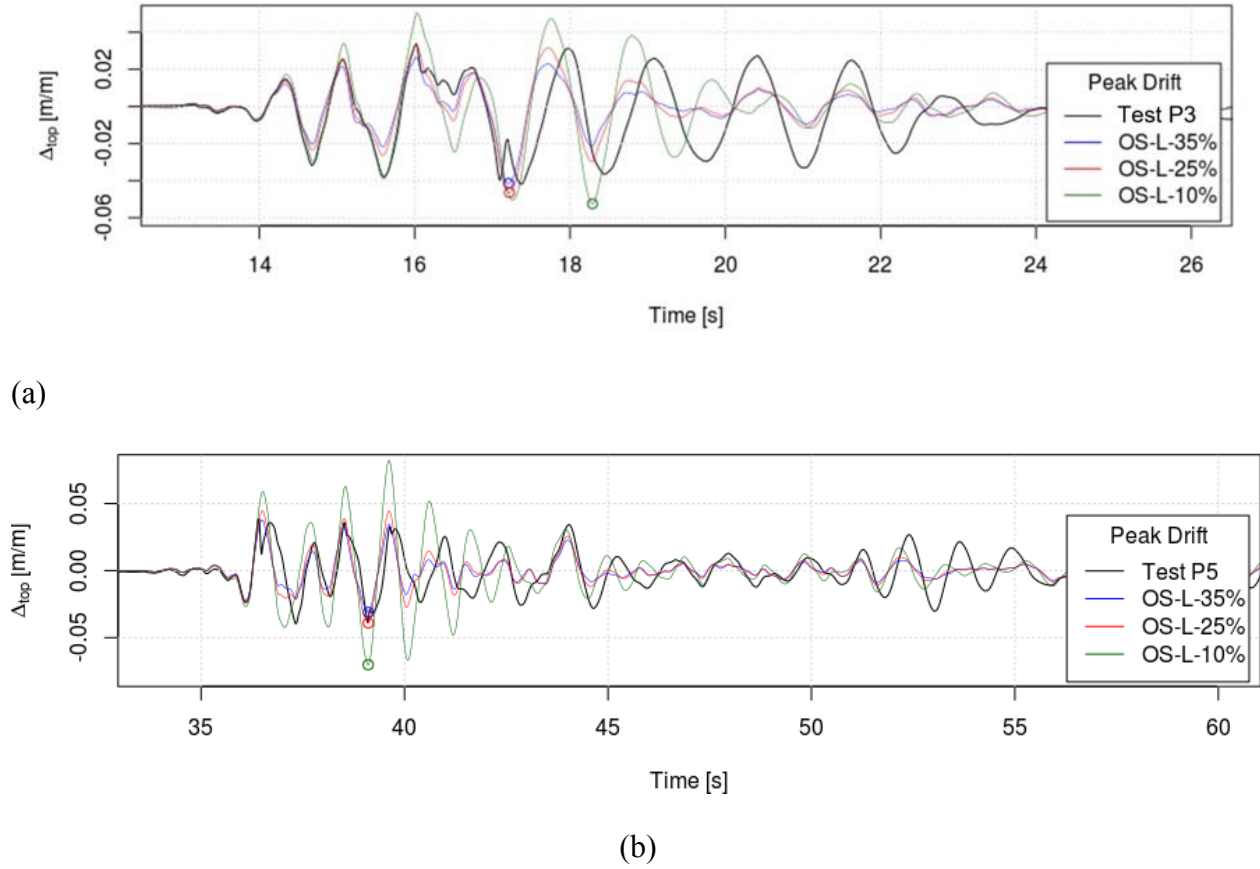


Figure 3-25: Influence of equivalent damping on displacement of the equivalent linear model for Tests: a) P3; and b) P5.

3.6 Numerical Seismic Response of Multi-level, Multi-bay Racks

3.6.1 Structures studied

In this section, the OpenSees numerical model is expanded to examine the seismic response of 6-bay rack structures having 3 to 6 levels to demonstrate how the proposed model may be used to further investigate more realistic rack configurations. The structures are subjected to the unscaled Q1 signal (Eastern Canada). For simplicity the column heights, beams lengths, connectors and pallet loads described in Figure 3-1 are retained. The frames are fix-connected at their bases and viscous damping is set at 2%.

In order to account for the increase in compression, C , on the base-plates, the previously developed yield line model (Figure 3-8) is used to adjust the flexural strength of the plate finite

element material. Table 3-5 shows the yield moment $M_{y,bpl}$ as determined by yield-line theory with the corresponding adjustment factors (AF) applied to the strength of the model base-plate material for different heights of rack and two different thicknesses of base-plate t_p .

Table 3-5: Strength adjustment factors for different base-plate thickness and compression level

Levels	t_p	C	$M_{y,bpl}$	AF
-	mm	kN	kN-m	-
3	6.35	40.0	3.89	1.55
3	12.7	40.0	10.61	4.23
4	6.35	53.4	4.45	1.77
4	12.7	53.4	11.17	4.45
5	6.35	66.7	4.99	1.98
5	12.7	66.7	11.72	4.67
6	6.35	80.1	5.55	2.21
6	12.7	80.1	12.27	4.89

Absent a similar model for the increase in stiffness, no direct attempt is made to account for this effect. An example of the effect of this scaling is shown with comparison to the Test F1 in Figure 3-26. Variation of strength/stiffness with axial load is small compared with the variation with thickness. For simplicity, these base-plate properties are assigned to all columns, neglecting the difference in gravity and seismic induced axial loads between interior and exterior columns. It is noted that the model cannot account for the variation of base reaction due to seismic demands and this possible limitation is examined next.

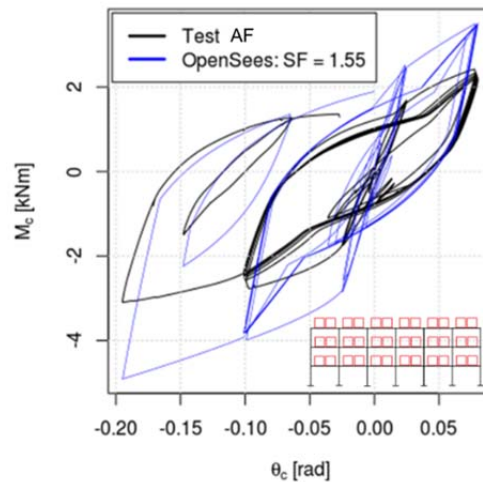


Figure 3-26: Effect of strength AF on base-plate hysteresis model, compression load for 3-level rack.

3.6.2 Seismic effects on column axial loads

Axial loads in the interior and exterior columns of the 3, 4, 5 and 6-level racks with the scaled 6.35 mm base-plates are evaluated under signal Q1. Figure 3-27 shows that, irrespective of the height of the rack, compression on the exterior base-plates varies within $\pm 15\%$ from its original value at 8.3% of the total seismic weight, W . For interior columns the variation in compression is below $\pm 10\%$. Since the variation of load is small, the error introduced by using a model with constant strength is also small. Likewise, by examining the increase in adjustment factor AF in Figure 3-26, doubling compression increases the stiffness of the base-plate by 30%, hence the error committed by using the same base-plate everywhere is slight.

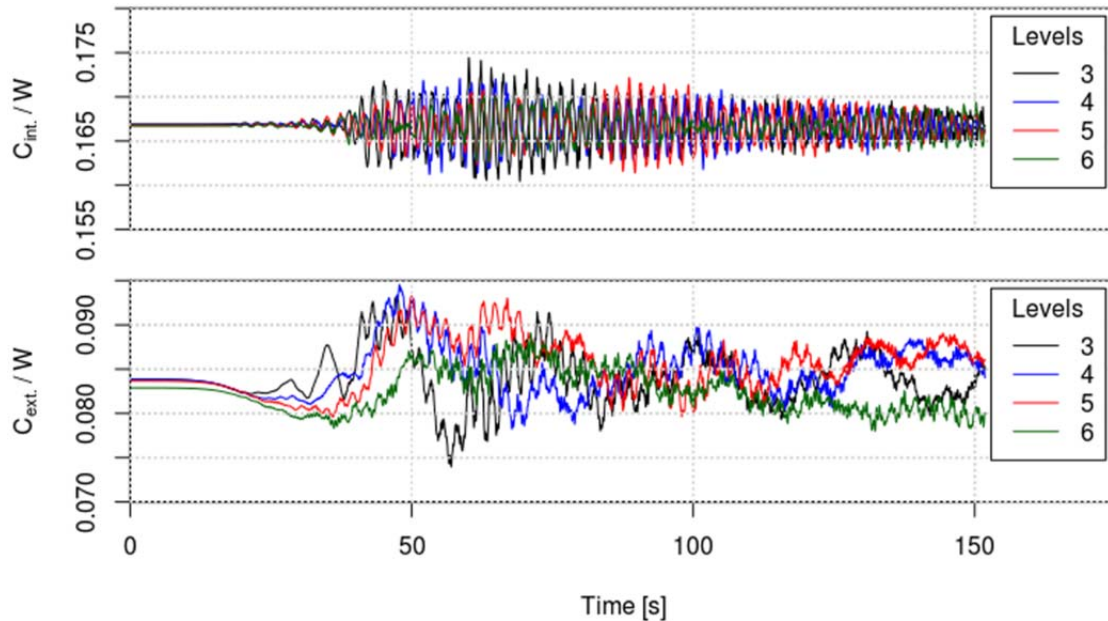


Figure 3-27: Variation of the base vertical reaction on interior and exterior columns.

3.6.3 Displacement profiles

The multi-level racks are subjected to signal Q1 at two different levels of intensity: scaling factor (SF) = 1.0 and 1.5. The displacement profile of each rack at the instant of peak drift of the top level, Δ_{top} , is shown in Figure 3-28b & c. For SF = 1.0, it is apparent from the profiles that all racks have displaced largely in their first mode although the drifts tend to concentrate in the first 3-levels for the 6-level frame. Drift concentration becomes more pronounced when the intensity of the accelerogram is increased by 1.5, causing collapse of the 6-level rack.

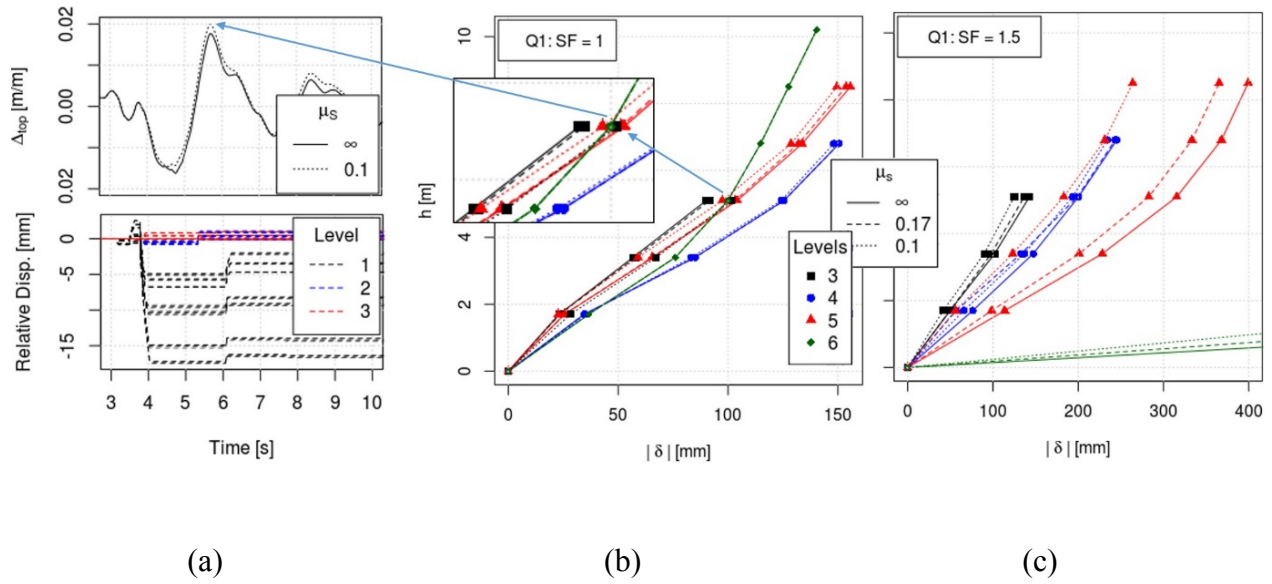


Figure 3-28: Drift profiles for multi-level racks subjected to Q1 ground motion at scale factors of 1.0 & 1.5 and $\zeta = 2\%$.

3.6.4 Pallet sliding

Figure 3-28b also shows drift profiles for racks with sliding permitted assuming static friction coefficients of $\mu_s = 0.17$ & $\mu_s = 0.1$. When the Q1 signal is unscaled and $\mu_s = 0.17$, sliding is in the order of 1- 2 mm and occurs only on the first level. Repercussion on the drift profile is almost imperceptible. Lowering the static coefficient to $\mu_s = 0.1$, which corresponds to the lowest coefficient observed in [14], made little difference, larger slip distances were observed but peak lateral displacements were unchanged except in the 3-level rack where sliding had an unfavourable effect on drifts. Figure 3-28a shows that drift increase was not due to increase P-delta effects (i.e. increased eccentricity of the pallet loads) since the masses moved to a favourable position with respect to the peak displacement, but because the rack underwent two large and opposed displacements during the quake: the first large displacement was reduced by pallet sliding, by consequent the second large displacement, which did not coincide with a sliding event, was enlarged. Sliding in this case was of larger magnitude (10 -15 mm) and occurred on all levels, though to a greater extent on the 1st level.

When the Q1 scale factor is increased to 1.5 sliding causes drift reductions in the all racks most significantly in the 5-level rack. The largest episodes of sliding occur on the lower levels and are in the order of 10 to 30 mm. The collapse of the 6-level rack is not prevented by sliding.

3.6.5 Drift-rotation relationship

Figure 3-29 presents the instantaneous connector rotations when Δ_{top} is at its peak under the unscaled Q1 ground motion (SF = 1.0). In the graph connector rotations in the frames are plotted for all multi-level frames as a function of the peak roof drift angle experienced by the corresponding frame. Connectors are not all subject to equal rotations. This is in part due to variations in displacements along the frame height, as previously discussed. This is also caused by gravity loads on beams. For the group of connectors undergoing rotations above 0.02 rad., seismic rotations are an unfavourable addition to gravity rotations. For this upper group, rotations vary between 0.02 rad and 0.038 rad. For the group of connectors below ≈ 0.01 rad seismic loads are favourable. Connectors in the upper group are paired with connectors in the lower group which are on the other side of a same bay. The upper and lower groups of rotations are the most tightly grouped for the 3-level rack, this is also the rack experiencing the most uniform inter-level drifts.

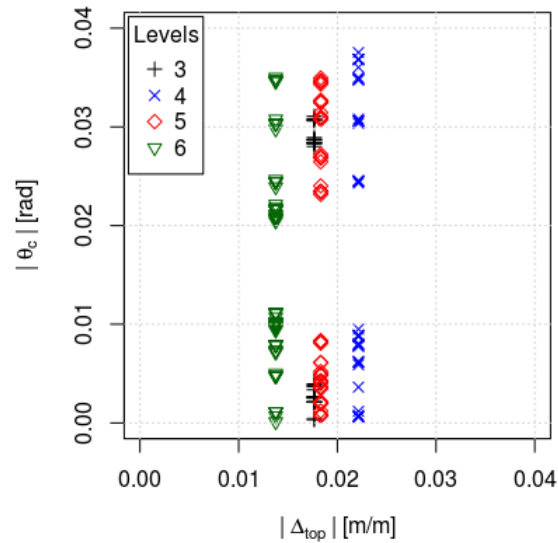


Figure 3-29: Peak rotations and drifts of multi-level racks without sliding subject to Q1 ground motion at SF = 1.0.

Table 3-6: Average peak connector rotations and top drifts of multi-level racks without sliding subject to Q1 ground motion at SF = 1.0

No. of Levels	Avg. Left $ \theta_c $ rad	Avg. Right $ \theta_c $ rad	Avg. $ \theta_c $ rad	$ \Delta_{top} $ m/m
-				
3	0.002	0.029	0.016	0.018
4	0.032	0.006	0.019	0.022
5	0.030	0.004	0.017	0.018
6	0.007	0.026	0.016	0.014

Table 3-6 presents a summary table of average connector rotations for each of the multi-level racks. Averages computed are for the whole height and width of the rack. The average connector rotations of the 6-level rack are greater than its peak drift. The average connection rotations are close to the roof drift angles but the demand placed on connectors undergoing the most extreme rotations due to gravity and seismic demands varies between 1.45 (4-level) to 1.86 (6-level) times the peak roof drift.

3.6.6 Influence of added viscous damping

As previously noted, small increases in viscous damping added to the model can have marked effect on response. Figure 3-30 compares displacement profiles at peak roof displacements for various levels of added damping. The results are for the ground motion scaled by 1.5. At 5% added damping, the 5-level rack experiences uniform drift demand; as added damping drops to 2% the rack exhibits drift concentration in the first 2 levels with almost 6% drift at its base; with 1% added damping there is collapse of that frame. In the shorter frames, displacements also increase as damping is reduced.

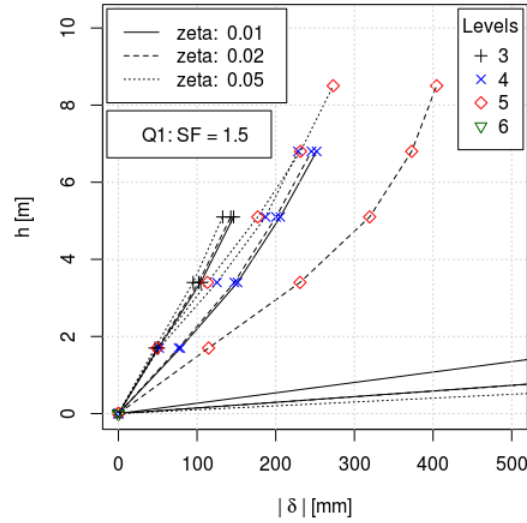


Figure 3-30: Influence of added viscous damping on peak drifts under Q1 ground motion at SF = 1.5.

3.6.7 Influence of base plate flexural strength

In Figure 3-31 the base-plate of the racks have been doubled in thickness and the racks have been subjected to the Q1 ground motion with increasing scale factor until collapse. The analyses were performed for three coefficients of friction. For SF = 1.0 and 1.5, the results can be compared to those in Figure 3-31. For these two cases, doubling the base-plate thickness reduces drift of the first level, concentrating the drifts on upper levels. This has the effect of accentuating peak displacements with respect to peak displacements with the thinner base-plate, see Figure 3-31b & c, except for the 5-level rack subjected to the Q1 signal scaled by 1.5.

Irrespective of friction coefficient, sliding had little effect on drifts when Q1 is left unscaled. In 3 and 4-level racks, depending on the scale of the Q1 signal, unfavourable drifts are observed when masses are free to slide. Modifications of drift profile (between sliding and non-sliding models) increase substantially as the Q1 scale factor increases. Drift also increases and collapse is observed in all but the 3-level rack at Q1 with SF = 3.0.

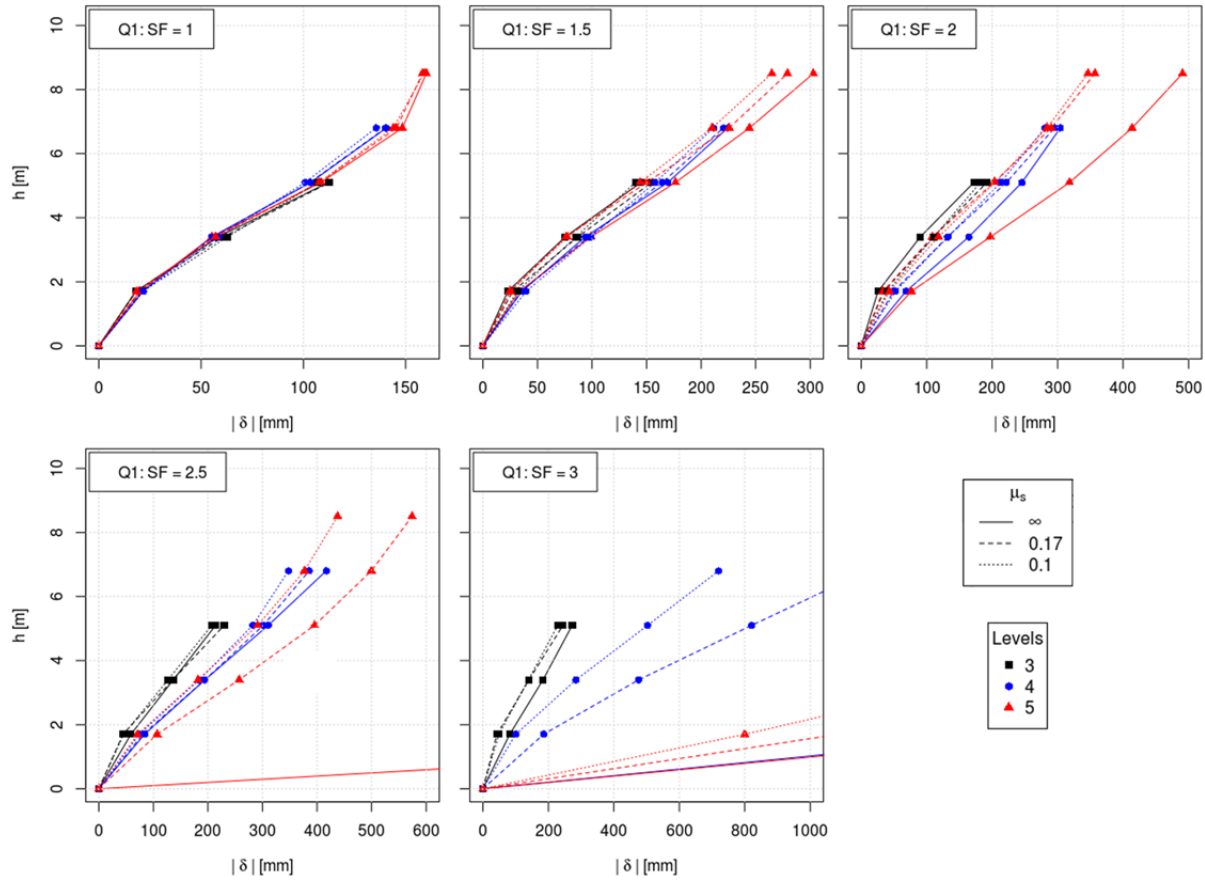


Figure 3-31: Drift profiles with stiffened base-plates and increasing scale factors on the Q1 signal.

3.7 Conclusions and Recommendations

A test program was performed on 11 one-level, one-bay cold formed rack specimens to generate data on the cyclic inelastic response of beam-to-column and base plate connections and seismic inelastic response of storage rack structures. Quasi-static, pull-back and seismic tests were performed. Loaded unattached wooden pallets were present in all tests. A numerical model was developed using the OpenSees framework to reproduce the observed connection and frame responses. Pallet sliding response was included in the model. The influence of viscous damping on the response was examined. A yield line model was proposed to assess the flexural strength of base plates including axial load effects. The model was then used to examine the influence of key parameters on the seismic response of 6-bay rack structures having 3 to 6 levels. The following conclusions can be drawn from this study:

- The beam-to-column connectors studied exhibited stable although pinched hysteretic response with moment capacity reached at a rotation of 0.14 rad, followed by gradual strength degradation. The column base plates also demonstrated stable inelastic cyclic response with greater energy dissipation capacity and could sustain up to 0.20 rad rotation capacity without failure. Pallet sliding was observed during all seismic tests. The frame specimens withstood the seismic demand through inelastic response in the connectors and base plates.
- The proposed numerical model is capable of reproducing the cyclic inelastic response of the beam-to-column and base plate connections studied as well as the inelastic seismic response of the specimens tested. Occurrences of sliding could also be captured by the model, though differences in sliding displacements were obtained between test and predicted values.
- The data from RMI unit tests of beam-to-column connectors are sufficient for calibrating models and predicting secant stiffness. Yield line theory can be used to estimate the flexural strength of rack base plates with consideration of axial compression. However, moment-rotation response of column base plates must be determined from cyclic tests including axial loads.
- For the pinned base tests, added viscous damping required to produce good correspondence between pull-back tests and the model was greater than that needed to match shake table tests; good agreement was found for the fixed base frame. In both cases, 2% viscous gave closest match to seismic tests. In spite of the apparent simplicity of the test set-up and careful calibration of non-linear elements, structural collapse remains difficult to predict and is strongly influenced by added damping. Consequently, time-history analysis producing large drifts and significant residual displacements should be treated as suspected collapse cases.
- For the racks studied, equivalent viscous damping in combination with secant stiffness properties in a linear model was a poor substitute for explicitly modelling energy dissipation through nonlinear modelling.
- Preliminary results indicate that:

- In addition to a low friction coefficient, sliding will only occur when the ground motion itself is strong enough to produce sufficient accelerations (agrees with [14])
- Flexible racks benefit more from sliding than do stiffer racks, however a minimum stiffness is needed to prevent collapse.
- On occasion pallet sliding may prove deleterious, the use of sliding to reduce design loads should be considered a niche, not a generality, and applied with caution.

Recommendations for future study:

- A key assumption inherent in this model is that beams and columns remain elastic. All plastic behavior is concentrated in the beam-column connections and base-plates. While this reflected the behaviour of the rack specimens studied and is consistent with current rack seismic design provisions, care must be taken to select weak connectors and strong beams and columns. Cold-formed columns may be subject to local buckling, distortional buckling and lateral torsional buckling, as they are uni-symmetric and loaded eccentrically from their shear centre. If these modes are expected, a more robust model integrating these modes, would be necessary.
- Further development of the base-plate model is needed to reflect behaviors such as stiffness increase with axial load, levering, bolt pull-out and concrete interaction all of which may be present in reality. Forces from loading in the transverse direction will also effect base-plate response and should be considered.
- Parametric studies on prototype structure must be performed to evaluate the validity of the assumptions and analysis methods used in rack seismic design.
- The study was limited to loading in one direction. The effects of loading in the transverse direction must also be considered.

3.8 Acknowledgements

Funding for this research was provided by the Natural Sciences and Engineering Research Council of Canada. The authors wish to thank undergraduate students Émile Lord and Aziz El

Meskini as well as research engineers Martin Leclerc and Romain Siguier for their invaluable assistance in the test program. The authors acknowledge the technical input from Post-Doctoral Fellow Poulad Daneshvar for the selection and scaling of ground motions as well as in the numerical modelling.

References

- [1] C. Clifton, M. Bruneau, G. MacRae, R. Leon and A. Fussel, "Steel Structures Damage From the Christchurch Earthquake Series of 2010 and 2011," *Bulletin of the New Zealand Society For Earthquake Engineering*, vol. 4, no. 44, pp. 297-318, 2011.
- [2] G. J. Beattie and U. S. R, *A Revised Guide for the Design, Construction and Operation of High Level Storage Racking Systems following the Darfield Earthquake*, Auckland, New Zealand: Proceedings of the Ninth Pacific Conference on Earthquake Engineering, 2011.
- [3] D. A. Bournas, P. Negro and F. F. Taucer, "Performance of industrial buildings during the Emilia earthquakes in Northern Italy and recommendations for their strengthening," *Bulletin of Earthquake Engineering* 12.5, vol. 5, no. 12, pp. 2383-2404, 2014.
- [4] CEN, "Steel static storage systems - Adjustable pallet racking systems - Principles for seismic design," European Committee for Standardization, Brussels, Belgium, 2016.
- [5] CSA, "A344.2-05, Standard for the design and construction of steel storage racks," Canadian standard Association, Mississauga, ON., 2005.
- [6] RMI, "ANSI MH16.1.12, Specification for the Design, Testing and Utilization fo Industrial Steel Storage Racks," Rack Manufacturer's Institute, Charlotte, NC, 2012.
- [7] A. Filiatrault, R. E. Bachman and M. G. Mahoney, "Performance-based seismic design of pallet-type steel storage racks," *Earthquake spectra*, vol. 1, no. 22, pp. 47-64, 2006.
- [8] A. B. M. R. Haque and M. S. Alam, "Direct Displacement-Based Design of Industrial Rack Clad Buildings," *Earthquake Spectra*, vol. 4, no. 29, pp. 1311-1334, 2013.

- [9] E. Jacobsen, *Seismic Behaviour, Numerical Modelling and Displacement-Based Design of Steel Storage Rack Structures for Canadian Applications (Master's Thesis)*, Montreal, QC: Polytechnique Montreal, 2016.
- [10] M. Priestley, G. Calvi and M. Kowalsky, "Direct Displacement-Based Seismic Design of Structures," Pavia, IUSS Press, 2007, p. 721.
- [11] BSSC, "FEMA 460 Seismic Considerations for Steel Storage Racks Located in Areas Accessible to the Public. Prepared by the Building Seismic Safety Council for the Federal Emergency Management Agency, National Institute of Building Sciences," Building Safety Seismic Council, Washington, DC, 2005.
- [12] C. CSA, *CSA-S16-09: Design of Steel Structures*, Mississauga (Ontario, Canada): Canadian Standards Association, 2014.
- [13] G. E. N. R. Coutinho, "Numerical simulation of the seismic behavior of steel storage pallet racking systems," Instituto Superior Técnico, Lisbon, 2008.
- [14] I. Rosin, L. Calado, J. Proenca, P. Carydis, H. Mouzakis, C. Castiglioni, J. Brescianini, A. Plumier, H. Degee, P. Negro and others, "Report EUR 23744 Storage racks in seismic areas," European Commision, Luxembourg, 2009.
- [15] H. Degée and V. Denoël, "Numerical modelling of storage racks subjected to earthquake," in *Proceedings of COMPDYN 07, Conference on Computational Dynamics*, Rethymno, Crete, Greece, 2007.
- [16] A. B. M. R. Haque and M. S. Alam, "Force-Based Seismic Design of Industrial Rack Clad Buildings," University of British Columbia, Okanagan, 2012.
- [17] C. Bernuzzi and M. Simoncelli, "An advanced design procedure for the safe use of steel storage pallet racks in seismic zones," *Thin-Walled Structures*, no. 109, pp. 73-87, 2016.
- [18] H. Krawinkler, "Experimental study on seismic behavior of industrial storage racks," in *4th*

International Specialty Conference on Cold-Formed Steel Structures, 1978.

- [19] A. Filiatrault, P. S. Higgins, A. Wanitkorkul, J. A. Courtwright and R. Michael, "Experimental seismic response of base isolated pallet-type steel storage racks," *Earthquake Spectra*, vol. 3, no. 24, pp. 617-639, 2008.
- [20] B. P. Gilbert and K. J. Rasmussen, "Determination of the base plate stiffness and strength of steel storage racks," *Journal of Constructional Steel Research*, vol. 6, no. 67, pp. 1031-1041, 2011.
- [21] N. Baldassino and C. Bernuzzi, "Analysis and behaviour of steel storage pallet racks," *Thin-Walled Structures*, vol. 37, no. 4, pp. 277-304, 2000.
- [22] N. Baldassino and R. Zandonini, "Performance of base-plate connections of steel storage pallet racks," in *5th international colloquium on coupled instabilities in metal structures*, Sydney, 2008.
- [23] A. T. Sarawit and T. Peköz, "Cold-formed steel frame and beam-column design," American Iron and Steel Institute, Cornell, 2003.
- [24] A. Firouzehhaji, A. Saleh and B. Samali, "Australian Conference On The Mechanics Of Structures And Materials," in *CRC press/Balkema*, 2013.
- [25] A. Kanyilmaz, C. A. Castiglioni, G. Brambilla and G. P. Chiarelli, "Experimental assessment of the seismic behavior of unbraced steel storage pallet racks," *Thin-Walled Structures*, no. 108, pp. 391-405, 2016.
- [26] C. Bernuzzi and C. A. Castiglioni, "Experimental analysis on the cyclic behaviour of beam-to-column joints in steel storage pallet racks," *Thin-Walled Structures*, vol. 10, no. 39, pp. 841-859, 2001.
- [27] C. Aguirre, "Seismic behavior of rack structures," *Journal of Constructional Steel Research*, vol. 61, no. 5, pp. 607-624, 2005.

- [28] N. Baldassino and C. Bernuzzi, "Analysis and behaviour of steel storage pallet racks," *Thin-Walled Structures*, vol. 4, no. 37, pp. 277-304, 2000.
- [29] H. Degée and V. Denoël, "An investigation on the sliding of pallets on storage racks subjected to earthquake," in *Proceedings of the 7th National Congress on Theoretical and Applied Mechanics*, Mons, 2006.
- [30] P. Sideris, "Seismic behavior of palletized merchandise in steel storage racks (Master's Thesis)," ProQuest Information and Learning Company, Ann Arbor, MI, 2008.
- [31] Y. Gao, "Seismic Evaluation and Performance Enhancement of Industrial Storage Racks," Case Western Reserve University, Cleveland, 2013.
- [32] B. Gilbert, R. Badet, L. Teh and K. Rasmussen, "Determination of the influence of the pallets on the design of drive-in steel storage racks," Centre for Infrastructure Engineering and Management, Griffith University, Queensland, 2013.
- [33] M. Pollino, Y. Gao and R. Michael, "Seismic Response and Protection of Steel Storage Rack Palleted Merchandise," in *10th U.S. National Conference on Earthquake Engineering Frontiers of Earthquake Engineering*, Anchorage, 2014.
- [34] P. Sideris, A. Filiatrault, M. Leclerc and R. Tremblay, "Experimental investigation on the seismic behavior of palletized merchandise in steel storage racks," *Earthquake Spectra*, vol. 1, no. 26, pp. 209-233, 2010.
- [35] C. Chen, R. E. Scholl and J. A. Blume, "Seismic Study of Industrial Steel Storage Racks," URS/John A. Blume & Associates, San Francisco, 1980.
- [36] A. Filiatrault, P. S. Higgins, A. Wanitkorkul and J. Courtwright, "Experimental stiffness of pallet-type steel storage rack tier drop connectors," *Practice Periodical on Structural Design and Construction*, vol. 4, no. 12, pp. 210-215, 2007.
- [37] F. McKenna and G. Fenves, "Open System for Earthquake Engineering Simulation," Pacific

Earthquake Engineering Research Center (PEER), University of California, Berkeley, CA., 2014.

- [38] R. Tremblay, G. Atkinson, N. Bouaanani, P. Daneshvar, P. Léger and S. Koboevic, "Selection and scaling of ground motion time histories for seismic analysis using NBCC 2015," in *Proc. 11th Canadian Conference on Earthquake Engineering, Paper No. 99060*, Victoria, BC, 2015.
- [39] NRCC, "National Building Code of Canada, 14th ed.," National Research Council, Ottawa, ON, 2015.
- [40] R. Szilard, *Theories and Applications of Plate Analysis: Classical Numerical and Engineering Methods*, John Wiley & Sons, 2004.
- [41] A. Zsarnóczyay, "Steel4 Material," University of California Regents, Berkeley, 2015.
- [42] M. Scott, F. Filippou and S. Mazzoni, "Hysteretic Material," University of California Regents, Berkeley, 2016.
- [43] M. Scott, F. Filippou and S. Mazzoni, "OpenSees Wiki," University of California Regents, 30 09 2013. [Online]. Available: http://opensees.berkeley.edu/wiki/index.php/Hysteretic_Material. [Accessed 13 11 2016].
- [44] A. Zsarnóczyay, "OpenSees Wiki," University of California Regents, 20 02 2015. [Online]. Available: http://opensees.berkeley.edu/wiki/index.php/Steel4_Material. [Accessed 13 11 2016].
- [45] N. Mitra, "Pinching4 Material," 2012. [Online]. Available: http://opensees.berkeley.edu/wiki/index.php/Pinching4_Material. [Accessed 1 9 2015].
- [46] A. K. Chopra, *Dynamics of Structures Vol. 3*, New Jersey: Prentice Hall, 2005.
- [47] A. Schellenberg, "Flat Slider Bearing Element," 8 May 2014. [Online]. Available: http://opensees.berkeley.edu/wiki/index.php/Flat_Slider_Bearing_Element. [Accessed 13

April 2017].

- [48] A. Schellenberg, "OpenSees Wiki," University of California, Berkeley, 18 September 2014. [Online]. Available: http://opensees.berkeley.edu/wiki/index.php/Velocity_Dependent_Friction. [Accessed 12 April 2017].
- [49] M. Priestley, G. Calvi and M. Kowalsky, "Direct displacement-based seismic design of structures," in *5th New Zealand Society for Earthquake Engineering Conference*, 2007.
- [50] G. Beattie and B. Deam, *Design Guide Seismic Design of High Level Storage Racking Systems with Public Access*, Porirua City, New Zealand: Branz, 2006.

CHAPTER 4 DISPLACEMENT-BASED DESIGN OF RACKS ACCORDING TO ANNEX N AND COMPARISON WITH NON-LINEAR TIME HISTORY ANALYSIS

4.1 Introduction

This section aims to test the displacement-based design provisions of S16 Annex N for feasibility and safety. Several 3, 4, 5 and 6 level prototypes are designed (with little or no over-strength) to be used in multi-parameter non-linear time history analyses in Vancouver and Montreal sites C and E conditions. The hypotheses and method for a displacement-based procedure are outlined in §4.2. Pertinent Annex N articles are reproduced in APPENDIX A . Force based-design is examined in APPENDIX C .

In §4.3 detailed displacement based design is given for a 3-level, 6-bay rack in Vancouver, site C (where the deformation limits of Annex N govern design) as well as a detailed design for a 6-level, 6-bay rack in Montreal site E conditions (where minimum lateral strength in Annex N governs). Design summaries are presented and discussed for the other 14 prototypes in §4.4.

Using the model developed in the previous section with the modifications discussed in detail in APPENDIX D , the base-line series of non-linear time history analyses are performed on the prototype racks and the results are examined in §4.5.

4.2 A proposed displacement-based design method for racks

As previously noted, the connectors and base-plates should be the fuse element in a rack designed to withstand earthquake effects in the non linear range. Design is satisfactory when the rotation capacity of the connectors, $\theta_{c,max}$, match rotation demands placed on the connectors, θ_{demand} .

With respect to displacement-based seismic design of rack moment frames Annex N §11.4.5.3 stipulates that:

- (a) The effective properties of the equivalent single-degree-of-freedom system shall be determined from an appropriate model representing the rack structure inelastic first mode response with the effective stiffness of the beam-to-column and column base connections determined at the seismic design displacement;

(b) The effective stiffness and energy dissipation capacity of the beam-to-column and column base connections shall be determined from the qualification procedure specified in Clause 10.9;

(c) P-delta effects shall be taken into account;

(d) The seismic design displacement shall be determined using the design displacement spectrum specified in Clause 10.5.3 using the effective period of the fundamental period and the equivalent damping properties of the rack structure; and

(e) The structure equivalent viscous damping properties shall be based on the energy dissipation capacity of the beam-to-column and column base connections as specified in b). It may also include the inherent damping of the structure up to 3%.

In addition, the proposed Annex N requires that other drift and minimum resistance criteria be validated (see §10.7). Furthermore, capacity design dictates that beams and columns be designed to cede after the connectors.

The following method, adapted from [15], [16] and [85], and making direct use of connector qualification tests adheres to the above stipulations and delineates the design of the rack based on the rotation of the connector. The numbered design steps are illustrated in Figure 4-3:

- 1) A first hypothesis of connector rotation-demand is made, $\theta_{d,i}$ i.e. a design or target rotation is chosen. In practical terms this consists of choosing a connector and base-plate with a certain rotation capacity, $\theta_{c,max}$, which the designer supposes will be adequate to accommodate both gravity rotations, θ_D , and seismic rotations, θ_E . In the context of Annex N two articles influence the adequacy of a connector: §10.7a, which gives overall drift limits, and : §10.7b in conjunction with §11.8.2.1.3, which limits the rotation imposed by “gravity loads plus two times the seismic design displacements” to be less than rotation capacity of the connections, $\theta_{c,max}$. One method of satisfying these deformation conditions is to suppose a certain relationship between connector rotations and overall drift to determine which limit in §10.7 governs keeping in mind that allowable connector rotation should be reduced to account for gravity rotations.
- 2) From the cyclic test data of the chosen connections the secant stiffness, k_c & k_{bpl} , and the energy dissipated per cycle, EDC_c & EDC_{bpl} , are calculated at the target rotation. In Figure 4-1 the calculation of secant stiffness using the average of positive and negative

slopes (as mandated in the proposed Annex N 10.9) in a cycle is shown. Because the target rotation lies between tested rotations the secant stiffness is interpolated.

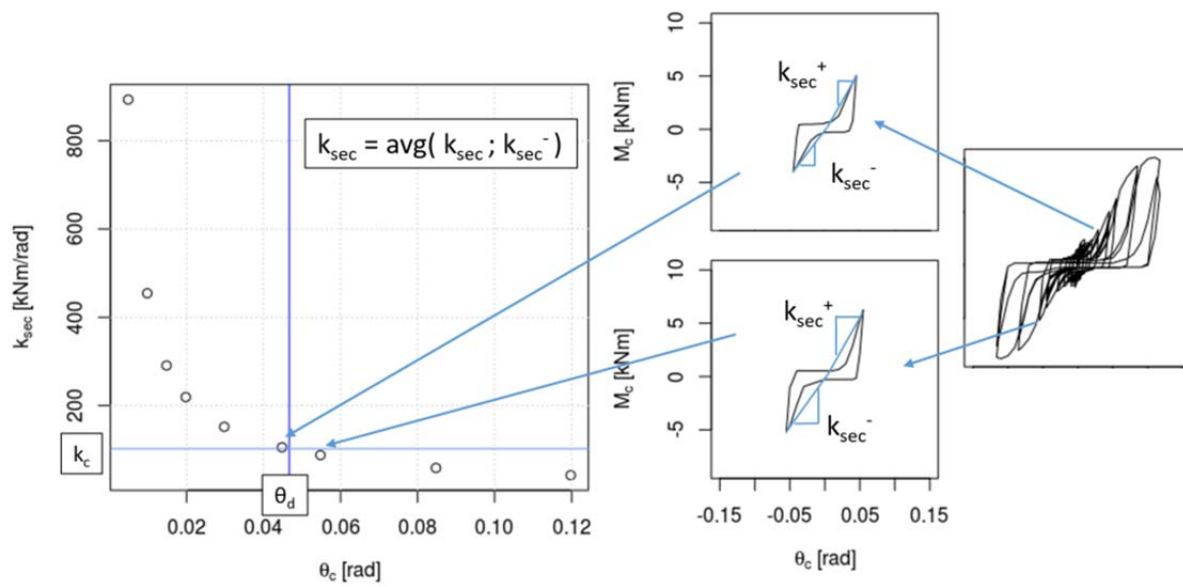


Figure 4-1: Calculation of secant stiffness, cycle by cycle, from experimental connector test data.

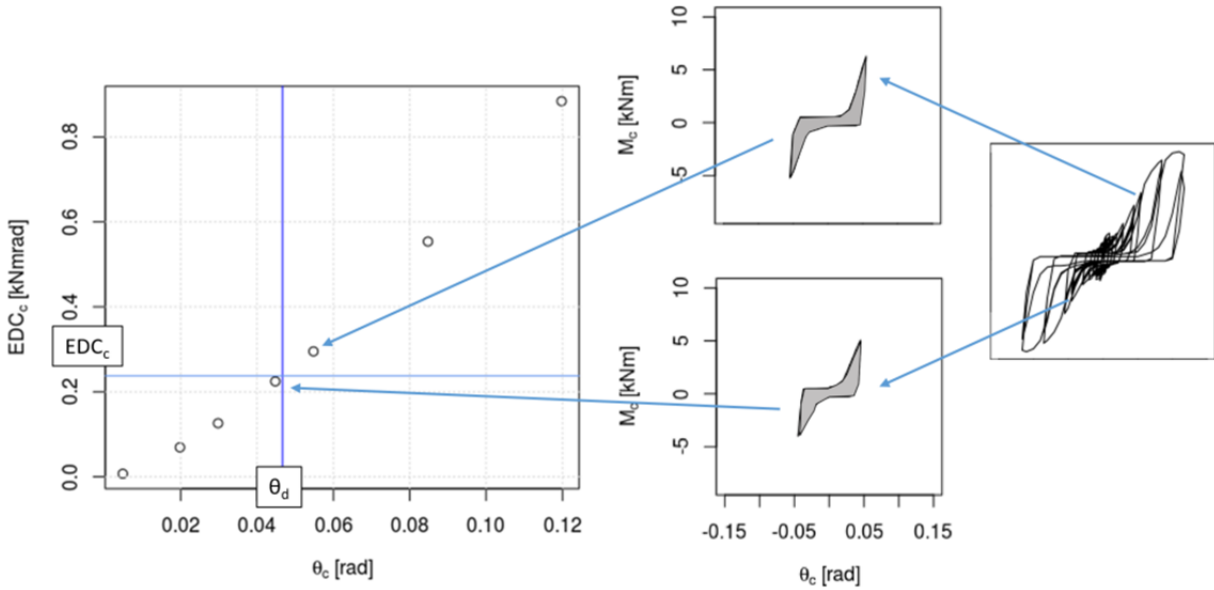


Figure 4-2 : Calculation of energy dissipated, cycle-by-cycle, from experimental connector test data.

- 3) The effective fundamental period, T_{eff} , of the substitute SDOF structure is calculated. This can be accomplished by performing eigenvalue analysis on an FEM model of the rack with its beam-column connections at k_c and base-plates at k_{bpl} or, when appropriate, by using a simplified equation see [15] or Annex G.
- 4) The effective lateral stiffness of the rack, k_{eff} , is reduced to account for P-delta effects. See discussion in section 2.4.5 and [43]. The fundamental period is hence elongated, $T_{eff,aug}$.
- 5) The energy dissipated by the connectors is transformed into effective damping, β_{eff} , of the whole rack according to eq. (4-1) (adapted from [16]). In the equation, β_{el} is the inherent damping of the structure encompassing energy dissipation by all other mechanisms aside yielding of the base-plates and connectors i.e. sliding of pallets.

$$\beta_{eff} = \beta_{hyst.} + \beta_{el.} = \frac{N_{bpl}EDC_{bpl} + N_cEDC_c}{2\pi \cdot k_{eff,rack,red.} \cdot \delta_d^2} + \beta_{el.} \quad (4-1)$$

- 6) The elastic spectral displacement, which can be calculated from the design (acceleration) spectrum $S(T)$ using eq. (4-2) and by linear interpolation for intermediate values:

$$S_{d5\%} = S \cdot g \cdot \frac{T^2}{4\pi^2} \quad (4-2)$$

$S_{d5\%}$ is adjusted (reduced by the factor R_β see eq. (4-4) drawn from [86]) from 5% damping to the effective damping level of the rack.

$$S_{d\beta} = S_{d5\%} \times R_\beta \quad (4-3)$$

Where:

$$R_\beta = [0.1 / (0.05 + \beta_{eff})]^{0.5} \quad (4-4)$$

- 7) The displacement of the substitute SDOF, $S_{d\beta}$, is calculated from the reduced spectrum at the augmented effective period $T_{eff,aug}$. A hypothesis must then be made as to the relationship between displacement of the SDOF and rotation of the connectors. If the target rotation in step 1 agrees with the rotation demand found in step 7, the connector, and its rotation capacity, are deemed satisfactory.

4.3 Design according to proposed Annex N provisions

4.3.1 Properties, dimensions and loads

The following typical rack geometries and loadings were supplied by industry collaborators. Test data for beam-to-column connectors AC175 and AC200, typically used in such racks were also supplied. Cyclic test data for these connections is presented in the subsequent sections §0 & §4.3.1.2. No such data was available for the base plates, as such numerical data was produced (see §4.3.1.3). The product load in Table 4-1 refers to the load of 1 pallet, of which there are two, per-bay, per-level as indicated in Figure 4-4.

Table 4-1: Connectors and product loads for prototype racks.

Levels	Connectors	Product Load	
		kip	kN
3	AC175	3.3	14.679
4	AC175	2.5	11.121
5	AC175 or AC200	2.5	11.121
6	AC200	2.5	11.121

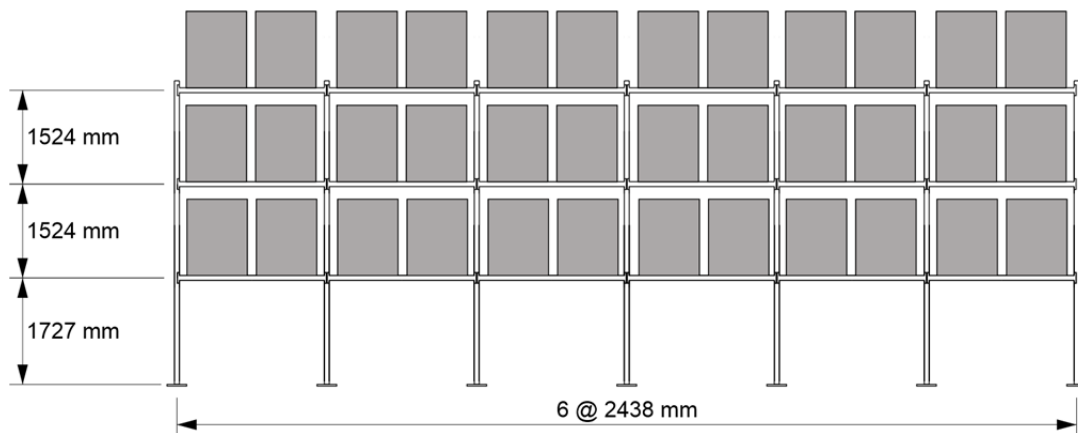


Figure 4-4: Geometry of prototype racks.

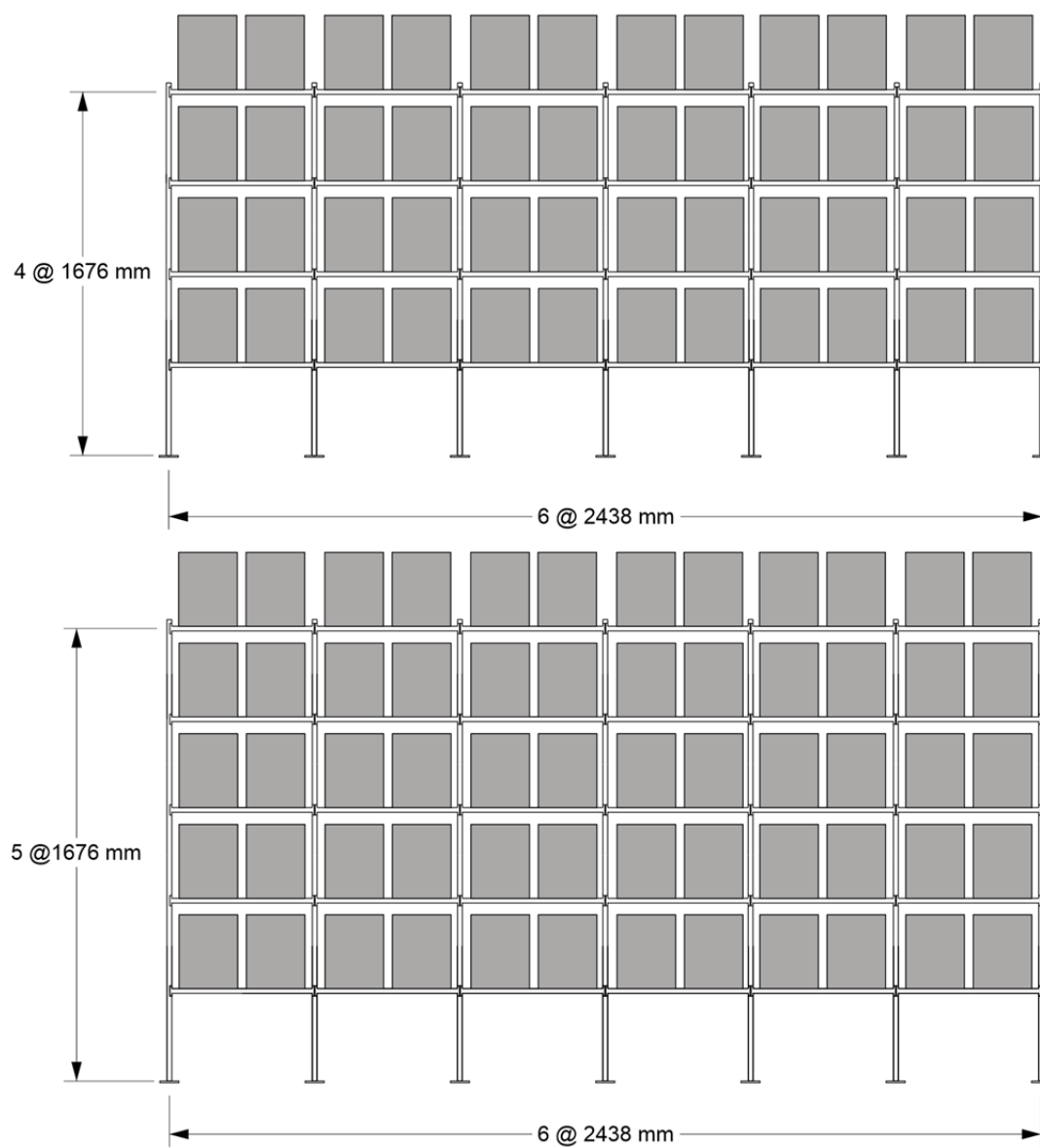


Figure 4-4 : Suite : Geometry of prototype racks

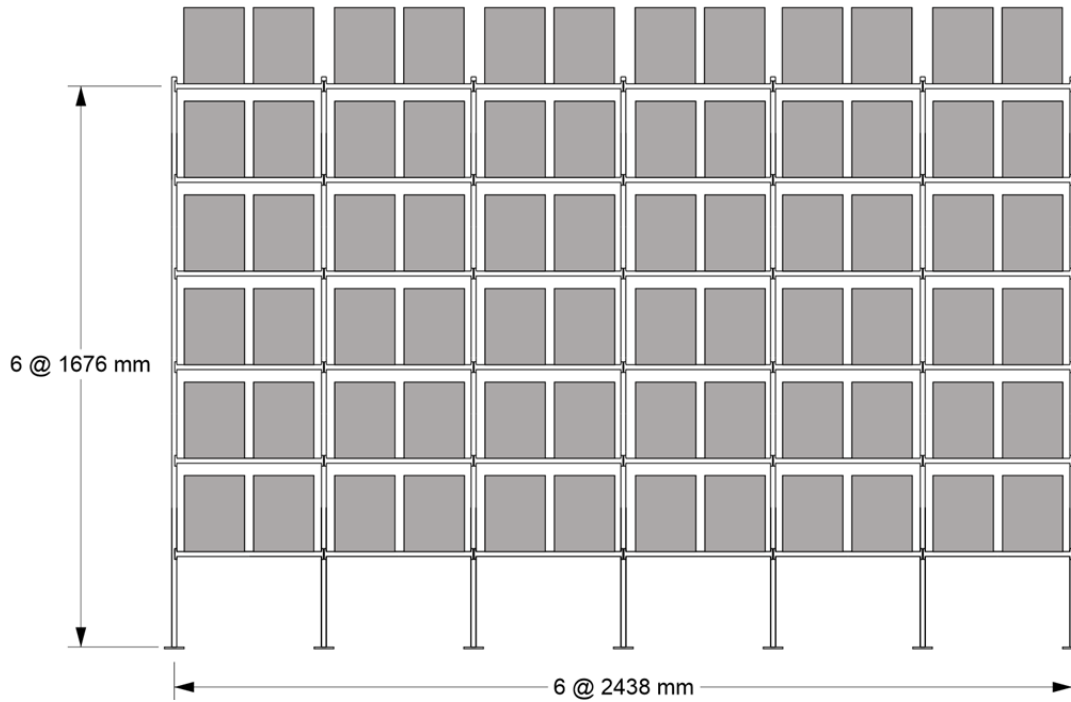


Figure 4-4 : Suite : Geometry of prototype racks

4.3.1.1 AC175 Connector Properties

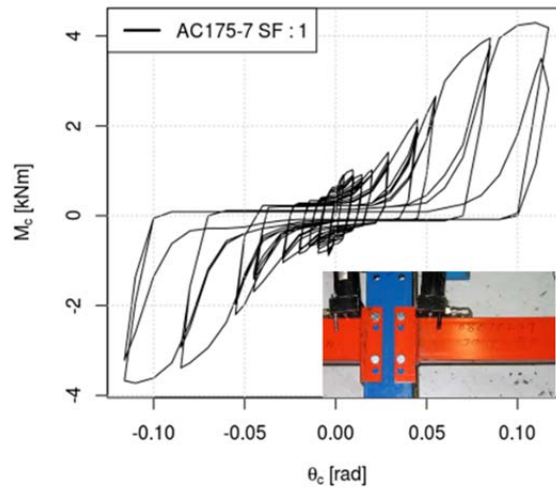


Figure 4-5: Moment-rotation hysteresis of a single 2-bolt connector AC175.

According to S16 Annex N §11.8.1 the connection rotation capacity is taken as the peak average rotation in the last loading cycle during which $M_{c,peak} \geq 0.8M_{c,max}$. This connector shows no deterioration in the range of tested rotations, cycle 43 (the last cycle, see Annex H.4) will be taken as the last at which $M_{c,peak} \geq 0.8M_{c,max}$, hence $\theta_{c,max} = (0.117+0.116)/2 = 0.1165$ rad and $M_{c,max} = (4.290 \text{ kNm} + 3.730 \text{ kNm})/2 = 4.01 \text{ kNm}$.

4.3.1.2 AC200 Connector Properties

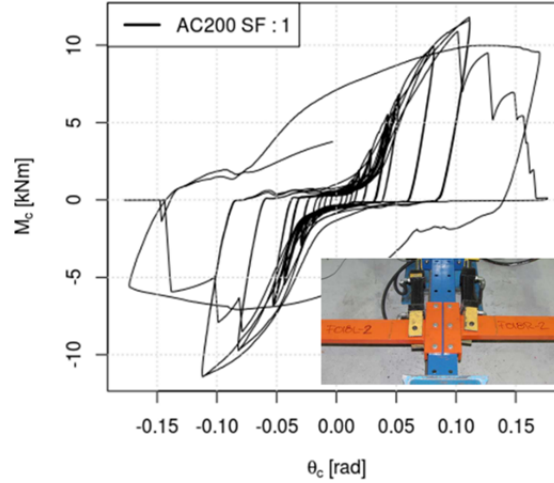


Figure 4-6: Moment-rotation hysteresis of a single 3-bolt connector AC200.

$M_{c,max}$ occurs during cycle 44 (see Annex 15.1H.5H.5) : $M_{c,max} = (11.800 \text{ kNm} + 11.417 \text{ kNm})/2 = 11.6085 \text{ kNm} \Rightarrow 0.8 * M_{c,max} = 9.2868$. The last cycle in which the connector maintains $M_{c,max}$ is also cycle 44 $\Rightarrow \theta_{c,max} = (0.1114 + 0.1123)/2 = 0.1119 \text{ rad}$.

4.3.1.3 Base-plate properties

No specific base-plate was supplied with prototype rack geometries, the base-plate configuration in Figure 4-7 was adopted.

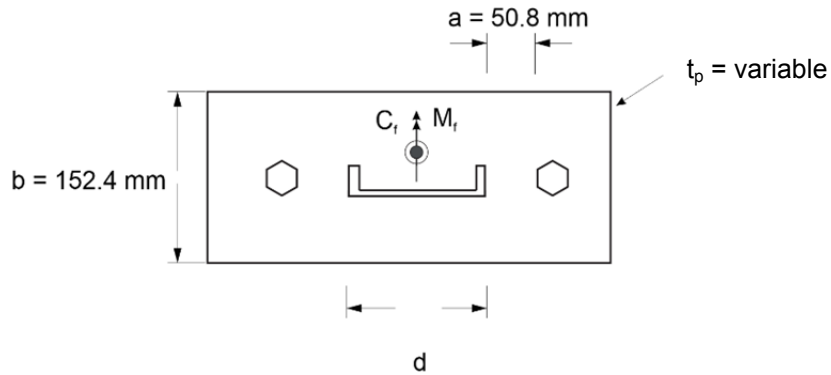


Figure 4-7: Base-plate dimensions for prototype racks.

As discussed in APPENDIX E , these base-plates have the advantage of being simple to recreate as a 2D finite element model, the verification of which is easily performed by yield line theory. The cyclic test data necessary to carry-out the displacement-based design outlined in the previous section was produced following the procedure outlined in APPENDIX E . In short

pseudo-cyclic tests were performed with appropriate levels of compression on the OpenSees model of the base-plate. This produced the secant stiffness and energy dissipation data seen in Figure 4-13, Figure 4-15, Figure 4-21 & Figure 4-23.

Base-plates have been chosen for each rack to have a stiffness similar to the beam-column connectors; this was accomplished by reducing the thickness of the plate fiber elements used in the base-plate assembly (see Appendix D.2.1). This reduces the reliance of the design on the base-plate's behaviour.

4.3.1.4 Material properties

Steel is assumed to have the usual mass of 77000 kg/m^3

Table 4-2: Material properties.

	Norm	F_y		F_u or X_u		E	
		ksi	MPa	ksi	MPa	ksi	MPa
Channels	ASTM A572 Grade 50 UNO	50	345	65	450	29000	200000

4.3.1.5 Seismic data

NBCC 2015 seismic data is used for designs. The design spectra for the four sites are given in Table 4-3 and Figure 4-8.

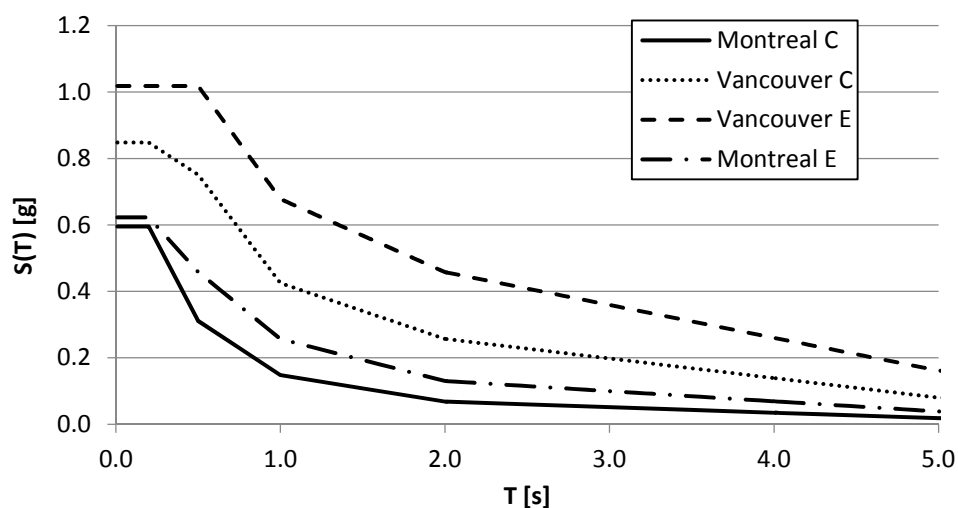


Figure 4-8 : Design spectra for Montreal and Vancouver Sites C & E from NBCC 2015.

Table 4-3 : Spectral values for Montreal and Vancouver Sites C & E from NBCC 2015.

	Montreal		Vancouver	
	C	E	C	E
T	S			
s	g			
0.2	0.60	0.62	0.85	1.02
0.5	0.31	0.46	0.75	1.02
1	0.15	0.26	0.43	0.68
2	0.07	0.13	0.26	0.46
5	0.02	0.04	0.08	0.16
10	0.01	0.01	0.03	0.06

4.3.2 Design of 3-level, 6-bay rack in Vancouver site C

The next paragraphs follow the design path of §4.3.2.1 in detail for the last iteration of design of a 3-level, 6-bay rack (see Figure 4-4) in Vancouver site C conditions meeting exactly the deformation limits in S16 Annex N §11.7. Iterations were made on the stiffness of connectors, base-plates and accompanying beam and column sections. Given that data does not exist for connector that would exactly meet the needs of this design, ficticiously strong connectors have been created by scaling the strength of the AC175 connectors. Likewise, base-plate thickness is increased to give appropriate stiffness values. When larger column sections are needed, the column is first boxed and only once this section becomes insufficient is a larger channel selected. Beams are not boxed, only larger channels are taken.

The same connectors are used throughout except on the top-level interior joints where connectors have half the resistance of the other connectors. Current design practice does not account for weaker connectors to be connected to the top interior columns as would be necessary for a weak connector, strong beam and column capacity design as assumed in S16 Annex N.

The frame is considered perfectly straight and the material properties are known. As such, no reduction will be made for accidental out-of-plumb erection of the rack and material phi coefficients shall be taken as 1.

The following sections and connectors were chosen:

- Beams : C100x9 ($1.77 \times 10^6 \text{ mm}^4$), $F_{yb} = 329 \text{ MPa}$

- Columns : C100x7 ($1.53 \times 10^6 \text{ mm}^4$), boxed at all three levels, $F_{yc} = 216 \text{ MPa}$
- Connectors : AC175 strength scaled by 2.36
- Base-plates : $t_p = 5.5 \text{ mm}$ (all other dimensions as seen in §4.3.1.3)

4.3.2.1 Design Path

1. Check applicability,
2. Determine drift and rotation limits and establish by pushover which limit governs,
3. Adjust connector and base-plate to achieve the required level of energy dissipation and secant stiffness such that deformation limits are satisfied,
4. Adjust columns and beams to cede after connectors,
5. Check minimum lateral resistance.

1. Applicability

The rack is 4.775 m high $< 7.6 \text{ m} \Rightarrow$ This rack is admissible for displacement-based design of the MRF direction under S16 Annex N §10.5.1 limitations.

2. Deformation limits

According to S16 Annex N §11.7a, the first seismic design deformation to respect is a drift limit, Δ_{lim} , of 0.05 rad. The rack is considered perfectly straight, hence no reduction for out-of-plumb erection. Were erection tolerance to be taken into account, the allowable drift could be reduced as shown in eq. (4-5).

$$\Delta_d = \frac{0.05 \text{ rad} - \text{erection tolerance}}{I_E} = \frac{0.05 - 1/240}{1} = 0.046 \text{ rad} \quad (4-5)$$

The second deformation limit stated in S16 Annex N §11.7b refers to connector rotation capacity:

- According to S16 Annex N §11.7 the connection rotation capacity is taken as the peak average rotation in the last loading cycle during which $M_{c,peak} \geq 0.8M_{c,max}$. As previously noted, this connector shows no deterioration in the range of tested rotations and thus the peak cycle shown in Figure 4-5 is assumed to be the last at which $M_{c,peak} \geq 0.8M_{c,max}$. Thus $\theta_{c,max}$ shall be taken as 0.11 rad.

- Following S16 Annex N §11.8.2.1.3 and by assuming that gravity rotations θ_D act on an essentially pinned-pinned beam:

$$\theta_d = \frac{(\theta_{c,max} - \theta_D)}{2} = \frac{\left(\theta_{c,max} - \frac{Pl^2}{24EI}\right)}{2} \quad (4-6)$$

Thus:

$$\theta_d = \frac{\left(0.11 \text{ rad} - \frac{14679 \text{ N} \cdot (2438 \text{ mm})^2}{24 \cdot 200000 \text{ MPa} \cdot 1.77 \times 10^6 \text{ mm}^4}\right)}{2}$$

$$\Rightarrow \theta_d = (0.11 \text{ rad} - 0.01 \text{ rad})/2 = 0.05 \text{ rad}$$

The design drifts and rotations need not be further reduced as the importance factor $I_E = 1.0$.

A pushover analysis is performed on the rack to determine which of the preceding deformation limits is reached first. Pushover is performed using a triangular loading pattern with maximum force applied at the top rack. The connector for which rotation is most critical changes throughout the pushover (the left-most and right-most connectors on the 1st and 2nd levels are at turns critical); Figure 4-9 shows the most critical rotation occurring in the rack vs. drift at the top level.

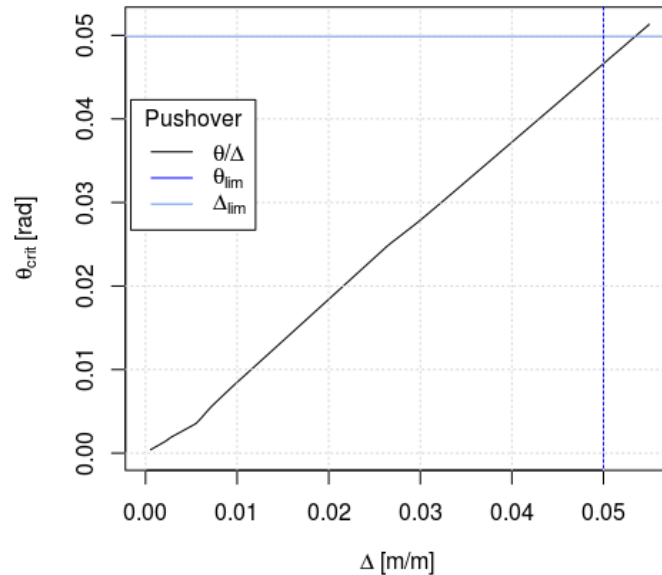


Figure 4-9: Drift vs. rotation relationship issue from non-linear pushover of a 3-level rack.

Critical drift is reached slightly before connector rotation; hence the drift limit governs. The design drift is thus: $\Delta_d = \Delta_{lim} = 0.05 \text{ rad}$, and the design rotation is: $\theta_d = 0.047 \text{ rad}$ (taken at the instant of critical drift).

3. Verification that deformation limits are satisfied given connector and base-plate properties

The hypothesis is made that all the nodes in the rack experience a similar rotation when the design drift occurs. The secant stiffness and energy dissipated per cycle of the scaled AC175 beam-column connectors at θ_d may be interpolated from Figure 4-12 & Figure 4-14. These curves have been calculated following the procedure illustrated in Figure 4-1 & Figure 4-2 using the scaled physical unit tests (as proscribed in S16 Annex N art. 10.9.3) and as shown in Figure 4-10. Secant stiffness and EDC of the base-plates are interpolated from Figure 4-13 & Figure 4-15 which are calculated from FEM unit tests as described in APPENDIX E .

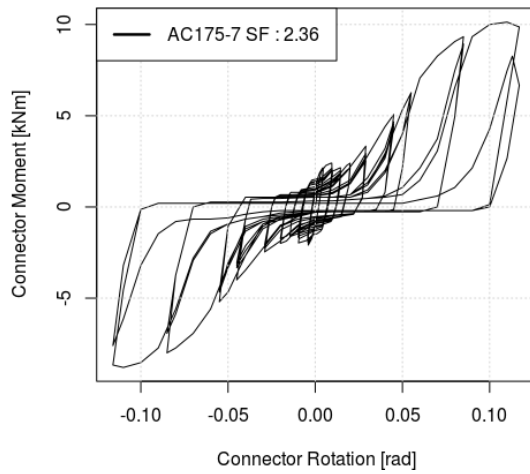


Figure 4-10: Moment rotation behaviour determined from physical unit tests and strength scaled by a factor of 2.36.

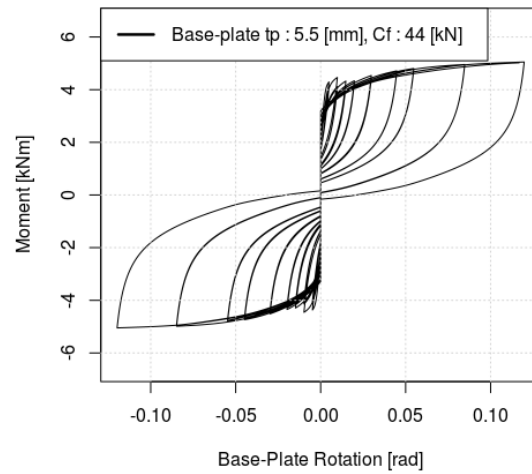


Figure 4-11: Moment-rotation behaviour as determined from FEM tests.

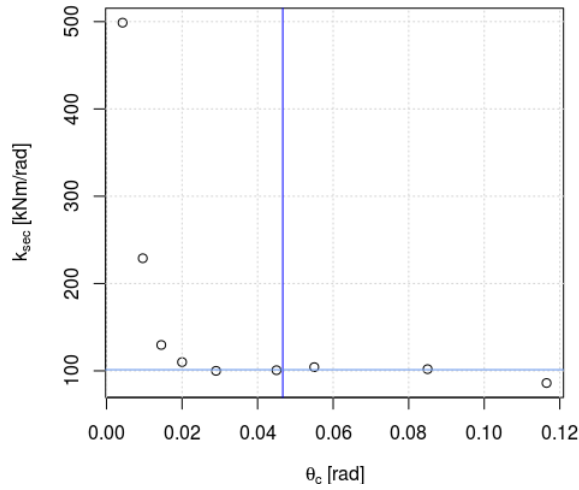


Figure 4-12: 1st pass secant stiffness of AC175 connector strength scaled by a factor of 2.36.

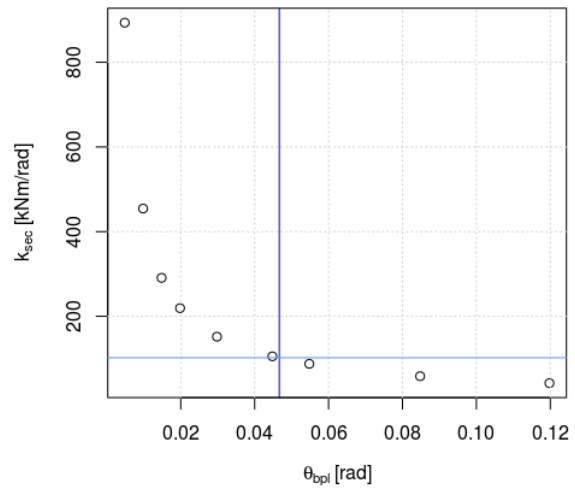


Figure 4-13: 1st pass secant stiffness of 5.5mm base-plates under compressive load of $C_f = 44$ kN.

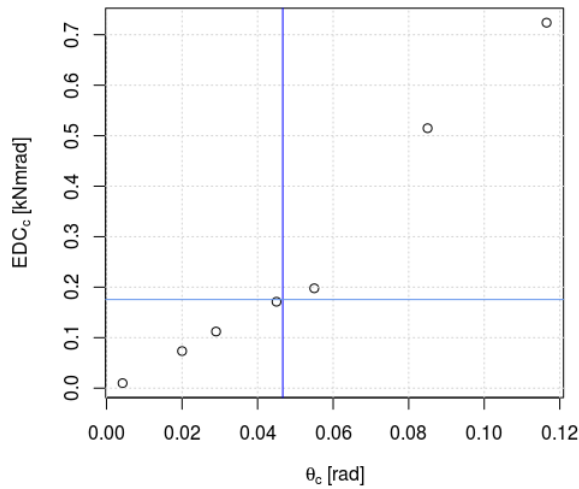


Figure 4-14: 1st pass energy dissipation of AC175 connector calculated from physical tests and strength scaled by a factor of 2.36.

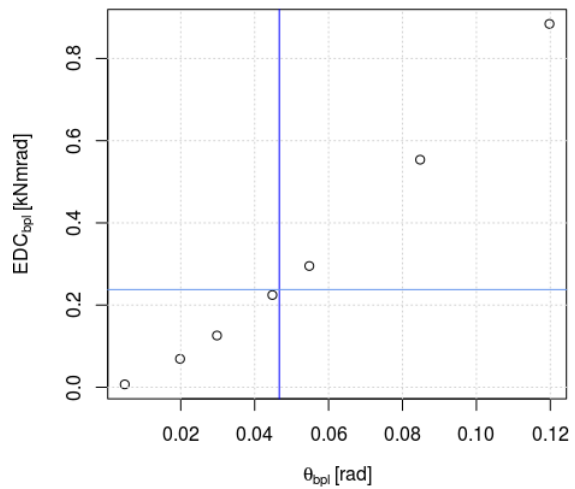


Figure 4-15: 1st pass energy dissipation of base-plates 5.5mm base-plates under compressive load of $C_f = 44$ kN.

To construct the equivalent SDOF, eigenvalue analysis on a FEM model with beam-column connectors at $k_{sec} = 101.3$ kNm/rad and base-plates at $k_{bpl} = 102.18$ kNm/rad is performed. Reductions of seismic weight allowed by Annex N for sliding of the mass and for expected

loading (see §11.2.1) of the rack are not taken into account. The full weight of the pallets is used to calculate the seismic weight. The rack's effective lateral stiffness is then obtained from that period using (4-7):

$$k_{eff,rack} = m_{eff} \cdot \left(\frac{2\pi}{T_{eff}} \right)^2 \quad (4-7)$$

$$T_{eff} = 1.99 \text{ s} \Rightarrow k_{eff,rack} = 24032 \text{ kg} \cdot \left(\frac{2\pi}{1.99} \right)^2 = 238.65 \text{ kN/m}$$

Where the effective mass, m_{eff} , is found from the generalized displacement, Δ_{gen} , using the deformation profile already available from the pushover used to determine deformation limits and by noting that the masses are equal at each level. When they are equal, their value is arbitrary since they cancel out in eq. (4-8):

Table 4-4: Finding the generalised displacement coordinate.

Level	h_x	δ_i / δ_{max}	$(\delta_i / \delta_{max})^2$
-	m	-	-
3	4.775	1.000	1.000
2	3.251	0.719	0.518
1	1.727	0.399	0.159
Σ		2.118	1.677

$$\delta_{gen} = \sum (m_i \delta_i^2) / \sum (m_i \delta_i) \quad (4-8)$$

$$m_{eff} = \left(\sum m_i \delta_i \right) / \Delta_{gen} \quad (4-9)$$

From eq. (4-8) & (4-9):

$$\frac{\delta_{gen}}{\delta_{max}} = 1.677 / 2.118 = 0.79 \Rightarrow m_{eff} = 24032 \text{ kg}$$

The rack's effective lateral stiffness is then reduced to account for P-delta by eq. (4-10):

$$k_{eff,rack} - P_{eff} / \delta_{gen} h \quad (4-10)$$

Thus:

$$k_{eff,rack,red.} = 238.65 - (24032 \cdot 9.81)/(0.79 \cdot 4.775) = 176.3 \text{ kN/m}$$

In this expression P_{eff} is the effective seismic weight of the SDOF. The augmented fundamental period is calculated from eq. (4-11):

$$T_{eff,aug.} = 2\pi \sqrt{\frac{m_{eff}}{k_{eff,rack,red.}}} \quad (4-11)$$

Thus:

$$T_{eff,aug.} = 2\pi \sqrt{\frac{24032}{176.3}} = 2.31 \text{ s}$$

The total energy dissipated per cycle by the 36 connectors, EDC_c , and 7 base-plates is $36(0.176 \text{ kNmrad}) + 7(0.238 \text{ kNmrad}) = 6.34 + 1.67 = 8.01 \text{ kNmrad}$. Despite the larger energy dissipation capacity of the base-plate, their contribution to effective damping is much less than that of the connectors. The effective damping is calculated and 3% inherent damping added as permitted in S16 Annex N §11.5.2(e). Eq. (4-1) is repeated below :

$$\beta_{eff} = \frac{N_{bpl}EDC_{bpl} + N_cEDC_c}{2\pi \cdot k_{eff,rack,red.} \cdot \delta_d^2} + 0.03 = 0.23$$

The 5% damped displacement is found from NBCC spectral values, S , at the augmented effective period. Eq. (4-2) is repeated and applied below (intermediate displacement spectra values should be interpolated between ordinates):

$$S_{d5\%} = S \cdot g \cdot \frac{T_{eff,aug.}^2}{4\pi^2} = 0.237 \cdot 9.8065 \cdot \frac{(2.33)^2}{4\pi^2} = 0.319 \text{ m}$$

The effective damped displacement, $S_{d\beta}$, (of the SDOF) in Vancouver site C is found by multiplying the 5% spectral displacement, $S_{d5\%}$, by R_β .

The damping coefficient, R_β , applied to the displacement spectra is calculated from eq. (4-3) repeated and applied below:

$$R_\beta = [0.1 / (0.05 + \beta_{eff})]^{0.5} = 0.60$$

This can be compared to the design displacement of the equivalent SDOF. This is found from design drift and the generalised displacement (which occurs at h_n): $\delta_d = \Delta_d 0.79 h_n = (0.05)(0.79)(4.775) = 0.189 \text{ m}$.

$$S_{d\beta} = S_{d5\%} \cdot R_{\beta} = 0.189 \text{ m} = \delta_d = 0.189 \Rightarrow \text{OK}$$

4. *Check that beams and columns respect capacity design i.e. that they cede after connectors and base-plates*

Beams: must satisfy S16 Annex N §11.8.4 (resist 1.2 times the ultimate flexural capacity of the beam-to-column connections). Assuming that beams are sufficiently restrained along their length such that yielding is the only limit state which must be checked $S_x > (11.32 \text{ kNm}) / (1.0) / (345 \text{ MPa}) = 32.8 \times 10^3 \text{ mm}^3 < S_{x,C100 \times 9} = 34.6 \times 10^3 \text{ mm}^3 \Rightarrow \text{Beams OK}$. The yield strength of the beams may be reduced to 329 MPa in the FEM model to check that the capacity design proscription is adequate.

Columns: must satisfy §11.8.3b) by ensuring that they can withstand full gravity loads combined with member forces induced at 1.2 times the ultimate flexural capacity of the beam-to-column connectors. The later is calculated (see §0 for connector strength values):

$$M_f = 1.2 \cdot SF_c \cdot M_{c,max} = 1.2 \cdot 2.36 \cdot \left(\frac{4.29 \text{ kNm} + 3.73 \text{ kNm}}{2} \right) = 11.32 \text{ kNm}$$

The moment induced by the base-plates will be:

$$M_{p,bpl} = 4.6 \text{ kNm}$$

Which is lower than the moment imposed by the connectors.

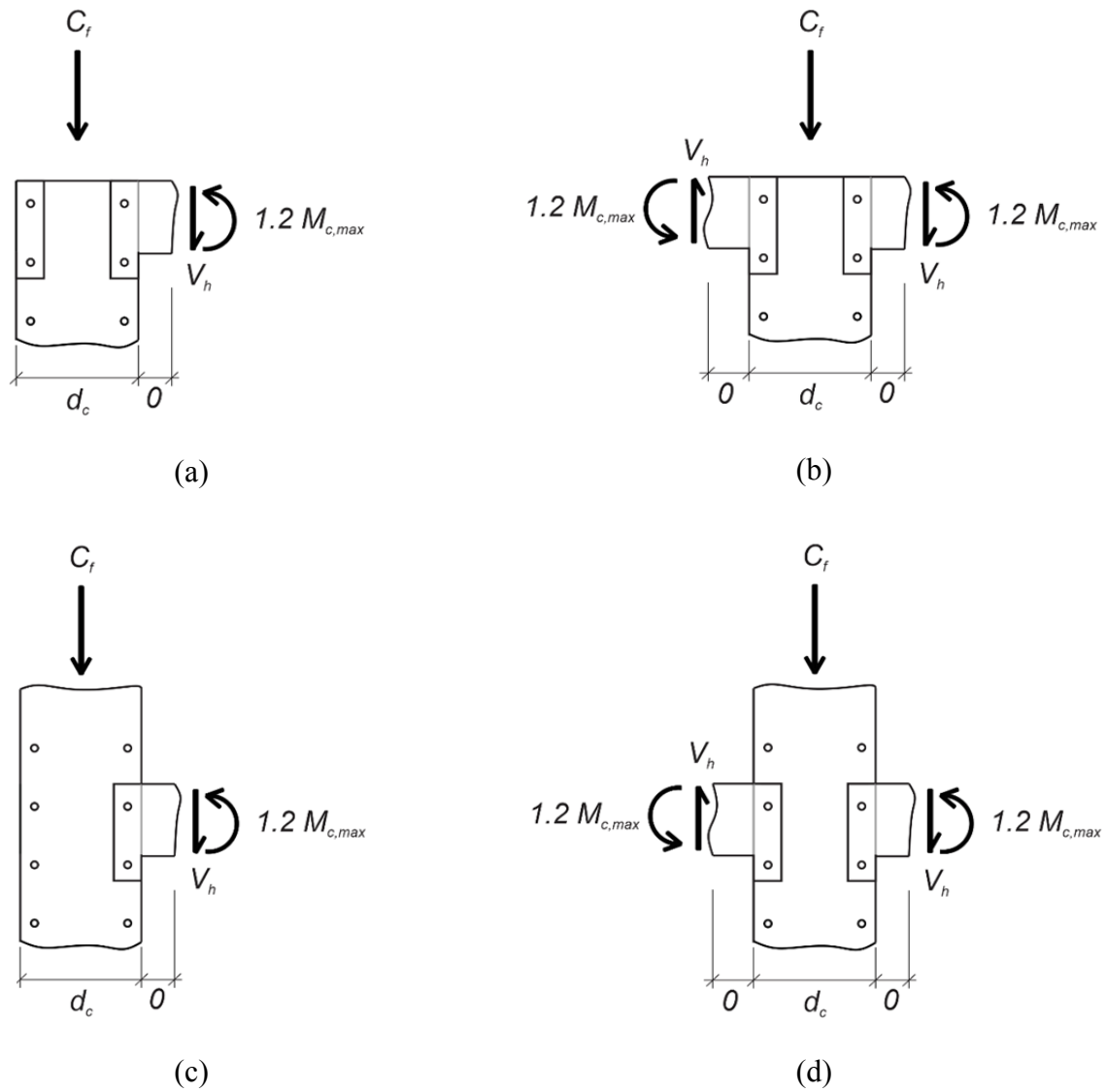


Figure 4-16 : Actions on joints of the rack frame a) Top exterior joint b) Top interior joint, c) Middle or bottom exterior joint d) Middle or bottom interior joint.

Table 4-5: Column Design Moments

Level	Exterior		Interior	
	-	kNm	-	kNm
Top	$1.2M_{c,max}$	11.32	$2(1.2M_{c,max}/2) = 1.2M_{c,max}$	11.32
Middle	$0.5(1.2M_{c,max}) = 0.6M_{c,max}$	5.66	$1.2M_{c,max}$	11.32
Base	$1.2M_{bpl}$	5.52	$1.2M_{bpl}$	5.52

Table 4-6: Column gravity loads

	Exterior	Interior
Level	kN	kN
Top	7.4	14.7
Middle	14.7	29.4
Base	22.0	44.1

The same boxed channel section is used along the total height of all the columns, thus only the most critical lower level interior column need be checked. Columns are channels resisting bending moments and axial loads and must thus satisfy S16 §13.8.3. Flexural torsional buckling need not be considered because boxed column. The column is verified for cross-sectional strength and in-plane buckling:

Cross-sectional strength:

$$C_r = \frac{\phi A F_y}{(1 + \lambda^{2n})^{\frac{1}{n}}} = \frac{(1.0)(2 \cdot 892 \text{ mm}^2)(345 \text{ MPa})}{(1 + 0)^{\frac{1}{1.34}}} = 615 \text{ kN}$$

$$M_r = \phi Z F_y = (1.0)(68810 \text{ mm}^3)(345 \text{ MPa}) = 23.74 \text{ kNm (becomes Class 2 when boxed)}$$

$$Z \cong [2bd^2 - (2b - 2w)(d - 2t)^2]/4 = 68810 \text{ mm}^2$$

$$U_{1x} = \frac{\omega_1}{1 - \frac{C_f}{C_e}} = \frac{0.4}{1 - \frac{44.1 \text{ kN}}{2025 \text{ kN}}} = 0.41 \leq 1.0 \Rightarrow U_{1x} = 1.0$$

$$\omega_1 = 0.6 - 0.4\kappa = 0.6 - 0.4 \frac{5.52}{11.32} = 0.4$$

$$C_e = \frac{\pi^2 EI}{L^2} = \frac{\pi^2 (200\,000 \text{ MPa}) \cdot 2 \cdot (1.53 \times 10^6 \text{ mm}^4)}{(1727)^2} = 2025 \text{ kN}$$

$$C_f/C_r + U_1 (M_f/M_r) = 44.1 \text{ kN}/615 \text{ kN} + 11.32 \text{ kNm}/23.74 \text{ kNm} = 0.55$$

In-plane buckling:

$$C_r = \frac{\phi A F_y}{(1 + \lambda^{2n})^{\frac{1}{n}}} = \frac{(1.0)(2 \cdot 892 \text{ mm}^2)(345 \text{ MPa})}{(1 + 0.55^{2 \cdot 1.34})^{\frac{1}{1.34}}} = 536 \text{ kN}$$

$$\lambda = \sqrt{F_y/F_e} = 0.55, F_e = \frac{\pi^2 E}{(KL/r_x)^2} = \frac{\pi^2 (200\,000 \text{ MPa})}{(1 \cdot 1727/41.4)^2} = 1134 \text{ MPa}$$

$$M_r = 23.74$$

$$U_{1x} = 1.0 \text{ (unbraced)}$$

$$C_f/C_r + U_1 (M_f/M_r) = 44.1 \text{ kN}/536.2 \text{ kN} + (11.32 \text{ kNm}/23.74 \text{ kNm}) = 0.56 < 1 \Rightarrow \textbf{OK}$$

In-plane buckling controls; the yield strength of the column may be reduced to 216 MPa in the FEM model to check that the capacity design proscription is adequate.

5. Check minimum lateral resistance

In accordance with S16 Annex N §11.5.4 the frame must have a minimum lateral resistance at every level to resist P-delta effects at twice the anticipated displacements, i.e. $2\sum C_f \Delta/h_s$. The resistance at each level is evaluated by performing a pushover of the rack (triangular pattern with largest load at top level), without P-delta effects, and checking that the shear at each level, when the rack reaches twice the design displacement, is larger than $V_{r,min}$:

Table 4-7: Calculation of minimum lateral resistance.

Level	h_s	$\sum C_f$	δ	$\delta_i - \delta_{i-1} = \Delta_{inter}$	$V_{r,min}$	V_r	
-	m	kN	m	m	kN	kN	
3	1.524	88.1	0.239	0.067	7.76	42.1	OK
2	1.524	176.1	0.172	0.077	17.7	70.8	OK
1	1.727	264.2	0.095	0.095	29.1	86.1	OK

4.3.3 Design of 6-level, 6-bay rack in Montreal site E

During design iterations it was found that a rack flexible enough to achieve the deformation limits of S16 Annex N §11.7 in Montreal site E conditions will not have sufficient lateral resistance to satisfy with S16 Annex N §11.5.4. i.e. strength to resist P-delta controls design and not deformation.

The following sections and connectors were chosen:

- Beams : C100x7 ($1.53 \times 10^6 \text{ mm}^4$), $F_{yb} = 297 \text{ MPa}$
- Columns : C100x9 ($1.77 \times 10^6 \text{ mm}^4$) simple channel at all levels, $F_{yc} = 322 \text{ MPa}$
- Connectors : AC175 strength scaled by 1.85 (AC200 was found excessively strong)
- Base-plates : $t_p = 2.7 \text{ mm}$ (all other dimensions as seen in §4.3.1.3)

1. Applicability

The total height of the rack is $10.056 \text{ m} > 7.6 \text{ m} \Rightarrow$ This rack would not be admissible for displacement-based design under current proposed S16 Annex N provisions. The design check is never-the-less carried-out.

2. Deformation limits

Since there is no reduction for out-of-plumb erection: $\Delta_d = 0.05 \text{ rad}$

The connector rotation limit is calculated with eq. (4-6)

$$\Rightarrow \theta_d = (0.11 \text{ rad} - 0.01 \text{ rad})/2 = 0.05 \text{ rad}$$

Pushover (triangular pattern, maximum load at top) is performed and it is found that rotation controls (see Figure 4-17):

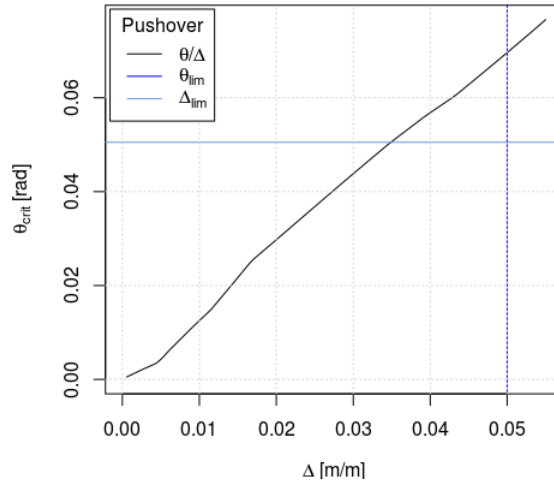


Figure 4-17: Drift vs. rotation relationship issue from non-linear pushover of a 6-level rack.

The design drift is thus: $\Delta_d = 0.035 \text{ rad}$, and the design rotation is: $\theta_d = 0.05 \text{ rad}$.

2. *Verification that deformation limits are satisfied given connector and base-plate properties*

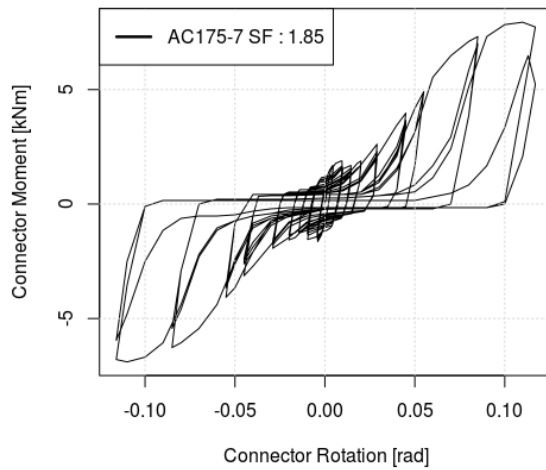


Figure 4-18: Moment rotation behaviour determined from physical unit tests and strength scaled by a factor of 1.85.

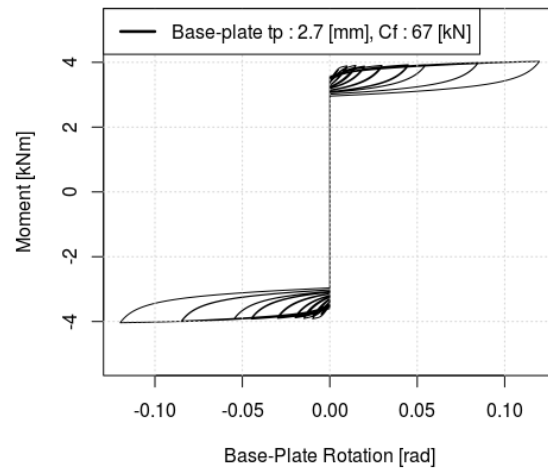


Figure 4-19: Moment-rotation behaviour as determined from FEM tests under compressive load of $C_f = 66.7 \text{ kN}$.

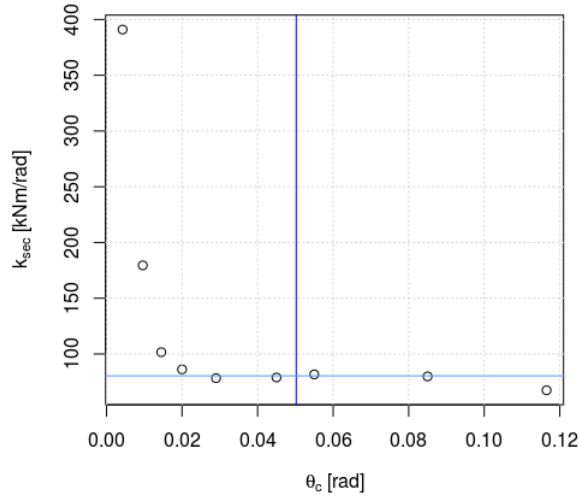


Figure 4-20: 1st pass secant stiffness of AC175 connector strength scaled by a factor of 1.85.

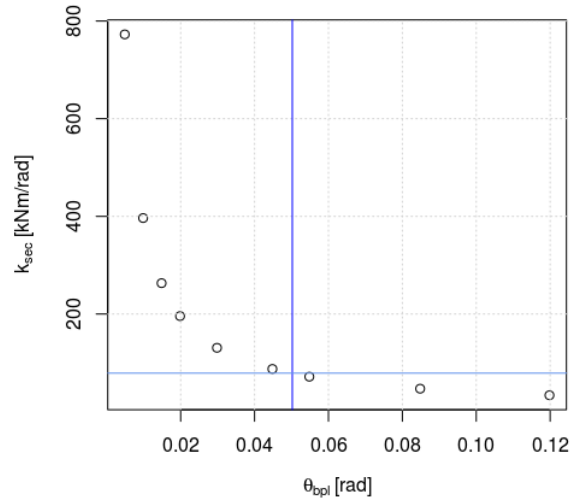


Figure 4-21: 1st pass secant stiffness of 2.7mm base-plates under compressive load of $C_f = 66.7$ kN.

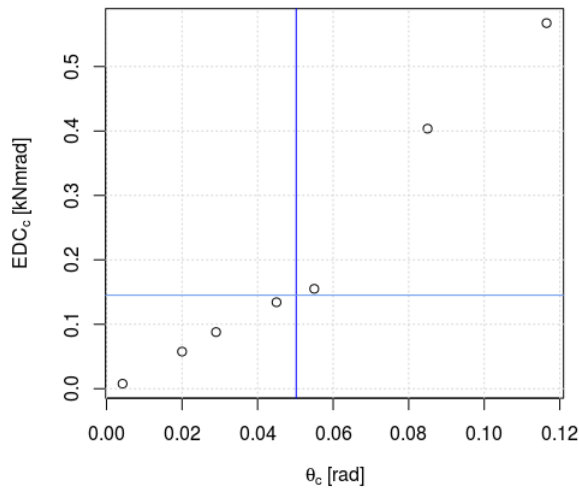


Figure 4-22: 1st pass energy dissipation of AC175 connector calculated from physical tests and strength scaled by a factor of 1.85.

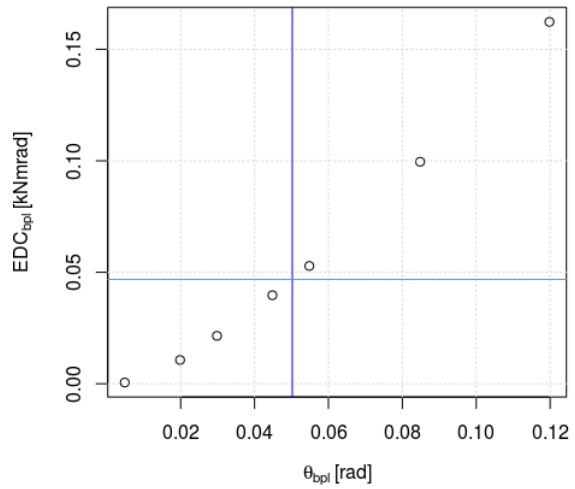


Figure 4-23: 1st pass energy dissipation of 2.7mm base-plates under compressive load of $C_f = 66.7$ kN.

The secant stiffness and EDC of the base-plates and the scaled AC175 connectors is interpolated at the design rotation of 0.035 rads from Figure 4-20 & Figure 4-21.

The effective mass is found from the generalized displacement using the deformation profile already available from the pushover used to determine deformation limits.

Table 4-8: Finding the generalised displacement coordinante of a 6-level rack.

Level	h_x	δ_i / δ_{\max}	$(\delta_i / \delta_{\max})^2$
-	m	-	-
6	10.056	1	1
5	8.38	SxS63	0.928
4	6.704	0.885	0.784
3	5.028	0.746	0.556
2	3.352	0.544	0.296
1	1.676	0.289	0.083
Σ		4.427	3.647

From eq. (4-8) & (4-9):

$$\frac{\delta_{gen}}{\delta_{max}} = 3.647/4.427 = 0.82$$

$$m_{eff} = 36562 \text{ kg}$$

From eigenvalue analysis of the rack with connectors and base-plates at respective stiffness's of 80.4 kNm/rad and 79.0 kNm/rad, the rack's effective period is:

$$T_{eff} = 3.85 \text{ s}$$

The effective lateral stiffness according to eq. (4-7) is:

$$36562 \text{ kg} \cdot \left(\frac{2\pi}{3.85} \right)^2 = 97.1 \text{ kN/m}$$

The rack's effective lateral stiffness is then reduced to account for P-delta, from eq. (4-10) :

$$k_{eff,rack,red.} = 97.1 - (36562 \cdot 9.81)/(0.82 \cdot 10.056) = 53.8 \text{ kN/m}$$

The augmented fundamental period is thus: $T_{eff,aug.} = 2\pi \sqrt{\frac{36562}{53.8}} = 5.18 \text{ s}$

The design displacement of the equivalent SDOF can be calculated from the design drift: $\delta_d = \Delta_d 0.82 h_n = (0.035)(0.82)(10.058) = 0.287 \text{ m}$.

The effective damping is calculated from eq. (4-1) :

$$\beta_{eff} = \frac{N_{bpl}EDC_{bpl} + N_cEDC_c}{2\pi \cdot k_{eff,rack,red.} \cdot \delta_d^2} + 0.03 = 0.42$$

The 5% damped displacement derived from NBCC spectral values is (see eq. (4-2)). Intermediate displacement spectra values should be interpolated between ordinates :

$$S_{d5\%} = S \cdot g \cdot \frac{T_{eff,aug}^2}{4\pi^2} = 0.0384 \cdot 9.8065 \cdot \frac{(5.18)^2}{4\pi^2} = 0.26$$

The damping coefficient applied to the 5% displacement spectra is calculated from eq. (4-3):

$$R_\beta = [0.1 / (0.05 + \beta_{eff})]^{0.5} = 0.46$$

The effective damped displacement (of the SDOF) in Vancouver site C is:

$$S_{d\beta} = S_{d5\%} \cdot R_\beta = 0.116 \text{ m} < \delta_d = 0.287 \text{ m} \Rightarrow \text{OK}$$

The real damped displacement is slightly lower than 0.116 m because successive iterations of displacement-based analysis using more realistic initial values of design drift (and/or rotation) will reduce the displacement. However, the displacement found at the end of the initial iteration is close to the final value; see as an example Table 4-14.

3. Check that beams and columns respect capacity design (cede after connectors and base-plates)

Beams: must satisfy S16 Annex N §11.8.4. Assuming they are sufficiently restrained along their length such that yielding is the only limit state which must be checked $S_x > (8.9\text{kNm})/(1.0)/(345 \text{ MPa}) = 25.8 \times 10^3 \text{ mm}^3 > S_{x,C100 \times 7} = 30.0 \times 10^3 \text{ mm}^3 \Rightarrow$ **Beams OK**. The yield strength of the beams may be reduced to 297 MPa in the FEM model to check that the capacity design proscription is adequate.

Columns: must satisfy §11.8.3b), see §0 for connector strength values:

$$M_f = 1.2 \cdot SF_c \cdot M_{c,max} = 1.2 \cdot 1.85 \cdot \left(\frac{4.29 \text{ kNm} + 3.73 \text{ kNm}}{2} \right) = 8.9 \text{ kNm}$$

$$M_{p,bpl} = 3.8 \text{ kNm}$$

Table 4-9: Column Design Moments.

	Exterior		Interior	
Level	-	kNm		kNm
Top	$1.2M_{c,max}$	8.9	$2(1.2M_{c,max}/2)$	8.9
Intermediate	$0.5(1.2M_{c,max})$	4.45	$1.2M_{c,max}$	8.9
Bottom	$1.2M_{bpl}$	4.56	$1.2M_{bpl}$	4.56

Table 4-10: Column gravity loads.

	Exterior	Interior
Level	kN	kN
6	5.6	11.1
5	11.1	22.2
4	16.7	33.4
3	22.2	44.5
2	27.8	55.6
1	33.4	66.7

Only the most critical lower level interior column need be checked because the same channel section is used along the total height of the columns, (see also Figure 4-16) :

Cross-sectional strength S16 §13.8.3 (a):

$$C_r = \frac{\phi A F_y}{(1 + \lambda^{2n})^{\frac{1}{n}}} = \frac{(1.0)(1190 \text{ mm}^2)(345 \text{ MPa})}{(1 + 0)^{\frac{1}{1.34}}} = 411 \text{ kN}$$

$$M_r = \phi S F_y = (1.0)(34600 \text{ mm}^3)(345 \text{ MPa}) = 11.9 \text{ kNm (simple channel is class 3)}$$

$$U_{1x} = \frac{\omega_1}{1 - \frac{C_f}{C_e}} = \frac{0.4}{1 - \frac{66.7 \text{ kN}}{1243 \text{ kN}}} = 0.43 \leq 1.0 \Rightarrow U_{1x} = 1.0$$

$$\omega_1 = 0.6 - 0.4\kappa = 0.6 - 0.4 \frac{4.56}{8.9} = 0.4, C_e = \frac{\pi^2 EI}{L^2} = \frac{\pi^2 (200\,000 \text{ MPa}) \cdot (1.77 \times 10^6 \text{ mm}^4)}{(1676)^2} = 1243 \text{ kN}$$

$$C_f/C_r + U_1 (M_f/M_r) = 66.7 \text{ kN}/411 \text{ kN} + (8.9 \text{ kNm}/11.9 \text{ kNm}) = 0.91$$

In-plane buckling S16 §13.8.3 (b)::

$$C_r = \frac{\phi A F_y}{(1 + \lambda^{2n})^{\frac{1}{n}}} = \frac{(1.0)(1190 \text{ mm}^2)(345 \text{ MPa})}{(1 + 0.582^{2 \cdot 1.34})^{\frac{1}{1.34}}} = 352 \text{ kN}$$

$$\lambda = \sqrt{F_y/F_e}, F_{ex} = \frac{\pi^2 E}{(KL/r_x)^2} = \frac{\pi^2 (200\,000 \text{ MPa})}{(1 \cdot 1676/38.5)^2} = 1042 \text{ MPa}$$

$$M_r = 11.9 \text{ kNm}, U_{1x} = 1.0 \text{ (unbraced)}$$

$$C_f/C_r + U_1 (M_f/M_r) = 66.7 \text{ kN}/351 \text{ kN} + 1(8.9 \text{ kNm}/11.9 \text{ kNm}) = 0.93 < 1 \Rightarrow \text{OK}$$

Out-of-plane buckling (assuming weak-axis bracing at mid-height of column) :

C_r according to S16 §13.3 (x and y axes are inversed):

$$F_{ey} = \frac{\pi^2 E}{(KL/r_y)^2} = \frac{\pi^2 (200\,000 \text{ MPa})}{(1 \cdot 1676/2/11.5)^2} = 371 \text{ kN}$$

$$F_{ez} = \left(\frac{\pi^2 E C_w}{(KL)^2} + GJ \right) \frac{1}{A \bar{r}_o^2} = 1020 \text{ kN}, \text{ with } KL = 1676 \text{ mm}$$

$$\Omega = 0.25$$

$$F_{exz} = f(F_{ex}, F_{ez}) = 552 \text{ kN} \Rightarrow \lambda = \sqrt{F_y/F_{ey}} = \sqrt{345/371} = 0.96 \Rightarrow C_r = 255 \text{ kN}$$

M_r according to S16 §13.6 (b) :

$$\omega_2 = \frac{4M_{max}}{\sqrt{M_{max}^2 + 4M_a^2 + 7M_b^2 + 4M_c^2}} = \frac{4 \cdot 8.89}{\sqrt{8.89^2 + 4 \cdot 5.54^2 + 7 \cdot 2.17^2 + 4 \cdot 1.20^2}} = 2.3$$

$$M_u = \frac{\omega_2 \pi}{L} \sqrt{EI_y GJ + \left(\frac{\pi E}{L} \right)^2 I_y C_w} = 39.66 \text{ kNm}, \quad L = 1676 \text{ mm}$$

$$M_y = (30 \times 10^3 \text{ mm}^3)(345 \text{ MPa}) = 10.35 \text{ kNm}$$

$$\S i): M_r = 11.03 \text{ kNm} \geq M_y \Rightarrow M_r = 10.35 \text{ kNm}$$

$$U_{1x} = 1.0 \text{ (unbraced)}$$

$$C_f/C_r + U_1 (M_f/M_r) = 66.7 \text{ kN}/255 \text{ kN} + (8.9 \text{ kNm}/10.35 \text{ kNm}) = 1.16 \Rightarrow \text{governs}$$

Because the FEM model used in NLTH cannot reproduce this mode of instability. The yield strength has been adjusted to be a close-design for in-plane buckling of the column \Rightarrow reduced to 322 MPa.

4. Check minimum lateral resistance

The rack is then checked for minimum lateral resistance in accordance with S16 Annex N §11.5.4 which stipulates that, at every level, the frame shall have a minimum lateral resistance equal to $2\Sigma C_f \Delta/h_s$. Pushover is performed to twice the design displacement (with and without P-

delta effects) to establish the lateral resistance at each level => **Strength is found to be sufficient at every level** (see Table 4-11).

Table 4-11 : Minimum lateral resistance.

Level	h_s	$\sum C_f$	δ	$\delta_i - \delta_{i-1} = \Delta_{inter}$	$V_{r,min}$	V_r	
-	m	kN	m	m	kN	kN	
6	1.676	66.7	0.349	0.013	1.03	13.75	OK
5	1.676	133.5	0.336	0.027	4.33	25.21	OK
4	1.676	200.2	0.308	0.049	11.61	34.38	OK
3	1.676	266.9	0.26	0.07	22.44	41.25	OK
2	1.676	333.6	0.189	0.089	35.37	45.84	OK
1	1.676	400.4	0.1	0.1	47.98	48.13	OK

4.4 Summary of design of prototype racks

In examining Table 4-12, design is governed by deformation limits in Vancouver and by minimum lateral resistance requirements in Montreal. For this reason only one design is necessary for both Montreal sites C & E. In Vancouver, the 4-level rack, because of its greater mass (and consequently longer period), needed weaker connectors and base-plates than did the 3-level rack. Increasing column inertia, either by increasing the section or doubling (boxing) the column had a significant impact on displacements in design. In general the strength of the column was mainly taken-up by the moment imposed by the connectors on the columns and not by the compressive load, which is why, when the column was doubled, it was usually doubled at every level.

Table 4-12: Sections and section inertias (I_b & I_c), material yield limits (F_{yb} & F_{yc}), connectors, scaling factors (SF_c) and base-plate thickness (t_p).

		Beam	I_b	F_{yb}	Column	I_c	F_{yc}	Boxed Levels	Connector	SF_c	t_p
		-	10^6 mm^4	MPa	-	10^6 mm^4	MPa	-	-	-	mm
M tl C & E	3	C75x5	0.635	270	C100x7	1.53	170	0	AC175	0.73	1
	4	C75x5	0.635	251	C100x7	1.53	193	0	AC175	0.87	1
	5	C100x7	1.53	212	C100x7	1.53	281	0	AC175	1.32	1
	6	C100x7	1.53	297	C100x9	1.77	322	0	AC175	1.85	2.7
V a n C	3	C100x9	1.77	329	C100x7	1.53	216	3	AC175	2.36	5.5
	4	C100x7	1.53	328	C100x9	1.77	327	0	AC175	2.04	5.2
	5	C100x7	1.53	233	C100x7	1.53	302	0	AC200	0.5	2.3
	6	C100x7	1.53	259	C100x7	1.53	329	1	AC200	0.557	2
V a n E	3	C150x12	5.36	328	C100x11	1.91	328	3	AC175	4.8	9.3
	4	C150x12	5.36	276	C100x9	1.77	303	4	AC175	4.04	8.8
	5	C150x12	5.36	336	C100x11	1.91	341	5	AC200	1.7	9.4
	6	C150x16	6.21	321	C130x13	3.66	249	6	AC200	1.88	9.1

For 3 and 4 level racks drift was the criteria that controlled design (see Table 4-13), while for 5 and 6 level racks it was the rotation of the critical connector. Except for the racks designed for Montreal it was possible to have base-plates with a stiffness similar to the connectors. In general, due to their relatively fat hysteresis, the base-plates dissipated more energy (per joint) than did

the connectors, but given that they were out-numbered by more than three-fold for all configurations of rack their influence is diluted.

Table 4-13: Deformation limits (θ_{lim} & Δ_{lim}), design deformations (θ_d & Δ_d) and corresponding connector and base-plate and secant stiffness (k_c & k_{bpl}) and energy dissipated by cycle (EDC_c & EDC_{bpl}).

		θ_{lim}	Δ_{lim}	Δ_d	θ_d	k_c	k_{bpl}	EDC_c	EDC_{bpl}
		rad	m/m	m/m	rad	kNm/rad	kNm/rad	kNmrad	kNmrad
Mtl C	3	0.041	0.050	0.018	0.016	38.5	146.7	0.018	0.000
	4	0.044	0.050	0.011	0.010	78.3	225.4	0.013	0.000
	5	0.050	0.050	0.007	0.008	183.3	422.2	0.013	0.000
	6	0.050	0.050	0.006	0.006	338.3	718.5	0.012	0.001
Mtl E	3	0.041	0.050	0.029	0.027	31.6	88.0	0.032	0.001
	4	0.044	0.050	0.021	0.021	40.1	112.8	0.029	0.001
	5	0.050	0.050	0.014	0.020	61.4	144.3	0.042	0.001
	6	0.050	0.050	0.012	0.017	95.5	238.4	0.047	0.009
Van C	3	0.050	0.050	0.050	0.047	101.3	102.2	0.176	0.238
	4	0.050	0.050	0.050	0.051	88.8	89.8	0.161	0.232
	5	0.050	0.050	0.042	0.051	64.6	64.0	0.094	0.032
	6	0.050	0.050	0.039	0.051	71.9	73.4	0.105	0.023
Van E	3	0.053	0.050	0.050	0.049	207.6	204.8	0.369	0.889
	4	0.054	0.050	0.050	0.052	176.9	176.6	0.327	0.864
	5	0.054	0.050	0.050	0.054	220.0	202.4	0.361	1.037
	6	0.054	0.050	0.049	0.054	243.1	243.5	0.408	1.188

The effective fundamental period, T_{eff} , of the substitute structure (before correction for P-delta) varied from a low of 1.5 s in a 3-level racks configuration to over 4 s in a 6-level configuration (see Table 4-15). Due to the effective damping, β_{eff} , the 5% damped displacement spectrum could be reduced by between 40-55%.

Since the design of racks for Montreal sites C & E was governed by minimum lateral resistance (Annex N 10.5.4) $\Delta_d \neq \Delta_{lim}$ nor does $\theta_d \neq \theta_{lim}$ in Table 4-15. The displacement of the rack is found by iterations using $S_{d\beta}$ as the design displacement (via drift) at the start of each iteration as illustrated for the 3-level rack in Montreal site C in Table 4-14 until $S_{d\beta} = \delta_d$.

Table 4-14: Iterations to converge on displacement of 3-level rack in Montreal Site C.

Itr.	Δ_d	θ_d	k_c	k_{bpl}	EDC_c	EDC_{bpl}	T_{eff}	k_{eff}	$k_{eff,red.}$	$T_{eff,aug.}$	β_{eff}	$S_{d\beta}$	δ_d
1	0.0435	0.0409	31.1	58.4	0.048	0.002	3.26	88.9	26.7	5.95	0.42	64	164
2	0.0184	0.0167	37.6	140.5	0.019	0.000	2.70	127.4	65.9	3.75	0.37	66	69
3	0.0176	0.0159	38.5	146.7	0.018	0.000	2.66	130.7	69.2	3.66	0.37	66	66

The effective damping values, β_{eff} , found for racks designed to meet minimum lateral resistance criteria are much higher than for racks designed according to displacement-based criteria. This is mainly due to their relatively low lateral stiffness and low expected displacements both of which appear in the denominator of the the effective damping eq. (4-1).

Table 4-15: Effective period (T_{eff}) and lateral stiffness (k_{eff}) of the structure of the substitute SDOF structure, reduced lateral stiffness ($k_{eff,red.}$) and augmented natural period ($T_{eff,aug.}$) to account for P-delta, effective damping (β_{eff}), spectral reduction coefficient for damping (R_β), spectral displacement of the substitute SDOF at 5% and at β ($S_{d5\%}$ & $S_{d\beta}$), design displacement of the SDOF and design displacement of the real structure (δ_d & δ_{tot}).

		T_{eff}	k_{eff}	$k_{eff,red.}$	$T_{eff,aug.}$	β_{eff}	R_β	$S_{d5\%}$	$S_{d\beta}$	δ_d	δ_{top}
		s	kN/m	kN/m	s	-	-	mm	mm	mm	mm
Mtl C	3	2.66	130.7	69.2	3.66	0.37	0.49	134	66	66	84
	4	2.52	144.1	100.5	3.02	0.31	0.52	116	61	59	76
	5	2.23	227.3	184.8	2.47	0.35	0.50	91	45	7	58
	6	2.18	274.5	232.9	2.37	0.32	0.52	86	45	45	58
Mtl E	3	3.05	100.4	38.6	4.92	0.44	0.45	246	111	109	139
	4	3.30	84.5	40.3	4.78	0.49	0.43	256	110	108	141
	5	3.40	103.3	60.1	4.47	0.70	0.36	271	99	99	121
	6	3.37	124.5	81.9	4.15	0.67	0.37	276	103	102	125
Van C	3	2.00	237.7	175.4	2.33	0.23	0.59	319	190	189	239
	4	2.53	145.7	101.1	3.03	0.25	0.57	448	257	257	332
	5	3.58	91.0	46.2	5.03	0.30	0.54	507	272	275	355
	6	4.04	86.0	41.6	5.81	0.35	0.50	608	304	303	387
Van E	3	1.42	473.9	411.6	1.52	0.24	0.59	323	190	190	239
	4	1.78	289.9	245.6	1.94	0.24	0.59	440	258	258	336
	5	2.01	281.3	237.2	2.19	0.22	0.60	522	315	316	415
	6	2.22	273.6	229.5	2.42	0.22	0.61	607	369	371	492

4.5 Summary of force-based designs

In APPENDIX C the equivalent static force method proposed in Annex N is applied to the 3-level, 6-bay rack shown in §4.3.1. Two design iterations are given. The principal commentaries emitted during design are summarised below:

- It is found that in to meet the drift limit in Annex N §11.7 of 0.05 rad a connector scaled to roughly 10 times the strength of the AC175 connector is necessary. This was in part due to the way the stiffness of the connector is defined by Annex N when applying force-based methods. Such a connector would be infeasible.
- Increased connector stiffness also resulted in increased beam and column sections further stiffening the rack and increasing base-shear
- It was found for this particular rack that using NBCC §4.1.8.11. 3)d)v) (softening the rack to get longer periods past the limits of stated in Annex N) did not result in acceptable deflections.
- Because of the way connector stiffness is defined, every connector that passes the rotation limit set out in S16 Annex N §11.7b is automatically qualified to verify the resistance requirement as set out in S16 Annex N §11.8.2.1.1 & §11.9.

4.6 Discussion of preliminary results of NLTH trials

The following paragraphs discuss the first in series of non-linear time history analyses on the 3, 4, 5 & 6 level racks whose displacement based design is summarized in §4.4. It is considered the base-line series because no modifications of geometry have been made, the global out-of-plumb imperfection is zero and no sliding is permitted between beams and columns. Trials varying these parameters are to be examined in future studies. The designed racks are subjected to representative ground motions for Montreal, QC (11 quakes) and Vancouver, BC (33 quakes) sites C & E conditions.

4.6.1 FEM model

The 2D concentrated plasticity model developed in §3.3 which included non-linear material rules of base-plates and connectors calibrated from physical tests as well as geometric non-linearity, was modified for these trials to include :

- Fiber base-plate assemblies (replacing the zero-length elements calibrated in §3.3.1) that adapt strength and stiffness depending on the level of imposed compression and the thickness of the base-plate used. See §D.2.1 as well as APPENDIX E for further details,
- Distributed plasticity columns (fiber columns) which can capture yielding and in-plane buckling. See §D.2.2,
- Elastic beams with fiber ends. See §D.2.3.

Sliding elements (see §3.6.4) remained in the model but were inactive (constraints between pallet and beam nodes) for the analyses discussed in the following paragraphs.

4.6.2 Displacement profiles

Displacement profiles of the racks (at the instant of the peak displacement of the top level) issue from NLTH are illustrated in Figure 4-24, Figure 4-25, Figure 4-26 & Figure 4-27. Three comparison curves are added to the displacement profiles

1. DBD values as indicated in Table 4-15 and found at each level by non-linear pushover,
2. Mean values of peak displacement, σ_{NLTH} , for all records that did not produce a collapse (where collapse is defined as peak value greater than 0.1 rad),
3. Drift profile when the rotations \approx drifts assumption is used (the top level displacement is taken from DBD, see Table 4-15).

Displacement graphs are presented in a windows up to 5% top-level drift.

4.6.2.1 Vancouver C & E

Figure 4-24 & Figure 4-25 show that in all instances, the prediction of peak displacement by DBD is higher than the average displacement of stable racks. Except in the case of the Vancouver site C 5 & 6-level racks which experienced large numbers of collapse, the prediction by DBD is

only surpassed by a handful of non-linear time history analyses. In most cases the racks have deformed in a shape similar to that predicted by DBD.

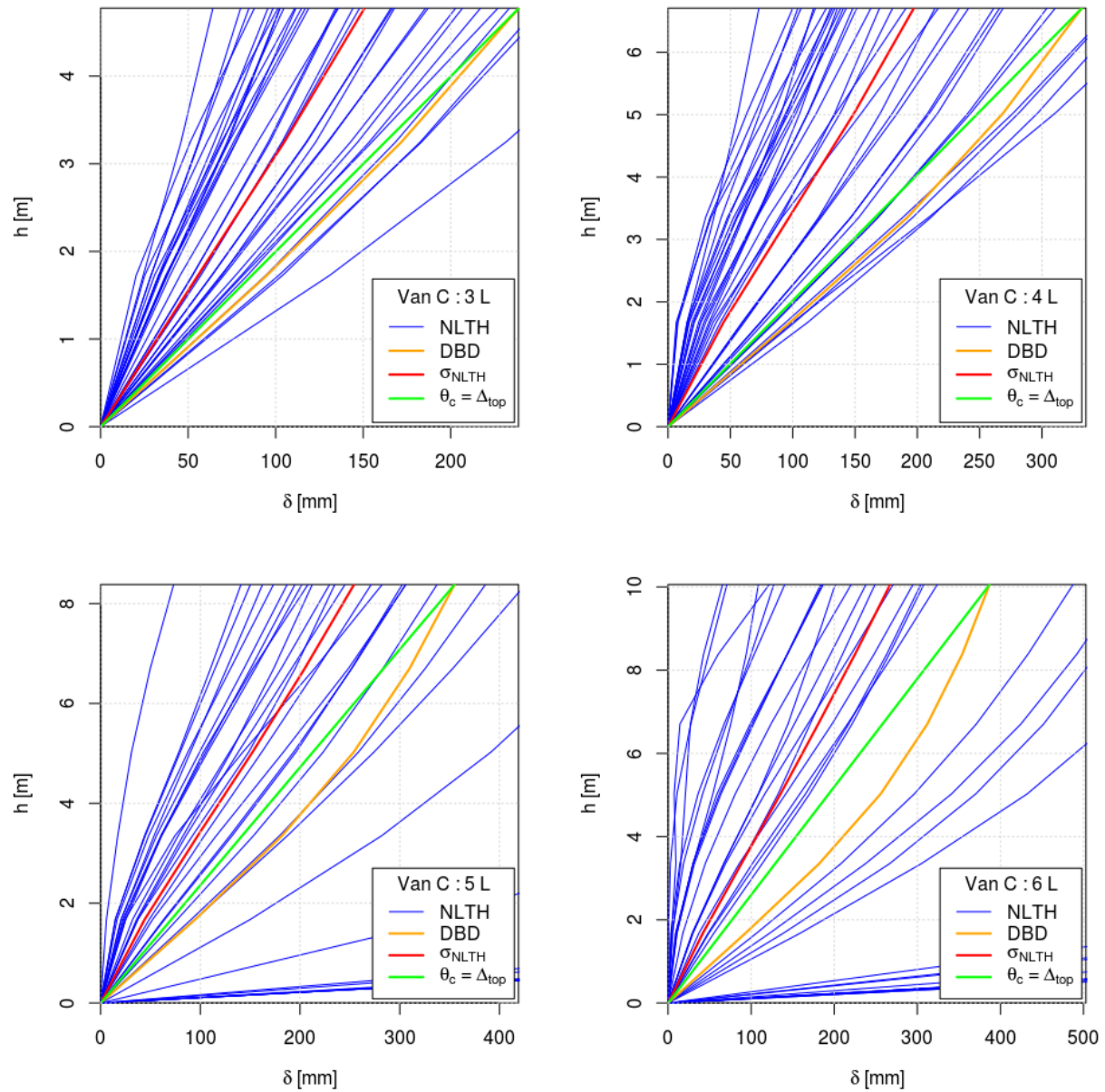


Figure 4-24: Displacement profiles from NLTH for racks located in Vancouver site C.

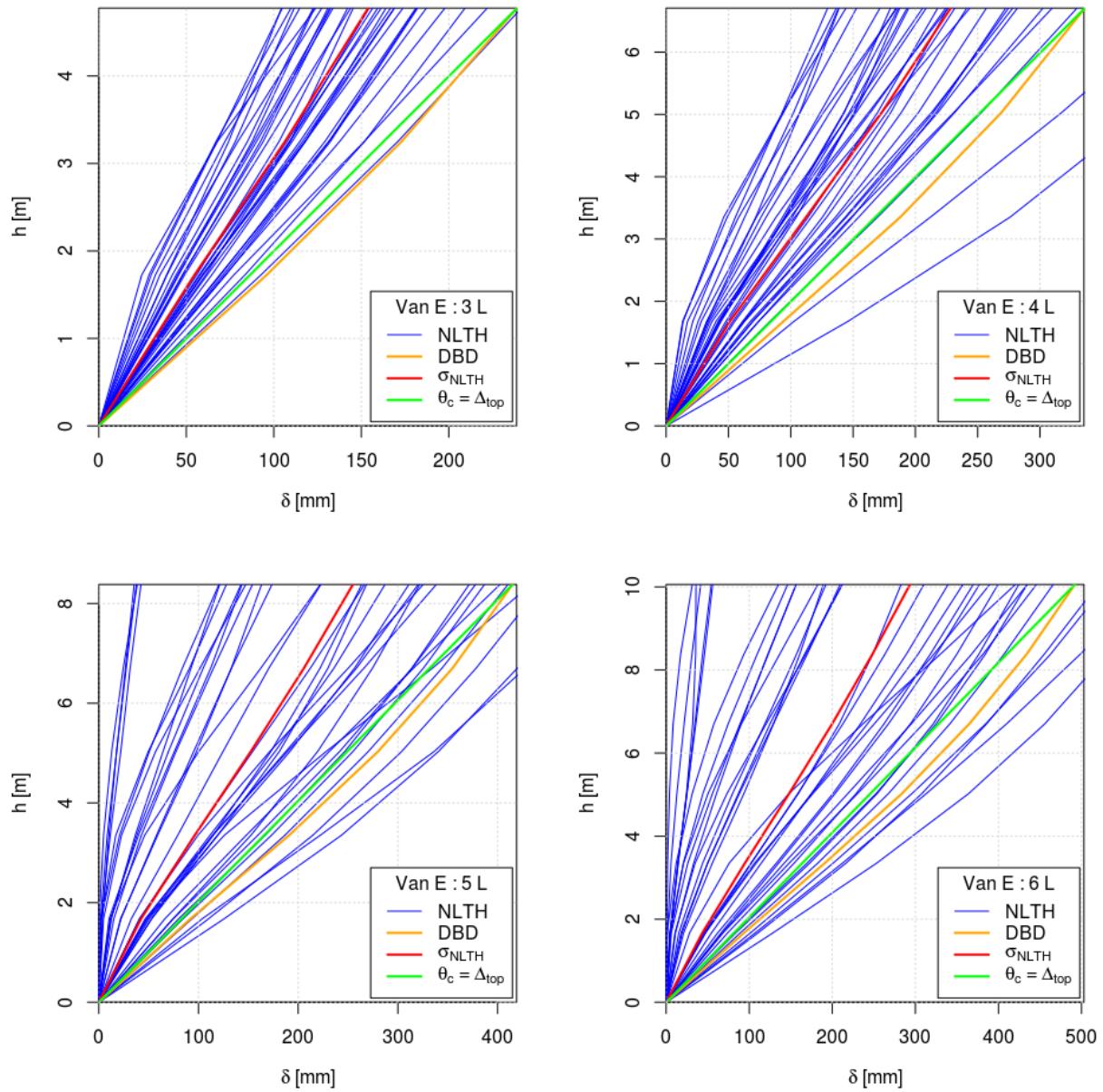


Figure 4-25: Displacement profiles from NLTH for racks located in Vancouver site E.

4.6.2.2 Montreal C & E

The same design of rack is used for Montreal site C & E because the design of these racks is governed by minimum lateral resistance requirements. However, peak drift as computed by DBD differs between the two sites. Peak drift from DBD is as estimated $S_{dB}/0.78$ (see Table 4-15 and discussion in §4.4). Comparison of Figure 4-26 & Figure 4-27 shows (as expected) that drifts are larger in site E conditions than site C conditions. No collapses are recorded, although Figure 4-27

for the 3-level rack has one possible collapse case when in ME7 the rack's peak top-level displacement is 0.078 rad. The displacements predicted by DBD are close to the mean value of displacements.

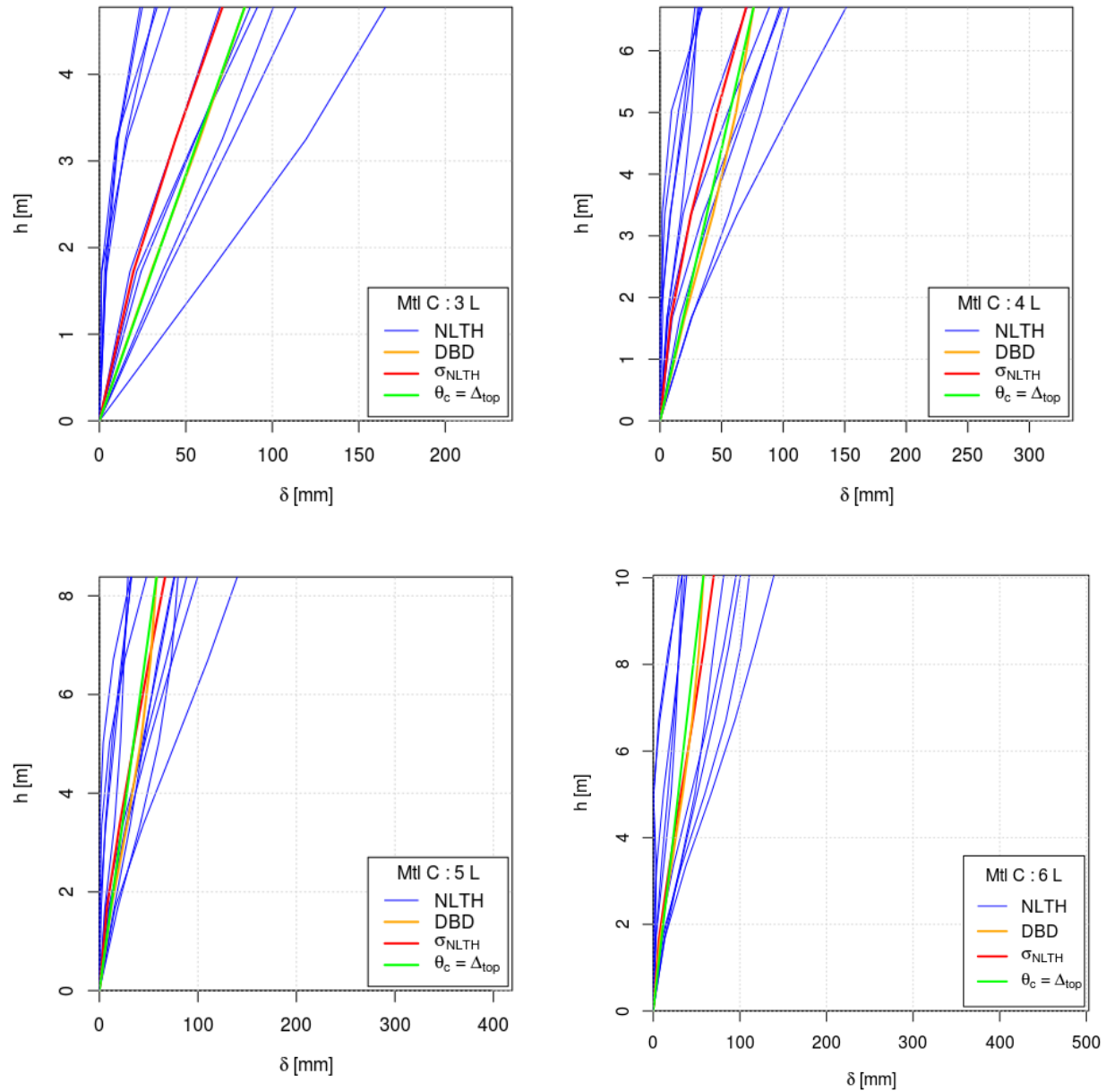


Figure 4-26: Displacement profiles from NLTH for racks located in Montreal site C.

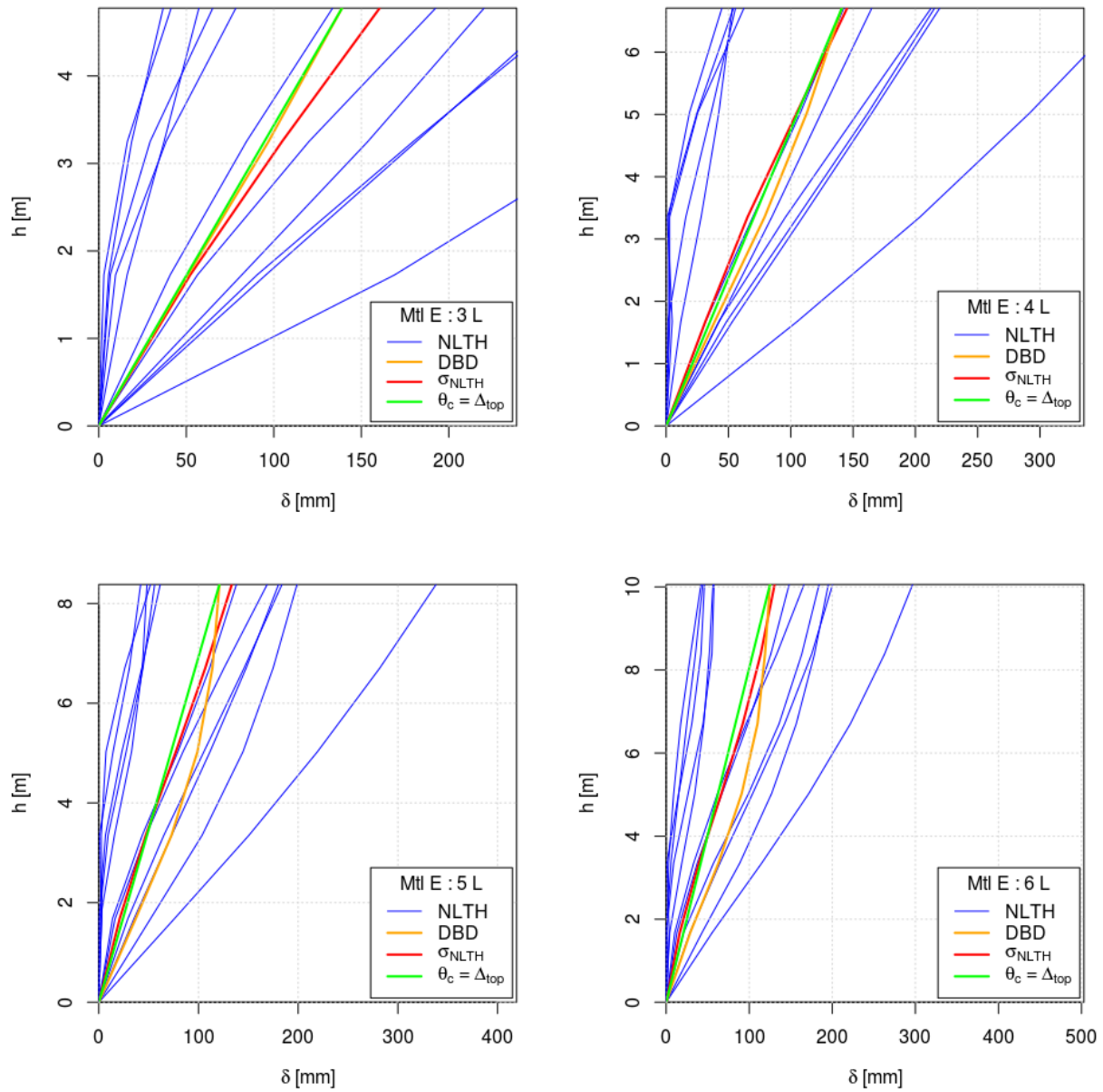


Figure 4-27: Displacement profiles from NLTH for racks located in Montreal site E.

4.6.3 Summary of results DBD vs. NLTH

Figure 4-28 & Figure 4-29 show that among racks that did not collapse those designed for Vancouver generally had displacements over-predicted by displacement-based design in comparison to NLTH. For racks in Montreal over-predictions and under-predictions of drift are about equal.

4.6.3.1 Displacements

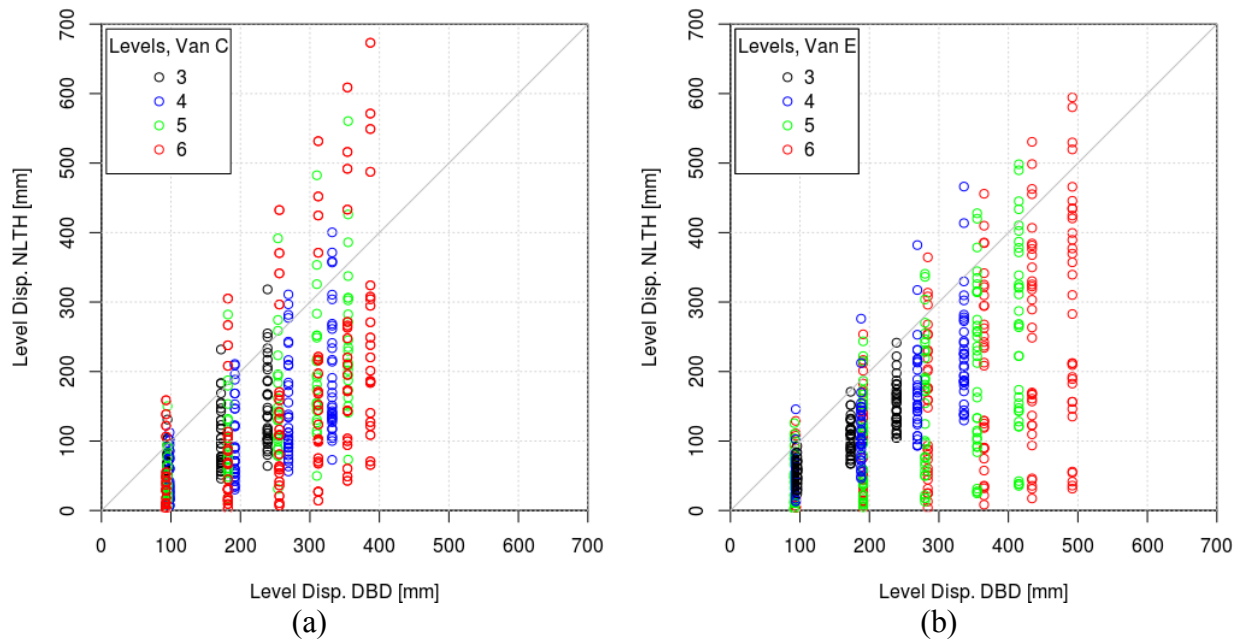


Figure 4-28: Comparison of level drifts from non-linear time history analysis and displacement-based design for racks which did not collapse in a) Vancouver site C and b) Vancouver site E.

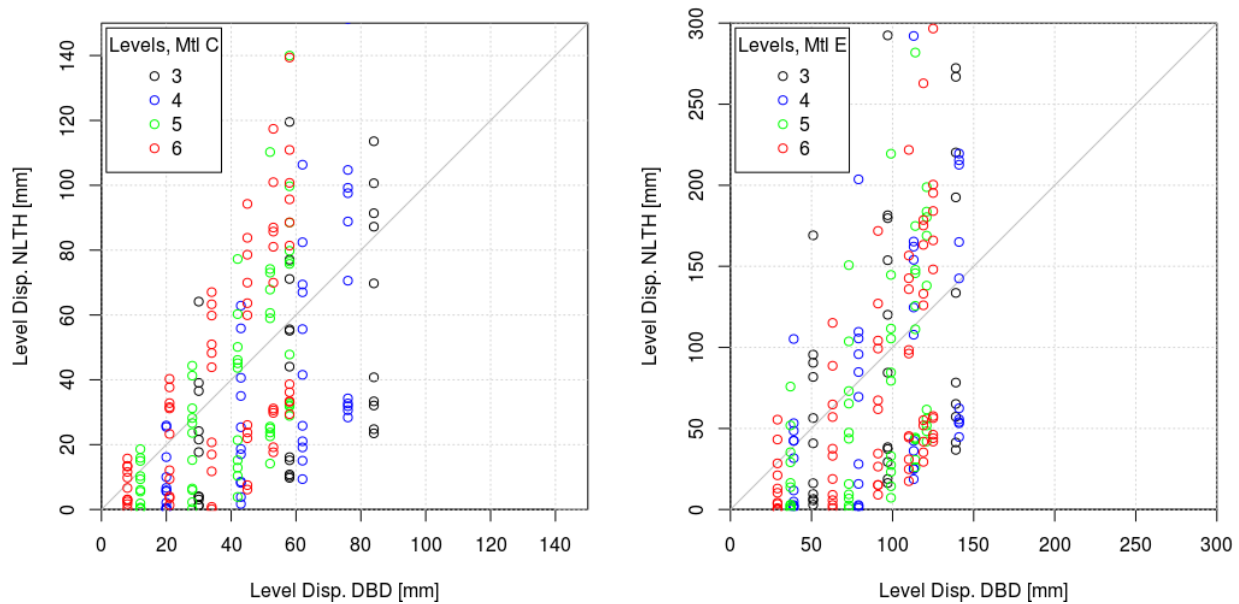


Figure 4-29: Comparison of level drifts from non-linear time history analysis and displacement-based design for racks which did not collapse in a) Montreal site C and b) Montreal site E.

4.6.3.2 Rotations

During design it was assumed that there would be shake-down of the beam-column connectors and that post-quake the gravity loads would act on an essentially pinned-pinned beam (for the purpose of gravity rotation calculations), eqn. (4-6) is repeated:

$$\theta_d = \frac{(\theta_{c,max} - \theta_D)}{2} = \frac{\left(\theta_{c,max} - \frac{Pl^2}{24EI}\right)}{2}$$

For both connectors used in the designs in CHAPTER 4 , $\theta_{c,max} = 0.11 \text{ rad}$. As was the case with the multi-level racks studied in §3.6, rotations are not equal when the rack reaches it's peak displacement.

Table 4-16 shows the gravity rotations assumed during design, θ_D , the peak connector rotation $\theta_{c,max}$ which for these two connectors is always 0.11 rad, the design rotation, θ_d , the initial gravity rotation, $\theta_{D,init}$, as computed at the beginning of the non-linear time history analysis, the average value of absolute connector rotations at the instant of peak displacement, $\mu|\theta_c|$, and the standard deviation of connector rotations at the instant of peak displacement, $\sigma|\theta_c|$, as well as the peak drift of the top level, $|\Delta_{top}|$. Table 4-16 shows that the average rotation undergone by connectors is almost always lower than the peak connector rotation, however, with the addition of the standard deviation it is clear that many connectors are undergoing much larger rotations.

Table 4-16: Summary of expected and calculated connector rotations.

		I_c	θ_D	$\theta_{c,max}$	θ_d	$\theta_{D,init.}$	$\mu \theta_c $	$\sigma \theta_c $	$ \Delta_{top} $
		10^6 mm^4	rad	rad	rad	rad	rad	rad	rad
Mtl C	3	0.635	0.029	0.11	0.041	0.0005	0.041	0.007	0.018
	4	0.635	0.022	0.11	0.044	0.0006	0.031	0.007	0.011
	5	1.53	0.009	0.11	0.05	0.0000	0.018	0.005	0.007
	6	1.53	0.009	0.11	0.05	0.0000	0.016	0.005	0.006
Mtl E	3	0.635	0.029	0.11	0.041	0.0005	0.056	0.021	0.029
	4	0.635	0.022	0.11	0.044	0.0006	0.040	0.013	0.021
	5	1.53	0.009	0.11	0.05	0.0000	0.026	0.011	0.014
	6	1.53	0.009	0.11	0.05	0.0000	0.021	0.009	0.012
Van C	3	1.77	0.010	0.11	0.05	0.0000	0.038	0.011	0.050
	4	1.53	0.009	0.11	0.05	0.0000	0.037	0.012	0.050
	5	1.53	0.009	0.11	0.05	0.0008	0.041	0.013	0.042
	6	1.53	0.009	0.11	0.05	0.0005	0.040	0.019	0.039
Van E	3	5.36	0.003	0.11	0.053	0.0000	0.035	0.006	0.050
	4	5.36	0.003	0.11	0.054	0.0000	0.037	0.011	0.050
	5	5.36	0.003	0.11	0.054	0.0001	0.036	0.017	0.050
	6	6.21	0.002	0.11	0.054	0.0000	0.035	0.017	0.049

Figure 4-30 shows that there is little correlation between the peak drift and the amount of dispersion of connector rotations.

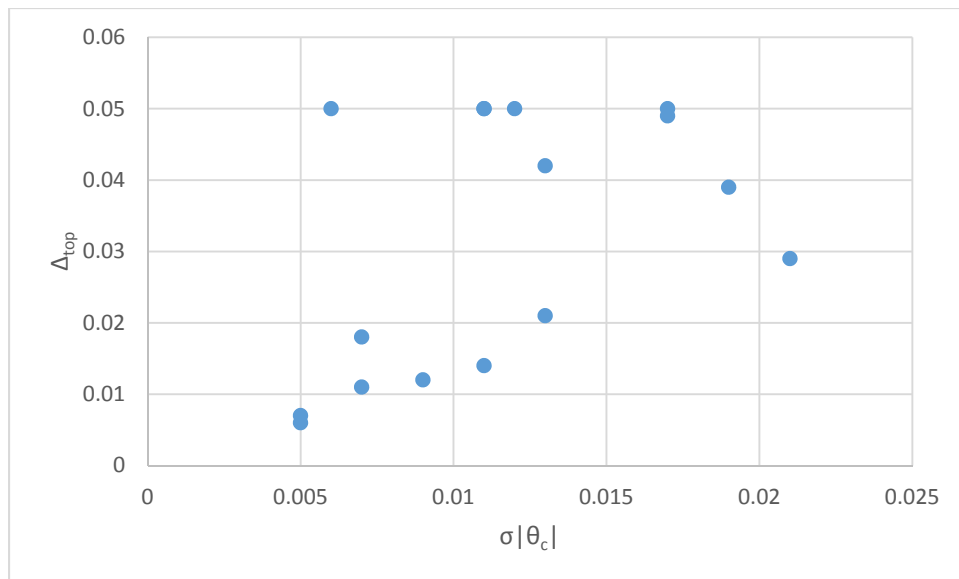


Figure 4-30: Standard deviation in function of peak level drift.

4.6.4 Collapse Case

Collapses were observed for a number of 5 & 6 level racks in Vancouver site C conditions. The collapse of the 5-level rack under the VC30 earthquake was typical of the collapse of these racks. Figure 4-31 shows the full VC30 ground motion as well as close-ups during the times when the strongest shaking and the collapse of a 5-level rack occurs.

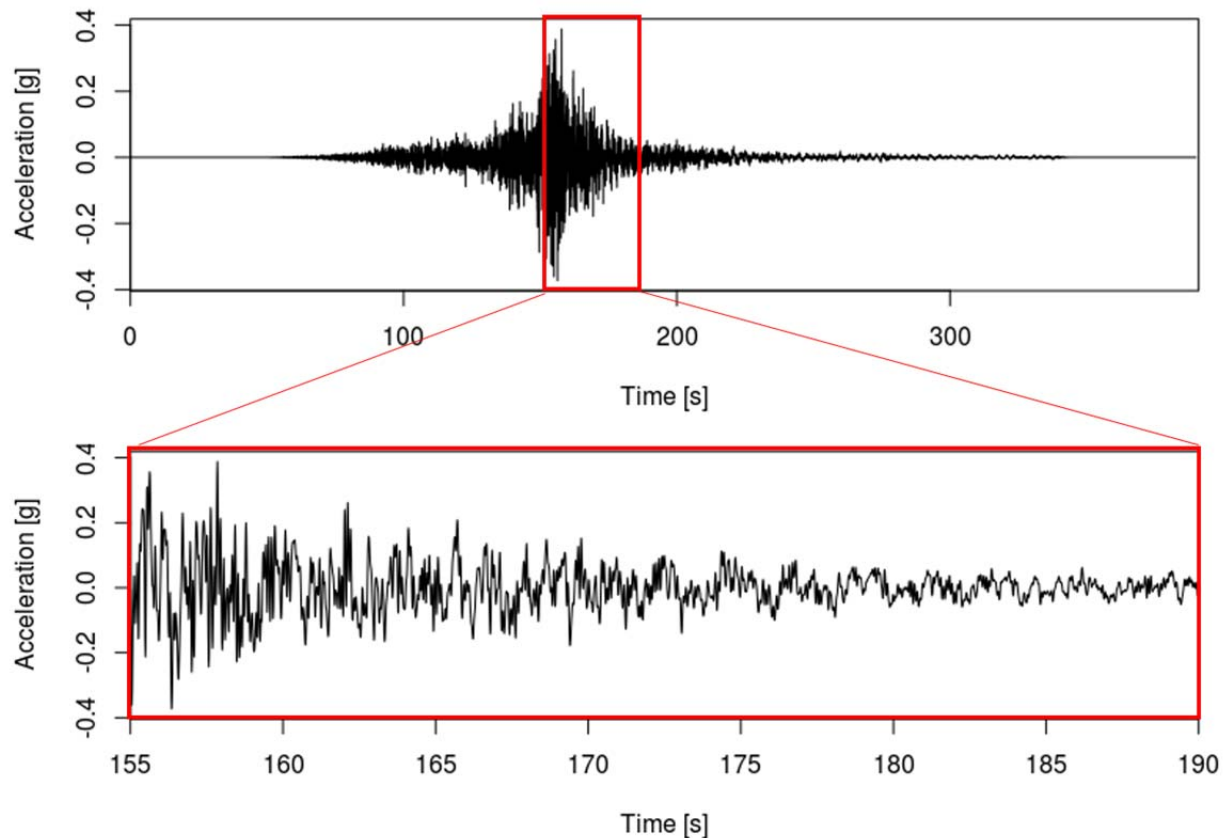


Figure 4-31: VC30 ground motion.

Figure 4-32 presents three simplified snap-shots of the deformed shape of the rack showing participation of higher modes. For ease of rendering, the height to width ratio of the figure has been changed. Also, beams appear straight, whereas in the real model they are deformed; the nodes have been omitted in the figure for simplicity of rendering. The representation of columns has also been simplified to show only the bottom, middle and top nodes of columns (there are 8 nodes along the height of each column). Curvature of the column is thus approximative. Figure 4-33 shows the displacement time history of each level of the 5-level rack subjected to the VC30 ground motion (as seen in Figure 4-33). The episodes of higher mode deformation shown in

Figure 4-32, when bottom floors and top floors are drifting in opposite directions, are also indicated.

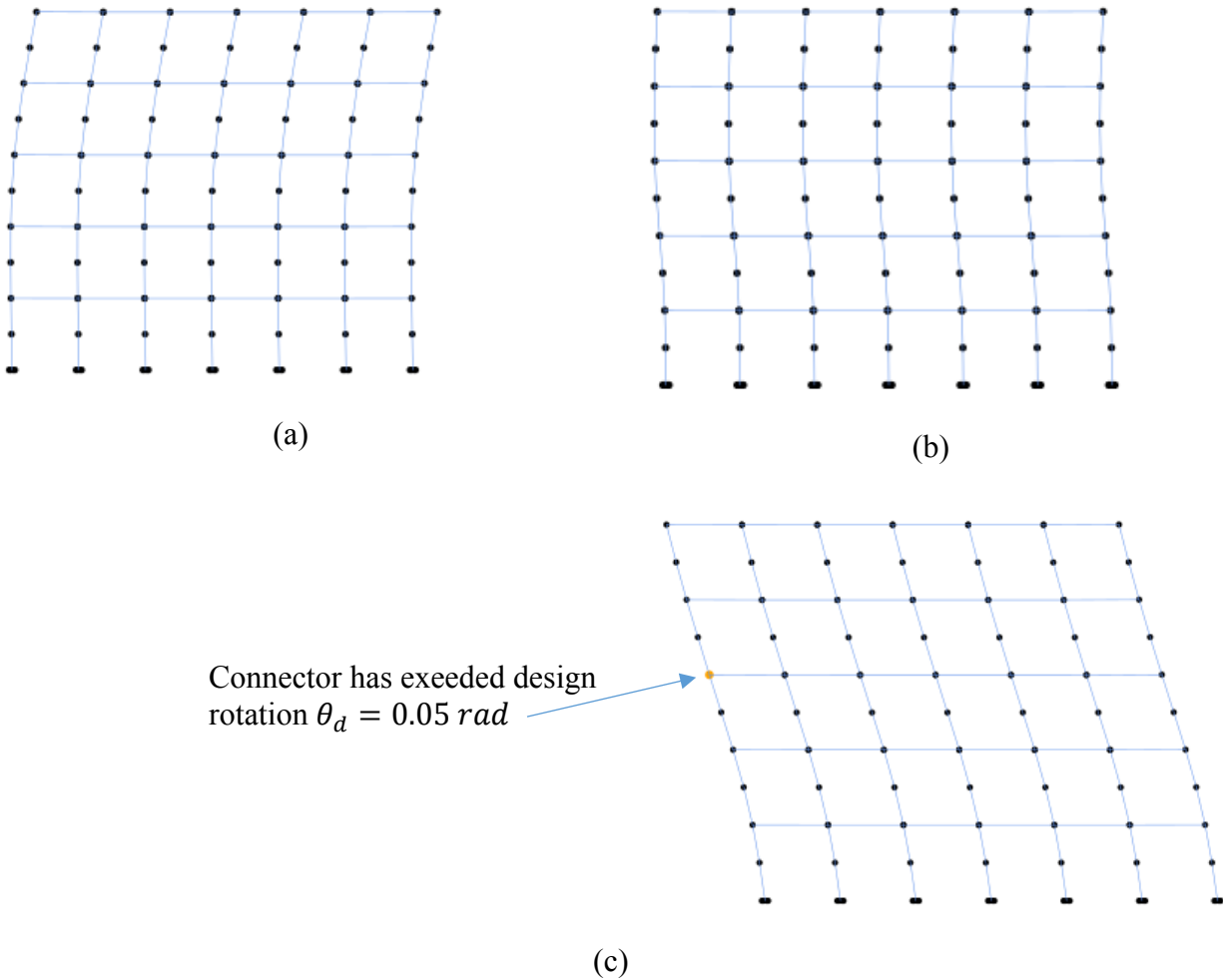


Figure 4-32 : Select deformed shapes of the rack during the VC30 ground motion at: a) $t = 160.05 \text{ s}$; b) $t = 160.7 \text{ s}$; c) $t = 166.4 \text{ s}$.

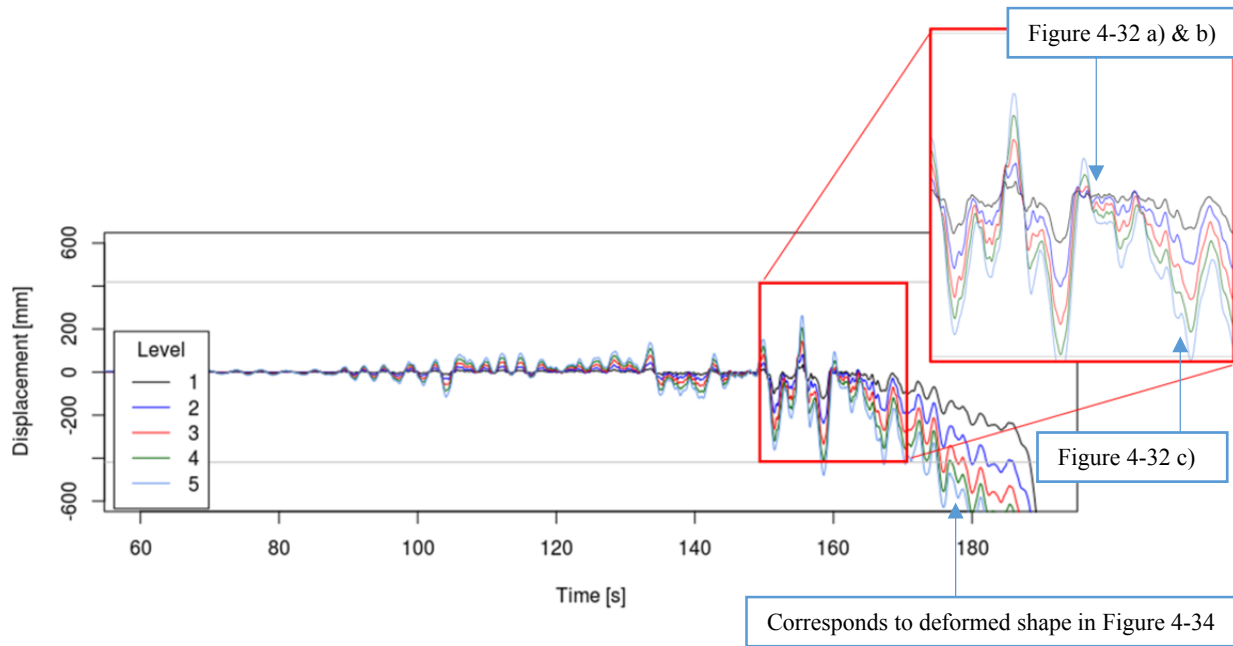


Figure 4-33 : Displacement time history of each level of a 5-level collapsed rack.

The deformed shape of the rack just before collapse at $t = 179.6$ s is shown in Figure 4-34. The same simplifications as for Figure 4-32 have been made when rendering the model. Beam-column connectors at nodes indicated in orange have exceeded their design rotation of 0.05 rad. Connectors at nodes indicated in red have exceeded their rotation capacity of 0.11 rad. Two joints have been indicated in Figure 4-34. These exterior joints are unfavourably loaded with

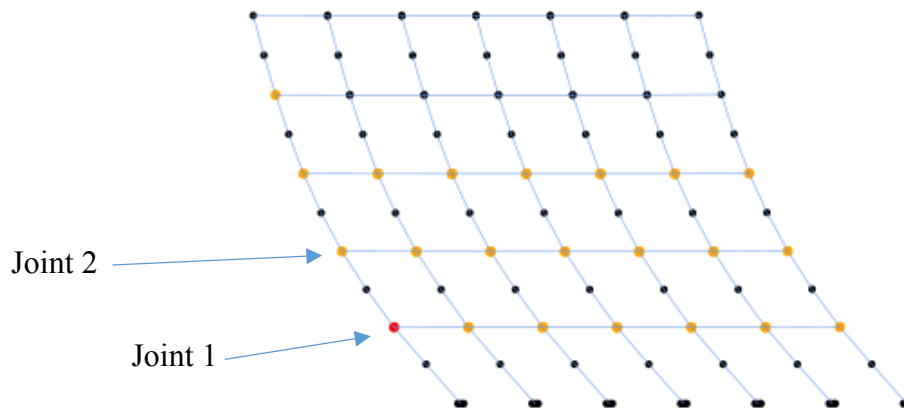


Figure 4-34 : Deformed shape of rack just before collapse during the VC30 acceleration at $t = 179.6$ s and 8 % drift.

gravity loads which are approximately -0.01 rad (see Table 4-16). Joint 1 is also the first joint to reach its rotation capacity. Their rotation time histories are shown in Figure 4-35. Joints 1 & 2 exceed the seismic design rotation, θ_d , slightly at several occasions. As the rack collapses, the

connector rotation at joint 1 exceeds the peak design capacity of the connector, $\theta_{c,max}$ just before 180 s.

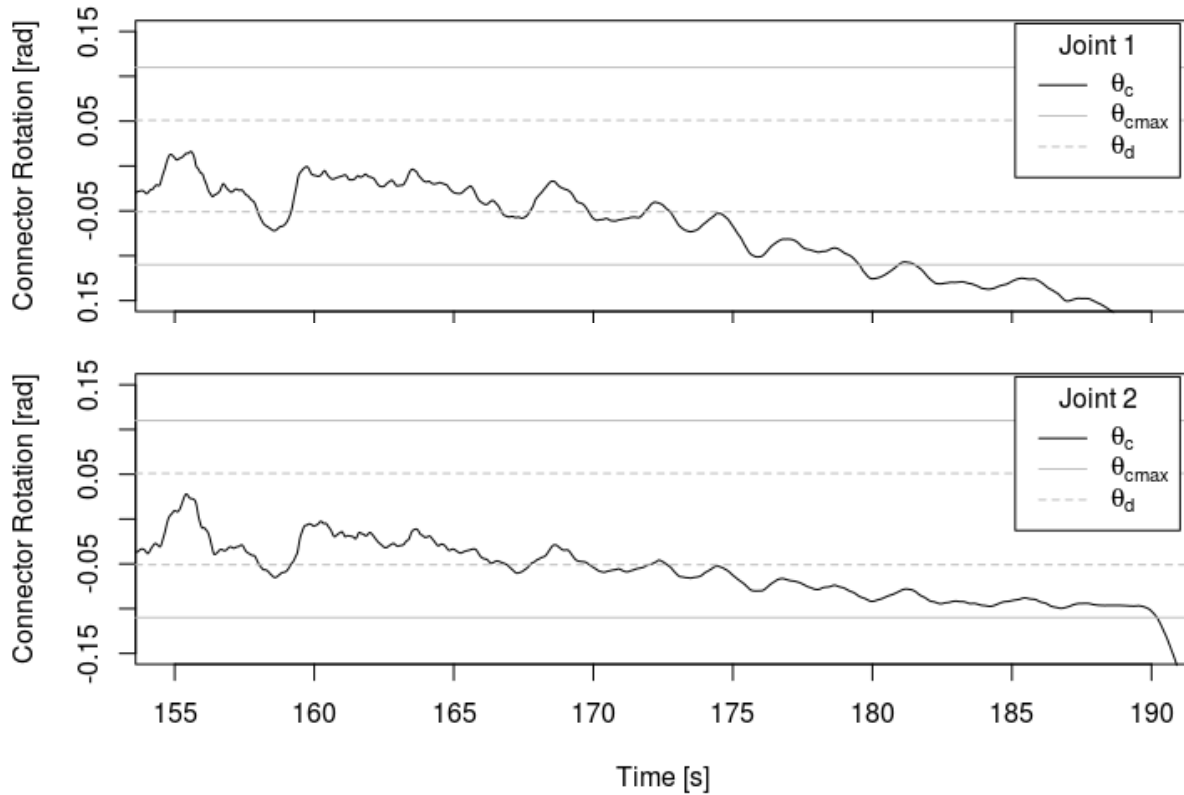


Figure 4-35 : Rotation time histories of connectors at joints 1 and 2.

The controlling limit state for the columns is in-plane buckling. Their yield strength has been adjusted down from 345 MPa to 302 MPa such that buckling will occur when connections impose the code prescribed $M_f = 1.2M_{c,max}$ in the columns. The factor of 1.2 accounts for possible overstrength of the connectors. Although in the model there is no overstrength, the columns were sized including the overstrength factor. In the case of the AC200 connectors which have been strength scaled by $SF_c = 0.5$, this corresponds to:

$$M_f = 1.2 \cdot SF_c \cdot M_{c,max} = 1.2 \cdot 0.5 \cdot \left(\frac{11.8 \text{ kNm} + 11.417 \text{ kNm}}{2} \right) \cong 7.0 \text{ kNm}$$

The same column is used for both interior and exterior columns and throughout each level of the rack, thus the design moment is dictated by the interior columns that have two adjacent connectors (see Figure 4-16). This moment is assumed distributed evenly to columns above and

below the joint. The factored axial load is greatest for the interior columns, at their first level $C_f = 55.6 \text{ kN}$. The interaction equation used for interior column design is thus:

In-plane buckling according to S16 §13.8.3 (b) [20]:

$$C_r = \frac{\phi A F_y}{(1 + \lambda^{2n})^{\frac{1}{n}}} = \frac{(1.0)(892 \text{ mm}^2)(302 \text{ MPa})}{(1 + 0.5^{2 \cdot 1.34})^{\frac{1}{1.34}}} = 242 \text{ kN}$$

$$\lambda = \sqrt{F_y/F_e}, F_{ex} = \frac{\pi^2 E}{(KL/r_x)^2} = \frac{\pi^2 (200\,000 \text{ MPa})}{(1 \cdot 1676/41.4)^2} = 1204 \text{ MPa}$$

$$M_r = \phi S F_y = (1.0)(30000 \text{ mm}^3)(302 \text{ MPa}) = 9.06 \text{ kNm},$$

$$U_{1x} = 1.0 \text{ (unbraced frame)}$$

$$C_f/C_r + U_{1x} (M_f/M_r) = 55.6 \text{ kN}/242 \text{ kN} + 1(7.0 \text{ kNm}/9.06 \text{ kNm}) = 1.0$$

For comparison, cross-sectional strength according to S16 §13.8.3 (a) [20]:

$$C_r = \frac{\phi A F_y}{(1 + \lambda^{2n})^{\frac{1}{n}}} = \frac{(1.0)(892 \text{ mm}^2)(302 \text{ MPa})}{(1 + 0)^{\frac{1}{1.34}}} = 269 \text{ kN}$$

$$M_r = \phi S F_y = (1.0)(30000 \text{ mm}^3)(302 \text{ MPa}) = 9.06 \text{ kNm (simple channel is class 3)}$$

$$U_{1x} = \frac{\omega_1}{1 - \frac{C_f}{C_e}} = \frac{0.4}{1 - \frac{55.6 \text{ kN}}{1075 \text{ kN}}} = 0.42 \leq 1.0 \Rightarrow U_{1x} = 1.0$$

$$\omega_1 = 0.6 - 0.4\kappa = 0.6 - 0.4 \frac{4.56}{8.9} = 0.4, C_e = \frac{\pi^2 EI}{L^2} = \frac{\pi^2 (200\,000 \text{ MPa}) \cdot (1.53 \times 10^6 \text{ mm}^4)}{(1676)^2} = 1075 \text{ kN}$$

$$C_f/C_r + U_1 (M_f/M_r) = 55.6 \text{ kN}/269 \text{ kN} + (7.0 \text{ kNm}/9.06 \text{ kNm}) = 0.98$$

Cross sectional strength is close to buckling. In addition, the interaction equations are dominated by bending as was typical of the racks studied. The exterior columns are subjected to less axial load, however unbalanced shears from all the yielding beam-column connectors on the exterior column must be added (see also Figure 4-16c):

$$V_h = 2 \cdot S F_c \cdot M_{c,max}/L = (2)(0.5)(5.8)/(2.438) = 2.38 \text{ kN}$$

Only half the moment from the connectors their interaction equation gives:

In-plane buckling according to S16 §13.8.3 (b) [20]:

$$(C_f + \sum V_h)/C_r + U_{1x} (M_f/M_r) = (27.8 \text{ kN} + 5 \cdot 2.38 \text{ kN})/242 \text{ kN} + 1(3.5 \text{ kNm}/9.06 \text{ kNm}) \\ = 0.55$$

or for yielding according to S16 §13.8.3 (a) [20]:

$$(27.8 \text{ kN} + 5 \cdot 2.38 \text{ kN})/269 \text{ kN} + 1(3.5 \text{ kNm}/9.06 \text{ kNm}) = 0.53$$

This indicates that axial loads, moments and moment distribution would need to be significantly different to cause these columns to fail. From the interaction equation for yielding, $M_{f-yield} = 7.72 \text{ kNm}$ would be needed in order to yield the exterior column below joint 1. Figure 4-36 shows the moment in the exterior column above and below each joint along with the connector moment and their sum. This figure also shows that the inflexion point cannot be directly at mid-column height nor is moment equally distributed to the columns above and below the joints. This causes the exterior column below joint 1 to attain/surpass $M_{f-yield}$ at several occasions starting at $t = 175.9 \text{ s}$. Finally the factored moment resistance $M_r = 9.06 \text{ kNm}$ is reached beginning near $t = 180 \text{ s}$; almost at the same instant, the connector's moment capacity, $M_{c,max}$ is also attained. Equilibrium at each joint is maintained until the rack is in the last stages of collapse after $t = 188 \text{ s}$. Several important times (175.9 s, 179.6 s, 180.3 s, 183.8 s) in the response history, that will be discussed further in Figure 4-36, are marked in dotted lines.

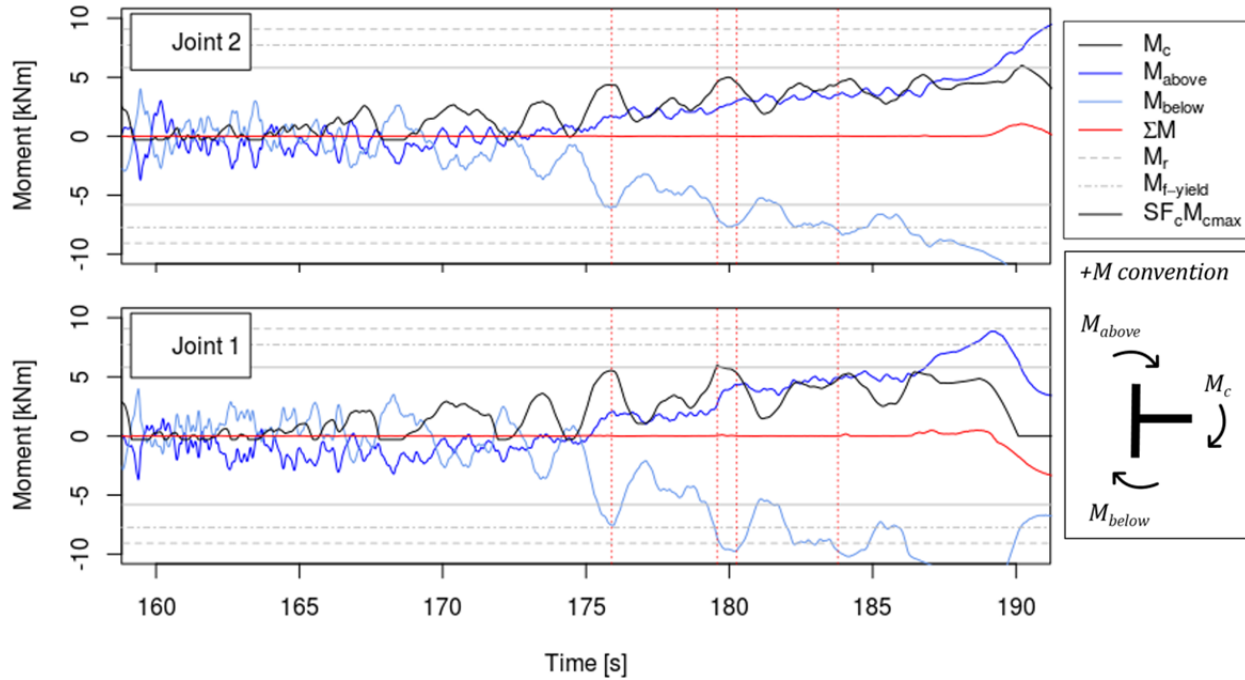


Figure 4-36 : Moments and equilibrium $\sum M = M_c + M_{above} + M_{below}$ histories around joint 1 & 2, factored moment resistance M_r of the exterior column, moment needed to cause yielding $M_{f-yield}$ (including axial interaction) and the connector moment capacity scaled for design

$$SF_c \cdot M_{c,max}.$$

Figure 4-37a & b show the moment-curvature relations in the exterior columns below joints 1 & 2. Figure 4-37c shows the history of the interaction equation S16 §13.8.3 (a) (yielding) in the columns directly below these joints. The connector moment rotation hysteresses at these joints is shown in Figure 4-37d & e. In c, at 175.9 s the column below joint 1 exceeds the interaction limit. A comparison with Figure 4-37a shows that this instant corresponds to yielding of the column below joint 1. The column below joint 2 remains elastic at this point. When comparing with Figure 4-36 it appears that the column has begun to yield before the extreme fibers of the section reach $F_{yc} = 302 \text{ MPa}$. This is because a kinematic hardening rule is defined for the column's Steel4 material. This property defines a relatively smooth transition radius between elasticity and rupture without a clear yield point (see [85]). As a result some non-linearity begins before F_y is reached. Thus, there is some slight non-linearity in what appears as the elastic phase shown in Figure 4-37a & b. By comparing Figure 4-37d with Figure 4-37c, at 179.57 s, the connector at Joint 1 can be seen to reach its moment capacity $SF_c \cdot M_{c,max} = 0.5 \cdot 11.6 = 5.8 \text{ kNm}$ while the column below the joint continues yielding as its interaction equation makes a

long excursion above 1.0. The peak of this excursion is marked at 180.25 s. By 183.78 s the column below joint 2 has also yielded as its interaction equation passes 1.0.

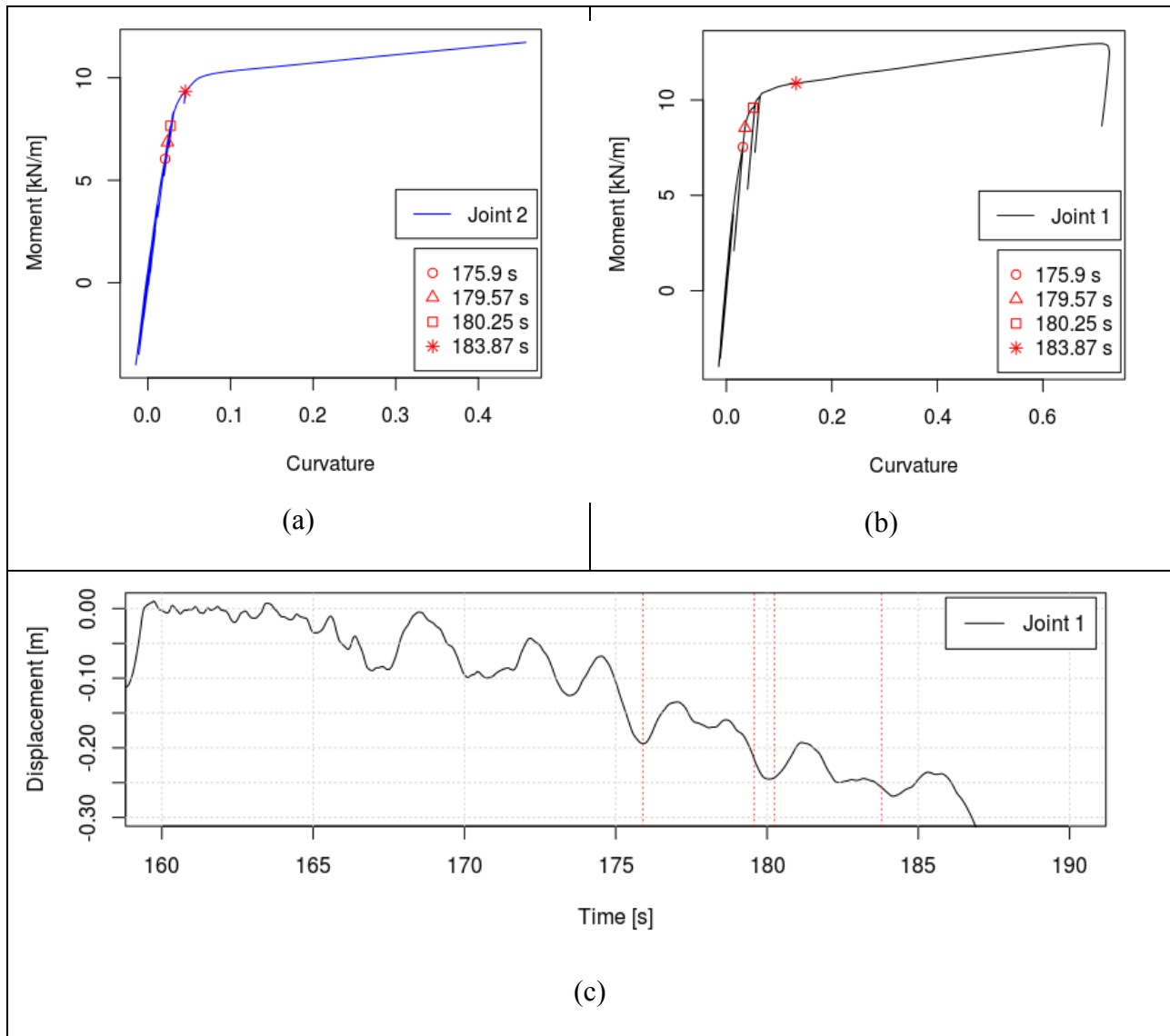
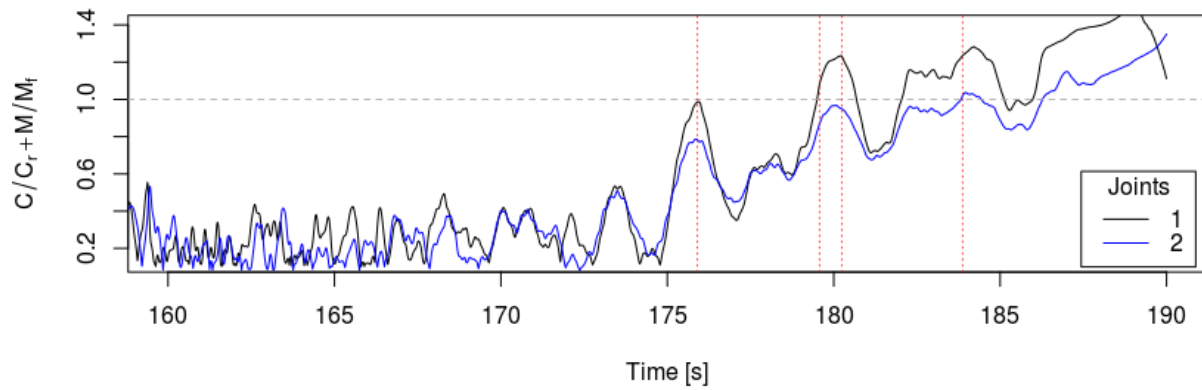
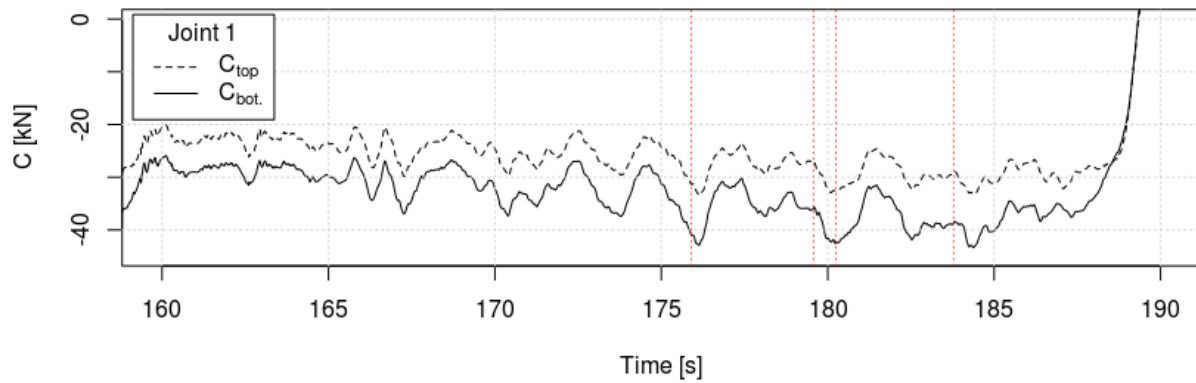


Figure 4-37 : Behavior at below joints 1 & 2: a) & b) Moment-curvature in the exterior column segment below the joints; c) Displacement history of joint 1; d) Time history of interaction equation S16 §13.8.3 (a) (yielding) in the column segments below the joints; e) Column axial load history above and below joint 1; f) Column shear history above and below joint 1; g) & h) connector hysteresis at the joints.

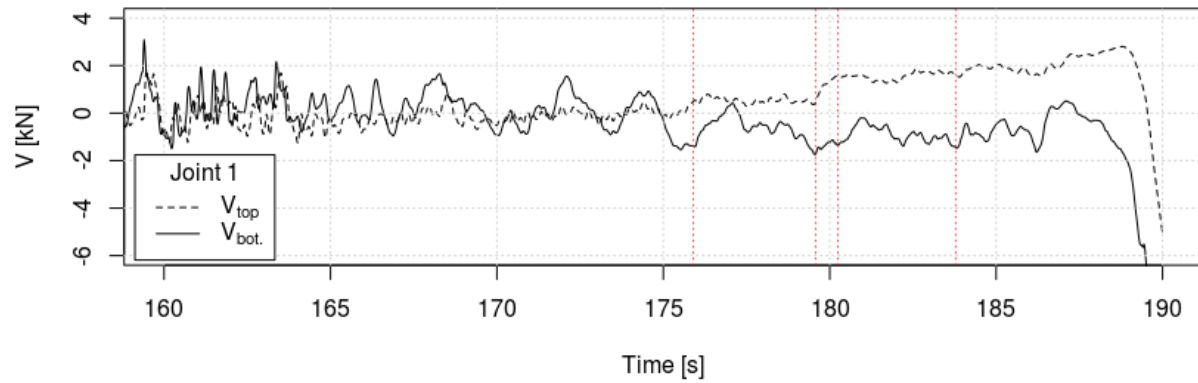


(d)

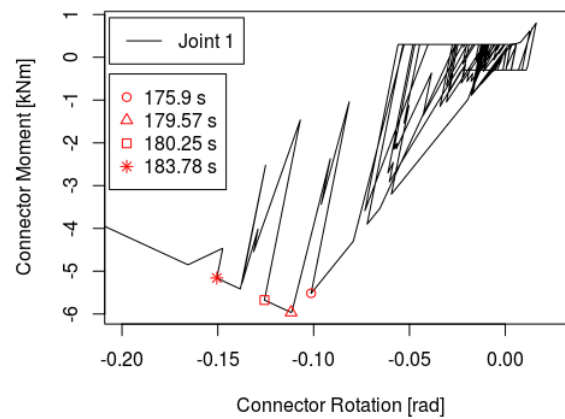


(e)

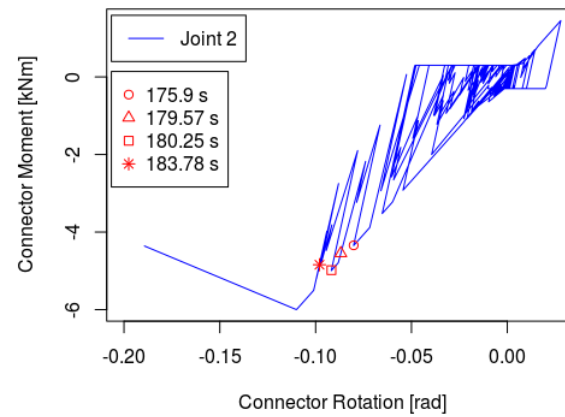
Figure 4-37 : Suite : Behavior at below joints 1 & 2: a) & b) Moment-curvature in the exterior column segment below the joints; c) Displacement history of joint 1; d) Time history of interaction equation S16 §13.8.3 (a) (yielding) in the column segments below the joints; e) Column axial load history above and below joint 1; f) Column shear history above and below joint 1; g) & h) connector hysteresis at the joints



(f)



(g)



(h)

Figure 4-37 : Suite : Behavior at below joints 1 & 2: a) & b) Moment-curvature in the exterior column segment below the joints; c) Displacement history of joint 1; d) Time history of interaction equation S16 §13.8.3 (a) (yielding) in the column segments below the joints; e) Column axial load history above and below joint 1; f) Column shear history above and below joint 1; g) & h) connector hysteresis at the joints

Figure 4-38 shows a close-up of the deformed shape of the column at the instants discussed in Figure 4-37. The profiles confirm that the column is not buckling but rather yielding at these times.

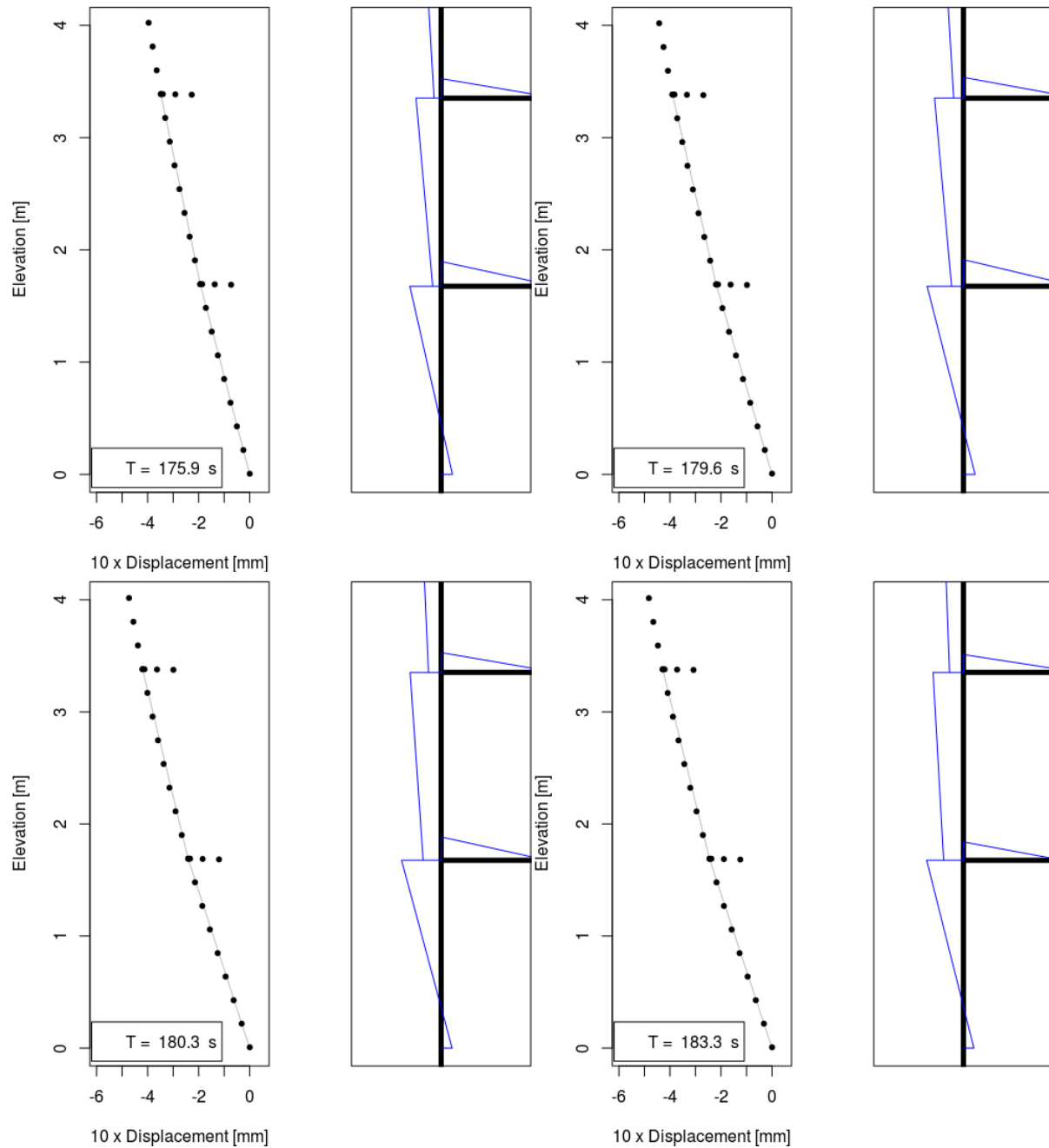


Figure 4-38 : Close-up deformed shape of exterior column at times of interest with forms of moment diagram.

Figure 4-39a shows the distribution of moments over the first two levels of the exterior column at $t = 175.9$ s (the instant when yielding occurs in the column below joint 1). Figure 4-39b shows the free-body diagram of the deformed exterior column below joint 1.

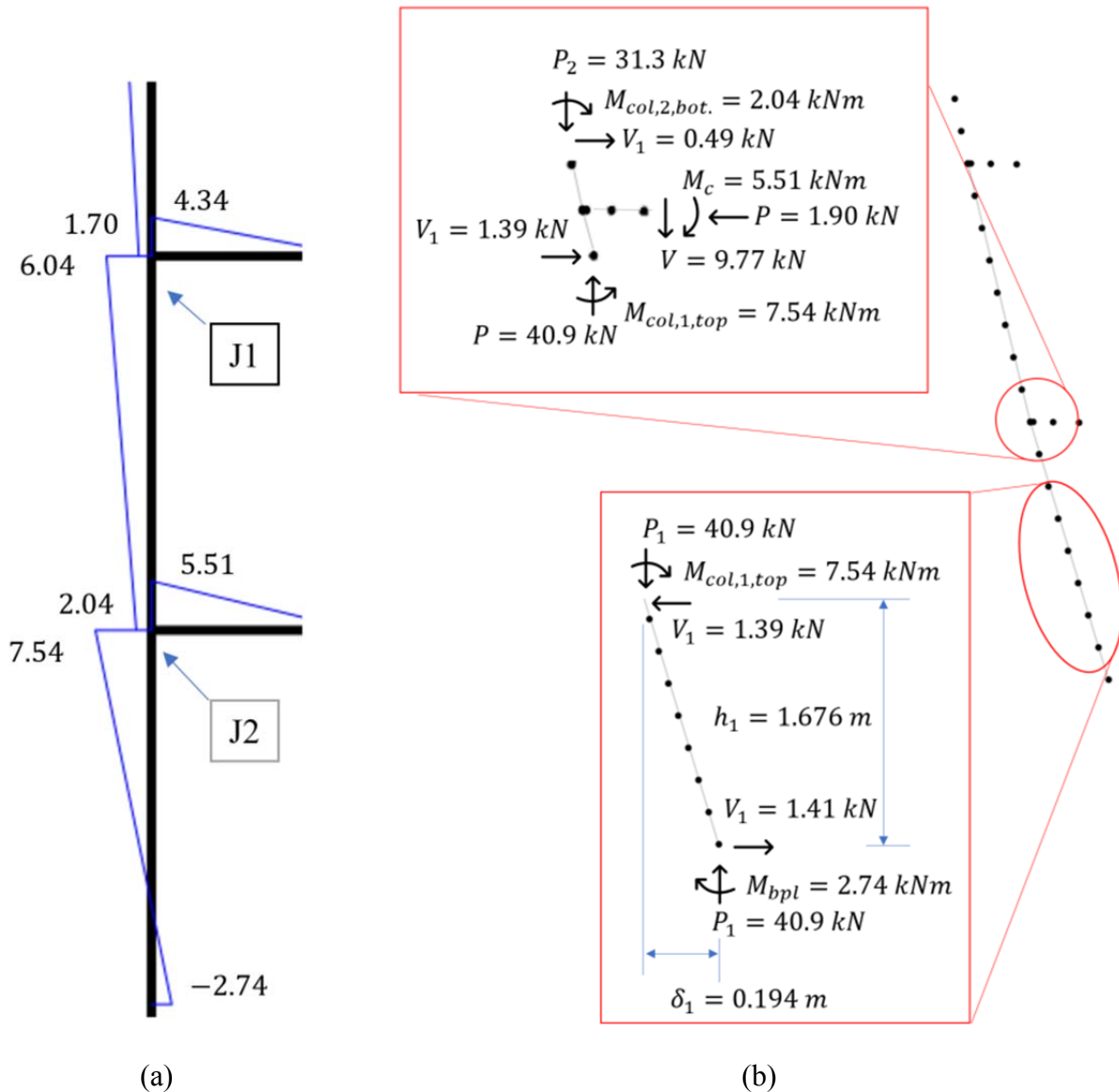


Figure 4-39 : Moment distribution in the column at the instant of yielding: a) Form of moment distribution near joints 1 & 2 at 175.9 s; b) Free-body diagram of deformed column above and below joint 1.

Figure 4-39b shows that at $t = 175.9$ s, the moment at the top end of the first level column is (see efforts and displacements at joint 1 reported in Figure 4-37):

$$M_{col,1,top} = M_{bpl} + P_1 \cdot \delta_1 + V_1 \cdot h_1 \quad (4-12)$$

$$M_{col,1,top} = -2.74 \text{ kNm} + 40.9 \text{ kN} \cdot 0.194 \text{ m} + 1.41 \text{ kN} \cdot 1.676 \text{ m}$$

$$M_{col,1,top} \cong -2.74 \text{ kNm} + 7.93 \text{ kNm} + 2.36 \text{ kNm} \cong 7.5 \text{ kNm}$$

Axial load predicted for the interaction equation was $(27.8 \text{ kN} + 5 \cdot 2.38 \text{ kN}) = 39.7 \text{ kN}$. This is only slightly lower than the axial load of 40.9 kN seen in the model. Conversely, the moment imposed by the connector is larger than was assumed in design following the current provisions of the S16: $M_c \cong 5.51 \text{ kNm} > 3.5 \text{ kNm}$. However the moment imposed by P-delta: $40.9 \text{ kN} \cdot 0.194 \text{ m} = 7.93 \text{ kNm}$ is much more important. This effect has not been explicitly addressed in S16 provisions, where currently P-delta effect on the column is accounted for by using the base-shear calculated at twice the design displacement (to account for uncertainties in drift prediction): $V_{P-delta} = P \cdot (2 \cdot \delta_d)/h_s$ and increasing capacity at the joint by $(V_{P-delta}/2) \cdot h_s$. As demonstrated in the above discussion and in Figure 4-39b, this increase in capacity is less than the moment imposed by P-delta.

The neglect in the moment caused by P-delta is compounded by the large drifts imposed on the column. Indeed, the drift predicted at joint 1 by displacement based design is approximately (see Table 4-13) 0.042 m/m. The margin for variability in drift prediction (twice the design drift) is exceeded: $2 \cdot 0.042 = 0.084 < \frac{0.194}{1.676} = 0.12 \text{ m/m}$.

The column should be designed to take into account the moment caused by ceding of the connectors $1.2 \cdot M_{c,max}$ in addition to the moment imposed by $P_1 \cdot \delta_1$. The moment in the base-plate may be neglected as its contribution is opposite.

CHAPTER 5 GENERAL DISCUSSION

With the goal of developping a non-linear FEM model to test the design provisions of the proposed Annex N of S16, a series of tests were carried out on 1-bay, 1-level cold-form rack specimens: three quasi-static tests, two pull-back tests with free vibration and finally six shake table tests. The quasi-static tests isolated the behaviour of the base-plates and beam-column connectors thereby allowing the development of detailed models of these elements where:

- Material properties of the connectors and base-plates were calibrated to match three response properties i.e. general hysteresis shape, secant stiffness and energy dissipation,
- The data gathered on beam-column connectors matched well independent test data and permitted the calibration of materials to mimic the connector action,
- Cyclic response of the base-plate (for which no data was previously available) was generated allowing the development of an analytical and FEM model.

Free vibration tests were used to measure period and damping properties of the racks. Shake table tests were carried out with ground motions from eastern and western Canada scaled to cause significant damage to the specimens. Theses shake table tests verified the ability of the models created from quasi-static tests to reproduce the response of the racks, including collapse, provided that low levels of viscuous damping were added. The seismic tests also provided valuable information on the interaction of rack structures and pallet sliding such that friction elements could be added to the finite element model to mimic sliding.

With the model developped from laboratory tests, several preliminary studies were performed on multi-level, multi-bay configurations of cold-form racks subject to a single ground motion. Studies were performed on the influence of base-plate axial load and thickness, axial load on exterior and interior columns, drift-rotations relationship, influence of damping on response, influence of sliding on response, and the interaction of base-plates, sliding and increased ground motion. The findings of this phase showed which parameters should be included in further multi-parameter tests.

Following the preliminary studies on a multi-bay, multi-level rack, the model was expanded to included buckling of the columns in plane, plastification of the beam-ends and compression

dependent base-plate assemblies. These adjustments allowed the examination of different configurations of beam/column/connector/base-plate/height while ensuring that the hypotheses of elastic beams and columns can be validated. Although further physical testing would improve confidence in this model, the calibration of non-linear elements from smaller unit tests was judged to be adequate. This latest model provided assurance that beams and columns remain elastic (or that their entry into plasticity will not go un-noticed).

Several configurations of prototype racks were designed according to the proposed Annex N of S16. The feasibility and resulting designs of the proposed design methods were examined in detail. Both displacement-based design and force-based design were applied, however, the force-based method resulted in unfeasible designs due in part to incoherence in the definition of lateral stiffness of the rack. As a result only the racks designed according to displacement based design were subjected to non-linear time history analysis with a representative number of earthquakes (11 from Montreal and 33 from Vancouver).

The results of these non-linear time history analyses were compiled and discussed. A particular mechanism causing soft-story collapse of several prototype racks was identified. This mechanism was explained in detail and a design remedy was proposed.

CHAPTER 6 CONCLUSIONS AND RECOMMENDATIONS

6.1 Conclusions

The following conclusions and recommendations refer to the overall project. For more detailed conclusions and recommendations specific to the testing and modeling of the 1-bay, 1-level rack specimens and the multi-level multi-level specimens which included pallet sliding see §3.7.

- The quasi-static tests performed validated the hypothesis that yielding is confined to the connectors and base-plates of these racks. Data collected on the inelastic response of beam-column connectors was found to match data generated from more simple cruciform tests. Base-plate inelastic response was measured and it was found that flexural strength (including axial load effects) can be predicted from yield line theory. Shake table tests confirmed that rack response (and even collapse) can be predicted by a concentrated plasticity model (plasticity at beam-column and base joints) incorporating geometric second order effects (large and small p -delta), base-plate and connector non-linearity and pallet sliding.
- It was found that viscous damping (mass dependant rayleigh damping) provided an imperfect representation of damping in the racks.
- Based on these findings the numerical model can be generalised to predict the response of multi-level, multi-bay racks with various combinations of beam/column/connector/base-plate/height configurations provided that the hypothesis that beams and columns remain elastic is verified.
- Preliminary results on several cold-formed racks subjected to a single ground motion indicated that :
 - Response is dominated by the first mode of vibration,
 - Base-plate thickness was much more important than axial load in modifying the stiffness and strength of these particular base-plates,
 - Axial load in the columns varied little over the course of the quake,

- Rotations were not equal in all the connectors at the moment of peak displacement, but that the average connector rotation was close to the value of the top level drift ratio,
- Pallet sliding was found to have more influence on the drift profile of racks when ground motion was strong, when sliding coefficients were low and when racks were more flexible. Both negative and positive impacts on the drift profile were observed.
- The displacement-based design method proposed in Annex N in high seismic zones leads to the specification of larger beams, columns and connectors than are used currently in industry, however these larger sections and stronger base-plates are not so strong as to be unfeasible.
- The force-based design method proposed in Annex N lead to infeasably large sections connectors (nearly 10 times the measured strength of available connectors) and an incoherance in the definition of lateral stiffness and strength of the rack was identified.
- Tests performed on a number of representative racks with a large number of quakes for Vancouver and Montreal sites C & E indicate that:
 - Displacement-based design did not always lead to safe design when compared with non-linear time history analyses. A significant portion of the 5 & 6 level racks in Vancouver site C conditions and 3 & 4 level racks in Montreal site E experienced collapse or suspected collapse. Design according to Annex N lead to very flexible racks (T_n near 5 s) in these cases. The minimum lateral resistance requirement of Annex N was applied but did not prevent the colllapses.
 - Collapses were caused by failure of the columns in yielding due to the increased moment from P-delta. This created a soft first story. This P-delta moment was larger than the design moment imposed by the connector; this design moment had itself been increased in an effort to account for P-delta, but was insufficient.
 - The assumption that, on average, rotations \approx drifts is adequate because the drift-rotation relationship derived from pushover was not more accurate when compared to non-linear time history analysis.

- Rotations, due to gravity and lateral loads, cannot be said to be equal amongst themselves and/or to peak drift throughout the structure. However, average connector rotations are generally near to the value of the drift ratio.

6.2 Recommendations

6.2.1 Modelling

- When using the model developed in this project, low levels of added damping should be used if fictitious stability is to be avoided.
- The base-plate assemblies developed could be easily modified by the addition of different material rules to the four support springs to account for the flexibility of the concrete slab and for bolt pull-out.
- Given that rack columns are uni-symmetric and loaded outside their shear centre, a more robust mode would account for flexural-torsional buckling of the columns.

6.2.2 Design

- That top interior beams should be designed with connectors having half the capacity of other connectors are to satisfy capacity design requirements.
- In most cases, the displacement-based design method proposed in Annex N lead to satisfactory performance of the racks, the exception being very flexible racks for which an unexceptable number of collapses were recorded.
 - The minimum lateral resistance requirement of Annex N should be revisited (to prevent the collapse of very flexible racks) by imposing a greater margin of safety than 2 on drift prediction;
 - Guidance must be given on how to asses the minimum lateral resistance of racks since the current method used required non-linear pushover.
- That the definition of stiffness be revisited in cases where force-based methods or resistance checks must be performed. An iterative method of finding coherant stiffness, strength and displacement values should be investigated. Either eigenvalue analysis should be used to determine periods or the approximate equation outlined in Annex G.

- Columns should be explicitly designed to resist the moment imposed by P-delta times, at least, twice the design displacement, in addition to the yielding of the beams.

6.2.3 Further reasearch

- The results of non-linear time history analysis herein should be expanded to include variations in geometry along the height of the rack, sliding of pallets, the vertical component of ground motions and erection imperfections.
- More information is needed about the cyclic response of base-plates with different geometries in realistic situations incorportaing stiffness of the concrete floor, varying compression bolt pull-out and levering.
- Lack of publicly available test data on connectors and base-plates greatly impedes the development of codes and consignes many studies to piecemeal examination of a particular manufacturer's product line. Recognising that manufacturers have an unassailable interest in protecting their designs but also in the development of modern design codes and in research projects whose results may be generalised, an anonymised database of connector and base-plate qualification tests should be developed and maintained. The availabilty of this data will lend more legitimacy to rack research as a whole by giving manufacturers and researchers the means to compare and scrutinize; it will facilitate and expidite parametric studies necessary to dispel the impulse toward overly conservative code provisions; and it will build trust between all stake-holders that design guidelines are backed-up by solid empirical evidence.
- As a minimum, such a database should include the data points from qualification tests, corresponding beam and column properties, approximate corresponding product loads and the seismic spectrum for which the design is intended.

BIBLIOGRAPHY

- [1] S. Uma and G. Beattie, "Observed Performance of Industrial Pallet Rack Storage Systems in the Canterbury Earthquakes," *Bulletin of the New Zealand Society for Earthquake Engineering*, vol. 44, no. 4, pp. 388-393, 2011.
- [2] D. A. Bournas, P. Negro and F. F. Taucer, "Performance of Industrial Buildings During the Emilia Earthquakes in Northern Italy and Recommendations for Their Strengthening," *Bulletin of Earthquake Engineering*, vol. 12, no. 5, pp. 2383-2404, 2014.
- [3] C. Clifton, M. Bruneau, G. MacRae, R. Leon and A. Fussel, "Steel Structures Damage from the Christchurch Earthquake Series of 2010 and 2011," *Bulletin of the New Zealand Society for Earthquake Engineering*, vol. 44, no. 4, pp. 297-318, 2011.
- [4] Bruneau, M. et al, "Steel Building Damage from the Christchurch Earthquake of February 22, 2011," *Unpublished draft*, 2011.
- [5] J. Crosier, M. Hannah and D. Mukai, "Damage to Steel Storage Racks in Industrial Buildings in the Darfield Earthquake," *Bulletin of the New Zealand Society for Earthquake Engineering*, vol. 43, no. 4, p. 425, 2010.
- [6] S. Uma and G. Beattie, "Observed Performance of Industrial Pallet Rack Storage Systems in the Canterbury Earthquakes," *Bulletin of the New Zealand Society for Earthquake Engineering*, vol. 44, no. 4, 2011.
- [7] China Quality Suppliers, "Selective Pallet Racking," China Good Quality Selective Pallet Rack, Industrial Pallet Racks and Double Deep Pallet Rack International Trade Site, 2015. [Online]. Available: <http://www.selectivepallettracking.com/sale-4117546-long-span-industrial-racking-systems-pallet-adjustable-for-stores-cargo-storing.html>. [Accessed 2016 12 20].
- [8] Cisco-Eagle, "Cisco-Eagle," 2016. [Online]. Available: <http://www.cisco->

eagle.com/catalog/p-7718-structural-pallet-rack-42d-x-144h-x-96w-9800-lbs-cap-3-beam-levels-starter.aspx. [Accessed 20 12 2016].

- [9] Efficiency Systems Inc., "Efficiency Systems Inc," 2016. [Online]. Available: <http://www.efficiencysystemsinc.com/wp-content/uploads/2014/12/Palletier.jpg>. [Accessed 20 12 2016].
- [10] North American Wholesale Logistics , "Nawl Usa," 2016. [Online]. Available: <http://www.nawlusa.com/our-products/pallet-rack/>. [Accessed 20 12 2016].
- [11] 3D Storage Solutions, "3dstoragesolutions," 2016. [Online]. Available: <http://www.3dstoragesolutions.com/pallet-rack>. [Accessed 20 12 2016].
- [12] Material Storage Systems Inc., "msshouston.com," Crest Media, 20009. [Online]. Available: <http://msshouston.com/roll-formed-racks.html>. [Accessed 20 12 2016].
- [13] Steel King, "steelking.com," Ecreativeworks , 2016. [Online]. Available: https://www.steelking.com/newsdesk.php?news_id=23. [Accessed 20 12 2016].
- [14] R. Haque and S. Alam, "Force-Based Seismic Design of Industrial Rack Clad Buildings," 2012.
- [15] A. Filiatrault, R. E. Bachman and M. G. Mahoney, "Performance-based seismic design of pallet-type steel storage racks," *Earthquake spectra*, vol. 22, no. 1, pp. 47-64, 2006.
- [16] R. Haque and S. Alam, "Direct Displacement-Based Design of Industrial Rack Clad Buildings," *Earthquake Spectra*, vol. 29, no. 4, pp. 1311-1334, 2013.
- [17] H. Krawinkler, "Experimental Study on Seismic Behavior of Industrial Storage Racks," 1978.
- [18] C. Chen, R. Scholl and J. Blume, "Earthquake Simulation Tests of Industrial Steel Storage Racks," in *Proceedings of the Seventh World Conference on Earthquake Engineering*,

Istanbul, Turkey, 1980.

- [19] NBCC, *National Building Code of Canada*, Ottawa, Canada: National Research Council of Canada, 2015.
- [20] C. CSA, *CSA-S16-09: Design of Steel Structures*, Mississauga (Ontario, Canada): Canadian Standards Association, 2014.
- [21] C. Chen, R. W. Clough, R. E. Scholl and J. A. Blume, *Seismic Study of Industrial Steel Storage Racks*, URS/John A. Blume & Associates, 1980.
- [22] B. S. S. Council, *Seismic Considerations for Steel Storage Racks Located in Areas Accessible to the Public, FEMA 460*, 2005.
- [23] Fédération Européenne de la Manutention, *FEM 10.2.08 Recommendations for the Design of Static Steel Pallet Racks in Seismic Conditions*, 2011.
- [24] I. Rosin, L. Calado, J. Proenca, P. Carydis, H. Mouzakis, C. Castiglioni, J. Brescianini, A. Plumier, H. Degee, P. Negro and others, "Storage Racks in Seismic Areas," *Report EUR*, vol. 23744, 2009.
- [25] G. Beattie and B. Deam, *Design Guide Seismic Design of High Level Storage Racking Systems with Public Access*, Porirua City, New Zealand: Branz, 2006.
- [26] G. J. Beattie and U. S. R., *A Revised Guide for the Design, Construction and Operation of High Level Storage Racking Systems Following the Darfield Earthquake*, Auckland, New Zealand: Proceedings of the Ninth Pacific Conference on Earthquake Engineering, 2011.
- [27] A. Filiatrault and A. Wanitkorkul, "Shake Table Testing of Frazier Industrial Storage Pallet Racks," in *Report No. CSEE-SEESL-2004-02*, Buffalo, NY, 2005.
- [28] A. Filiatrault, P. S. Higgins, A. Wanitkorkul and J. Courtwright, "Experimental stiffness of pallet-type steel storage rack tier drop connectors," *Practice Periodical on Structural*

Design and Construction, vol. 12, no. 4, pp. 210-215, 2007.

- [29] M. Godley, R. Beale and X. Feng, "Analysis and Design of Down-Aisle Pallet Rack Structures," *Computers & Structures*, vol. 77, no. 4, pp. 391-401, 2000.
- [30] C. Bernuzzi, A. Gobetti, G. Gabbianelli and M. Simoncelli, "Simplified Approaches to Design Medium-Rise Unbraced Steel Storage Pallet Racks. 2: Fundamental Period Estimates," *ASCE*, 2015.
- [31] N. Baldassino and C. Bernuzzi, "Analysis and Behaviour of Steel Storage Pallet Racks," *Thin-Walled Structures*, vol. 37, no. 4, pp. 277-304, 2000.
- [32] B. P. Gilbert and K. J. Rasmussen, "Determination of the Base Plate Stiffness and Strength of Steel Storage Racks," *Journal of Constructional Steel Research*, vol. 67, no. 6, pp. 1031-1041, 2011.
- [33] N. Baldassino and R. Zandonini, "Performance of Base-Plate Connections of Steel Storage Pallet Racks," in *5th International Colloquium on Coupled Instabilities in Metal Structures. The University of Sydney*, 2008.
- [34] A. T. Sarawit and P. Teoman, "Cold-formed Steel Frame and Beam-Column Design," American Iron and Steel Institute, Cornell, 2003.
- [35] ANSI, *ANSI MH16.1: 2012 Specification for the Design, Testing and Utilization of Industrial Steel Storage Racks*, 2008.
- [36] G. Beattie, "A Design Guide for High Level Storage Racking with Public Access," in *NZSEE Conference*, 2006.
- [37] H. Degée and V. Denoël, "Numerical Modelling of Storage Racks Subjected to Earthquake," 2007.
- [38] H. Degée and V. Denoël, "An Investigation on the Sliding of Pallets on Storage Racks Subjected to Earthquake," in *NCTAM, 7th National Congress on Theoretical and Applied*

Mechanics, 2006.

- [39] P. Sideris, "Seismic Behavior of Palletized Merchandise in Steel Storage Racks," ProQuest, 2008.
- [40] Y. Gao, "Seismic Evaluation and Performance Enhancement of Industrial Storage Racks," Case Western Reserve University, Cleveland, 2013.
- [41] J. J. Bommer and R. Mendis, "Scaling of Spectral Displacement Ordinates with Damping Ratios," *Earthquake Engineering & Structural Dynamics*, vol. 34, no. 2, pp. 145-165, 2005.
- [42] J. D. Pettinga and M. N. Priestley, Accounting for P-delta Effects in Structures When Using Direct Displacement-Based Design, IUSS Press, 2007.
- [43] M. Priestley, G. Calvi and M. Kowalsky, "Direct Displacement-Based Seismic Design of Structures," in *2007 NZSEE Conference*, 2007.
- [44] G. Calvi and G. Kingsley, "Displacement-Based Seismic Design of Multi-Degree-of-Freedom Bridge Structures," in *Second International Workshop on Seismic Design of Bridges*, Queenstown, New Zealand, 1994.
- [45] X. Cui, X. Liang and L. Xin, "Direct Displacement-Based Seismic Design Method of High-Rise Buildings Considering Higher Mode Effects," *Computational Structural Engineering*, pp. 253-265, 2009.
- [46] C. Clifton, M. Bruneau, G. MacRae, R. Leon and A. Fussel, "Steel Structures Damage From the Christchurch Earthquake Series of 2010 and 2011," *Bulletin of the New Zealand Society For Earthquake Engineering*, vol. 4, no. 44, pp. 297-318, 2011.
- [47] D. A. Bournas, P. Negro and F. F. Taucer, "Performance of Industrial Buildings During the Emilia Earthquakes in Northern Italy and Recommendations for Their Strengthening," *Bulletin of Earthquake Engineering* 12.5, vol. 5, no. 12, pp. 2383-2404, 2014.

- [48] CEN, "Steel Static Storage Systems - Adjustable Pallet Racking Systems - Principles for Seismic Design," European Committee for Standardization, Brussels, Belgium, 2016.
- [49] CSA, "A344.2-05, Standard for the Design and Construction of Steel Storage Racks," Canadian standard Association, Mississauga, ON., 2005.
- [50] RMI, "ANSI MH16.1.12, Specification for the Design, Testing and Utilization fo Industrial Steel Storage Racks," Rack Manufacturer's Institute, Charlotte, NC, 2012.
- [51] A. Filiatrault, R. E. Bachman and M. G. Mahoney, "Performance-Based Seismic Design of Pallet-Type Steel Storage Racks," *Earthquake spectra*, vol. 1, no. 22, pp. 47-64, 2006.
- [52] A. Haque and M. Alam, "Direct Displacement-Based Design of Industrial Rack Clad Buildings," *Earthquake Spectra*, vol. 4, no. 29, pp. 1311-1334, 2013.
- [53] M. Priestley, G. Calvi and M. Kowalsky, "Direct Displacement-Based Seismic Design of Structures," Pavia, IUSS Press, 2007, p. 721.
- [54] BSSC, "FEMA 460 Seismic Considerations for Steel Storage Racks Located in Areas Accessible to the Public," Building Safety Seismic Council, Washington, DC, 2005.
- [55] C. CSA, *CSA-S16-09: Design of Steel Structures – Amendment no. 1.*, Mississauga (Ontario, Canada): Canadian Standards Association, 2014.
- [56] G. E. N. R. Coutinho, "Numerical Simulation of the Seismic Behavior of Steel Storage Pallet Racking Systems," Instituto Superior Técnico, Lisbon, 2008.
- [57] I. Rosin, L. Calado, J. Proenca, P. Carydis, H. Mouzakis, C. Castiglioni, J. Brescianini, A. Plumier, H. Degee, P. Negro and others, "Report EUR 23744 Storage Racks in Seismic Areas," European Commision, Luxembourg, 2009.
- [58] H. Degée and V. Denoël, "Numerical Modelling of Storage Racks Subjected to Earthquake," in *Proceedings of COMPDYN 07, Conference on Computational Dynamics*,

Rethymno, Crete, Greece, 2007.

- [59] R. Haque and S. Alam, "Force-Based Seismic Design of Industrial Rack Clad Buildings," University of British Columbia, Okanagan, 2012.
- [60] C. Bernuzzi and M. Simoncelli, "An Advanced Design Procedure for the Safe Use of Steel Storage Pallet Racks in Seismic Zones," *Thin-Walled Structures*, no. 109, pp. 73-87, 2016.
- [61] H. Krawinkler, "Experimental Study on Seismic Behavior of Industrial Storage Racks," in *4th International Specialty Conference on Cold-Formed Steel Structures*, 1978.
- [62] A. Filiatrault, P. S. Higgins, A. Wanitkorkul, J. A. Courtwright and R. Michael, "Experimental seismic response of base isolated pallet-type steel storage racks," *Earthquake Spectra*, vol. 3, no. 24, pp. 617-639, 2008.
- [63] B. P. Gilbert and K. J. Rasmussen, "Determination of the base plate stiffness and strength of steel storage racks," *Journal of Constructional Steel Research*, vol. 6, no. 67, pp. 1031-1041, 2011.
- [64] N. Baldassino and R. Zandonini, "Performance of Base-Plate Connections of Steel Storage Pallet Racks," in *5th international colloquium on coupled instabilities in metal structures*, Sydney, 2008.
- [65] A. T. Sarawit and P. Teoman, "Cold-formed Steel Frame and Beam-Column Design," American Iron and Steel Institute, Cornell, 2003.
- [66] A. Firouzhianhaji, A. Saleh and B. Samali, "Australian Conference On The Mechanics Of Structures And Materials," in *CRC press/Balkema*, 2013.
- [67] A. Kanyilmaz, C. A. Castiglioni, G. Brambilla and G. P. Chiarelli, "Experimental Assessment of the Seismic Behavior of Unbraced Steel Storage Pallet Racks," *Thin-Walled Structures*, no. 108, pp. 391-405, 2016.

- [68] C. Bernuzzi and C. A. Castiglioni, "Experimental Analysis on the Cyclic Behaviour of Beam-to-Column Joints in Steel Storage Pallet Racks," *Thin-Walled Structures*, vol. 10, no. 39, pp. 841-859, 2001.
- [69] C. Aguirre, "Seismic Behavior of Rack Structures," *Journal of Constructional Steel Research*, vol. 61, no. 5, pp. 607-624, 2005.
- [70] N. Baldassino and C. Bernuzzi, "Analysis and Behaviour of Steel Storage Pallet Racks," *Thin-Walled Structures*, vol. 4, no. 37, pp. 277-304, 2000.
- [71] H. Degée and V. Denoël, "An investigation on the sliding of pallets on storage racks subjected to earthquake," in *Proceedings of the 7th National Congress on Theoretical and Applied Mechanics*, Mons, 2006.
- [72] P. Sideris, "Seismic Behavior of Palletized Merchandise in Steel Storage Racks (Master's Thesis)," ProQuest Information and Learning Company, Ann Arbor, MI, 2008.
- [73] Y. Gao, "Seismic Evaluation and Performance Enhancement of Industrial Storage Racks," Case Western Reserve University, Cleveland, 2013.
- [74] B. Gilbert, R. Badet, L. Teh and K. Rasmussen, "Determination of the influence of the pallets on the design of drive-in steel storage racks," Centre for Infrastructure Engineering and Management, Griffith University, Queensland, 2013.
- [75] M. Pollino, Y. Gao and R. Michael, "Seismic Response and Protection of Steel Storage Rack Palleted Merchandise," in *10th U.S. National Conference on Earthquake Engineering Frontiers of Earthquake Engineering*, Anchorage, 2014.
- [76] P. Sideris, A. Filiatrault, M. Leclerc and R. Tremblay, "Experimental Investigation on the Seismic Behavior of Palletized Merchandise in Steel Storage Racks," *Earthquake Spectra*, vol. 1, no. 26, pp. 209-233, 2010.
- [77] C. Chen, R. E. Scholl and J. A. Blume, "Seismic Study of Industrial Steel Storage Racks,"

URS/John A. Blume & Associates, San Francisco, 1980.

- [78] A. Filiatrault, P. S. Higgins, A. Wanitkorkul and J. Courtwright, "Experimental stiffness of pallet-type steel storage rack tier drop connectors," *Practice Periodical on Structural Design and Construction*, vol. 4, no. 12, pp. 210-215, 2007.
- [79] F. McKenna and G. Fenves, "Open System for Earthquake Engineering Simulation," Pacific Earthquake Engineering Research Center (PEER), University of California, Berkeley, CA., 2014.
- [80] NRCC, "National Building Code of Canada, 14th ed.," National Research Council, Ottawa, ON, 2015.
- [81] M. Scott, F. Filippou and S. Mazzoni, "OpenSees Wiki," University of California Regents, 30 09 2013. [Online]. Available:
http://opensees.berkeley.edu/wiki/index.php/Hysteretic_Material. [Accessed 13 11 2016].
- [82] A. Zsarnóczyay, "OpenSees Wiki," University of California Regents, 20 02 2015. [Online]. Available: http://opensees.berkeley.edu/wiki/index.php/Steel4_Material. [Accessed 13 11 2016].
- [83] A. K. Chopra, Dynamics of Structures ed. 3, New Jersey: Prentice Hall, 2005.
- [84] M. Priestley, G. Calvi and M. Kowalsky, "Direct Displacement-Based Seismic Design of Structures," in *5th New Zealand Society for Earthquake Engineering Conference*, 2007.
- [85] M. Priestley, G. Calvi and M. Kowalsky, Displacement-Based Seismic Design of Structures, Pavia: IUSS Press, 2007.
- [86] C. CSA, *S6-09 Canadian Bridge Design Code*, Mississauga: Canadian Standards Association, 2009.
- [87] OpenSees, "<http://opensees.berkeley.edu/>," UC Regents, 2006. [Online]. Available:

<http://opensees.berkeley.edu/>. [Accessed 20 12 2016].

- [88] N. Priestley, *Fundamentals of Direct Displacement-Based Seismic Design and Assessment*, Springer, 2007.
- [89] "Supplementary Agenda for the 2010-08 Meeting of the Standing Committee on Earthquake Design," 2014.
- [90] R. Balbaa, "Industrial Racking Failures," 9 2003.
- [91] C. Bernuzzi, A. Gobetti, G. Gabbianelli and M. Simoncelli, "Simplified Approaches to Design Medium-Rise Unbraced Steel Storage Pallet Racks. 1: Elastic Buckling Analysis," *ASCE*, 2015.
- [92] S. Mazzoni, "PEER Ground Motion Database," University of California, Berkeley, 2013. [Online]. Available: <http://ngawest2.berkeley.edu/>. [Accessed 25 Novembre 2015].
- [93] A. Gupta and H. Krawinkler, "STESSA 2000: Behaviour of Steel Structures in Seismic Areas: Proceedings of the Third International Conference STESSA 2000," F. Mazzolani and R. Tremblay, Eds., CRC Press, 2000, pp. 687-694.
- [94] CTokas, *Microsoft PowerPoint - US Building Code Seismic Testing Requirements for Nonstructura_Hndoutl.ppt*.
- [95] S. CSI, "CSI Analysis Reference Manual," *Berkeley (CA, USA): Computers and Structures INC*, 2015.
- [96] S. Avgeriou, *Seismic Performance of Steel Pallet Racks*, 2012.
- [97] 3D Storage Solutions Ltd., "3D Storage Solutions," 2016. [Online]. Available: <http://www.3dstoragesolutions.com/pallet-rack>. [Accessed 20 12 2016].
- [98] R. J. Micheal, *Design and Developement of Seismic Isolation System for Commercial Storage Racks*, Case Western Reserve University, 2013.

- [99] Shelving Product Group, "Storage Equipment Information Bulletin No. 2 Latest Developments in the Harmonization of the Design and Use of Storage Equipment," European Racking Federation, 2010.
- [100] B. Alavi and A. Gupta, "Performance-Based Seismic Design of an Industrial Storage Rack System," in *2008 Structures Congress--Crossing Borders*, 2008.
- [101] C. Bernuzzi and C. A. Castiglioni, "Experimental Analysis on the Cyclic Behaviour of Beam-to-Column Joints in Steel Storage Pallet Racks," *Thin-Walled Structures*, vol. 39, no. 10, pp. 841-859, 2001.
- [102] A. Bhaskararao and R. Jangid, "Seismic Analysis of Structures Connected with Friction Dampers," *Engineering Structures*, vol. 28, no. 5, pp. 690-703, 2006.
- [103] J. J. Bommer and A. S. Elnashai, "Displacement Spectra for Seismic Design," *Journal of Earthquake Engineering*, vol. 3, no. 01, pp. 1-32, 1999.
- [104] B. Brown, "Seismic Design of Pallet Racking Systems," 1983.
- [105] W. I. Cameron and R. A. Green, "Damping Correction Factors for Horizontal Ground-Motion Response Spectra," *Bulletin of the Seismological Society of America*, vol. 97, no. 3, pp. 934-960, 2007.
- [106] C. Castiglioni, P. Carydis, P. Negro, L. Calado, H. Degee and I. Rosin, "Seismic Behaviour of Steel Storage Racking Systems," in *STESSA 2009 Conference*, 2009.
- [107] A. K. Chopra, *Dynamics of Structures*, vol. 3, Prentice Hall New Jersey, 1995.
- [108] C. Clifton, M. Bruneau, G. MacRae, R. Leon and A. Fussell, "Steel Structures Damage from the Christchurch Earthquake Series of 2010 and 2011," *Bulletin of the New Zealand Society for Earthquake Engineering*, vol. 44, no. 4, pp. 297-318, 2011.
- [109] C. E. de Normalisation, *Eurocode 8 - Design of Structures for Earthquake Resistance -*

Part 1: General Rules, Seismic Actions and Rules for Buildings, vol. 1, 1998.

- [110] E. Faccioli, R. Paolucci and J. Rey, "Displacement Spectra for Long Periods," *Earthquake Spectra*, vol. 20, no. 2, pp. 347-376, 2004.
- [111] F. FEMA, "273: NEHRP Guidelines for the Seismic Rehabilitation of Buildings," *Federal Emergency Management Agency*, 1997.
- [112] A. Filiatrault, "Building Code Seismic Testing Requirements for Nonstructural Components".
- [113] A. Filiatrault, P. S. Higgins, A. Wanitkorkul, J. A. Courtwright and R. Michael, "Experimental seismic response of base isolated pallet-type steel storage racks," *Earthquake Spectra*, vol. 24, no. 3, pp. 617-639, 2008.
- [114] A. Firouzhianhaji, A. Saleh and B. Samali, "Finite Element Modeling of a Beam-Column Connection in Industrial Storage Racking Structures," 2013.
- [115] B. Gilbert, R. Badet, L. Teh and K. Rasmussen, "Determination of the Influence of the Pallets on the Design of Drive-In Steel Storage Racks," 2013.
- [116] P. S. Higgins, "Drawing FZ-01, CSA S16 - Annex N Test Model Rack Hot Rolled Material Frazier Racks Standard Details," 2015.
- [117] Y. Lin and K. Chang, "Study on Damping Reduction Factor for Buildings Under Earthquake Ground Motions," *Journal of Structural Engineering*, vol. 129, no. 2, pp. 206-214, 2003.
- [118] V. Mohan, P. Prabha, J. Rajasankar, N. R. Iyer, N. Raviswaran, V. Nagendiran and S. Kamalakannan, "Cold-Formed Steel Pallet Rack Connection: An Experimental Study," *International Journal of Advanced Structural Engineering (IJASE)*, vol. 7, no. 1, pp. 55-68, 2015.

- [119] F. Naeim and C. A. Kircher, "On the Damping Adjustment Factors for Earthquake Response Spectra," *The Structural Design of Tall Buildings*, vol. 10, no. 5, pp. 361-369, 2001.
- [120] N. M. Newmark and W. J. Hall, *Earthquake Spectra and Design*, vol. 1, 1982.
- [121] M. Pollino, Y. Gao and R. Michael, "Seismic Response and Protection of Steel Storage Rack Palleted Merchandise," 2014.
- [122] M. Priestley, G. Calvi and K. M.J., *Displacement-Based Seismic Design of Structures*, IUSS Press, 2007.
- [123] K. K. Sangle, K. M. Bajoria and R. S. Talicotti, "Elastic Stability Analysis of Cold-Formed Pallet Rack Structures with Semi-Rigid Connections," *Journal of Constructional Steel Research*, vol. 71, pp. 245-262, 2012.
- [124] P. Sideris, A. Filiatrault, M. Leclerc and R. Tremblay, "Experimental Performance Evaluation of Inclined Shelving for Steel Pallet Type Storage Racks".
- [125] Federation Europeenne de la Manutention, *Recommendation for the Design of Static Steel Pallet Racks Under Seismic Conditions, FEM 10.2. 08*, European Racking Federation, Birmingham, 2010.
- [126] RMI-Rack Manufacturers Institute, *ANSI MH 16.1-04 Specification for the Design, Testing and Utilization of Industrial Steel Storage Racks*, 2008.
- [127] Canadian Standards Association, "CAN/CSA--S16. 1 Limit States Design of Steel Structures," *Mississauga, Ontario, December*, 2015.
- [128] A. Belleri, M. Torquati and P. Riva, "P-Delta Effects in Displacement Based Assessment of RC Hinged Frames," in *2ECEES: 2nd European Conference on Earthquake Engineering and Seismology*, 24-29, Istanbul, Turkey, 2014.

- [129] Building Seismic Safety Council, *NEHRP Commentary on the Guidelines for the Seismic Rehabilitation of Buildings*, Federal emergency management agency, 1997.
- [130] EN CEN and others, *Steel Static Storage Systems - Adjustable Pallet Racking Systems - Principles for Structural Design*, CEN European Committee for Standardization, 2009.
- [131] Building Seismic Safety Council, *NEHRP Recommended Provisions for Seismic Regulations for New Buildings (FEMA 450)*, 2003.
- [132] E. Jacobsen, *Proposition de recherche initiale (Unpublished)*, Montreal: École Polytechnique de Montréal, 2015.
- [133] Industrial Systems Technical Committee On Commercial Storage Racking, *A344.1-05/A344.2-05 (Reaffirmed 2011) User Guide for Steel Storage Racks / Standard for the Design and Construction of Steel Storage Racks*, 2005.
- [134] Rack Manufacturer's Institute, FEMA 460.
- [135] Building Seismic Safety Council, "Prestandard and Commentary for the Seismic Rehabilitation of Buildings, FEMA-356," *Federal Emergency Management Agency, Washington, DC*, 2000.
- [136] G. E. N. R. Coutinho, *Numerical Simulation of the Seismic Behavior of Steel Storage Pallet Racking Systems*, Lisbon, Portugal: Instituto Superior Técnico, 2008.
- [137] M. Priestley, G. Calvi and M. Kowalsky, "Displacement-Based Seismic Assessment," in *Displacement-Based Seismic Design of Structures*, Pavia, Italy, IUSS Press, 2007, pp. 653-656.

APPENDIX A EXTRACTS FROM ANNEX N ON SEISMIC DESIGN

10.1 Notional and minimum horizontal loads

10.1.1

Rack structures and their elements (columns, beams, bracing, connections, etc.) shall be designed to withstand the forces of notional loads combined with factored loads. Notional loads are introduced to account for the effect of out-of-plumb on the stability of a framed structure and unique characteristics of rack structures.

10.1.2

At every level, notional loads shall be equal to the notional load coefficient, ϕ_N , multiplied by the factored gravity load contributed by that level, where the notional load coefficient is defined as:

$$\phi_N = (0.003 + \text{erection tolerance as defined in Clause 14.1})$$

Erection tolerance shall include any out-of-plumb effects caused by floor slope.

Commentary: For example, if the erection tolerance is equal to 1:240 plus an out-of-plumb of 1% due to floor slope, then ϕ_N would be equal to $0.003 + (1 / 240) + (0.01) = 0.0172$.

11.1.2.3

When the seismic design is performed in accordance with Clause 10.1.2.1(b)²:

- a) the height shall not exceed 10 m to the topmost beam level when $I_E F_a S_a(0.2)$ is greater than or equal to 0.35;

Commentary: For storage racks exceeding 10m, the structure is to be designed using rational, recognized engineering principles and current engineering practice that demonstrate compliance with the intent of the applicable building code. The design review for these racks needs to be carried out by Professional Engineers experienced and knowledgeable in seismic analysis methods and with proper modeling and testing of the actual rack's behaviour. The rack design must have a clearly defined, seismic force resisting system that validates a stable, seismic response.

the provisions of Clause 27.1.2 shall apply;

- a) the seismic weights and gravity loads at every level shall be determined as defined in Clause 10.2;
- b) earthquake effects shall be determined using the methods described in Clauses 10.3 to 10.5, as applicable;
- c) stability effects shall be as specified in Clause 11.6;
- d) drift limits as specified in Clause 11.7 shall be satisfied;
- e) special design requirements specified in Clause 10.8 shall be satisfied; and

² i.e. if seismic design is performed according to Annex N and not Clause 27 of S16

- f) for the moment frame direction, the performance of the beam-to-column and column base connections shall be demonstrated through a qualification procedure, as specified in Clause 10.9.

11.2

11.2.1 Seismic weight

11.2.1.1 Calculation

The seismic weight shall be calculated by including the dead load of the structure plus the expected loading as specified by the storage rack user, but not less than 100% of the design product load in the cross-aisle direction and not less than 60% of the design product load in the moment frame direction. Well-substantiated product statistics from the user of the storage rack that account for the facility's loading practices shall support any reduction of the product load.

Commentary:

- i. *The seismic weight may be reduced by the dynamically active fraction of the load by up to 2/3 of the product load.*
- ii. *Research has shown that the stored goods do not move entirely in unison with the rack structure and the 2/3 factor accounts for this damping-of-the-load behaviour. If the designer knows that for a particular application the dynamic portion of the load is likely to be greater than 67%, then such a higher magnitude will be used in the determination of the lateral forces.*
- iii. *The products placed on the storage rack shelves are often less than the capacity for which the individual shelves are designed. In most operating warehouses these are several open product slots available for storing incoming product. Therefore, the total row seismic mass, for computing the down-aisle seismic effects may be reduced by the product of a probabilistic factor to account for the amount of load expected on the rack at the time of an earthquake. Reduction in the cross-aisle direction and for the vertical load is not permitted.*

11.4.1 Seismic force modification factors

The force modification factors shall be those used for conventional construction: $R_d = 1.5$, $R_o = 1.3$. In the moment frame direction, $R_o = 1.0$ when non-normalized connection test data is used in design and R_d may be taken equal to 2.0 provided that the requirements of Clause 10.8.1.2 are satisfied.

11.4.2 Importance factor

The seismic importance factor, IE, shall be taken equal to the importance factor applicable to the building in which the rack is located.

11.4.3 Connection stiffness

In the moment frame direction, the rotational stiffness of the beam-to-column and base connections shall be taken equal to the initial secant stiffness obtained at 60% of the connection's moment capacity, $M_{c \max}$, as determined from the connection qualification procedures specified in Clause 10.9.

11.4.5.1

The equivalent static force procedure may be used for rack structures at the ground level and if:

- (a) $IEFaSa(0.2)$ is less than 0.35; or
- (b) the total height h_n is less than 6.0 m and the fundamental period T_a is less than 1.0 s in the braced frame direction and less than 2.0 s in the moment frame direction.

11.4.5.2 Periods

The fundamental period of racks shall not be evaluated using the formulas for the fundamental period of building structures in Part 4 of the National Building Code of Canada. When determining earthquake forces, the period T_a in any direction shall be determined from methods of mechanics, except that the so-computed period for determining base shear and earthquake forces shall not exceed $0.15 h_n$ in the braced frame direction and to $0.3 h_n$ in the moment frame direction. In the moment frame direction, the rotational stiffness of the beam-to-column and base connections shall not be less than the stiffness determined as specified in Clause 10.4.3.

11.4.5.3

The static distribution of load provides a good distribution of load if the weight on the racks is similar at all levels but is less accurate if the mass distribution is not equal. Racks that have a large mass on the bottom level can get unreasonably high overturning moments if this is not accounted for. Under these circumstances the rack designer may elect to use dynamic analysis to get a more accurate distribution of the overturning forces acting on the rack.

11.5.2 Method

- (a) The effective properties of the equivalent single-degree-of-freedom system shall be determined from an appropriate model representing the rack structure inelastic first mode response with the effective stiffness of the beam-to-column and column base connections determined at the seismic design displacement;
- (b) The effective stiffness and energy dissipation capacity of the beam-to-column and column base connections shall be determined from the qualification procedure specified in Clause 10.9;
- (c) P-delta effects shall be taken into account;
- (d) The seismic design displacement shall be determined using the design displacement spectrum specified in Clause 10.5.3 using the effective period of the fundamental period and the equivalent damping properties of the rack structure; and
- (e) The structure equivalent viscous damping properties shall be based on the energy dissipation capacity of the beam-to-column and column base connections as specified in b). It may also include the inherent damping of the structure up to 3%.

11.5.3 Design Displacement Spectrum

The design spectral displacement values $S_d(T)$ at periods $T = 0.0, 0.2, 0.5, 1.0, 2.0, 5.0$ and 10.0 s shall be determined using $S_d(T) = 250 S(T) T^2$ (in millimeters). Values for intermediate values of T shall be determined using linear interpolation.

11.5.4 Minimum lateral resistance

At every level, the frame shall have a minimum lateral resistance in the moment frame direction equal to $2 \sum C_f \Delta / h_s$ where Δ and h_s are defined in Clause 10.6.2, unless it can be demonstrated through nonlinear dynamic analysis as described in the NBCC that the rack has stable seismic response and the drift limits specified in Clause 10.7 are satisfied. As a minimum, the required analysis shall account for the inelastic

cyclic response of the connections as obtained from the qualification procedure specified in Clause 10.9, including strength degradation, if any, and P-delta effects.

11.6 Stability effects

11.6.1 Notional loads

Notional lateral loads as specified in Clause 9.2 shall be applied when using a force-based analysis method. Notional loads need not be considered when determining drifts.

11.6.2 P-delta effects

When using force-based methods of analysis, P-delta effects shall be considered for members and connections for which inelastic response is expected by multiplying forces due to lateral load at every level by the factor U_2 :

$$U_2 = 1 + \frac{\sum 2C_f \Delta}{V_f h_s}$$

where Δ is the relative lateral displacement occurring in the level, as obtained from the seismic design displacements, V_f is the total horizontal shear force at the level, and h_s is the height of the level.

11.7 Drift limits

In the moment frame direction, the seismic displacement shall be such that:

- (a) at any level, the drift angle corresponding to the seismic design displacements does not exceed 0.05 radians; and
- (b) be such that the total rotation imposed on the beam-to-column connections from gravity loads plus the rotation from the amplified seismic displacements does not exceed the rotation capacity of connections, as prescribed in Clause 10.8.1.2.

11.8 Special design requirements

11.8.2.1 Moment connections

11.8.2.1.1

When using force-based analysis methods, the connection strength may be taken as the connection moment capacity, $M_{c,max}$, as defined in Clause 10.9.3.

11.8.2.1.2

When using force based analysis methods for moment-resisting frames, the total rotation imposed on the beam-to-column connections from gravity loads plus R_d times the seismic design displacements shall not exceed the rotation capacity of the connections, $\theta_{c,max}$, as defined in Clause 10.9.3.5.

11.8.2.1.3

When using displacement based analysis methods, the total rotation imposed on the beam-to-column connections from gravity loads plus two times the seismic design displacements shall not exceed the rotation capacity of the connections, $\theta_{c,max}$, as defined in Clause 11.9.3.5

11.8.3

Column design

Column members shall be designed to resist: (a) in the braced frame direction, the axial loads due the combination of the gravity loads plus the earthquake loads corresponding to a force modification factor of $R_d R_o = 1.3$;

(b) in the moment frame direction, the full gravity loads in combination with the bending moments induced at each level by the lesser of the combination of the gravity loads and the earthquake loads corresponding to the values obtained using a force modification of $R_d R_o = 1.0$ or 1.2 times the ultimate flexural capacity of the beam-to-column connections; and

(c) when braces are absent in the braced frame direction, as permitted in Clause 10.1.1, column members shall resist combined axial load and bending moments from gravity loads plus earthquake loads determined with $R_d R_o = 1.3$.

11.8.4

Beam design In the moment frame direction, beams must resist a moment equal to 1.2 times the combined bending moments and shears induced at each level by the lesser of the combination of the gravity loads and the earthquake loads corresponding to the values obtained using a force modification of $R_d R_o = 1.0$ or 1.2 times the ultimate flexural capacity of the beam-to-column connections or that will develop at the attainment of the maximum moment capacity of the beam-to-column connections used at their ends.

11.9.3.4

Connection moment capacity:

The connection moment, M_c , shall be taken as (see Figure 3):

$$M_c = 0.5 (PL + PR) L$$

The connection moment capacity, $M_{c,max}$, shall be taken as the maximum value of $M_{c,max,cycle}$ among all loading cycles, where $M_{c,max,cycle}$ is the average of the peak positive and peak negative moments M_c , in absolute values, reached within the same loading cycle (see Figure 4a).

11.9.3.5

Connection rotation capacity

The connection rotation, θ_c , is obtained by subtracting from the drift angle θ the drift angle due to elastic flexural deformation of the beams (see Figure 3):

$$\theta_c = \theta - 0.5 (PL + PR) L^2 / 3EI_b$$

When significant, the effect of the flexural deformations of the columns on connection rotation shall also be subtracted using the same procedure. The connection rotation capacity, $\theta_{c,max}$, is taken as the peak connection rotation $\theta_{c,peak}$ in the last loading cycle during which M_c peak is equal to or greater than 0.80 times $M_{c,max}$, where $M_{c,peak}$ and $\theta_{c,peak}$ are respectively the average of the positive and negative moments M_c and rotation θ_c , in absolute values, reached at the maximum positive and negative drift angles in the same loading cycle (see Figure 4). Presentation of test results shall be properly reduced to actual values by correcting, where appropriate, initial readings.

Note: Since rotations are measured at the beam end, the raw displacement data is a sum of beam deflection, connector rotation and column deflection. To obtain the true connector rotation data, the beam deflection value is to be subtracted from the data. Since the column is fixed at both ends, its deflections may be neglected in the data process due to its very small values.

15.1 Tolerances

The rack erection tolerance on out-of-plumb shall not exceed 1:240. If the rack is deliberately installed on a sloped floor, the additional out-of-plumb from the floor slope may be added to the erection tolerance. The maximum out-of-plumb erection tolerance shall be considered in the design. If the erection tolerance considered in design differs from 1:240, it must be shown on the rack design drawings.

APPENDIX B LABORATORY TESTS

Table : B-1: Testing matrix

Name	Date	Base Fixity	Beam- Column Fixity	Load Protocol
F1	11/26/2015- 11/27-2015	base- plate	pinned	Quasi-static displacement control (see Figure 3-4)
P1	12/15/2015	pinned	cold-form	
F2	12/04/2015 – 12/09/2015	base- plate		
P2	01/22/2016 – 01/25/2016	pinned		Pull-back tests
F3	01/29/2016 – 02/01/2016	base- plate		
P3	02/19/2016	pinned		
P4	03/11/2016			Re-Scaled_NGAKKiK_Major_H2_623_s scaled by 0.85 (see Figure 3-5)
P5	03/18/2016			Re-Scaled_RSN769_LOMAP_G06000 scaled by 1.02 (see Figure 3-5)
F4	04/07/2016	base- plate		Re-Scaled_F19.6_A112.2_BRUT_Trial1_s scaled by 3.2
F5	04/14/2016			Re-Scaled_RSN769_LOMAP_G06000 scaled by 1.45
F6	04/21/2016			Re-Scaled_NGAKKiK_Major_H2_623_s scaled by 1.9

B.1.Quasi-static tests

B.1.1Test F1

- 238
mm



Figure B-1 : Over all deformation Test F1

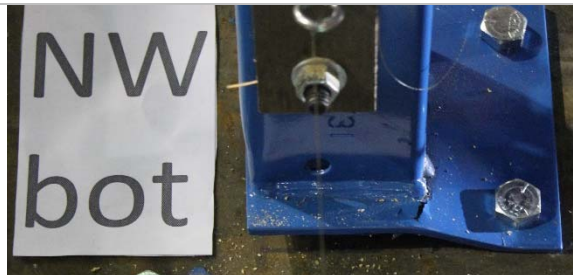


Figure B-2: Typical damaged to base-plate test F1



Figure B-3 : Typical damage to base plate
test F1

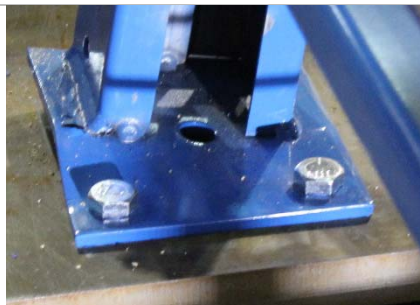





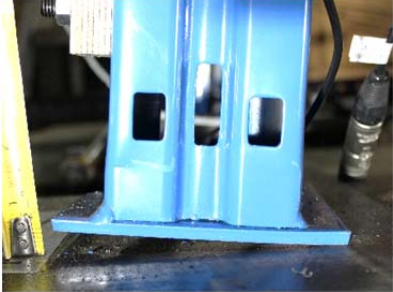

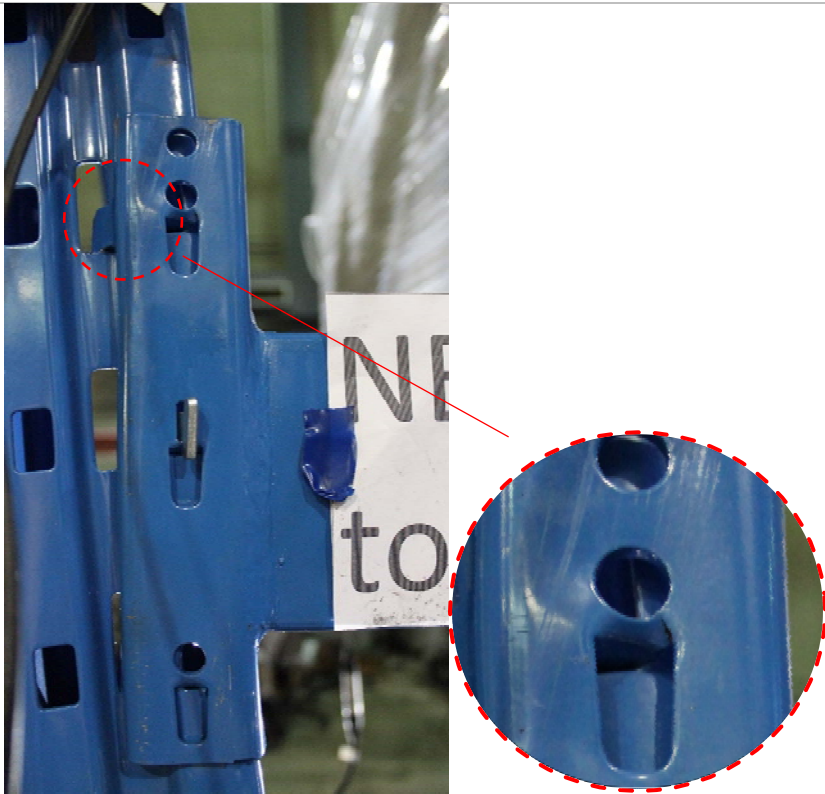






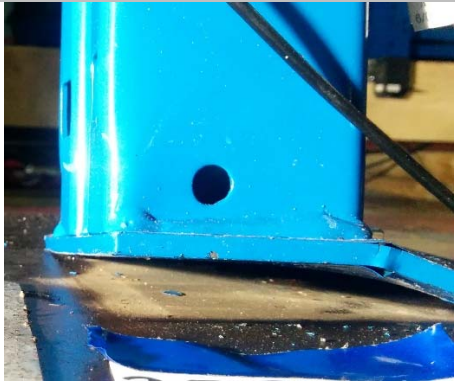
Figure B-4 : Typical damage to base-plate test F1

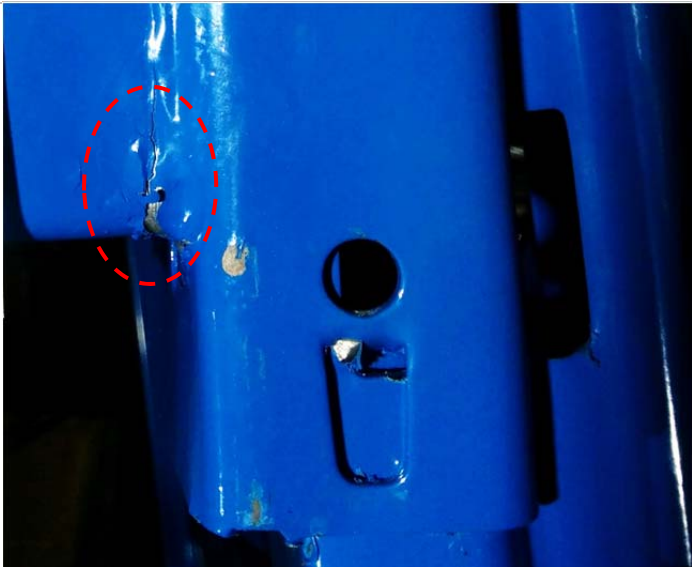
B.1.2 Test F2

Drift	Damage Observed	Photos of Damage	
cycles @ +/- 5mm followed by 4 cycles @ +/- 10 mm		No damage observed	
4 cycles @ +/- 50 mm	No perceptible damage to beam-column connections or base-plates; slight up-lift at corners of base-plates and rotation of connectors	 <p>Figure B-5 : Base-plate uplift</p>	 <p>Figure B-6 : Connectors are not visibly damaged</p>
1 st cycle @ - 180 mm	Top, bottom and middle exterior tabs bent out; interior tabs start to shear; base-plate near plastification close to weld and bolt; levering of base-plate	 <p>Figure B-7 : Shearing of top interior tab and bending out of top exterior tab (eastern side)</p>	 <p>Figure B-8 : Shearing of bottom interior tab and bending out of middle and lower exterior tabs (western side)</p>


		 <p>Figure B-9 : Plastic hinging of base-plate</p>	 <p>Figure B-10 : Lever effect at base-plate</p>
		 <p>Figure B-11 : Vue of the combination of plastic hinging (accompanied by paint flaking) and lever effect</p>	
+140 mm	No new damage observed		


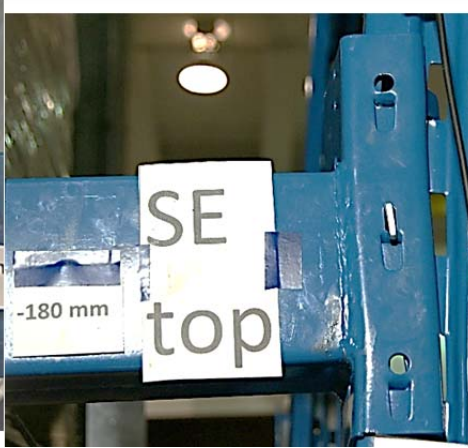

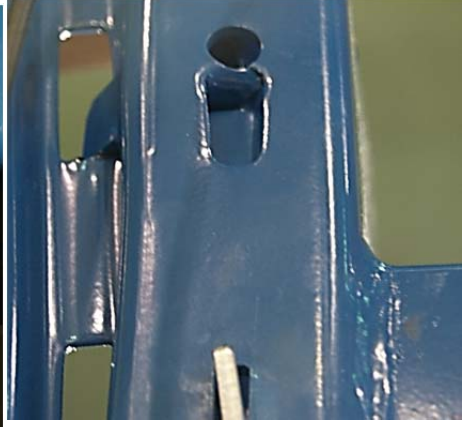
2 nd cycle @ - 180 mm	complete shearing of <u>some</u> top interior tabs	 <p>Figure B-12 : Complete shearing of interior top tabs</p>
+140 mm		 <p>Figure B-13 : Bearing of sheared interior tabs on connector body</p>
-180 mm	No new damage observed	
+140 mm		
-180 mm		
+140 mm		
-180		

mm			
+145 mm			
mm			
+238 mm	<p>Lateral torsional buckling of columns; progression of shearing of connector tabs; damage to some beam-connector welds; local buckling and global torsion of connectors; progression of base-plate plastification</p>	 <p>Figure B-14 : Level is held against the braced frame to emphasize the lateral torsional buckling</p>	 <p>Figure B-15 : Lateral torsional buckling of the columns</p>
		 <p>Figure B-16 : Local buckling</p>	 <p>Figure B-17 : Progression of base-plate plastic hinging</p>

		 <p>Figure B-18 : Beam-connector weld damage as well as progression of tab shearing</p>
-238 mm		Photos missing
+300 mm		Photos missing

B.1.3 Test P1

Drift	Damage Observed	Photo of Damage	
4 cycles @ +/- 5 mm	None visible	-	-
4 cycles @ +/- 50 mm	Some deformation of the 1st tabs; one end of the connector butts up against column while the tension end is visibly disengaged	 <p>Figure B-19 : Close-up for torn 2nd tab on NE connection</p>	

1 st cycle @ -180 mm	Shearing of some of the 1 st tabs and visible deformation of the 2 nd tabs; twisting of the connection on the tension side and deformation of the connection on the compression side	 <p>Figure B-20 : Twisting of connection</p>	 <p>Figure B-21 : Twisting</p>
+140 mm	No new damage observed	-	-
2 nd cycle @ -180 mm	Progression of shearing of the 1 st tab on SW, SE & NW connectors; complete shearing of the 1 st tab on the NE connector; paint cracking reveals the beginning of damage to the beam-to-connector weld on tension side	 <p>Figure B-22 : SW close-up</p>	 <p>Figure B-23 : NE connector close-up showing rupture of 1st tab</p>
Suite of cycles @ +140 & -180	No new damage observed	-	-




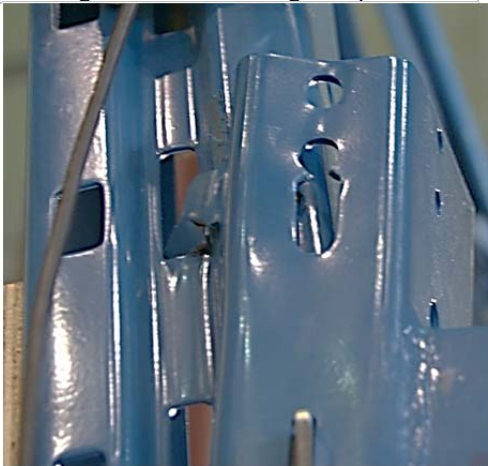


+238 mm	Loss of 1 st tabs on NE connection; complete shearing of 1 st tab on SW connection	 <p>Figure B-24 : Lost tab</p>	 <p>Figure B-25 : Shearing of top tab</p>
-238 mm	Shearing of 2 nd tab on NE connection; complete shearing of 1 st tab on NW connection	 <p>Figure B-26 : Complete shear first (top) tab</p>	 <p>Figure B-27 : Close-up for torn 2nd tab on NE connection</p>
+300 mm	All 1 st tabs are completely torn or missing; all 2 nd tabs have begun shearing; NE top has cracking of weld on tension side	 <p>Figure B-28 : Typ. Shearing and/or loss of 1st and 2nd tabs</p>	 <p>Figure B-29 : Close-up of NE weld rupture</p>



Figure B-30 : Column damage typ.: deformation is most pronounced around bottom connector hole



Figure B-31 : Typ. All deformation is taking place in the connection



Figure B-32 : Typ. Local buckling on the face of the connector



Figure B-33 : Typ. Connector after test



Figure B-34 : Full frame after testing

APPENDIX C FORCE-BASED ANALYSIS AND DESIGN ACCORDING TO ANNEX N DRAFT

In §C.3 an industry provided 3-level, 6-bay prototype rack is checked against S16 Annex N provisions using a force-based method. Using the same geometry, the same rack is then redesigned (given stronger connectors, base-plates, columns and beams). Given some feasibility issues encountered during force-based design some amendments to S16 Annex N are recommended.

C.1. Design Parameters

All geometries properties and loading are as outlined in §4.3.1.

No guidance is given in S16 Annex N as to the determination of base-plate stiffness. Thus when mechanical methods are used to determine the fundamental period, it is assumed that the base-plate has the same stiffness as the beam-to-column connectors.

C.2. Design Path

1. Check S16 Annex N applicability
2. Estimate the fundamental period of the rack as $T_a = 0.3h_n$
3. Find connector stiffness that produces estimated rack period
4. Calculate base shear, distribute shear to rack as equivalent static forces (F_x), add notional loads (N_x) calculate inelastic drifts and check against drift limits
5. Calculate U_2 and check connector resistance under amplified forces
6. Select connector that can support imposed moments at required stiffness
7. Check that beams and columns cede after connection

C.3. Industry proposed prototype design check

- Beams : C100x7 ($1.53 \times 10^6 \text{ mm}^4$), $F_{yb} = 345 \text{ MPa}$
- Columns : C100x7 ($1.53 \times 10^6 \text{ mm}^4$), boxed at all three levels, $F_{yc} = 345 \text{ MPa}$
- Connectors : AC175 unscaled

Using the equivalent static force method, the 3-bay, 3-level prototype rack is analyzed to see if it satisfies code requirements in the context of Vancouver site C conditions:

- §11.4.4: The method is applicable $h_n \approx 4.8 \text{ m}$ [15'8"] $< 6.0 \text{ m}$

The AC175 is proposed for this prototype frame. As no degrading cycle is available from the test data, the assumption is made that $M_{c,max}$ occurs in the maximum cycle shown in Figure C-1. According to S16 Annex N §11.4.3 is taken as the secant stiffness at 60% of $M_{c,max}$. For the AC175 connector:

- $k_{sec} = avg \left\{ \frac{2.41}{0.052}; \frac{-2.41}{-0.061} \right\} \cong 42.92 \frac{kNm}{rad}$ [380 in. kip]
- the fundamental period of the rack (from eigenvalue analysis) is $T_n = 2.86 \text{ s} > 1.4 \text{ s} \rightarrow$ **S16 Annex N §11.4.4 is not respected.**

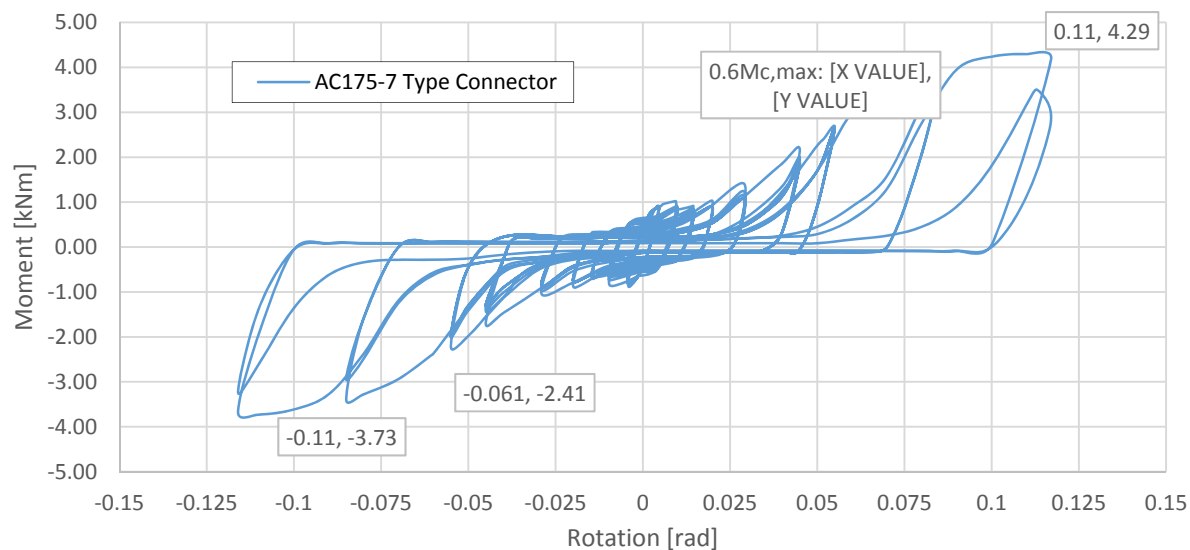


Figure C-1 : AC175 connector hysteresis as tested (un-scaled)

Base shear is calculated:

- S16 Annex N §11.4.1: $R_d R_o = (2.0)(1.0) = 2.0$
- S16 Annex N §11.4.2: I_E is assumed to be 1.0
- The seismic weight is calculated: $W = (1/2 \text{ frame})(14.679 \text{ kN unit-load/pallet})(2 \text{ pallets/beam})(3 \text{ levels})(6 \text{ bays}) = 264.2 \text{ kN}$ per 2D, 3-level, 6-bay moment frame
- The base shear according to NBCC §4.1.8.11.(2) is then:
- S_a calculated with real period, $T_n = 2.86 \text{ s}$, this period would only be valid for drift calculations but is used throughout the design check for demonstrative purposes

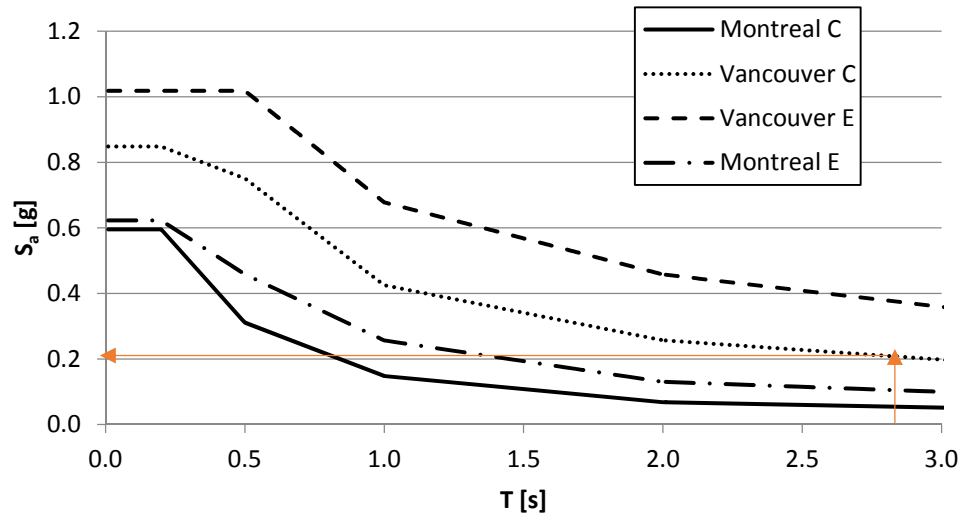


Figure C-2 : Finding acceleration from spectra

$$V = \frac{S(T_a)I_E W}{R_d R_o} = \frac{(0.205)(1.0)(1.0)(264.2 \text{ kN})}{(2.0)} = 27.14 \text{ kN [6.1 kips]}$$

According to §11.4.5.3 the equivalent static forces are distributed as follows:

$$F_x = \frac{V w_x h_x}{\sum_{i=1}^n w_i h_i}$$

Table C-1: Distribution of equivalent static forces

level	h_{sx}	h_x	w_i	$w_i h_i$	$w_i h_i^2$	F_x
-	m	m	kN	kNm	Nm ²	kN
3	1.524	4.775	88.074	420.55	2008142	13.29
2	1.524	3.251	88.074	286.33	930854	9.05
1	1.727	1.727	88.074	152.10	262683	4.81
Σ	4.775		264.222	858.99	3201680	27.14

A static analysis is performed on the frame under forces F_x to find story drifts:

Table C-2: Inelastic drift

	δ	h_{sx}	$\Delta_{inel.}$	$\Delta_{inel.}$
	m	m	m	m/m
3	0.311	1.524	0.16	0.10
2	0.227	1.524	0.19	0.12
1	0.127	1.727	0.24	0.14

$\rightarrow \Delta_{inel.} > 0.05 \text{ rads}$ **§11.7 (a) is not respected**

The notional load coefficient according to S16 Annex N §APPENDIX A $\phi_N = (0.003 + \text{erection tolerance}) = (0.003 + 1/240) = 0.0072$. Note that notional loads are insignificant in comparison to seismic loads:

Table C-3: Notional loads

level	h_{sx}	P_x	N_x	V_{F+N}
-	m	kN	kN	kN
3	1.524	88.07	0.63	13.92
2	1.524	176.15	0.63	23.60
1	1.727	264.22	0.63	29.04

P-delta amplification factors are calculated:

Table C-4: U2 factors

level	δ	h_{sx}	$\Delta_{inel.}$	$\Delta_{inel.}$	V_{F+N}	C_f	U_2
-	m	m	m	m/m	kN	kN	-
3	0.294	1.524	0.16	0.10	13.92	88.07	1.66
2	0.214	1.524	0.19	0.12	23.60	176.15	1.93
1	0.119	1.727	0.24	0.14	29.04	264.22	2.26

Unamplified connector moments are calculated from the FEM model:

Table C-5: Connector moments under gravity and lateral loads

		Column											
		1	2		3		4		5		6		7
		LH	RH	LH	RH	LH	RH	LH	RH	LH	RH	LH	RH
		kNm	kNm	kNm	kNm	kNm	kNm	kNm	kNm	kNm	kNm	kNm	kNm
Level	3	-2.07	-1.99	-1.98	-1.98	-1.98	-1.98	-1.98	-1.98	-1.98	-1.98	-1.98	-2.06
	2	-2.41	-2.39	-2.39	-2.39	-2.39	-2.39	-2.39	-2.39	-2.39	-2.39	-2.39	-2.40
	1	-2.83	-2.76	-2.76	-2.76	-2.76	-2.76	-2.76	-2.76	-2.76	-2.76	-2.76	-2.83
	0	-3.04	-3.07		-3.07		-3.07		-3.07		-3.07		-3.03

Table C-6: Connector moments under gravity and lateral loads

		Column											
		1	2		3		4		5		6		7
		LH	RH	LH	RH	LH	RH	LH	RH	LH	RH	LH	RH
		kNm	kNm	kNm	kNm	kNm	kNm	kNm	kNm	kNm	kNm	kNm	kNm
Level	3	-1.62	-2.44	-1.52	-2.45	-1.52	-2.44	-1.52	-2.44	-1.52	-2.44	-1.52	-2.51
	2	-1.94	-2.85	-1.93	-2.85	-1.92	-2.85	-1.92	-2.85	-1.92	-2.85	-1.93	-2.87
	1	-2.38	-3.22	-2.30	-3.22	-2.30	-3.22	-2.30	-3.22	-2.29	-3.22	-2.30	-3.28
	0	-3.03	-3.07		-3.07		-3.07		-3.07		-3.07		-3.04

U_2 amplified connector moments are calculated:

Table C-7: Amplified connector moments: $U_2 * M_E + M_D$

		Column											
		1	2		3		4		5		6		7
		LH	RH	LH	RH	LH	RH	LH	RH	LH	RH	LH	RH
		kNm	kNm	kNm	kNm	kNm	kNm	kNm	kNm	kNm	kNm	kNm	kNm
Level	3	-2.99	-3.76	-2.84	-3.76	-2.83	-3.76	-2.83	-3.76	-2.83	-3.76	-2.84	-3.88
	2	-3.86	-4.75	-3.83	-4.75	-3.82	-4.75	-3.82	-4.75	-3.82	-4.75	-3.82	-4.78
	1	-5.47	-6.24	-5.31	-6.23	-5.31	-6.23	-5.31	-6.23	-5.30	-6.23	-5.31	-6.37
	0	-6.86	-6.94		-6.94		-6.94		-6.93		-6.93		-6.85

The resistance of the connectors (see S16 Annex N §11.8.2.1.1 & §11.9) is checked against amplified seismic forces plus gravity loads:

$$M_c = U_2 M_E + M_D = \left(\frac{2.26 + 1.93}{2} \right) (-2.83) + (-2.83 + 3.28) = -6.37 \text{ kNm [56 in. kip]}$$

$$> M_{c,max} = (4.29 + 3.73)/2 = 4.01 \text{ kNm [35.5 in. kip]}$$

→ **Connector strength is insufficient**

The second drift limit which referred to in S16 Annex N §11.7b) states that the imposed rotations (S16 Annex N §11.8.2.1.2) must not exceed the capacity of the connectors as defined in S16 Annex N §11.9.3.5. The test data given does not show a degrading cycle, so the peak cycle as referred to in S16 Annex N §11.9.3.5 is taken as the maximum cycle in Figure C-1. It is assumed that this maximum cycle is also the last cycle in which $M_{c,peak}$ is 80% of $M_{c,max}$ thus $\theta_{c,max}$ shall be taken as 0.11 rad.

- The rotation imposed on beam-to-column connections by gravity loads, plus loads which produce R_d times the seismic design displacement is calculated using the maximum connector moments as computed in Table C-2 (notional loads are negligible) and Table C-3:

$$\theta_c = R_d \theta_E + \theta_D = \frac{R_d(R_d R_o M_E) + M_D}{k_{sec}} = \left| \frac{2(2 \cdot -2.83) - 0.46}{42.92 \text{ kNm/rad}} \right| = 0.27 \text{ rad} > 0.11 \text{ rad}$$

→ **Annex N §11.7(b) is not satisfied**

Beams and columns are checked in re-design.

C.4. Prototype re-design according to the equivalent static force method as proposed in S16 Annex N

According to S16 Annex N §11.4.5.2 the fundamental period may be computed using mechanics but must not exceed $0.3 h_n = (0.3)(4.775) \approx 1.4 \text{ s}$ nor must it exceed 2.0 s (S16 Annex N §11.4.4). Experience with this rack has shown that at periods past approximately 1.2 s , with Vancouver site C conditions, deflections become excessive. T_a is therefore taken as 1.2 s .

N.B. it was found for this particular rack that using NBCC §4.1.8.11. 3)d)v) (softening the rack to get longer periods past the limits of stated above) did not result in acceptable deflections.

Beam and column dimensions are unchanged in this iteration. Springs of equal stiffness at the base (this hypothesis should be verified in base-plate design) and between beams and columns are assumed. Using mechanics, a connector stiffness of 420 kNm/rad [3717 in. kip] is required to obtain a period of 1.2 s . This requires scaling the strength of the connection by a factor of 9.75. According to S16 Annex N §11.4.3 the connection stiffness is taken as the secant stiffness at 60% of $M_{c,max} = (0.6)(40.05) = 24.03 \text{ kN}$ (see Figure C-2)

- $k_{sec} = \text{avg} \left\{ \frac{23.47}{0.052}; \frac{-23.47}{-0.061} \right\} \cong 420 \frac{\text{kNm}}{\text{rad}}$ [3717 in. kip]

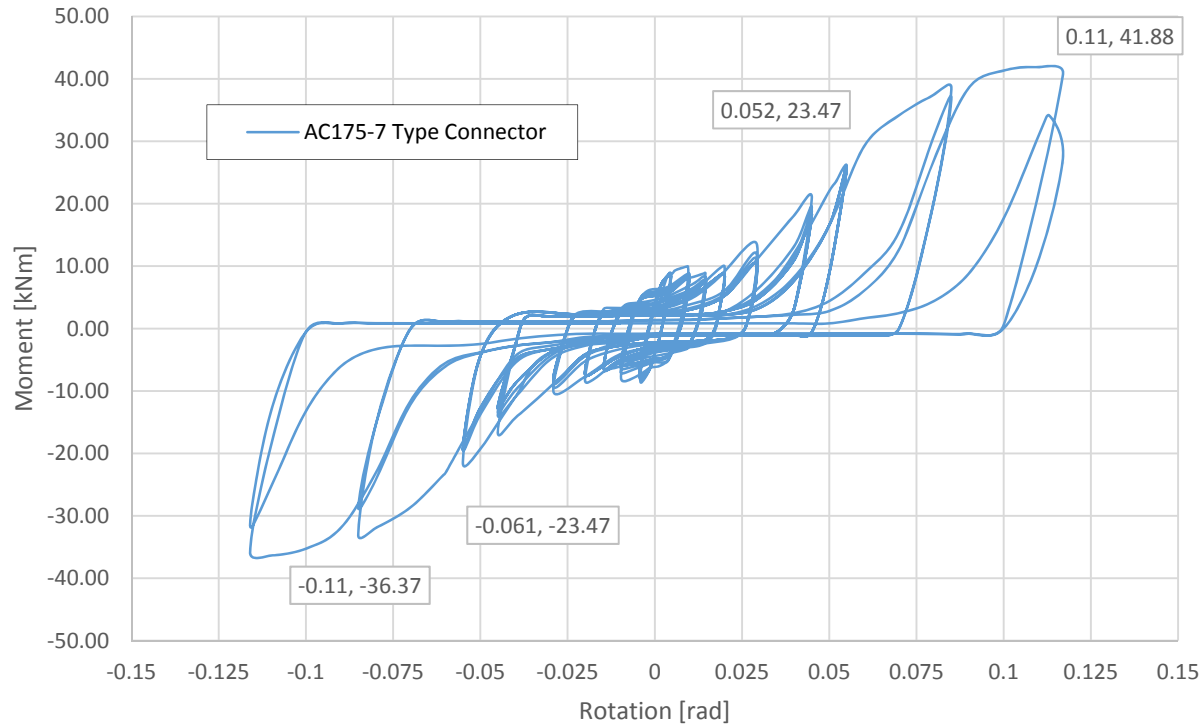


Figure C-3 : AC175 Connector with strength scaled by a factor of 9.75

Calculation of base-shear:

- S16 Annex N §11.3: $R_d R_o = (2.0)(1.0) = 2.0$
- S16 Annex N §11.4.2: I_E is assumed to be 1.0
- The seismic weight is calculated: $W = (1/2 \text{ frame})(14.679 \text{ kN unit-load/pallet})(2 \text{ pallets/beam})(3 \text{ levels})(6 \text{ bays}) = 264.2 \text{ kN}$ per 2D, 3-level, 6-bay moment frame
- Spectral acceleration is taken at 1.2 s

The base shear according to NBCC §4.1.8.11.(2) is then:

$$V = \frac{S(T_a) I_E W}{R_d R_o} = \frac{(0.387)(1.0)(1.0)(264.2 \text{ kN})}{(2.0)} = 51.16 \text{ kN [11.5 kips]}$$

Equivalent static forces are computed accordingly. Notional loads are unchanged:

Table C-8: Notional Loads

level	hsx	Px	Fx	Nx	FF+N
-	m	kN	kN	kN	kN
3	1.524	88.07	25.05	0.63	25.68
2	1.524	176.15	17.05	0.63	17.68
1	1.727	264.22	9.06	0.63	9.69
Σ			51.16		53.05

A static analysis is performed on the frame to find story drifts:

Table C-9: Inelastic drift

	$\delta_{el.}$	hsx	$\Delta_{inel.}$	$\Delta_{inel.}$	$\rightarrow \Delta_{inel.} < 0.05 \text{ rads} \quad \text{\textbf{\S 11.7(a) is respected}}$
	m	m	m	m/m	
3	0.098	1.524	0.044	0.029	
2	0.076	1.524	0.066	0.044	
1	0.042	1.727	0.085	0.049	

Table C-10: U2 factor

	$\delta_{el.}$	hsx	$\Delta_{inel.}$	$\Delta_{inel.}$	Vf	Cf	U2
	m	m	m	m/m	kN	kN	-
3	0.098	1.524	0.044	0.029	25.68	88.07	1.10
2	0.076	1.524	0.066	0.044	43.36	176.15	1.18
1	0.042	1.727	0.085	0.049	53.05	264.22	1.24

Unamplified connector moments are calculated from the FEM model:

Table C-11: Connector moments under lateral loads ($F_x + N_x$)

		Column											
		1	2		3		4		5		6		7
		LH	RH	LH	RH	LH	RH	LH	RH	LH	RH	LH	RH
		kNm	kNm	kNm	kNm	kNm	kNm	kNm	kNm	kNm	kNm	kNm	kNm
Level	3	-2.73	-2.42	-2.33	-2.34	-2.34	-2.33	-2.33	-2.33	-2.33	-2.31	-2.39	-2.69
	2	-4.44	-4.24	-4.19	-4.18	-4.17	-4.16	-4.16	-4.16	-4.16	-4.16	-4.21	-4.40
	1	-6.11	-5.60	-5.43	-5.44	-5.44	-5.44	-5.43	-5.43	-5.42	-5.40	-5.56	-6.06
	0	-6.96	-7.37		-7.35		-7.33		-7.32		-7.33		-6.90

Table C-12: Connector moments under gravity and lateral loads

		Column											
		1	2		3		4		5		6		7
		LH	RH	LH	RH	LH	RH	LH	RH	LH	RH	LH	RH
		kNm	kNm	kNm	kNm	kNm	kNm	kNm	kNm	kNm	kNm	kNm	kNm
Level	3	-1.10	-4.46	-0.35	-4.33	-0.36	-4.32	-0.35	-4.31	-0.34	-4.30	-0.35	-4.32
	2	-2.53	-6.23	-2.21	-6.17	-2.19	-6.15	-2.17	-6.14	-2.17	-6.13	-2.22	-6.31
	1	-4.34	-7.62	-3.44	-7.42	-3.46	-7.42	-3.45	-7.41	-3.44	-7.40	-3.55	-7.83
	0	-6.81	-7.37		-7.34		-7.33		-7.33		-7.33		-7.06

The second drift limit referring to connector rotation capacity is checked (S16 Annex N §11.7.b)):

$$\theta_c = R_d \theta_E + \theta_D = \frac{R_d(R_d R_o M_E) + M_D}{k_{sec}} = \left| \frac{2(2 \cdot -6.06) - 1.98}{420 \text{ kNm/rad}} \right| = 0.062 \text{ rad} < 0.11 \text{ rad}$$

→ **OK**

The resistance of the connectors (see S16 Annex N §11.8.2.1.1 is checked against amplified seismic forces plus gravity loads. For the critical connector (see Table C-6):

$$M_c = U_2 M_E + M_D = \left(\frac{1.18 + 1.24}{2} \right) (-6.06) + (-7.83 + 6.06) = -9.11 \text{ kNm} [80.6 \text{ in. kip}]$$

$$\ll M_{c,max} = (36.37 + 41.88)/2 = 40.05 \text{ kNm} [354 \text{ in. kip}]$$

→ **Connector strength is sufficient**

N.B.: Because of the way connector stiffness is defined, every connector that passes the rotation limit set out in S16 Annex N §11.7b is automatically qualified to verify the resistance requirement as set out in S16 Annex N §11.8.2.1.1 & §11.9.

Table C-13: P-delta amplified forces induced by lateral loads plus gravity loads: $U_2 M_E + M_D$

		Column											
		1	2		3		4		5		6		7
		LH	RH	LH	RH	LH	RH	LH	RH	LH	RH	LH	RH
		kNm	kNm	kNm	kNm	kNm	kNm	kNm	kNm	kNm	kNm	kNm	kNm
Level	3	-1.37	-4.70	-0.58	-4.56	-0.59	-4.55	-0.58	-4.54	-0.57	-4.53	-0.59	-4.59
	2	-3.14	-6.81	-2.79	-6.74	-2.76	-6.73	-2.75	-6.72	-2.74	-6.71	-2.80	-6.92
	1	-5.63	-8.80	-4.59	-8.57	-4.60	-8.57	-4.59	-8.56	-4.58	-8.54	-4.72	-9.11
	0	-8.67	-9.17		-9.14		-9.13		-9.12		-9.12		-8.59

Beams and columns are designed to be consistent with the FEM model in that only strong axis buckling will be permitted in columns and yielding in beams.

S16 Annex N §11.8.4 (refers to beams) and §11.8.3 (refers to columns) states that members should resist the lesser of:

- Forces induced by gravity loads and earthquake loads corresponding to values obtained using $R_d R_o = 1.0$; or
- Forces induced by gravity loads plus end moments equal to 1.2 times the maximum moment capacity of the beam-to-column connections.

When $R_d R_o = 1$, base shear is:

$$V = 2V_{RdRo=2} = 102.31 \text{ kN [23 kips]}$$

P-delta amplification factor is unchanged. Seismic forces double while gravity induced forces remain unchanged:

Table C-14: P-delta amplified forces induced by lateral loads plus gravity loads: $U_2 M_E + M_D$

		1	2		3		4		5		6		7
		LH	RH	LH	RH	LH	RH	LH	RH	LH	RH	LH	RH
		kNm	kNm	kNm	kNm	kNm	kNm	kNm	kNm	kNm	kNm	kNm	kNm
Level	3	-5.93	-5.26	-5.06	-5.08	-5.08	-5.07	-5.06	-5.06	-5.05	-5.02	-5.19	-5.84
	2	-14.15	-9.84	-9.71	-9.69	-9.67	-9.66	-9.65	-9.64	-9.64	-9.64	-9.76	-10.20
	1	-14.96	-13.71	-13.31	-13.32	-13.32	-13.31	-13.30	-13.29	-13.27	-13.23	-13.62	-14.84
	0	-17.03	-18.03		-17.97		-17.94		-17.91		-17.92		-16.88

Since $1.2M_{c,max} = (1.2)(40.05 \text{ kNm}) = 48.06 \text{ kNm} \gg 14.96 \text{ kNm}$, beams and columns are designed using forces under $R_d R_o = 1.0$

To prevent yielding, the section modulus of the beams must satisfy: $S_x > (15 \text{ kNm}) / (0.9)(345 \text{ MPa}) = 48.3 \times 10^3 \text{ mm}^3 > S_{x,C100 \times 7} = 30 \times 10^3 \text{ mm}^3$. A C130x10 [C5x6.7] will be appropriate.

The controlling columns are the interior columns with $C_f = 44.1 \text{ kN [9.91 kips]}$ and $M_f = 18 \text{ kNm [159 in. kip]}$. This requires a C150x12 [C6x8.2].

The larger sections have the effect of stiffening the rack somewhat, reducing the period and slightly increasing base-shear. This stiffened system sees reduced drifts and thus the strength of the connections can be reduced. The process becomes iterative as connection forces are diminished under softer connections allowing smaller beams and columns.

After some iterations C130x13 [C5x9] columns, C130x10 [C5x6.7] beams, with connections at 280 kNm/rad [2478 in. kip] are chosen:

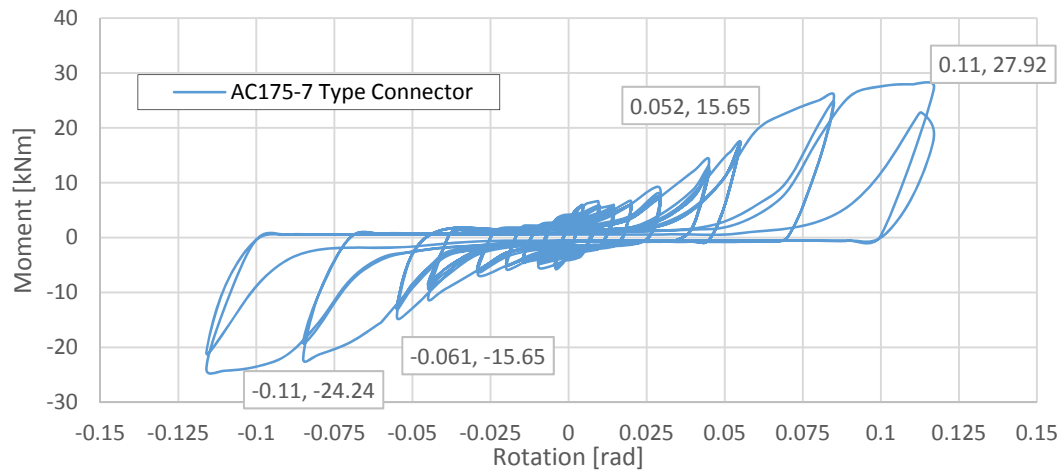


Figure C-4 : AC175 Connector with strength scaled by a factor of 6.5 to have a secant stiffness of 280 kNm/rad

The fundamental period from eigenvalue analysis is $T_a = 1.23$ s, giving a spectral acceleration of 0.384 g.

Base shear is calculated: $V = (S(T_a)I_E W)/(R_d R_o) = ((0.384)(1.0)(1.0)(264.2 \text{ kN}))/((2.0)) = 50.8 \text{ kN}$ [11.4 kip]

Drift angles and P-delta amplification factors are (largely) un-changed: $\rightarrow \Delta_{inel.} < 0.05$ rads §11.7 (a) is respected.

Table C-15: Calculation of U_2 factors

	$\delta_{el.}$	h_{sx}	$\Delta_{inel.}$	$\Delta_{inel.}$	V_f	C_f	U_2
	m	m	m	m/m	kN	kN	-
3	0.099	1.524	0.049	0.032	25.52	88.07	1.11
2	0.075	1.524	0.065	0.043	43.10	176.15	1.17
1	0.042	1.727	0.085	0.049	52.74	264.22	1.25

Connector moments are somewhat reduced (see comparison with Table C-11 and Table C-16):

Table C-16: Connector moments under lateral loads ($F_x + N_x$)

		Column											
		1	2		3		4		5		6		7
		LH	RH	LH	RH	LH	RH	LH	RH	LH	RH	LH	RH
		kNm	kNm	kNm	kNm	kNm	kNm	kNm	kNm	kNm	kNm	kNm	kNm
Level	3	-3.23	-3.00	-2.99	-2.99	-2.99	-2.98	-2.98	-2.98	-2.98	-2.97	-3.02	-3.24
	2	-4.31	-4.23	-4.24	-4.23	-4.23	-4.22	-4.22	-4.22	-4.22	-4.22	-4.24	-4.31
	1	-5.55	-5.29	-5.26	-5.26	-5.25	-5.25	-5.25	-5.24	-5.24	-5.24	-5.28	-5.54
	0	-6.30	-6.46		-6.45		-6.45		-6.44		-6.44		-6.26

Table C-17: P-delta amplified forces induced by lateral loads plus gravity loads

		Column											
		1	2		3		4		5		6		7
		LH	RH	LH	RH	LH	RH	LH	RH	LH	RH	LH	RH
		kNm	kNm	kNm	kNm	kNm	kNm	kNm	kNm	kNm	kNm	kNm	kNm
Level	3	-2.57	-4.48	-2.20	-4.45	-2.19	-4.44	-2.18	-4.44	-2.18	-4.43	-2.21	-4.62
	2	-3.82	-5.96	-3.72	-5.96	-3.70	-5.95	-3.69	-5.95	-3.69	-5.94	-3.71	-6.04
	1	-5.65	-7.53	-5.24	-7.49	-5.23	-7.48	-5.22	-7.47	-5.22	-7.47	-5.26	-7.77
	0	-7.85	-8.05		-8.04		-8.03		-8.02		-8.02		-7.80

The second drift limit referring to connector rotation capacity is checked (S16 Annex N §11.7.b)):

$$M_c = U_2 M_E + M_D = -8.05 \text{ [71 in.kip] kNm} \ll M_{c,max} = (27.92 + 24.24)/2 \\ = 26.08 \text{ kNm [230 in.kip]} \rightarrow \text{Connector strength is sufficient}$$

$$\theta_c = R_d \theta_E + \theta_D = \frac{R_d(R_d R_o M_E) + M_D}{k_{sec}} = \left| \frac{2(2 \cdot -5.29) - 1.13}{280 \text{ kNm/rad}} \right| = 0.08 \text{ rad} < 0.11 \text{ rad}$$

→ **Connector rotation is OK**

When static analysis is performed under loads produced by $R_d R_o = 1$, U_2 amplified connector moments including gravity loads are as follows:

Table C-18: Amplified moments

		1	2		3		4		5		6		7
		LH	RH	LH	RH	LH	RH	LH	RH	LH	RH	LH	RH
		kNm	kNm	kNm	kNm	kNm	kNm	kNm	kNm	kNm	kNm	kNm	kNm
Level	3	-7.10	-6.59	-6.56	-6.54	-6.54	-6.53	-6.53	-6.52	-6.52	-6.51	-6.59	-7.07
	2	-12.84	-9.80	-9.81	-9.79	-9.78	-9.77	-9.77	-9.76	-9.76	-9.76	-9.78	-9.96
	1	-13.61	-12.97	-	-12.88	-12.88	-12.87	-12.86	-12.85	-12.85	-12.84	-	-13.56
	0	-15.43	-15.83		-15.81		-15.79		-15.78		-15.76		-15.34

Beam yielding check: $S_x > (13.6 \text{ kNm}) / (0.9)(345 \text{ MPa}) = 43.8 \times 10^3 \text{ mm}^3 > S_{x,C130 \times 10} = 48.6 \times 10^3 \text{ mm}^3 \rightarrow \text{Beam OK}$ (assuming sufficient restraint such that yielding may develop).

Column check: To be consistent with modelling assumptions, only in-plane buckling is considered. $C_f/C_r + U_{1x}M_{rfx}/M_r = 44.1/446 + (1)(15.83)/17.88 = 0.984 < 1 \rightarrow \text{Columns OK}$. Given that columns are free to buckle in flexion and flexion-torsion and are in addition subjected to torsion from their connectors, additional restraint would be necessary to permit this assumption in reality.

A **base-plate** of sufficient strength and giving a rigidity equal to that of the beam-column connectors must be selected to be consistent with design assumptions.

APPENDIX D DESCRIPTION OF FEM MODEL OF RACK

OpenSees Version 2.5.0 (rev 6248) 32-Bit running on Ubuntu 16.04 was used for all FEM analyses.

D.1. OpenSees FEM used in predictions of experimental phase

During the experimental phase a 2D concentrated yielding model as shown in Figure D-1 is used.

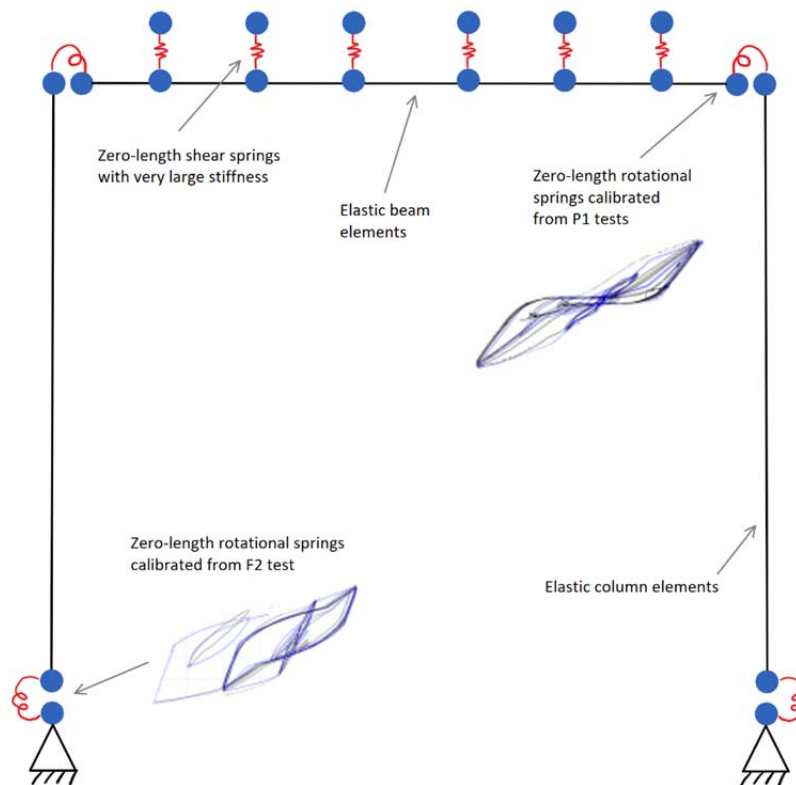


Figure : D-1: Preliminary FEM model of rack

D.1.1 Columns

Columns are elastic beam-column elements with a geometric transformation allowing inclusion of P-delta effects.

D.1.2 Beams

Beams are elastic beam-column elements with a linear geometric transformation (without inclusion of p-delta effects). The beams are divided into 7 sub-elements.

D.1.3 Zero-length pallet shear springs

Zero-length springs are present between the nodes to which mass is assigned and the beam nodes. The behaviour of these shear springs is calibrated from seismic tests. A velocity and normal force dependant friction model is used.

D.1.4 Zero-length beam-column connectors (see also §F.3 line 734)

Zero-length springs are calibrated from the quasi-static physical tests using Pinching4, a multi-linear pinched material including cyclic degradation.

D.1.5 Zero-length base-plates (see also §F.3 line 734)

The moment-rotation rule of the zero-length springs are calibrated from the quasi-static Test F2. Three materials are used in parallel to capture the multi-linear behaviour of the base-plates.

D.2. OpenSees FEM model used in parametric tests of prototype racks

A multi-bay, multi-level 2D model with fiber base-plate assemblies, fiber columns, elastic beams with fiber elements at their end points and zero length plastic hinge elements between beams and columns. The shear springs describing pallet sliding are as described in §D.1.3 and the beam-column connections are as described in §D.1.4.

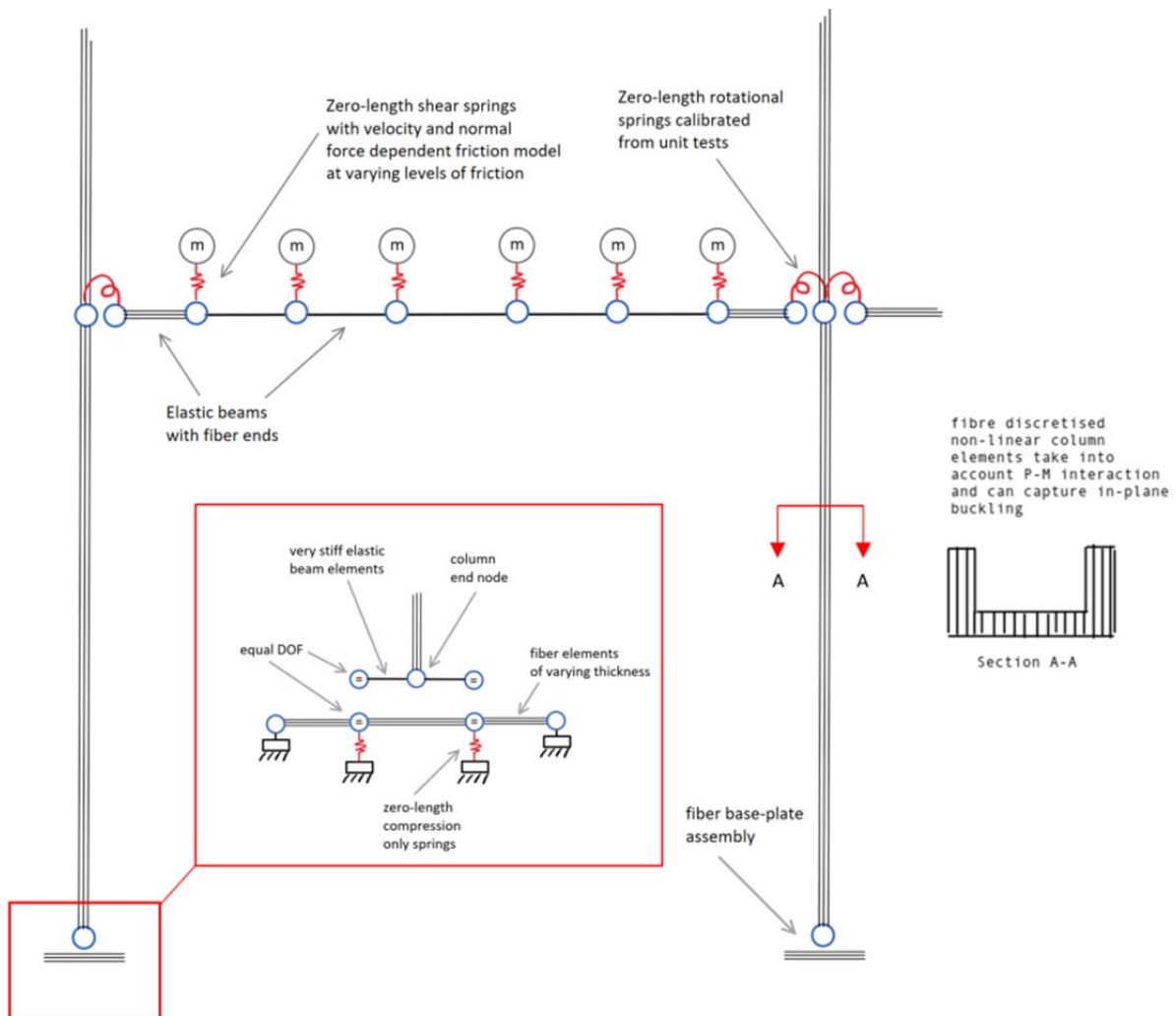


Figure : D-2 : Final FEM model of rack

D.2.1 Fiber Base-Plate Assemblies (see also §F.3 line 844)

The base-plate assemblies are made up of a 3 fiber plate elements connected between two fixed nodes (representing the position of the bolts) and two interior nodes representing the edge of the column section. Beneath the nodes representing the edges of the columns are two compression

only zero-length springs. Above the nodes representing the column edges are two nodes connected to very rigid elements, themselves connected to the end of the column. These last nodes are constrained to move with the nodes on the fiber base-plate which represent the edge of the column channel.

D.2.2 Fiber Columns (see also §F.3 line 1005)

Fiber columns are composed of 8 nonlinearBeamColumn sub-elements with 3 integration points. Each channel shaped fiber section (see also §F.3 line 1128) acts on a Steel4 material rule and has 4 fibers along the web depth and 8 fibers along the flange thickness. For buckling to occur these elements must be given a slight out of plane deflection at their mid-points.

D.2.3 Elastic Beams with Fiber Ends

Beams with this configuration have the last element before the junction with the non-linear connector made up of a nonlinearBeamColumn element with the fiber section constructed in the same manner as in §D.2.2.

APPENDIX E CYCLIC BASE-PLATE PSEUDO TESTS, FEM BASE-PLATE MODELS AND VERIFICATION BY YIELD-LINE METHOD

Base-plates used for prototype racks are symmetrical in the plane parallel to bending such that the finite element model is 2D and can accommodate variation of compressive load in concert with bending. Figure : & Figure : show the yield line model of the base-plate and the equivalent FEM model of the base-plate as it is constructed in OpenSees. Since no information is available, the base-plate model does not have a maximum rotation capacity after which stiffness would degrade.

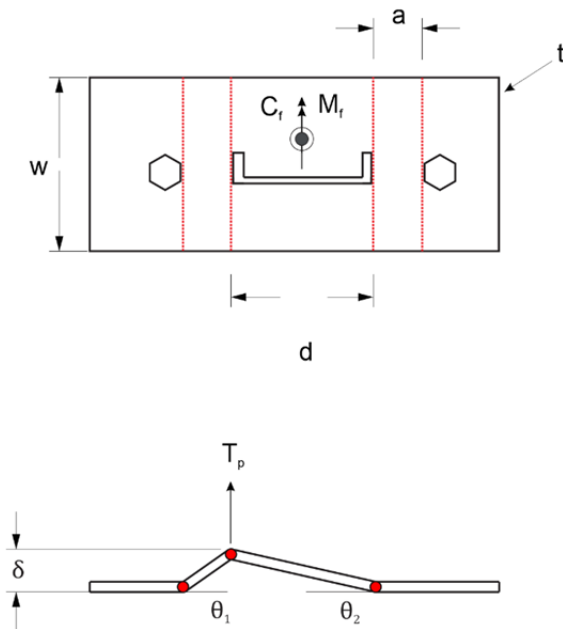


Figure : E-1 : Yield-line model of symmetrical base-plate

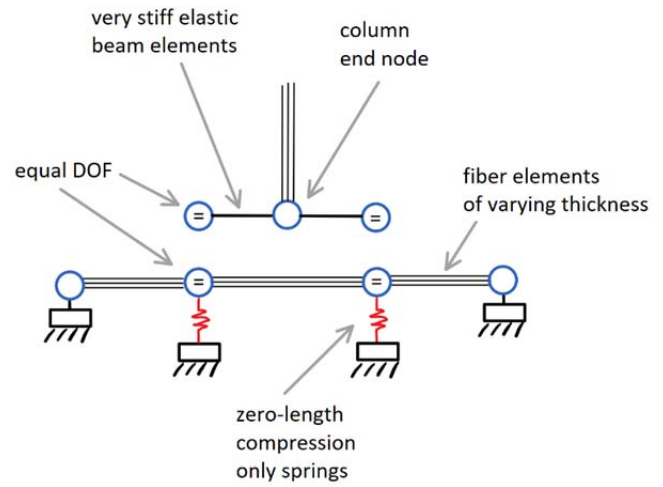


Figure : E-2 Finite element model of symmetrical base-plate

From the model in Figure E-1 the following relation is developed for the yield moment in function of compressive load:

$$W_E = W_I \Rightarrow T_p = 2 \cdot m_p \cdot w \cdot \left(\frac{1}{d} + \frac{1}{a} \right) \Rightarrow M_p = \left(T_p + \frac{C_f}{2} \right) d \quad (6-1)$$

As an example a FEM base-plate with the following parameters is verified using eq. (6-1): $a = 50.8$ mm, $d = 102$ mm, $w = 127$ mm, $t = 5.5$ mm with an applied compression of $C_f = 44$ kN and a yield strength of $F_y = 345$ MPa, the yield moment is this $M_p = 4.24$ kNm Figure E-3 shows the FEM OpenSees model subjected to the cyclic loading shown in E-4. The FEM model and the yield model agree.

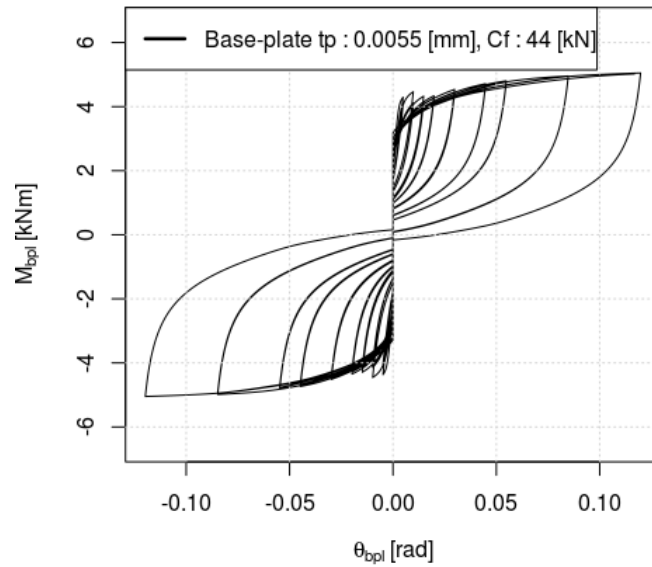


Figure : E-3 : Base-plate model subjected to RMI type cyclic loading

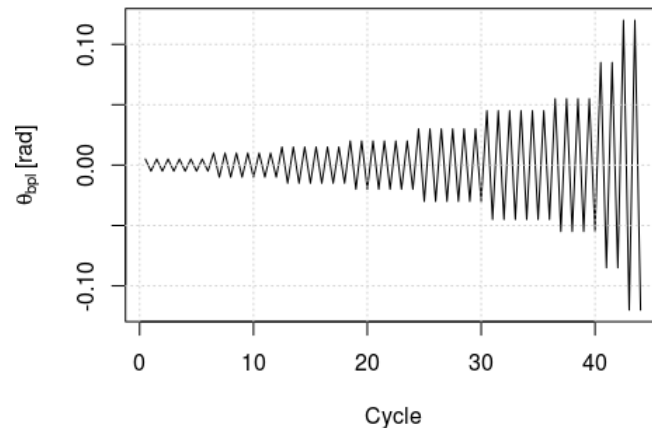


Figure : E-4 : Cyclic loading applied to FEM base-plate models

APPENDIX F TCL SCRIPTS FOR OPENSEES MODEL AND TIME HISTORY ANALYSIS

The following three sections describe and give the contents of the three principal scripts used to interact with the OpenSees framework and perform all the analysis in this paper. Each script is intended to be saved in a separate file in the same folder. Analysis is run by sourcing the script described in §F.1. Users are cautioned to understand and verify all results and are referred to the OpenSees user manual for instructions on how to download the free opensource software (Open System for Earthquake Engineering Simulation) and run analyses using the OpenSees framework [87]. The full project scripts including a database of channel sections and post-processing scripts are available at https://github.com/emjac/rack_moment_frames

F.1. Main input file to create model and run analysis

The following script gives an example of how a user may interact with the `rack_pack.tcl` collection of functions to efficiently construct a model of a rack, apply gravity loads, check that gravity loads are properly applied, see a display of the rack geometry, set recorders on some predefined lists of nodes and finally run a time-history analysis. The user must supply an accelerogram.

```
#####
# Procedure to run a series of time history analyses
#
# EJ
#####

# Set rack properties, see the rack_MRF function for other input options
# SI units
set h1 1.727; # First story height [m]
set hx 1.524; # Upper story heights [m]
set L 2.515; # Beam length c/c dimensions are used [m]
set beamPrfl "poly-cold-form-beam"; # See secProp for other sections, string
set colPrfl "poly-cold-form-col"; # See secProp for other sections, string
set Fyc 345e6; # Setting yield to strength to less than 345 MPa will invoke the use of fiber columns
set Fyb 345e6; # Setting yield to strength to less than 345 MPa will invoke the use of plastic
set boxed_levels 3; # How many of the columns levels, from the floor should be doubled channel sections
set PL 14679.; # Pallet weight [N]
set nB 6; # Number of bays [unitless]
set nL 3; # Number of levels [unitless]
set zeta 0.03; # Percent of critical damping (for Rayleigh damping). Ex. 0.02 means 2% of critical.
set muS 0.17; # Friction coefficient [unitless]
set muK 0.8; # Kinetic friction coefficient [unitless]
set sprOption "AC175"; # Name of a pre-calibrated connector
set bplOption "Parallel"; # Use fiber base-plate assemblies
set kc 2.36; # Strength scaling factor to apply to the connector material
```

```

set kctop [expr $kc/2]; # Strength scaling factor to apply to the top interior connectors
set kbp1 0.9; # Base-plate thickness or scale factor on base-plate material
set NL_geo "LargePdelta"; # Choose whether to include P-delta
set g_tol 0.0; # Global out-of-plumb drift [m/m]
set l_tol 0.0; # Local out-of-plumb drift at centre of columns [m/m]

# Includes the rack_pack package of modelling and analysis functions
lappend ::auto_path [eval pwd]
package require rack_pack
namespace import rack_pack::*

# Create rack model using the rackMRF function defined in rack_pack.tcl
rackMRF $h1 $hx $L $beamPrf1 $Fyb $colPrf1 $Fyc $boxed_levels $PL $nB $nL $zeta $muS $muK $sprOption $bp1Option $kc $kctop $kbp1 $NL_geo $g_tol $l_tol "";

# Apply gravity loads and check reaction using functions defined in rack_pack.tcl
record_rack "basenodes" "reaction"; # Recorders are set on the base-nodes
rack_gravity_static [expr $PL/6] "on_beams"; # Apply gravity loading
set message "Total vertical reaction is : "
set dof 2; # Degree of freedom for which reaction will be outputted
set step 10; # Step at which reaction will be computed
check_total_reaction $dof $step; # Check reaction by calling the function defined in rack_pack.tcl

# Ground motion accelerogram file
set accRecord "VC1.acc"
# Accelerogram time step
set dt 0.01;
# Accelerogram scale factor
set SF 1.0;

# Set displacement recorders on the exterior column nodes, see the record_rack function in rack_pack.tcl for more predefined recording options
record_rack "ext_col_nodes" "disp";

# Run time-history analysis
rack_TH $dt "" $accRecord $SF;

```

F.2.Package Index File

Save this script in a file named pkgIndex.tcl

```

# Tcl package index file, version 1.1
# This file is generated by the "pkg_mkIndex" command
# and sourced either when an application starts up or
# by a "package unknown" script. It invokes the
# "package ifneeded" command to set up package-related
# information so that packages will be loaded automatically
# in response to "package require" commands. When this
# script is sourced, the variable $dir must contain the
# full path name of this file's directory.

package ifneeded rack_pack 1.0 [list source [file join $dir rack_pack.tcl]]

```

F.3. Package of functions to build model and run analyses

The following script should be saved in a file called rack_pack.tcl

```
#####
# Package of commands for building a model of a rack semi-rigid moment
# frame, for running analysis on that frame and recording results
#
# rack_MRF is the principal function that calls other functions to
# construct a model of a rack
#
#####

# Create the rack_pack package

package provide rack_pack 1.0;
package require Tcl 8.5;
model BasicBuilder -ndm 2 -ndf 3

namespace eval ::rack_pack:: {

# Creates the rack_pack namespace with some common functions and variables

set version 1.0;

# Export functions such that they can be called by scripts outside the rack_pack file
namespace export rack_period;
namespace export triangular_pattern;
namespace export rack_gravity_static;
namespace export add_rayleigh_damping
namespace export rack_TH;
namespace export rackMRF;
namespace export check_total_reaction;
namespace export record_rack;
namespace export use_NL_spring;

# Default output directory
variable output_dir ""; # Set to null each time the package is called

# See get_tag
variable tagA 0; # Acceleration tag initialisation
variable tagT 0; # Time series tag initialisation
variable tagP 0; # Load pattern tag initialisation
variable tagM 0; # Material tag initialisation
variable tagS 0; # Section tag initialisation
variable tagG 0; # Geometric tags initialisation
variable tagF 0; # Friction tags initialisation

# Categorized lists of elements and nodes to make adding recorders and loads to groups of nodes easier
# Nodes are added to these lists when rackMRF is called and then they are available to all procedures in
# rack_pack
variable base_node_list {}; # List of nodes at the base of the structure
variable beam_node_list {}; # List of beam nodes not including the one coincident with the column
```

```

variable col_mid_node_list {}; # List of nodes in the middle of the columns (when fiber columns are used)
variable bpl_elem_list {}; # List of base-plate connector elements
variable col_elem_list {}; # List of column nodes
variable extcol_node_list {}; # List of nodes at each level where exterior column nodes are attached to beam-to-column connectors
variable intcol_node_list {}; # List of nodes at each level where interior column nodes are attached to beam-to-column connectors
variable connector_elem_list {}; # List of beam-to-column connector elements
variable beam_elem_list {}; # List of beam elements
variable beam_end_list {}; # List of fiber beam ends
variable pallet_elem_list {}; # List of elements between beams and pallet nodes
variable pallet_node_list {}; # List of nodes to which pallet masses are assigned

# Some modelling constants
variable pi [expr 2.0*asin(1.0)]; # Definition of pi
variable g 9.80665; # Gravity [m/s2]
variable E [expr 200.0e9]; # Steel elastic modulus [N/m2]
variable mSteel [expr 77000./$g]; # Unit mass of steel [kg/m3]
variable Fy_bpl 345e6; # !!!!! Careful : Changing this value will change beam and column plasticity !!!!!

}

proc ::rack_pack::get_Tag { tagType } {

#####
# Creates time, acceleration and pattern tags such that the same tag is
# not accidentally used twice by analysis procedures
#
# Example of creating a material tag and saving it to a variable:
# set sprMat [get_Tag "Material"];
#
# 11 july 2016, EJ
#####

variable tagA;
variable tagT;
variable tagP;
variable tagM;
variable tagS;
variable tagG;
variable tagF;

if { $tagType == "Section" } { incr tagS; return $tagS; };
if { $tagType == "Accel" } { incr tagA; return $tagA; };
if { $tagType == "Time" } { incr tagT; return $tagT; };
if { $tagType == "Pattern" } { incr tagP; return $tagP; };
if { $tagType == "Material" } { incr tagM; return $tagM; };
if { $tagType == "Geo" } { incr tagG; return $tagG; };
if { $tagType == "Fric" } { incr tagF; return $tagF; };

}

proc ::rack_pack::rackMRF { h1 hx L beamPrfl Fyb colPrfl Fyc boxed_levels PL nB nL zeta muSlow muFast sprOption bplOption { kc 1. } { kctop 1. } { kbpl 1. } {NL_geo
"LargePdelta"} {g_tol 0.} {l_tol 0.} {output_dir_append ""} {

#####
# Creates a 2D multi-story MRF with concentrated plasticity at column bases and beam to column joints, concentrated plasticity beams
# and distributed plasticity (fibre cross-section discretisation) of the columns allowing in-plane buckling
# First story column height can be specified differently than other column heights

```

```

# ALL UNITS SI
#
# INPUTS
# h1 := First level height, double [m]
# hx := Other level heights, double [m]
# L := Length of beams, double [m]
# beamPrfl := CISC designation for beam profile (other custom sections are available see proc secProp), string
# Fyb := Elastic limit for beams, double [N/m2] (if a value less than Fy_bpl = 345 MPa is used, plastic beams will be used)
# colPrfl := CISC designation for column profile (other custom sections are available see proc secProp), string
# Fyc := Elastic limit for columns, double [N/m2] (if a value less than Fy_bpl = 345 MPa is used, plastic columns will be used)
# boxed_levels := number of boxed levels, integer [unitless]
# PL := Weight of an individual pallet [N], the procedure assumes that there are two pallets per bay per level and that their weight is supported by 2 parallel MRF
# nB := Number of bays, integer [unitless]
# nL := Number of levels, integer [unitless]
# zeta := percent of critical damping to be used, default is 0. (Rayleigh damping) [%]
# muSlow := pallet friction coefficient [unitless], set to zero for no sliding
# muFast := kinetic friction coefficient [unitless]
# sprOption := "L" for linear springs, name of the non-linear spring if non-linear behaviour is wanted see use_NL_spring for some predefined options
# bplOption := "L" for linear springs, name of the non-linear spring if non-linear behaviour is wanted see use_NL_spring for some predefined options
# kc := When linear connections are used, kc represents the beam-column connector stiffness, double [Nm/rad]
# OR
# := When non-linear connections are used, kc represents the strength scaling factor to be applied to the non-linear material, double [unitless]
# kctop := Same as kc, but for the top interior connectors which may need to be a different scaling for strong column capacity design
# kbp1 := When linear connections are used, kbp1 represents the base-plate connector stiffness, double [Nm/rad]
# OR
# := When non-linear connections are used, kbp1 represents the a scaling factor to be applied to the non-linear material, double [unitless]
# In the special case that fiber sections are used, kbp1 represents the thickness of the plate, double [m]
# NL_geo := defines the kind of geometric non-linearity to be applied (default is to include P-delta effects), string [unitless]
# g_tol := initial global out of plumb condition (default is zero), double [mm/mm]
# l_tol := initial local column cambrure (default is zero), double [mm/mm]
# output_dir_append := a string to append to the default output directory
#
# Example :
#
# EJ
#####

# Remove existing models
wipe;

# Sets the name of the directory to save results in
set default_dir "rack_nL[expr $nL]nB[expr $nB]_"

# Creates output directory in which to save results
make_output_dir $default_dir$output_dir_append

# Saves and outputs modelling info
puts_and_save "h1: $h1"; puts_and_save "hx: $hx"; puts_and_save "L: $L"; puts_and_save "beamPrfl: $beamPrfl"; puts_and_save "Fyb: $Fyb";
puts_and_save "colPrfl: $colPrfl"; puts_and_save "Fyc: $Fyc"; puts_and_save "boxed_levels: $boxed_levels"; puts_and_save "PL: $PL"; puts_and_save "nB: $nB"; puts_and_save
"nL: $nL";
puts_and_save "zeta: $zeta"; puts_and_save "muSlow: $muSlow"; puts_and_save "muFast: $muFast"; puts_and_save "sprOption: $sprOption"; puts_and_save "bplOption:
$bplOption";
puts_and_save "kc : $kc"; puts_and_save "kctop : $kctop"; puts_and_save "kbp1: $kbp1"; puts_and_save "NL_geo: $NL_geo"; puts_and_save "g_tol: $g_tol"; puts_and_save
"l_tol: $l_tol";

# Loads some variables
variable g;

```

```

variable pi;
variable mSteel;
variable E;
variable Fy_bpl;
variable output_dir;

variable tagA; # Acceleration tag initialisation
variable tagT; # Time series tag initialisation
variable tagP; # Load pattern tag initialisation
variable tagM; # Material tag initialisation
variable tagS; # Section tag initialisation
variable tagG; # Geometric tags initialisation
variable tagF; # Friction ta initialisation

# Calculates some parameters
set mL [expr $PL/$g]; # Pallet mass
set nc [expr ($nB+1)]; # Number of upright base plate connections
set nb [expr $nL*$nc]; # Number of beam-connector connections

# Define geometric transformations
# For beam elements
set BeamTransf [get_Tag "Geo"];
geomTransf Linear $BeamTransf;
# For column elements
set ColTransf [get_Tag "Geo"];
if { $NL_geo == "noPdelta" } { geomTransf Linear $ColTransf };
if { $NL_geo == "Pdelta" } { geomTransf PDelta $ColTransf };
if { $NL_geo == "LargePdelta" } { geomTransf Corotational $ColTransf };

# Create array "h" of level heights and an array of elevations "hn"
set h(1) $h1;
set hn(1) 0;
set hn(2) $h1;
for { set i 2 } { $i <= $nL+1 } { incr i } {
  set h($i) $hx;
  set hn([expr $i+1]) [expr $hn($i)+$hx];
}

# Categorized lists of elements and nodes to make adding recorders and loads to groups of nodes easier
# Elements and nodes are appended to the appropriate lists as they are created
variable base_node_list {}; # List of nodes at the base of the structure
variable beam_end_list {}; # List of the beam sub elements connected directly to connectors
variable bpl_elem_list {}; # List of base-plate connector elements
variable col_elem_list {}; # List of column nodes
variable extcol_node_list {}; # List of nodes at each level where exterior column nodes are attached to beam-to-column connectors
variable intcol_node_list {}; # List of nodes at each level where interior column nodes are attached to beam-to-column connectors
variable connector_elem_list {}; # List of beam-to-column connector elements
variable beam_elem_list {}; # List of beam elements
variable pallet_elem_list {}; # List of elements between beams and pallet nodes
variable pallet_node_list {}; # List of nodes to which pallet masses are assigned
variable col_mid_node_list {}; # List of nodes in the middle of the columns (when fiber columns are used)
variable beam_node_list {}; # List of nodes along each beam

# Define nodes
for { set i 1 } { $i <= [expr $nL+1] } { incr i } {
  for { set j 1 } { $j <= $nc } { incr j } {
    # Column nodes

```

```

node $i$j [expr $L*($j-1) + $g_tol*$hn($i)] $hn($i);
# Column nodes are added to lists
if { $i == 1 } { lappend base_node_list $i$j }
if { $i != 1 } {
  if { $j==1 || $j==$nc } {
    lappend extcol_node_list $i$j;
  } else {
    lappend intcol_node_list $i$j;
  }
}
if { $i == 1 } {
  # do nothing
} elseif { $j < $nc } {
  # Beam nodes
  # the array pos contains the relative positions of the beam divisions
  array set pos {
    1 0
    2 0.03
    3 0.225
    4 0.48
    5 0.52
    6 0.745
    7 0.97
    8 1
  }
  set nb_div [array size pos]
  for { set k 1 } { $k <= $nb_div } { incr k } {
    if { $k == 1 || $k == $nb_div } {
      # Beam nodes coincident to columns
      node $i$j$k [expr $L*($j-1) + $g_tol*$hn($i) + $pos($k)*$L] $hn($i) -mass 0.0 0.0 0;
    } else {
      # Beam nodes not coincident with columns (will be given coincident pallet nodes)
      set node_mass [expr $mL/($nb_div-2)];
      node $i$j$k [expr $L*($j-1) + $g_tol*$hn($i) + $pos($k)*$L] $hn($i) -mass 1. 1. 0.;
      lappend beam_node_list $i$j$k;
      # Pallet nodes are given each an equal share of pallet mass
      set l 1; # Note numbering scheme : If beam node is 212 then corresponding pallet node is 2121
      node $i$j$k$l [expr $L*($j-1) + $g_tol*$hn($i) + $pos($k)*$L] $hn($i) -mass $node_mass $node_mass 0.;
      lappend pallet_node_list $i$j$k$l;
    }
  }
}
}
}
}

### Define Materials
# Define connector material
set sprMat [get_Tag "Material"];
set sprMatTop [get_Tag "Material"];
if { $sprOption == "L" } {
  use_linear_springs $sprMat $kc;
  use_linear_springs $sprMatTop $kctop;
} else {
  use_NL_spring $sprMat $sprOption $kc;
  use_NL_spring $sprMatTop $sprOption $kctop;
}
## Define base-plate material

```

```

set bplMat [get_Tag "Material"];
if { $bplOption == "L" } {
  use_linear_springs $bplMat $kbp1;
} else {
  use_NL_spring $bplMat $bplOption $kbp1;
}

## Pallet Material
## Friction Model
if { [expr $muSlow] > 0 } {
  set kInit 100.e6;
  set frnTag [get_Tag "Fric"];
  frictionModel VelDependent $frnTag $muSlow $muFast 0.6
  set matPyTag [get_Tag "Material"]; uniaxialMaterial Elastic $matPyTag 100.e6;
}

## Create column material and section if we are using fibre columns or concentrated plasticity columns
if { (($l_tol != 0.) || ($Fyc < $Fy_bpl)) } {

  set colMat [get_Tag "Material"];

  # Kinematic hardening parameters
  set b_k 0.01; set R_0 7.5; set r_1 0.9; set r_2 0.15;
  # Ultimate strength parameters
  set f_u [expr $Fyc/$Fy_bpl*450e6]; set R_u 20;
  uniaxialMaterial Steel4 $colMat $Fyc $E -kin $b_k $R_0 $r_1 $r_2 -ult $f_u $R_u;
  set NELEM 8;

  set dc [secProp $colPrf1 "D"];
  set bc [secProp $colPrf1 "B"];
  set tc [secProp $colPrf1 "T"];
  set wc [secProp $colPrf1 "W"];
  set xc [secProp $colPrf1 "X"];
  set xoc 0.; # Doesnt matter for planar
  set Ac [secProp $colPrf1 "A"];

  set mDc [expr $mSteel*$Ac]; #Mass per unit length
  set mDboxed [expr $mSteel*2*$Ac];

  # Both boxed section and the channel section are made and then when making the individual elements the appropriate tag is used
  set columnChannelTag [make_fibre_channel_section $colMat $dc $bc $tc $wc $xc [expr -$xoc]]
  set boxTag [make_fibre_boxed_channel_section $colMat $dc $bc $tc $wc $xc [expr -$xoc]]
}

## Create beam material and section if we are using concentrated plasticity beams
if { $Fyb < $Fy_bpl } {

  set beamMat [get_Tag "Material"];

  # Kinematic hardening parameters
  set b_k 0.01; set R_0 7.5; set r_1 0.9; set r_2 0.15;
  # Ultimate strength parameters
  set f_u [expr $Fyb/$Fy_bpl*450e6]; set R_u 20;
  uniaxialMaterial Steel4 $beamMat $Fyb $E -kin $b_k $R_0 $r_1 $r_2 -ult $f_u $R_u;

  set db [secProp $beamPrf1 "D"];

```



```

set bb [secProp $beamPrfl "B"];
set tb [secProp $beamPrfl "T"];
set wb [secProp $beamPrfl "W"];
set xb [secProp $beamPrfl "X"];
set xob 0.; # Doesnt matter for planar
set Ab [secProp $beamPrfl "A"];

set mDb [expr $mSteel*$Ab]; #Mass per unit length

set beamChannelTag [make_fibre_channel_section $beamMat $db $bb $tb $wb $xb [expr -$xob]]
}

# Base-plate material
variable Fy_bpl;
if { $bplOption == "fiber" } {

## Compression support elements
set matSup [get_Tag "Material"];
uniaxialMaterial ENT $matSup [expr $E*100];

set d_col [secProp $colPrfl "D"]; # Column section height
set wp [expr 8.5*25.4/1000]; # Base-plate width
set a [expr 2*25.4/1000]; # Base-plate bolt-to-column distance
set bp [expr 2*$a+$d_col]; # Bolt-to-bolt distance
set tp $kbpl; # Base-plate thickness
set nfh 1; set nfw 6;
set plateTag [get_Tag "Section"];
set plateMat [get_Tag "Material"];
# Kinematic hardening parameters
set b_k 0.01; set R_0 7.5; set r_1 0.9; set r_2 0.15;
# Ultimate strength parameters
set f_u 450e6; set R_u 20;
uniaxialMaterial Steel4 $plateMat $Fy_bpl $E -kin $b_k $R_0 $r_1 $r_2 -ult $f_u $R_u;
section fiberSec $plateTag {
patch rect $plateMat $nfw $nfh [expr -$tp/2] [expr -$wp/2] [expr $tp/2] [expr $wp/2];
}
}

# Define Elements
# Columns: named according to their start node and end node
for { set i 1 } { $i <= $nl } { incr i } {
for { set j 1 } { $j <= $nc } { incr j } {
set nodeI $i$j;
set nodeJ [expr $i+1]$j;
# Check to see if fibre or other columns should be used
if { $l_tol != 0. } {
# Check to see if the column is a simple channel or a boxed channel
if { $i <= $boxed_levels } {
use_fiber_columns $nodeI $nodeJ $NELEM $boxTag $mDboxed $ColTransf $l_tol; # Create sub-elements and add them to list of column elements
} else {
use_fiber_columns $nodeI $nodeJ $NELEM $columnChannelTag $mDc $ColTransf $l_tol; # Create sub-elements and add them to list of column elements
}
} else {
if { $Fyc < $Fy_bpl } {
# If Fyc is less than 345 MPa then columns are meant to be checked for plastification at their ends and a concentrated plasticity element is used

```

```

# Check to see if the column is a simple channel or a boxed channel
set l_pl [expr 0.05*$hx]; # Length of plastic hinge
if { $i <= $boxed_levels } {
  lappend col_elem_list [use_concentrated_plasticity_beamcolumns $nodeI $nodeJ $colPrfl $ColTransf $l_pl $boxTag $mDboxed ];
} else {
  lappend col_elem_list [use_concentrated_plasticity_beamcolumns $nodeI $nodeJ $colPrfl $ColTransf $l_pl $columnChannelTag $mDc ];
}
} else {
  # If Fyc = 345 MPa then plastification is not being checked and elastic elements can be used
  # Check to see if the column is a simple channel or a boxed channel
  if { $i <= $boxed_levels } { set boxed 2. } else { set boxed 1. }
  lappend col_elem_list [use_L_beamcolumns $nodeI $nodeJ $colPrfl $boxed $ColTransf]; # Create an elastic element and add it to list of column elements
}
}
}

# Beams: named according to their start node and end node
for { set i 1 } { $i <= $nL } { incr i } {
  for { set j 1 } { $j < $nc } { incr j } {
    for { set k 1 } { $k < $nb_div } { incr k } {
      set nodeI [expr $i+1]$j$k;
      set nodeJ [expr $i+1]$j[expr $k+1];
      if { $k == 1 || $k == $nb_div } {
        # Beam elements that are attached to connectors can be elastic or plastic
        if { $Fyb < $Fy_bpl } {
          # If Fyb is less than 345 MPa then beams are meant to be checked for plastification at their ends and a fiber element is used between the column and the pallet
          lappend beam_end_list [use_fiber_beam_ends $nodeI $nodeJ $beamChannelTag $mDb $BeamTransf];
        } else {
          # If Fyb = 345 MPa then plastification is not being checked and elastic elements can be used
          lappend beam_elem_list [use_L_beamcolumns $nodeI $nodeJ $beamPrfl 1. $BeamTransf]; # Create element and add it to list of beam elements
        }
      } else {
        # Add beam elements that are not directly connected to connectors
        lappend beam_elem_list [use_L_beamcolumns $nodeI $nodeJ $beamPrfl 1. $BeamTransf]; # Create element and add it to list of beam elements
      }
    }
  }
}

#Define pallet elements
if { $k == 1 || $k == $nb_div } {
  #do nothing
} else {
  set nodeK [expr $i+1]$j$k[expr 1]; # Pallet node

  if { [expr $muSlow] > 0 } {
    set tolSlider 10.e-6;
    set maxIterSlider 200;
    element flatSliderBearing $nodeI$nodeK $nodeI $nodeK $frnTag $kInit -P $matPyTag -Mz $matPyTag -orient 0 1 0 -1 0 0 -iter $maxIterSlider $tolSlider;
    equalDOF $nodeI $nodeK 3;
    lappend pallet_elem_list $nodeI$nodeK; # Add element to list of pallet elements
  } else {
    # Fixes pallets in place
    equalDOF $nodeI $nodeK 1 2 3;
  }
}
}
}
}

```

```

}

## Define beam-column connectors
# Lower level connectors
for { set i 2 } { $i <= $nL } { incr i } {
  for { set j 1 } { $j < $nc } { incr j } {
    # Left most connector in the bay at level i
    set k 1;
    set nodeI $i$j;
    set nodeJ $i$j$k;
    rotSpring2D $nodeI$nodeJ $nodeI $nodeJ $sprMat;
    lappend connector_elem_list $nodeI$nodeJ; # Add element to list of beam-column connectors
    # Right most connector in the bay at level i
    set k $nb_div;
    set nodeI $i[expr $j+1];
    set nodeJ $i$j$k;
    rotSpring2D $nodeI$nodeJ $nodeI $nodeJ $sprMat;
    lappend connector_elem_list $nodeI$nodeJ; # Add element to list of beam-column connectors
  }
}

## Top level connectors (for weak connector strong column design, inner top columns must have connectors half as strong)
for { set j 1 } { $j < $nc } { incr j } {
  if { $j == 1 || $j == $nc } { set Mat $sprMat; } else { set Mat $sprMatTop };
  # Left most connector in the bay at level i
  set i [expr $nL+1]
  set k 1;
  set nodeI $i$j;
  set nodeJ $i$j$k;
  rotSpring2D $nodeI$nodeJ $nodeI $nodeJ $Mat;
  lappend connector_elem_list $nodeI$nodeJ; # Add element to list of beam-column connectors
  # Right most connector in the bay at level i
  set k $nb_div;
  set nodeI $i[expr $j+1];
  set nodeJ $i$j$k;
  rotSpring2D $nodeI$nodeJ $nodeI $nodeJ $Mat;
  lappend connector_elem_list $nodeI$nodeJ; # Add element to list of beam-column connectors
}

# Define column base nodes and connectors fixities
if { $bplOption == "fiber" } {
  variable base_node_list {};
  for { set j 1 } { $j <= $nc } { incr j } {
    set nodeJ 1$j;
    set c [expr ($j-1)*$L]; # Centre de l'appui
    use_fiber_bpl $nodeJ $c $bp $a $tp $wp $plateTag $matSup;
  }
} else {
  for { set j 1 } { $j <= $nc } { incr j } {
    set k 0;
    node $j$k [expr [expr $j-1]*$L] 0;
    set nodeI $j$k;
    set nodeJ 1$j;
    fix $nodeI 1 1 1; # Assign column base fixities
    rotSpring2D $nodeI$nodeJ $nodeI $nodeJ $bplMat;
    lappend bpl_elem_list $nodeI$nodeJ; # Add element to list of base-plate connectors
  }
}

```

```

}

# Add viscous damping
add_rayleigh_damping $zeta;

puts "Model created";

# Outputs model information about nodes and elements to the output folder
print "$output_dir/nodes.out" -node
print "$output_dir/elements.out" -ele

}

proc ::rack_pack::rack_period { {n_modes 1} } {

#####
# Calculation of 1st fundamental period
# Prints period in the terminal and returns the period
#
# 8 mai 2016, EJ
#####

set pi [expr 2.0*asin(1.0)]; # Definition of pi

set omega [expr pow([eigen $n_modes], 0.5)];
set Tn [expr double(round([expr 20000 * $pi / $omega]))/10000];
puts "T1 = $Tn s";
return $Tn;

}

proc ::rack_pack::rack_gravity_static { Py load_placement } {

#####
# Adds a point load of Py either on beams or on columns
# When applied to columns, 1*Py is applied to exterior column nodes and 2*Py is applied to interior columns
# When applied to beam, 1*Py is applied to each node
# Then a static analysis is run, loads are held constant and time is reset to zero
#
# INPUTS :
# Py := scalar pallet weight in [N]
# load_placement := PL will either be placed "on_beams" "on_cols" "beam_left" "beams right"
#
# These two examples would give equivalent vertical reactions at base nodes :
# Example : rack_gravity_static $PL/6 "on_beams"; (assuming the default of six pallet nodes per beam)
# Example : rack_gravity_static $PL/2 "on_cols";
#
# Last mod. : 5 mai 2016, EJ
#####

# Lists of nodes constructed in rackMRF are included in the procedure, theses variables are part of the rack_pack
# namespace
variable right_pallet_node_list;
variable left_pallet_node_list;
variable pallet_node_list;
variable extcol_node_list;
variable intcol_node_list;

```

```

variable base_node_list;

# Pattern and time series tags are choosen automatically
set gravityPattern [ get_Tag "Pattern" ];
set timeSeriesTag [ get_Tag "Time" ];
timeSeries Linear $timeSeriesTag;

# Depending on the string in load_placement, loads are added to the appropriate nodes
pattern Plain $gravityPattern $timeSeriesTag {
  if { $load_placement == "on_beams" } {
    for { set n 0 } { $n < [llength $pallet_node_list] } {incr n} {
      set node [lindex $pallet_node_list $n];
      load $node 0.0 [expr -$Py] 0.0;
    }
  }
  if { $load_placement == "on_cols" } {
    if { [info exists extcol_node_list] == 1 } {
      for { set n 0 } { $n < [llength $extcol_node_list] } {incr n} {
        set node [lindex $extcol_node_list $n];
        load $node 0.0 [expr -$Py] 0.0;
      }
    }
    if { [info exists intcol_node_list] == 1 } {
      for { set n 0 } { $n < [llength $intcol_node_list] } {incr n} {
        set node [lindex $intcol_node_list $n];
        load $node 0.0 [expr -$Py*2] 0.0;
      }
    }
  }
}

constraints Plain; # Defines how to handle constraints between DOFs
numberer RCM; # Specify how OpenSees numbers the DOFs
system BandGeneral; # Save the system of equations

set tol 1.0e-6; # Convergence tolerance for test
set iter 6; # The max number of iterations to check before returning failure condition
test NormDispIncr $tol $iter; # Determine if convergence has been achieved at the end of an iteration step

# Algo for the resolution of the system of non-linear equations
algorithm Newton; # Use Newton's solution algorithm: updates tangent stiffness at every iteration

# integrator LoadControl $lambda <$numIter $minLambda $maxLambda>
set Nsteps 10; # Number of steps in which to apply load
set lambda [expr 1.0/$Nsteps]; # load increment
integrator LoadControl $lambda;

#Construct the analysis object
analysis Static;

# Run analysis in Nsteps
set ok [analyze $Nsteps]; # this will return zero if no convergence problems were encountered
set time 0.;
set message "Applied gravity loads... setting time to ";
if { $ok == 0 } { puts [append message $time " and holding load constant." ] };

```

```

loadConst -time $time; # Sets existing loading to be constant and resets time to 0.0
}

proc ::rack_pack::rack_TH { dt path accRecord SF {NTINCR 0}} {
#####
# Time-history analysis
#
# Warning : call graivty load analysis before to include P-delta effects
# dt := time step in file [s]
# path := full path to directory of acceleration file
# accRecord := string, file name of the accelerogram used
# NTINCR := number (default is the number of lines in the acceleration file), number of steps to be used in analysis
#
# Last mod. : 14 mars 2016, EJ
#####

# Dynamic Loading
# -----
variable g;
set accelSeries "Series -dt $dt -filePath $path$accRecord -factor [expr $g*$SF]";
set patternTag [get_Tag "Pattern"];
set dirX 1;
pattern UniformExcitation $patternTag $dirX -accel $accelSeries;

# Newmark Algorithm gamma=0.25; beta=0.5
# -----
set tol 0.000001;
set maxNumIter 300;
test EnergyIncr $tol $maxNumIter;
constraints Plain;
numberer Plain;
system BandGeneral;
algorithm Newton;
integrator Newmark 0.5 0.25;
analysis Transient;

#integrator HHT 0.9 0.3025 0.6; # Use if there are convergence problems with pallet sliding

# Check if NTINCR has been specified otherwise get number of lines in file
if {$NTINCR == 0} {
set infile [open $path$accRecord r];

while { [gets $infile line] >= 0 } {
incr NTINCR;
}
close $infile;
}

set dursism [expr $NTINCR*$dt];

# time step size for the analysis
set dt2 0.001;
puts_and_save "Time history time step:$dt2"
puts_and_save "Starting Time History Analysis with $accRecord at scale factor $SF";
set startTime [clock clicks -milliseconds]

```

```

set ok [analyze [expr int($dursism/$dt2)] $dt2];
set endTime [clock clicks -milliseconds]
set timeElapsed [expr ($endTime - $startTime)/1000]
if { $ok == 0 } { puts_and_save "TH Analysis Completed in $timeElapsed s" } else {
puts_and_save "TH Analysis failed after $timeElapsed s"
};
}

proc ::rack_pack::add_rayleigh_damping { zeta } {

variable pi;
variable col_elem_list; # List of column nodes
variable beam_elem_list; # List of beam elements
variable pallet_node_list; # List of nodes to which pallet masses are assigned

## Rayleigh Damping
set lambdaN [eigen [expr 2]];# eigenvalue analysis for nEigenJ modes
set w1 [expr pow([lindex $lambdaN 0],0.5)]; # w1 (1st mode circular frequency)
set w2 [expr pow([lindex $lambdaN 1],0.5)]; # w2 (2nd mode circular frequency)
set T1 [expr double(round([expr 2000*$pi/$w1]))/1000];
set T2 [expr double(round([expr 2000*$pi/$w2]))/1000];
puts_and_save "T1 = $T1 s";
puts_and_save "T2 = $T2 s";
# Calculate damping parameters (see Chopra p.419)
set a0 [expr $zeta*2.0*$w1*$w2/($w1 + $w2)]; # mass damping coefficient based on first and second modes
set a1 [expr $zeta*2.0/($w1 + $w2)]; # stiffness damping coefficient based on first and second modes

# Assign element and node lists to regions and apply damping
# Calling rayleigh damping : -rayleigh $alphaM $betaK $betaKinit $betaKcomm;
set cmd "region 1 -ele $col_elem_list -rayleigh $a0 0. 0. 0.";
eval $cmd;
set cmd "region 2 -ele $beam_elem_list -rayleigh $a0 0. 0. 0.";
eval $cmd;
set cmd "region 3 -node $pallet_node_list -rayleigh $a0 0. 0. 0.";
eval $cmd;
}

proc ::rack_pack::use_linear_springs { sprMat kc } {

#####
# Defines material moment-rotation curve to be used for linear zero-length connectors
#
# INPUTS:
# sprMat := material tag [an integer]
# kc := rotational stiffness [Nm/rad]
#
# Last mod. : 15 Juillet 2015, EJ
#####

puts_and_save "Using Linear Spring : $kc";

uniaxialMaterial Elastic $sprMat $kc; # Spring is perfectly elastic

}

proc ::rack_pack::use_NL_spring { sprMat NLsprName SF } {

```

```
#####
# Defines material moment rotation curve to be used for non-linear zero-length connectors
#
# INPUTS:
# sprMat := material tag [an integer]
# NLSprName := the name of the non-linear connector [text], see the list "Connector_name"
#
# exemple : use_NL_spring 3 "AC175"
#
# Last mod. : 10 mars 2016, EJ
#####
```

```
set material_picked 0;

if { $NLSprName == "AC175" } {
set ePd1 0.0036;
set ePf1 [expr $SF*900.];
set ePd2 0.025;
set ePf2 [expr $SF*1120.];
set ePd3 0.1;
set ePf3 [expr $SF*4700.];
set ePd4 0.4;
set ePf4 0.;
set rDispP 0.5;
set rForceP 0.04;
set uForceP 0.07;
set eNd1 [expr -$ePd1];
set eNf1 [expr -$ePf1];
set eNd2 [expr -$ePd2];
set eNf2 [expr -$ePf2];
set eNd3 [expr -$ePd3];
set eNf3 [expr -$ePf3];
set eNd4 [expr -$ePd4];
set eNf4 [expr -$ePf4];
set rDispN $rDispP;
set rForceN $rForceP;
set uForceN $uForceP;
set gK1 0.;
set gK2 0.;
set gK3 0.;
set gK4 0.;
set gKLim -0.1;
set gD1 0.;
set gD2 0.1;
set gD3 0.;
set gD4 0.1;
set gDLim 0.1;
set gF1 0.;
set gF2 0.;
set gF3 0.;
set gF4 0.;
set gFLim 0.01;
uniaxialMaterial Pinching4 $sprMat $ePf1 $ePd1 $ePf2 $ePd2 $ePf3 $ePd3 $ePf4 $ePd4 $eNf1 $eNd1 $eNf2 $eNd2 $eNf3 $eNd3 $eNf4 $eNd4 $rDispP $rForceP $uForceP $rDispN
$rForceN $uForceN $gK1 $gK2 $gK3 $gK4 $gKLim $gD1 $gD2 $gD3 $gD4 $gDLim $gF1 $gF2 $gF3 $gF4 $gFLim 1. "cycle";
set material_picked 1;
}
```



```

if { $NLsprName == "fiber" } {
# Fiber base-plates are largely constructed in the rackMRF procedure
set material_picked 1;
}
if { $NLsprName == "Parallel" } {
# This is the material that best replicates the behaviour of the base-plate in the F1 test
# Hysteretic + Parallel Steel 4 Test
set s1p [expr $SF*0.3*1000]
set e1p 0.005
set s2p [expr $SF*0.8*1000]
set e2p 0.02
set s3p [expr $SF*1.1*1000]
set e3p 0.08
set s1n [expr $SF*-0.3*1000]
set e1n -0.005
set s2n [expr $SF*-0.5*1000]
set e2n -0.02
set s3n [expr $SF*-1.0*1000]
set e3n -0.08
set pinchX 0.8
set pinchY 0.2
set damage1 0.
set damage2 0.
set beta 0.01

set hystMat [get_Tag "Material"];
set stl4_1Mat [get_Tag "Material"];
set stl4_2Mat [get_Tag "Material"];

uniaxialMaterial Hysteretic $hystMat $s1p $e1p $s2p $e2p $s3p $e3p $s1n $e1n $s2n $e2n $s3n $e3n $pinchX $pinchY $damage1 $damage2 $beta;
uniaxialMaterial Steel4 $stl4_1Mat [expr $SF*0.4*1000] [expr $SF*5.0*1000] -kin 0.08 15.0 0.925 0.15 -ult [expr 1.0*1000] 20.; # Initial portion of curve
uniaxialMaterial Steel4 $stl4_2Mat [expr $SF*1.0*1000] [expr $SF*45.0*1000] -kin 0.01 15.0 0.925 0.15 -ult [expr 2.2*1000] 20.; # 2nd portion of curve
uniaxialMaterial Parallel $sprMat $hystMat $stl4_1Mat $stl4_2Mat;

set material_picked 1;
}
if { $NLsprName == "MinMax" } {
set elMat [get_Tag "Material"];
uniaxialMaterial Elastic $elMat [expr $SF*10.e3];
uniaxialMaterial MinMax $sprMat $elMat -min -0.01 -max 0.01;
set material_picked 1;
}
if { $material_picked == 0 } {
#parse NLsprName to extract custom material string
set EOL [llength $NLsprName]; #Last element in the list
set mat_args [lrange $NLsprName 1 $EOL]; # isolate the
set NLsprName [lindex $NLsprName 0]
set cmd "uniaxialMaterial $NLsprName $sprMat $mat_args"
eval $cmd
}
}

proc ::rack_pack::use_fiber_bpl { originNode c bp a tp wp plateTag matSup } {

#####
# Makes a fibre base-plate assembly as seen below:
# -the node marked "o" is the originNode and is the point of attachment between the column and the base-plate assembly

```

```

# -the nodes marked "#" or "bolt#" are fixed nodes
# -the elements marked "fibre" are non-linear beam column elements with a fiber section (defined in rackMRF)
# -the elements marked "comp." are compression only zero-length elements
# -the elements marked "el." are very stiff elastic elements which allow a distribution of compression and moment from the column to the base-plate
#
#
#      |
#      y      col.
#      |      |
#      ---x      x---el.---o---el.---x
#      =          =
#
#      =          =
# bolt#---fibre---x-----fibre-----x---fibre---#bolt
#
#      comp.      comp.
#      |          |
#      #          #
#
# INPUTS:
# originNode := the Tag of the node at the start of the adjoining column
# c := the x coordinate of the originNode
# bp := the x-distance from originNode to the bolted end of the base-plate
# a := the x-distance between the bolt and the column section
# tp := the base-plate thickness
# wp := the base-plate width
# plateTag := the section tag of the fibre base-plate section (as defined in rackMRF)
# matSup := the material tag of the compression only material (as defined in rackMRF)
#
#
# OUTPUTS:
# The procedure has no outputs HOWEVER the base_node_list and the bpl_elem_list are constructed here.
# Since the interesting outputs are the reactions at the base and the uplift of the plate:
# - the base_node_list contains ONLY the four fixed nodes of the base-plate assembly
# - the bpl_elem_list contains ONLY the two zero-length compression springs
#
# EJ
#####

set hbp1 0.;
variable E;
variable base_node_list;
variable bpl_elem_list;

# Nodes along the fiber plate element
set node1 $originNode[expr 0][expr 0][expr 1];
node $node1 [expr $c-$bp/2] [expr -$hbp1];
node $originNode[expr 0][expr 0][expr 2] [expr $c-$bp/2+$a] [expr -$hbp1];
node $originNode[expr 0][expr 0][expr 4] [expr $c+$bp/2-$a] [expr -$hbp1];
set node5 $originNode[expr 0][expr 0][expr 5];
node $node5 [expr $c+$bp/2] [expr -$hbp1];
# End-nodes for tension only springs
set node6 $originNode[expr 0][expr 0][expr 6];
node $node6 [expr $c-$bp/2+$a] [expr -$hbp1];
set node7 $originNode[expr 0][expr 0][expr 7];
node $node7 [expr $c+$bp/2-$a] [expr -$hbp1];
lappend base_node_list $node1 $node5 $node6 $node7;
# Nodes for rigid "cadre" elements
node $originNode[expr 0][expr 0][expr 8] [expr $c-$bp/2+$a] 0.;

```

```

node $originNode[expr 0][expr 0][expr 9] [expr $c+$bp/2-$a] 0.;

fix $originNode[expr 0][expr 0][expr 1] 1 1 1;
fix $originNode[expr 0][expr 0][expr 5] 1 1 1;
fix $originNode[expr 0][expr 0][expr 6] 1 1 1;
fix $originNode[expr 0][expr 0][expr 7] 1 1 1;

equalDOF $originNode[expr 0][expr 0][expr 2] $originNode[expr 0][expr 0][expr 8] 1 2 3;
equalDOF $originNode[expr 0][expr 0][expr 4] $originNode[expr 0][expr 0][expr 9] 1 2 3;

# Cadre elements
set A 0.00102; set Iz 1.61e-6; set Ecadre [expr $E];
#element elasticBeamColumn $originNode[expr 0][expr 0][expr 4]$originNode[expr 0][expr 0][expr 9] $originNode[expr 0][expr 0][expr 4] $originNode[expr 0][expr 0][expr 9] $A $Ecadre $Iz 1
#element elasticBeamColumn $originNode[expr 0][expr 0][expr 2]$originNode[expr 0][expr 0][expr 8] $originNode[expr 0][expr 0][expr 2] $originNode[expr 0][expr 0][expr 8] $A $Ecadre $Iz 1
set Ar [expr $A]; set Izr [expr $Iz]; set Erigid [expr $Ecadre];
element elasticBeamColumn $originNode[expr 0][expr 0][expr 8]$originNode $originNode[expr 0][expr 0][expr 8] $originNode $Ar $Erigid $Izr 1
element elasticBeamColumn $originNode[expr 0][expr 0][expr 9]$originNode $originNode[expr 0][expr 0][expr 9] $originNode $Ar $Erigid $Izr 1

# Compression only support elements
set eleLeft $originNode[expr 0][expr 0][expr 2]$originNode[expr 0][expr 0][expr 6];
set eleRight $originNode[expr 0][expr 0][expr 4]$originNode[expr 0][expr 0][expr 7];
element zeroLength $eleLeft $originNode[expr 0][expr 0][expr 6] $originNode[expr 0][expr 0][expr 2] -mat $matSup -dir 1 -orient 0 1 0 -1 0 0;
element zeroLength $eleRight $originNode[expr 0][expr 0][expr 7] $originNode[expr 0][expr 0][expr 4] -mat $matSup -dir 1 -orient 0 1 0 -1 0 0;
lappend bpl_elem_list $eleLeft $eleRight;

# PlateElements
set npts 4;
set maxIters 100;
set tol 0.000001;
set ele2 $originNode[expr 0][expr 0][expr 1]$originNode[expr 0][expr 0][expr 2];
set ele4 $originNode[expr 0][expr 0][expr 2]$originNode[expr 0][expr 0][expr 4];
set ele5 $originNode[expr 0][expr 0][expr 4]$originNode[expr 0][expr 0][expr 5];
element nonlinearBeamColumn $ele2 $originNode[expr 0][expr 0][expr 1] $originNode[expr 0][expr 0][expr 2] $npts $plateTag 1;# -iter $maxIters $tol;
element nonlinearBeamColumn $ele4 $originNode[expr 0][expr 0][expr 2] $originNode[expr 0][expr 0][expr 4] $npts $plateTag 1;# -iter $maxIters $tol;
element nonlinearBeamColumn $ele5 $originNode[expr 0][expr 0][expr 4] $originNode[expr 0][expr 0][expr 5] $npts $plateTag 1;# -iter $maxIters $tol;

}

proc ::rack_pack::use_concentrated_plasticity_beamcolumns { s_node e_node elePrfl geoTransf l_pl secTag mD } {

#####
# This procedure is called by rackMRF to assign concentrated plasticity elements between 2 nodes
#
# INPUTS:
# s_node := the starting local column node, integer (defined in rackMRF) [unitless]
# e_node := the ending column node, integer (defined in rackMRF) [unitless]
# elePrfl := the name of the profile, string [unitless]
# geoTransf := geometric transformation tag, integer [unitless]
# l_pl := the length of the plastic hinge, double [m]
# secTag := the tag for the plastic hinge section, integer [unitless]
# mD := mass per unit length, double [kg/m2]
#
# OUTPUT:
# $s_node$e_node := the tag of the element created
#

```

```

# Last mod.: 8 aout 2016, EJ
#####

variable mSteel;

element forceBeamColumn $s_node$e_node $s_node $e_node $geoTransf "HingeRadau $secTag $l_pl $secTag $l_pl $secTag" -mass $mD; # <-iter $maxIters $tol>

return $s_node$e_node

}

proc ::rack_pack::use_L_beamcolumns { s_node e_node elePrfl boxed geoTransf } {

#####
# This procedure is called by rackMRF to assign elastic columns
# between 2 nodes
#
# INPUTS:
# s_node := the starting local column node, integer (defined in rackMRF) [unitless]
# e_node := the ending column node, integer (defined in rackMRF) [unitless]
# elePrfl := the name of the profile, string [unitless]
# boxed := used to double the inertia and area of a column profile when it is a boxed column, double [unitless]
# geoTransf := geometric transformation tag, integer [unitless]
#
# OUTPUT:
# $s_node$e_node := the tag of the element created
#
# Last mod.: 16 avril 2016, EJ
#####

variable mSteel;
variable E;

set A [expr $boxed*[secProp $elePrfl "A"]];
set Ix [expr $boxed*[secProp $elePrfl "Ix"]];
set mDc [expr $mSteel*$A]; #Mass per unit length

element elasticBeamColumn $s_node$e_node $s_node $e_node $A $E $Ix $geoTransf -mass $mDc;

return $s_node$e_node
}

proc ::rack_pack::use_fiber_beam_ends { s_node e_node beamSecTag mDb BeamTransf } {

#####
# This procedure is called by rackMRF to perform
# discretisation of beam end elements into multiple non-linear elements with
# fiber cross sections
#
# INPUTS:
# s_node := the starting local column node, integer (defined in rackMRF) [unitless]
# e_node := the ending column node, integer (defined in rackMRF) [unitless]
# beamSecTag := the fiber section specified in rackMRF
# mDb := mass per unit length of beam member
# BeamTransf := geometric transformation tag, integer [unitless]
#
# OUTPUT:

```

```

# beam_list := a list of the elements created
#
# EJ
#####

set npoint 3; # must be integer
set maxIters 1000;
set tol 0.000001;

# Creation of sub-elements
set beam_list {};
set nodeI $s_node;
set nodeJ $e_node;
element nonlinearBeamColumn $nodeI$nodeJ $nodeI $nodeJ $npoint $beamSecTag $BeamTransf -mass $mDb -iter $maxIters $tol;
lappend beam_list $nodeI$nodeJ;

# A list of column elements created is returned to add Rayleigh damping to the region in rackMRF
return $beam_list
}

proc ::rack_pack::use_fiber_columns { s_node e_node NELEM colSecTag mDc ColTransf l_tol } {

#####
# This procedure is called by rackMRF to perform
# discretisation of columns into multiple non-linear elements with
# fiber cross sections
#
# INPUTS:
# s_node := the starting local column node, integer (defined in rackMRF) [unitless]
# e_node := the ending column node, integer (defined in rackMRF) [unitless]
# NELEM := the number of sub elements, double
# colPrfl := the name of the profile, string [unitless]
# ColTransf := geometric transformation tag, integer [unitless]
# l_tol := initial local column cambrure, double [m/m]
#
# OUTPUT:
# col_list := a list of the elements created
#
# Last mod.: 16 avril 2016, EJ
#####

# Give a message while creating the first non-linear column
if { $s_node == "11" } { puts_and_save "Using non-linear columns with $NELEM sub-elements" };

variable pi;
variable g;
variable col_mid_node_list;
variable col_elem_list;

set npoint 3; # must be integer
# set maxIters 10;
# set tol 0.000001;

# Retrieve start and end coordinates of inputed nodes
set sx [nodeCoord $s_node 1]; set sy [nodeCoord $s_node 2];
set ex [nodeCoord $e_node 1]; set ey [nodeCoord $e_node 2];
set L [expr sqrt([expr pow([expr $sx-$ex],2)+pow([expr $sy-$ey],2)]]); # Distance between column end point and start point

```

```

# Angle of the column with respect to the positive x-axis
set sinT [expr ($sy-$ey)/$L];
set cosT [expr ($ex-$sx)/$L];

# Creation of nodes
# A sine curve is created with amplitude l_tol*L and length L and then is rotated and translated to fit the column end-points
set x(0) 0; set y(0) 0; set x1(0) $sx; set y1(0) $sy;
for { set i 1 } { $i <= [expr $NELEM-1] } { incr i } {
  if { [expr [expr $s_node/10]%2] != 0 } {
    # Impair levels
    # Sine curve with length L and amplitude l_tol*L
    set x($i) [expr $i*$L/$NELEM];
    set y($i) [expr $l_tol*$L*sin([expr $pi*($x($i)-0)/$L])];
    # Rotation and translation of coordinates
    set x1($i) [expr $x($i)*$cosT+$y($i)*$sinT + $sx];
    set y1($i) [expr -$x($i)*$sinT+$y($i)*$cosT + $sy];
  } else {
    # Pair levels
    # Sine curve with length L and amplitude l_tol*L
    set x($i) [expr $i*$L/$NELEM];
    set y($i) [expr -1*$l_tol*$L*sin([expr $pi*($x($i)-0)/$L])];
    # Rotation and translation of coordinates
    set x1($i) [expr $x($i)*$cosT+$y($i)*$sinT + $sx];
    set y1($i) [expr -$x($i)*$sinT+$y($i)*$cosT + $sy];
  }
  node $s_node[expr 0]$i $x1($i) $y1($i); # Add node to model
  if { $i == 4 } { lappend col_mid_node_list $s_node[expr 0]$i }
}

# Create first sub element
set nodeI $s_node;
set nodeJ $s_node[expr 0][expr 1];
element nonlinearBeamColumn $nodeI$nodeJ $nodeI $nodeJ $npoint $colSecTag $ColTransf -mass $mDc;# -iter $maxIters $tol;
lappend col_elem_list $nodeI$nodeJ;
# Create intermediate sub-elements
for { set i 1 } { $i <= [expr $NELEM - 2] } { incr i } {
  set nodeI $s_node[expr 0]$i;
  set nodeJ $s_node[expr 0][expr $i+1];
  element nonlinearBeamColumn $nodeI$nodeJ $nodeI $nodeJ $npoint $colSecTag $ColTransf -mass $mDc;# -iter $maxIters $tol;
  if { $i == 4 } { lappend col_elem_list $nodeI$nodeJ; }
}

# Create last sub element
set nodeI $s_node[expr 0][expr int($NELEM-1)];
set nodeJ $e_node;
element nonlinearBeamColumn $nodeI$nodeJ $nodeI $nodeJ $npoint $colSecTag $ColTransf -mass $mDc;# -iter $maxIters $tol;
lappend col_elem_list $nodeI$nodeJ;

}

proc ::rack_pack::make_fibre_channel_section { matTag d b t w x xo } {

#####
# This procedure is called by rack_MRF to make channel
# shaped fibre cross-sections
#

```

```

# INPUTS:
# (for more detail see tables of CISC Handbook)
# d := depth, double [m]
# b := flange width, double [m]
# t := flange thickness, double [m]
# w := web thickness, double [m]
# x := distance from neutral axis to exterior web, double [m]
# xo := position of loading vis-a-vis neutral axis, double (!!! be careful of sign!) [m]
#
# Example : Channel C100x7 section loaded in its shear centre : make_fibre_channel_section 0.102 0.040 0.0075 0.0032 0.0126 -0.0273
#
# OUTPUT : secTag := an identifier for the section, integer [unitless]
#
# Last mod.: 16 avril 2016, EJ
#####

set secTag [get_Tag "Section"];
set aggSecTag [get_Tag "Section"];

set nfd 4;# number of fibers along web depth
set nfw 1;# number of fibers along web thickness
set nfb 1;# number of fibers along flange width (you want this many in a bi-directional loading)
set nft 8;# number of fibers along flange thickness

# Some coordinates delineating channel web and flange
set z1 [expr {($d-2*$t)/2}]; # distance to nearest flange fibre from the c.g.
set z2 [expr {$d/2}]; # distance to the farthest flange fibre from the c.g.
set y1 [expr {-x-xo}]; # distance from the load centre to the web fibre nearest the shear centre
set y2 [expr {-x-xo+w}]; # distance from the load centre to the web fibre farthest from the shear centre
set y3 [expr {-x-xo+b}]; # distance from the load centre to the flange tip farthest from the shear centre

section fiberSec $secTag {
# Web
# patch quad $matTag $nfw $nfd $y1 [expr -$z1] $y2 [expr -$z1] $y2 $z1 $y1 $z1; # Weak axis in the plane
patch quad $matTag $nfd $nfw [expr -$z1] $y1 $z1 $y1 $z1 $y2 [expr -$z1] $y2; # Strong axis in the plane
# Top Flange
# patch quad $matTag $nft $nfb $y1 $z1 $y3 $z1 $y3 $z2 $y1 $z2; # Weak axis in the plane
patch quad $matTag $nfb $nft $z1 $y1 $z2 $y1 $z2 $y3 $z1 $y3; # Strong axis in the plane
# Bottom Flange
# patch quad $matTag $nft $nfb $y1 [expr -$z2] $y3 [expr -$z2] $y3 [expr -$z1] $y1 [expr -$z1]; # Weak axis in the plane
patch quad $matTag $nfb $nft [expr -$z2] $y1 [expr -$z1] $y1 [expr -$z1] $y3 [expr -$z2] $y3; # Strong axis in the plane
}

section Aggregator $aggSecTag $matTag My -section $secTag

return $aggSecTag;
}

proc ::rack_pack::make_fibre_boxed_channel_section { matTag d b t w x xo } {

#####
# This procedure is called by rack_MRF to make channel
# shaped fibre cross-sections
#
# INPUTS:
# (for more detail see tables of CISC Handbook)
# d := depth, double [m]

```

```

# b := flange width, double [m]
# t := flange thickness, double [m]
# w := we thickness, double [m]
# x := distance from neutral axis to exterior web, double [m]
# xo := position of loading vis-a-vis neutral axis, double (!!! be careful of sign!) [m]
#
# Example : Channel C100x7 section loaded in its shear centre : make_fibre_channel_section 0.102 0.040 0.0075 0.0032 0.0126 -0.0273
#
# OUTPUT : secTag := an identifier for the section, integer [unitless]
#
# Last mod.: 16 avril 2016, EJ
#####

set secTag [get_Tag "Section"];
set aggSecTag [get_Tag "Section"];

set nfd 4;# number of fibers along web depth
set nfw 1;# number of fibers along web thickness
set nfb 1;# number of fibers along flange width (you want this many in a bi-directional loading)
set nft 8;# number of fibers along flange thickness

#Some coordinates delineating channel web and flange
set z1 [expr ($d-2*$t)/2]; # distance to nearest flange fibre from the c.g.
set z2 [expr $d/2]; # distance to the farthest flange fibre from the c.g
set y1 [expr -$x-$xo]; # distance from the load centre to the web fibre nearest the shear centre
set y2 [expr -$x-$xo+$w]; # distance from the load centre to the web fibre farthest from the shear centre
set y3 [expr -$x-$xo+$b]; # distance from the load centre to the flange tip farthest from the shear centre

section fiberSec $secTag {
# Web1
patch quad $matTag $nfd $nfw [expr -$z1] $y1 $z1 $y1 $z1 $y2 [expr -$z1] $y2; # Strong axis in the plane
# Top Flange
patch quad $matTag $nfb $nft $z1 $y1 $z2 $y1 $z2 [expr 2*$y3-$y1] $z1 [expr 2*$y3-$y1]; # Strong axis in the plane
# Bottom Flange
patch quad $matTag $nfb $nft [expr -$z2] $y1 [expr -$z1] $y1 [expr -$z1] [expr 2*$y3-$y1] [expr -$z2] [expr 2*$y3-$y1]; # Strong axis in the plane
# Web2
patch quad $matTag $nfd $nfw [expr -$z1] [expr 2*$y3-$y2] $z1 [expr 2*$y3-$y2] $z1 [expr 2*$y3-$y1] [expr -$z1] [expr 2*$y3-$y1]; # Strong axis in the plane
}

section Aggregator $aggSecTag $matTag My -section $secTag

return $aggSecTag;
}

proc ::rack_pack::secProp { prflName prop } {
#####
# Returns a section from data base of properties of a CISC Channel or Miscellaneous Channel
#
# INPUTS:
# (for more detail see tables of CISC Handbook)
# D := depth, double [m]
# B := flange width, double [m]
# T := flange thickness, double [m]
# W := we thickness, double [m]
# X := distance from neutral axis to exterior web, double [m]
# Xo := position of loading vis-a-vis neutral axis, double (!!! be careful of sign!) [m]

```



```

# Ix := Strong axis interia, double [m4]
# Iy := Weak axis interia, double [m4]
# A := Area, double [m2]
#
# OUTPUT:
# The value of the requested section property of the specified section, double
#
# Example : secProp "C100x7" "D" would return 0.0102
#
# Last mod.: 23 mai 2016, EJ
#####

if { $prflName == "poly-cold-form-beam" } {
  if {$prop == "Ix"} { return [expr 1.8239*pow(25.4/1000,4)] };
  if {$prop == "A"} { return [expr 0.91936*pow(25.4/1000,2)] };
}
if { $prflName == "poly-cold-form-col" } {
  if {$prop == "Ix"} { return [expr 1.5606*pow(25.4/1000,4)] };
  if {$prop == "A"} { return [expr 0.9492*pow(25.4/1000,2)] };
} else {
  if { file exists StandardAndMiscChannels.db } {
    # Slurp up the data file
    set fp [open "StandardAndMiscChannels.db" r]
    set file_data [read $fp]
    close $fp
    # Process data file
    set data [split $file_data "\n"]
    set counter 0;
    foreach line $data {
      set counter [expr $counter+1];
      if { [string match *$prflName* $line] } {
        set sec_data [split $line "\t"]
        if {$prop == "D"} { return [expr double([lindex $sec_data 6])/1000] };
        if {$prop == "B"} { return [expr double([lindex $sec_data 7])/1000] };
        if {$prop == "T"} { return [expr double([lindex $sec_data 8])/1000] };
        if {$prop == "W"} { return [expr double([lindex $sec_data 9])/1000] };
        if {$prop == "X"} { return [expr double([lindex $sec_data 22])/1000] };
        if {$prop == "Xo"} { return [expr double([lindex $sec_data 25])/1000] };
        if {$prop == "Ix"} { return [expr double([lindex $sec_data 16])/1000000] };
        if {$prop == "Iy"} { return [expr double([lindex $sec_data 19])/1000000] };
        if {$prop == "A"} { return [expr double([lindex $sec_data 15])/1000000] };
      }
    }
  } else {
    # Get inertias from user
    puts "Data-base of sections was not found"
  }
}

proc ::rack_pack::record_rack { thing_to_record what_to_record {record_time 0} } {

#####
# Records nodes or elements according to previously constructed lists of nodes and elements
#
# INPUTS:
# thing_to_record := a string, designating the name of the list of elements or nodes to records i.e. "beams" or "connectors" etc.

```

```

# what_to_record := a string, that can be either "force" "deformation" "disp" "reaction" or "section_forces"
# record_time := double, output is recorded at specified time if greater than 0, default is zero
#
#####

variable output_dir
puts_and_save "Recorders:"

if { $thing_to_record == "beams" } { variable beam_elem_list; set ele_list $beam_elem_list ; puts_and_save "Beams Elements :" };
if { $thing_to_record == "beam_ends" } { variable beam_end_list; set ele_list $beam_end_list ; puts_and_save "Beam-End Elements :" };
if { $thing_to_record == "columns" } { variable col_elem_list; set ele_list $col_elem_list ; puts_and_save "Column Elements :" };
if { $thing_to_record == "base-plates" } { variable bpl_elem_list; set ele_list $bpl_elem_list ; puts_and_save "Base-Plate Elements :" };
if { $thing_to_record == "connectors" } { variable connector_elem_list; set ele_list $connector_elem_list ; puts_and_save "Connector Elements :" };
if { $thing_to_record == "pallets" } { variable pallet_elem_list; set ele_list $pallet_elem_list ; puts_and_save "Pallet Elements :" };

if { $thing_to_record == "palletnodes" } { variable pallet_node_list; set node_list $pallet_node_list ; puts_and_save "Pallet Nodes :" };
if { $thing_to_record == "beamnodes" } { variable beam_node_list; set node_list $beam_node_list ; puts_and_save "Beam Nodes :" };
if { $thing_to_record == "basenodes" } { variable base_node_list; set node_list $base_node_list ; puts_and_save "Base Nodes :";};
if { $thing_to_record == "ext_col_nodes" } { variable extcol_node_list; set node_list $extcol_node_list ; puts_and_save "Exterior Column Nodes @ Joints :";};
if { $thing_to_record == "int_col_nodes" } { variable intcol_node_list; set node_list $intcol_node_list ; puts_and_save "Interior Column Nodes @ Joints :";};
if { $thing_to_record == "col_mid_nodes" } { variable col_mid_node_list; set node_list $col_mid_node_list ; puts_and_save "Column Nodes @ Mid-Span :";};

if { $record_time > 0 } { set time_string "-dT $record_time"; } else { set time_string ""; }

if { $what_to_record == "section_forces" } {
puts_and_save "Recording all section forces for elements : $ele_list"
for { set i 0 } { $i <= [expr [llength $ele_list]-1] } { incr i } {
set e [lindex $ele_list $i];
set cmd "recorder Element -file [format $output_dir/ele_force$e.out] $time_string -ele $e force;"; eval $cmd;
}
}

if { $what_to_record == "force" } {
puts_and_save "Recording local forces for elements : $ele_list"
for { set i 0 } { $i <= [expr [llength $ele_list]-1] } { incr i } {
set e [lindex $ele_list $i];
set cmd "recorder Element -file [format $output_dir/ele_force$e.out] $time_string -ele $e localForce;"; eval $cmd;
}
}

if { $what_to_record == "deformation" } {
puts_and_save "Recording deformations for elements : $ele_list"
for { set i 0 } { $i <= [expr [llength $ele_list]-1] } { incr i } {
set e [lindex $ele_list $i];
set cmd "recorder Element -file [format $output_dir/ele_def$e.out] $time_string -ele $e deformation;"; eval $cmd;
}
}

if { $what_to_record == "disp" } {
puts_and_save "Recording displacements at nodes : $node_list"
for { set i 0 } { $i <= [expr [llength $node_list]-1] } { incr i } {
set n [lindex $node_list $i];
set cmd "recorder Node -file [format $output_dir/node_disp$n.out] $time_string -node $n -dof 1 2 3 disp;"; eval $cmd;
}
}

if { $what_to_record == "reaction" } {
puts_and_save "Recording reactions at nodes : $node_list"

```

```

for { set i 0 } { $i <= [expr [llength $node_list]-1 ] } { incr i } {
set n [lindex $node_list $i];
set cmd "recorder Node -file [format $output_dir/node_reac$n.out] $time_string -node $n -dof 1 2 3 reaction;"; eval $cmd;
}
}
if {$what_to_record == "accel"} {
puts_and_save "Recording reactions at nodes : $node_list"
for { set i 0 } { $i <= [expr [llength $node_list]-1 ] } { incr i } {
set n [lindex $node_list $i];
set cmd "recorder Node -file [format $output_dir/node_acc$n.out] $time_string -node $n -dof 1 2 3 accel;"; eval $cmd;
}
}
}

proc ::rack_pack::check_total_reaction { dof step } {

#####
# Calculates the total reaction at the base nodes in a specified direction at a specified time step
#
# INPUTS :
# dof := an integer, direction the reaction [unitless] (1=x,2=y,3=z)
# step := the time step at which the reaction is to be calculated
#
# Example :
#
# EJ
#####

variable base_node_list;
variable output_dir;

# Base-plate recorders must be closed before reading the files
remove recorders;

set base_nodes [llength $base_node_list];
set total_reaction 0.;

# Read recorded out files node by node
for { set i 0 } { $i < $base_nodes } { incr i } {
set nodeI [lindex $base_node_list $i]; # Get item "i" in list of base nodes
if { [catch {set fp [open $output_dir/node_reac$nodeI.out]} errmsg] } {
puts_and_save "Verify that base-node recorders are set: $errmsg";
return 0.;
}
set file_data [read $fp]; # Slurp up data in file
close $fp; # Close connection
file delete $output_dir/node_reac$nodeI.out -force; # Delete the reaction output file
# Treat slurped up data to get reaction at the specified step
set data [split $file_data "\n"];
set lastline [lindex $data [expr $step-1]]; # Parse data to get last line which contains the reactions at the end of static analysis
set node_reaction [lindex $lastline [expr $dof-1]];
set total_reaction [expr $total_reaction + $node_reaction];
}

# Add-up and display total seismic weight
set message "Total vertical reaction is : "

```

```

puts_and_save [append message $total_reaction];

return $total_reaction;

}

proc ::rack_pack::make_output_dir { dirname } {

variable output_dir;

set output_dir $dirname;
set i 1;

# If an analysis has already been run in the output directory then make the output directory the default with a number appended
while { [file exists $output_dir$i] == 1 } { set i [expr $i+1] };

set output_dir $output_dir$i;
file mkdir $output_dir;
puts "Writing output to $output_dir";

}

proc ::rack_pack::puts_and_save { string_to_save } {

variable output_dir;
set out_file [open "$output_dir/a_model_and_analysis_info.out" "a+"]
puts $string_to_save
puts $out_file $string_to_save
close $out_file

}

proc rotSpring2D {eleID nodeR nodeC matID} {

# SETS A MULTIPOINT CONSTRAINT ON THE TRANSLATIONAL DEGREES OF FREEDOM,
# SO DO NOT USE THIS PROCEDURE IF THERE ARE TRANSLATIONAL ZEROLENGTH
# ELEMENTS ALSO BEING USED BETWEEN THESE TWO NODES
#
# Written: MHS
# Date: Jan 2000
#
# Formal arguments
#eleID - unique element ID for this zero length rotational spring
#nodeR - node ID which will be retained by the multi-point constraint
#nodeC - node ID which will be constrained by the multi-point constraint
#matID - material ID which represents the moment-rotation relationship
#for the spring

# Create the zero length element
element zeroLength $eleID $nodeR $nodeC -mat $matID -dir 6
# Constrain the translational DOF with a multi-point constraint
# retained constrained DOF_1 DOF_2 ... DOF_n
equalDOF $nodeR $nodeC 1 2

}

```

APPENDIX G AN APPROXIMATE EQUATION FOR THE FUNDAMENTAL PERIOD OF A RACK MOMENT FRAME

G.1. Developpement of approximate equation:

To find the total rigidity of the frame, base-plate and beam-column connectors are replaced with torsional springs, Figure : a. Assuming beam inflexion points at mid-span the frame can be replaced by the equivalent system shown in Figure G-1b.

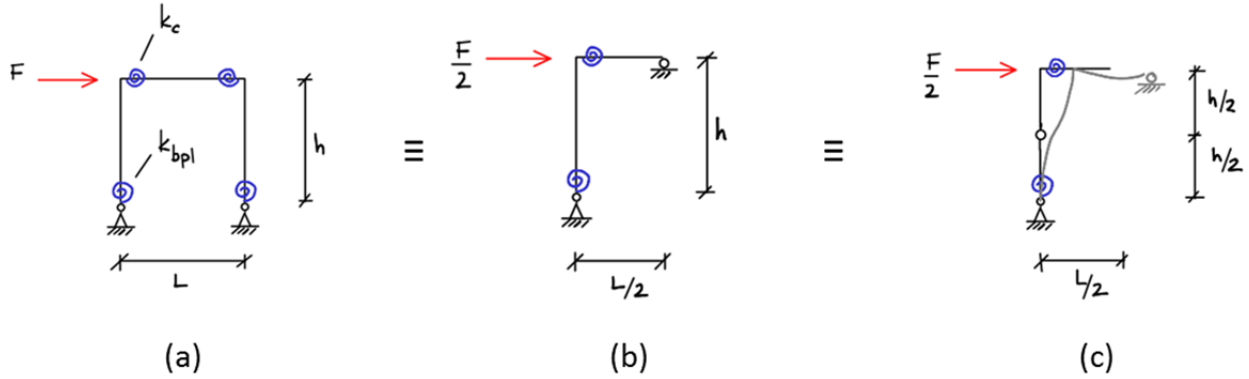


Figure : G-1 Simplification of a rack moment frame

It is assumed that column inflexion points are located at mid-height as in Figure G-1c. Using this assumption, lateral story deflection due to beam and connector rigidity can be written:

$$\Delta_1 = \theta_{b,c} \cdot \frac{h}{2} \quad (1)$$

Where: $\theta_{b,c}$:= rotation of the joint allowed by beam and connector

Since beam and connector act in series:

$$\Delta_1 = M_{bc} \frac{(k_c + k_{b\theta})}{k_c k_{b\theta}} \cdot \frac{h}{2} = 2 \left(\frac{F}{2} h \right) \cdot \frac{(k_c + k_{b\theta})}{k_c k_{b\theta}} \cdot \frac{h}{2} \quad (2)$$

$$\text{Thus: } k_1 = 2 \cdot k_c k_{b\theta} / (k_c + k_{b\theta}) \cdot \text{where } k_{b\theta} = 3EI_b / (L/2) = 6EI_b / L \quad (3)$$

Story deflection due to the top-half of column deflection is: $\Delta_2 = F / \left(3EI_c / (h/2)^3 \right)$

Thus: $k_2 = 24EI_c / h^3$

Story deflection due to the bottom half of the column in series with the base-plate is:

$$\Delta_3 = \theta_{col,c} \cdot \frac{h}{2}$$

Where: $\theta_{col,c} :=$ rotation of the joint allowed by half of column and base plate

$$\Delta_3 = M_{col,c} \frac{(k_c + k_{col\theta})}{k_c k_{col\theta}} \cdot \frac{h}{2} = Fh \cdot \frac{(k_c + k_{col\theta})}{k_c k_{col\theta}} \cdot \frac{h}{2}$$

Thus : $k_3 = 2 \cdot k_c k_{col\theta} / (k_c + k_{col\theta})$ where $k_{col\theta} = 3EI_{col} / (h/2) = 6EI_{col} / h$

The top of the column (k_2) acts in series with the beam and connector (k_1); since the rotule is considered at mid-height of the column, the base plate and column bottom (k_3) are in parallel with the rest of the structure:

$$k_{tot} = \frac{N_b}{2} \left[\frac{1}{k_1} + \frac{1}{k_2} \right]^{-1} + \frac{N_c}{2} k_3 \quad (4)$$

Since fundamental period is a function of stiffness and mass only, pallet height centre of gravity should not influence the fundamental period. Note that the generalised mass is the same whether calculated using the displacements at pallet centres of gravity or at beam levels because the shape function is the same.

$$T_n = 2\pi \sqrt{\frac{\sum W_{p,i} h_{x,i}^2}{g \cdot k_{tot}}} \quad (5)$$

Where:

$W_{p,i} :=$ weight of all the pallets at the level i

$h_{x,i} :=$ height of the level

G.2. Comparisons of approximate fundamental period equation with RMI equation and eigenvalue analysis

The approximate equation for fundamental period developed in §Appendix G is compared with the approximate equation developed in [15] and with fundamental periods issue from eigenvalue analysis. The following combinations are plotted

- Number of levels 1 through 9
- Number of bays 1 through 9
- Connector stiffness 50 kNm/rad through 500 kNm/rad (by increments of 50)

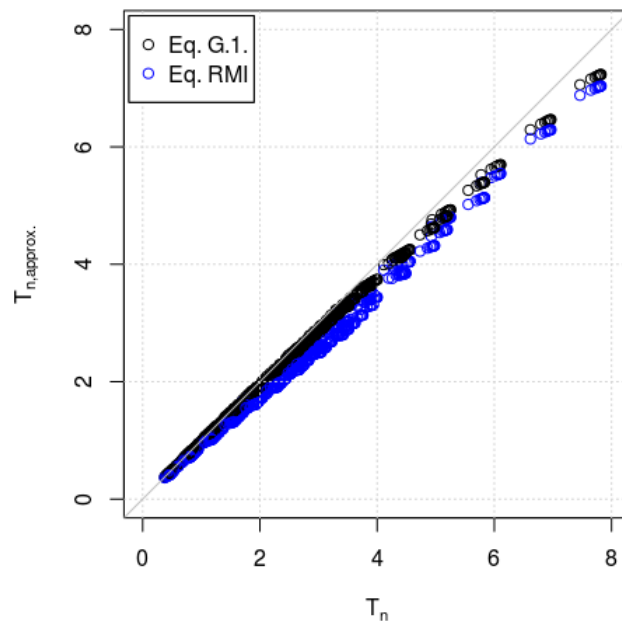


Figure : G-2 : Comparision of two approximate equations for fundamental period with periods issue from eigenvalue analys

A numeric experiment further illustrates that pallet centre of gravity should not influence fundamental period. A 3-level, 1-bay rack with 200 kNm/rad beam-column and base-plate connections is loaded with eccentric pallets (Figure G-2) or at beam-level loads (Figure G-5). Weight totals 14.68 kN per level. Very rigid beams are used in both models such that the stiffness of the pallet assemblies does not influence fundamental period. Column inertia is $1.315\text{E-}06 \text{ m}^4$. Member self-weight is neglected. As can be seen by comparing Figure G-4 and G-5, pallet height does not influence fundamental period.

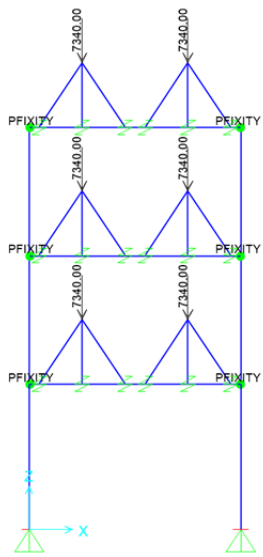


Figure : G-3 : Rack
with eccentric loads

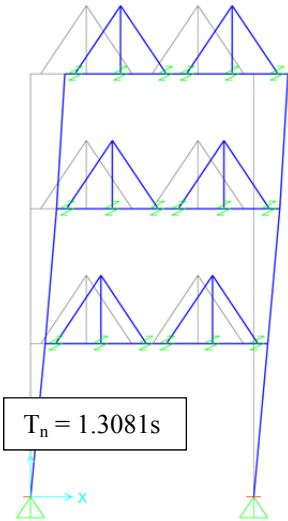


Figure G-4 :
Fundamental period
with eccentric loads

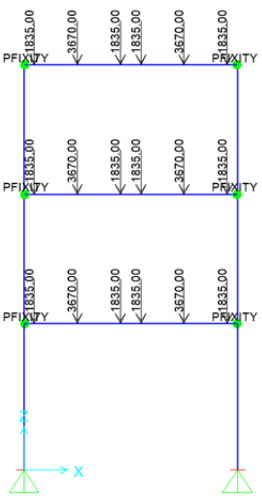


Figure : G-5 : Rack
with beam-level
masses

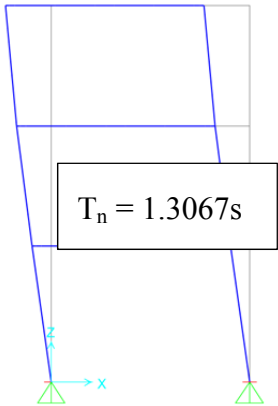
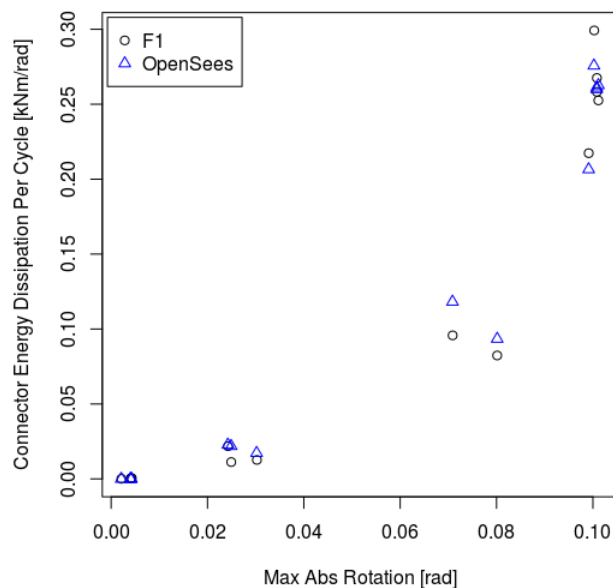
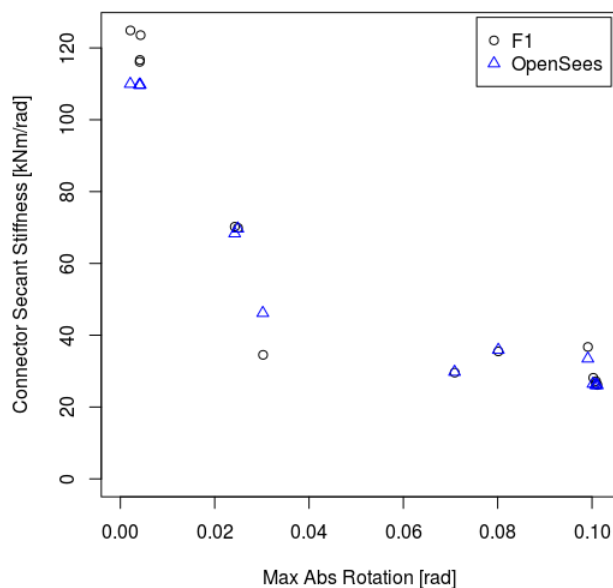


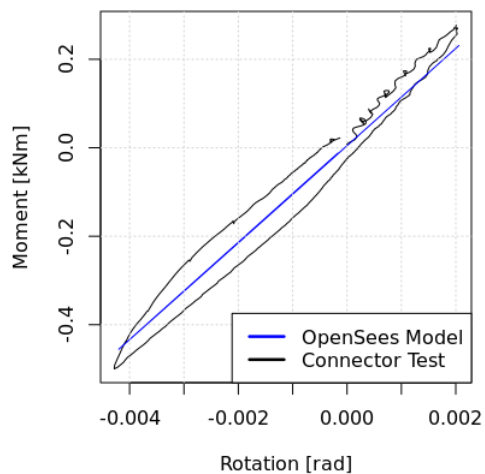
Figure : G-6 :
Fundamental period
with beam-level loads

APPENDIX H CYCLE BY CYCLE CURVE MATCHING OF NON-LINEAR CONNECTORS AND BASE-PLATES

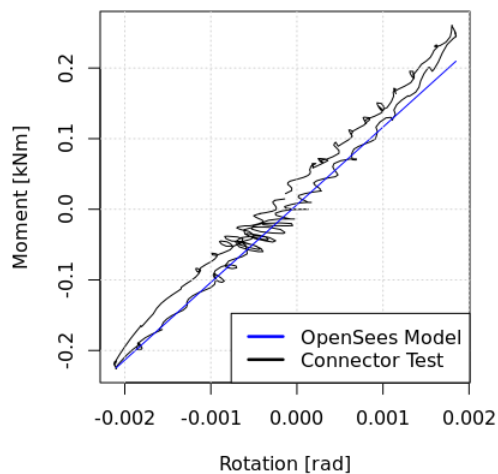
H.1. Polytechnique Base-Plate vs. Test F1



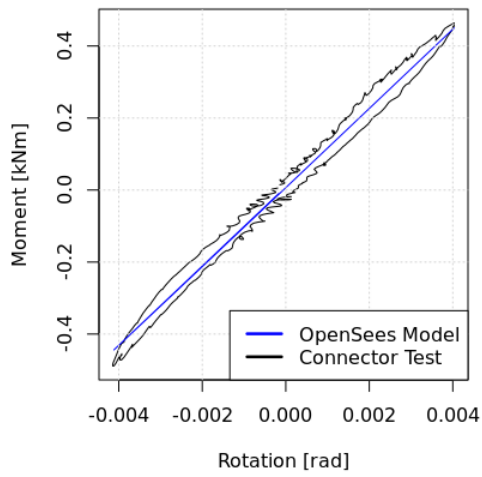
Cycle 1 Max Real Moment: 0.2773 [Nm], Min Real Moment: -0.5 [kNm]
 Max Real Rot.: 0.002 [rad], Min Real Rot.: -0.0043 [rad]
 vs. Max Model Moment : 0.230999 [Nm], Min Model Moment : -0.45561 [kNm]
 Max Model Rot.: 0.0021 [rad], Min Model Rot.: -0.0042 [rad]



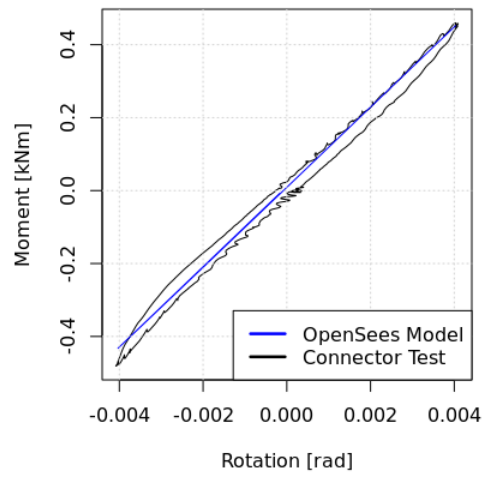
Cycle 2 Max Real Moment: 0.2608 [Nm], Min Real Moment: -0.2261 [kNm]
 Max Real Rot.: 0.0018 [rad], Min Real Rot.: -0.0021 [rad]
 vs. Max Model Moment : 0.209651 [Nm], Min Model Moment : -0.224476 [kNm]
 Max Model Rot.: 0.0018 [rad], Min Model Rot.: -0.0021 [rad]



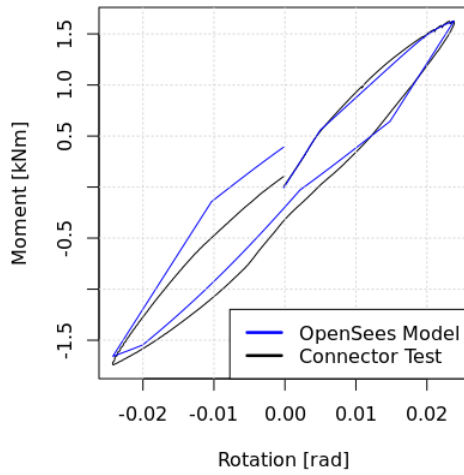
Cycle 3 Max Real Moment: 0.4642 [Nm], Min Real Moment: -0.4889 [kNm]
 Max Real Rot.: 0.004 [rad], Min Real Rot.: -0.0041 [rad]
 vs. Max Model Moment : 0.450024 [Nm], Min Model Moment : -0.4439 [kNm]
 Max Model Rot.: 0.004 [rad], Min Model Rot.: -0.0041 [rad]



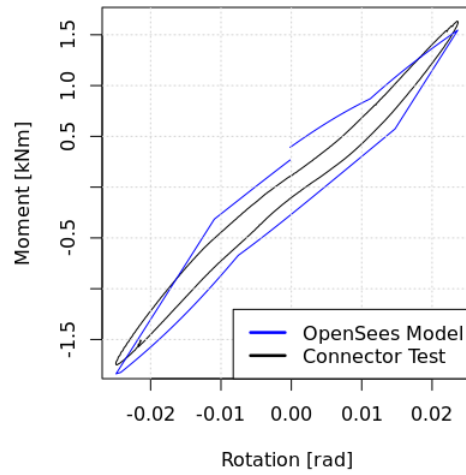
Cycle 4 Max Real Moment: 0.4599 [Nm], Min Real Moment: -0.4813 [kNm]
 Max Real Rot.: 0.0041 [rad], Min Real Rot.: -0.0041 [rad]
 vs. Max Model Moment : 0.452354 [Nm], Min Model Moment : -0.432428 [kNm]
 Max Model Rot.: 0.004 [rad], Min Model Rot.: -0.004 [rad]



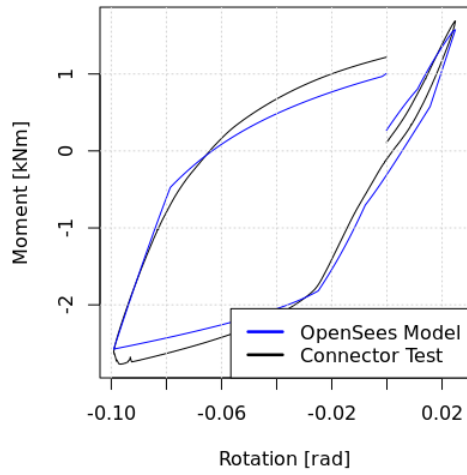
Cycle 5 Max Real Moment: 1.6255 [Nm], Min Real Moment: -1.7413 [kNm]
 Max Real Rot.: 0.0239 [rad], Min Real Rot.: -0.0243 [rad]
 vs. Max Model Moment : 1.62624 [Nm], Min Model Moment : -1.65697 [kNm]
 Max Model Rot.: 0.0238 [rad], Min Model Rot.: -0.0242 [rad]



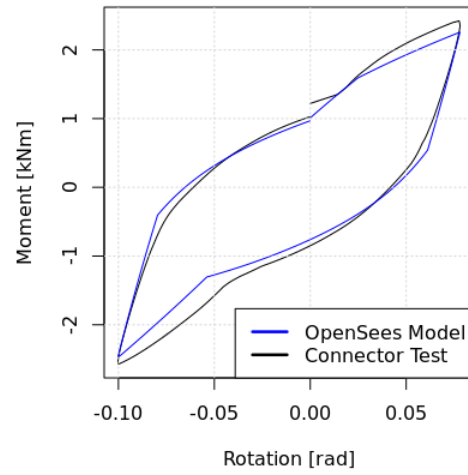
Cycle 6 Max Real Moment: 1.6348 [Nm], Min Real Moment: -1.7496 [kNm]
 Max Real Rot.: 0.0237 [rad], Min Real Rot.: -0.0249 [rad]
 vs. Max Model Moment : 1.54538 [Nm], Min Model Moment : -1.83727 [kNm]
 Max Model Rot.: 0.0236 [rad], Min Model Rot.: -0.0249 [rad]



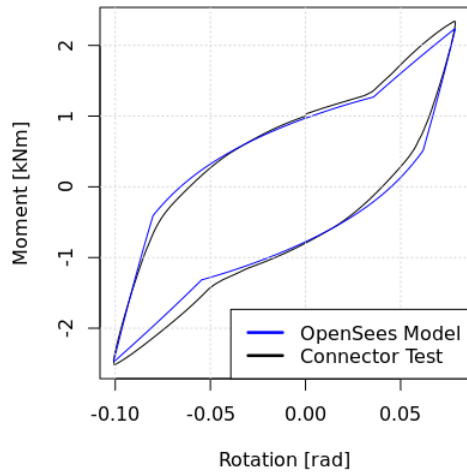
Cycle 7 Max Real Moment: 1.6896 [Nm], Min Real Moment: -2.7699 [kNm]
 Max Real Rot.: 0.0248 [rad], Min Real Rot.: -0.0991 [rad]
 vs. Max Model Moment : 1.5745 [Nm], Min Model Moment : -2.57457 [kNm]
 Max Model Rot.: 0.0248 [rad], Min Model Rot.: -0.0991 [rad]



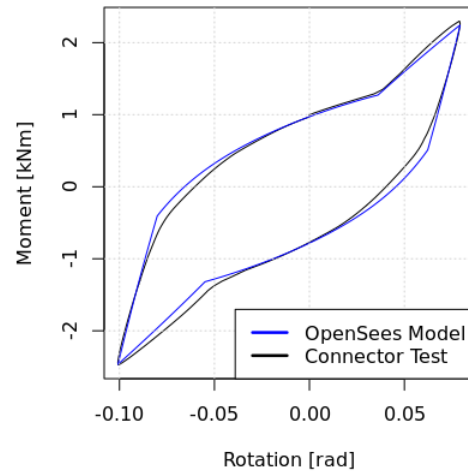
Cycle 8 Max Real Moment: 2.4222 [Nm], Min Real Moment: -2.5725 [kNm]
 Max Real Rot.: 0.0781 [rad], Min Real Rot.: -0.1003 [rad]
 vs. Max Model Moment : 2.25805 [Nm], Min Model Moment : -2.4599 [kNm]
 Max Model Rot.: 0.078 [rad], Min Model Rot.: -0.1002 [rad]



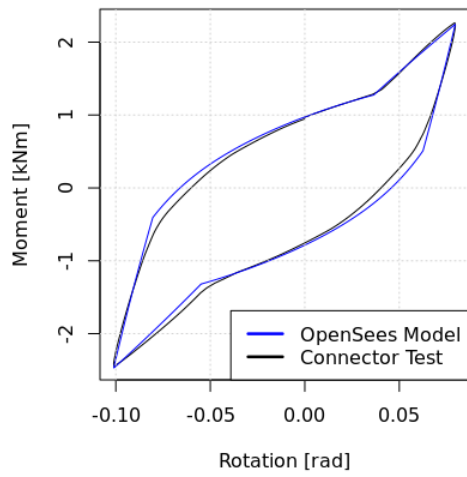
Cycle 9 Max Real Moment: 2.3437 [Nm], Min Real Moment: -2.5184 [kNm]
 Max Real Rot.: 0.0787 [rad], Min Real Rot.: -0.1008 [rad]
 vs. Max Model Moment : 2.23461 [Nm], Min Model Moment : -2.46697 [kNm]
 Max Model Rot.: 0.0787 [rad], Min Model Rot.: -0.1008 [rad]



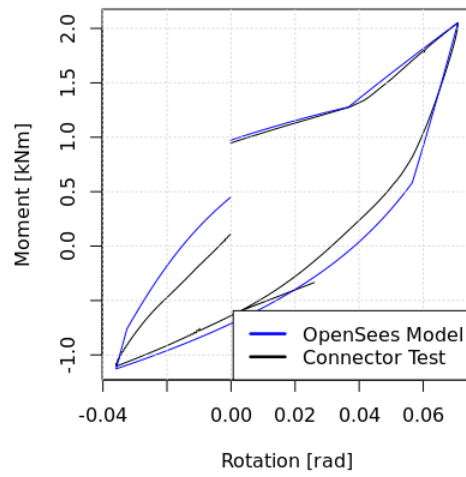
Cycle 10 Max Real Moment: 2.2989 [Nm], Min Real Moment: -2.4732 [kNm]
 Max Real Rot.: 0.0793 [rad], Min Real Rot.: -0.1008 [rad]
 vs. Max Model Moment : 2.24002 [Nm], Min Model Moment : -2.46581 [kNm]
 Max Model Rot.: 0.0793 [rad], Min Model Rot.: -0.1008 [rad]



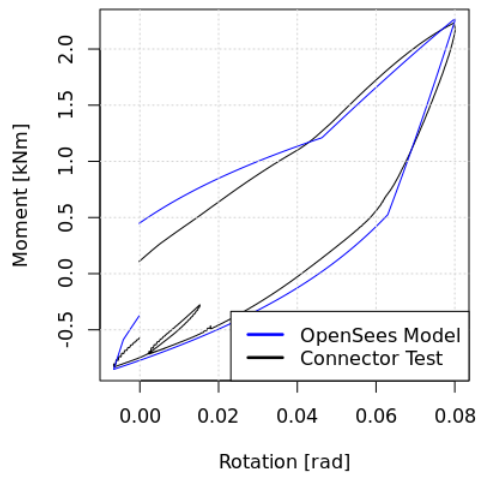
Cycle 11 Max Real Moment: 2.2645 [Nm], Min Real Moment: -2.445 [kNm]
 Max Real Rot.: 0.0796 [rad], Min Real Rot.: -0.1011 [rad]
 vs. Max Model Moment : 2.24299 [Nm], Min Model Moment : -2.46845 [kNm]
 Max Model Rot.: 0.0796 [rad], Min Model Rot.: -0.1011 [rad]



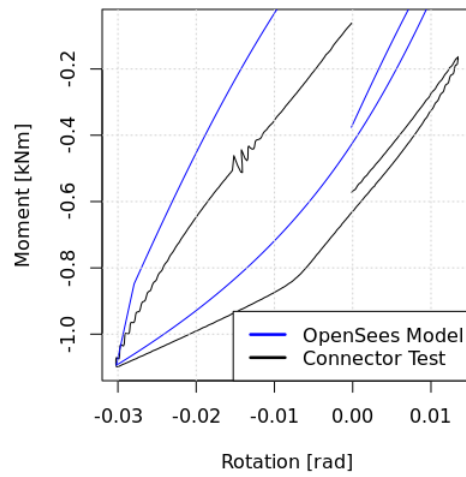
Cycle 12 Max Real Moment: 2.0506 [Nm], Min Real Moment: -1.1025 [kNm]
 Max Real Rot.: 0.0709 [rad], Min Real Rot.: -0.036 [rad]
 vs. Max Model Moment : 2.05301 [Nm], Min Model Moment : -1.1275 [kNm]
 Max Model Rot.: 0.0709 [rad], Min Model Rot.: -0.0359 [rad]



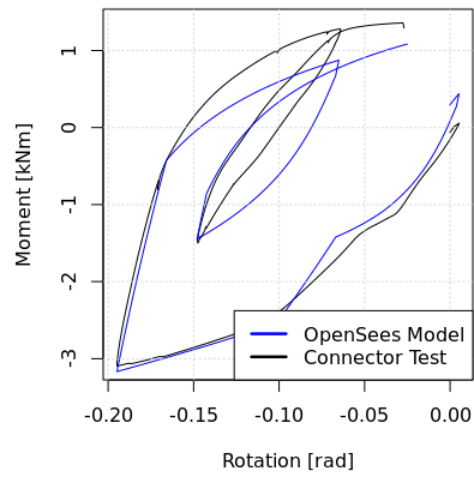
Cycle 13 Max Real Moment: 2.2308 [Nm], Min Real Moment: -0.8299 [kNm]
 Max Real Rot.: 0.0801 [rad], Min Real Rot.: -0.0067 [rad]
 vs. Max Model Moment : 2.26472 [Nm], Min Model Moment : -0.851314 [kNm]
 Max Model Rot.: 0.0801 [rad], Min Model Rot.: -0.0066 [rad]



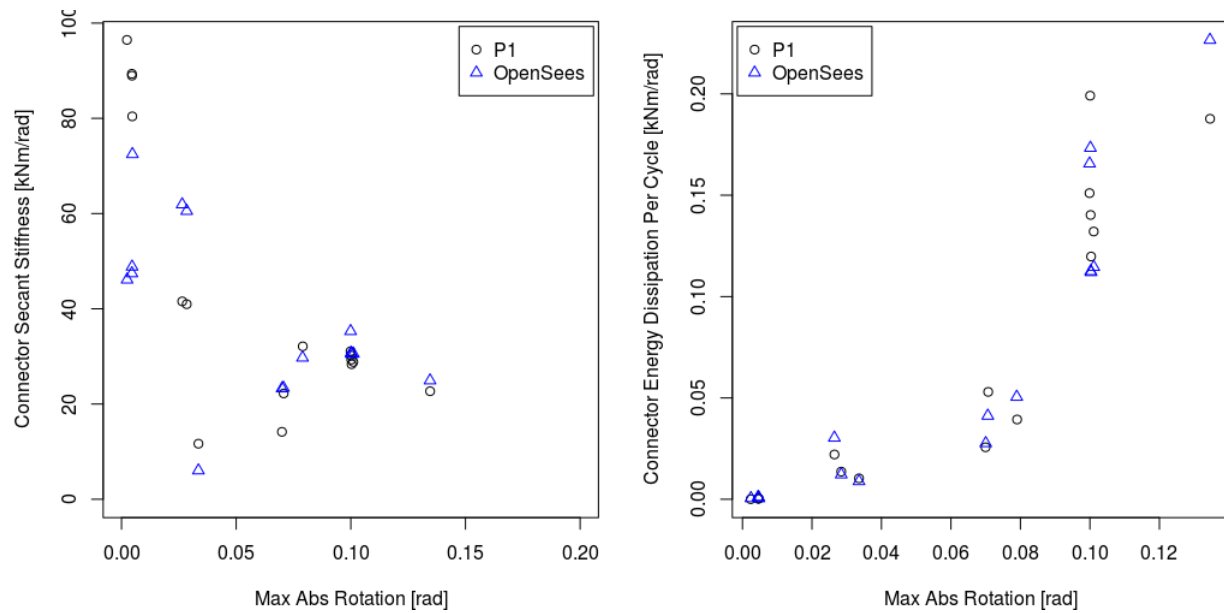
Cycle 14 Max Real Moment: -0.0617 [Nm], Min Real Moment: -1.0987 [kNm]
 Max Real Rot.: 0.0135 [rad], Min Real Rot.: -0.0303 [rad]
 vs. Max Model Moment : 0.29297 [Nm], Min Model Moment : -1.09373 [kNm]
 Max Model Rot.: 0.0134 [rad], Min Model Rot.: -0.0302 [rad]



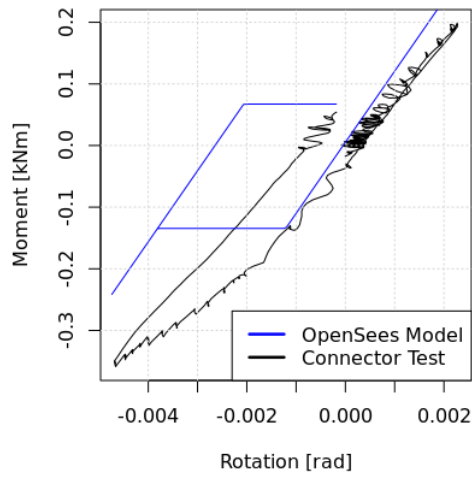
Cycle 15 Max Real Moment: 1.3594 [Nm], Min Real Moment: -3.0968 [kNm]
 Max Real Rot.: 0.0053 [rad], Min Real Rot.: -0.1949 [rad]
 vs. Max Model Moment : 1.08463 [Nm], Min Model Moment : -3.16795 [kNm]
 Max Model Rot.: 0.0052 [rad], Min Model Rot.: -0.1948 [rad]



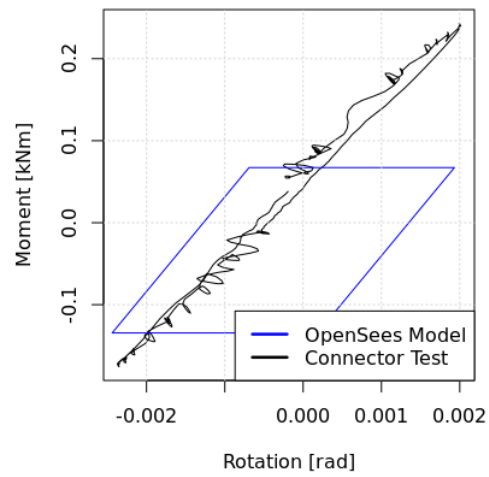
H.2. Polytechnique Connector Cold-form vs. Test P1



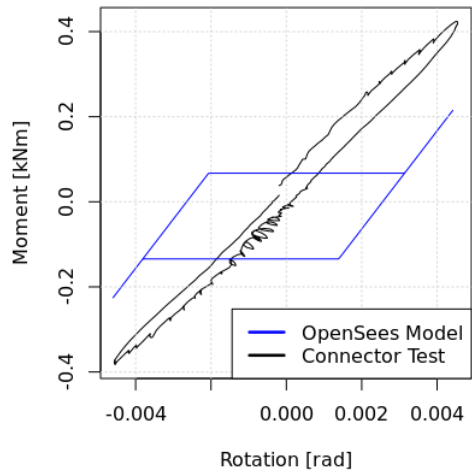
Cycle 1 Max Real Moment: 0.1983 [Nm], Min Real Moment: -0.3588 [kNm]
 Max Real Rot.: 0.0023 [rad], Min Real Rot.: -0.0047 [rad]
 vs. Max Model Moment : 0.265382 [Nm], Min Model Moment : -0.241372 [kNm]
 Max Model Rot.: 0.0023 [rad], Min Model Rot.: -0.0047 [rad]



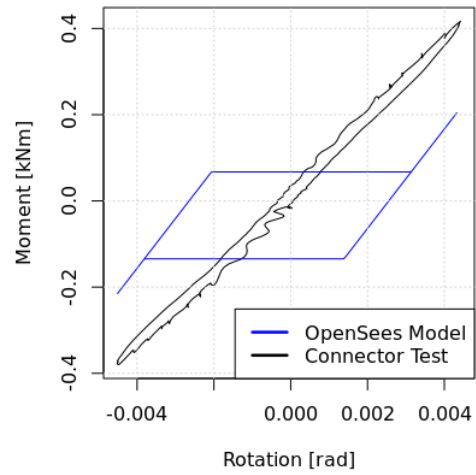
Cycle 2 Max Real Moment: 0.2432 [Nm], Min Real Moment: -0.1756 [kNm]
 Max Real Rot.: 0.002 [rad], Min Real Rot.: -0.0024 [rad]
 vs. Max Model Moment : 0.0672001 [Nm], Min Model Moment : -0.1344 [kNm]
 Max Model Rot.: 0.0019 [rad], Min Model Rot.: -0.0024 [rad]



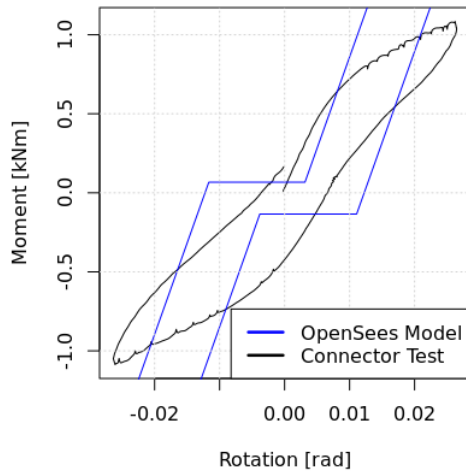
Cycle 3 Max Real Moment: 0.4243 [Nm], Min Real Moment: -0.3829 [kNm]
 Max Real Rot.: 0.0045 [rad], Min Real Rot.: -0.0046 [rad]
 vs. Max Model Moment : 0.214845 [Nm], Min Model Moment : -0.225449 [kNm]
 Max Model Rot.: 0.0044 [rad], Min Model Rot.: -0.0046 [rad]



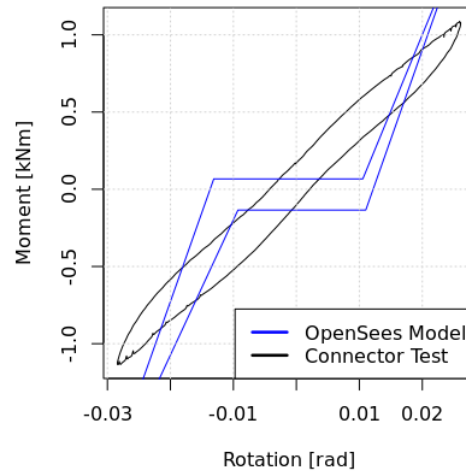
Cycle 4 Max Real Moment: 0.4167 [Nm], Min Real Moment: -0.38 [kNm]
 Max Real Rot.: 0.0044 [rad], Min Real Rot.: -0.0045 [rad]
 vs. Max Model Moment : 0.20423 [Nm], Min Model Moment : -0.214834 [kNm]
 Max Model Rot.: 0.0043 [rad], Min Model Rot.: -0.0045 [rad]



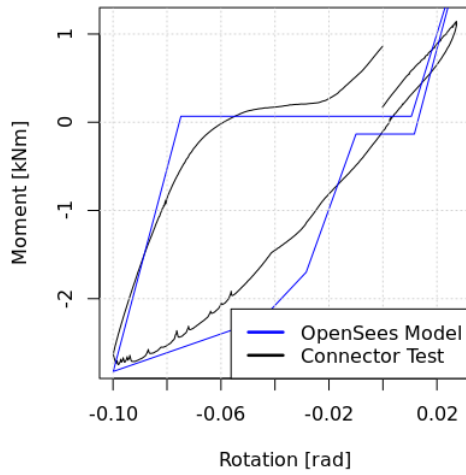
Cycle 5 Max Real Moment: 1.0849 [Nm], Min Real Moment: -1.0873 [kNm]
 Max Real Rot.: 0.0265 [rad], Min Real Rot.: -0.0264 [rad]
 vs. Max Model Moment : 1.63861 [Nm], Min Model Moment : -1.63412 [kNm]
 Max Model Rot.: 0.0264 [rad], Min Model Rot.: -0.0264 [rad]



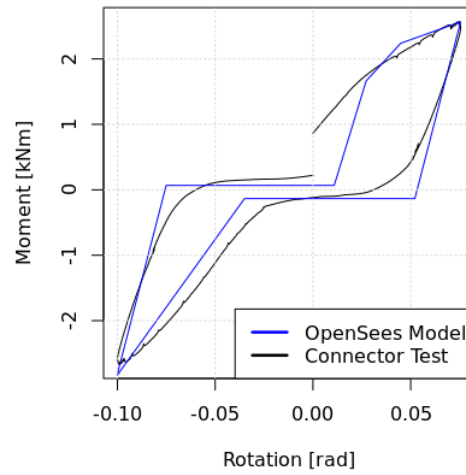
Cycle 6 Max Real Moment: 1.0875 [Nm], Min Real Moment: -1.1358 [kNm]
 Max Real Rot.: 0.0261 [rad], Min Real Rot.: -0.0284 [rad]
 vs. Max Model Moment : 1.59769 [Nm], Min Model Moment : -1.6999 [kNm]
 Max Model Rot.: 0.026 [rad], Min Model Rot.: -0.0284 [rad]



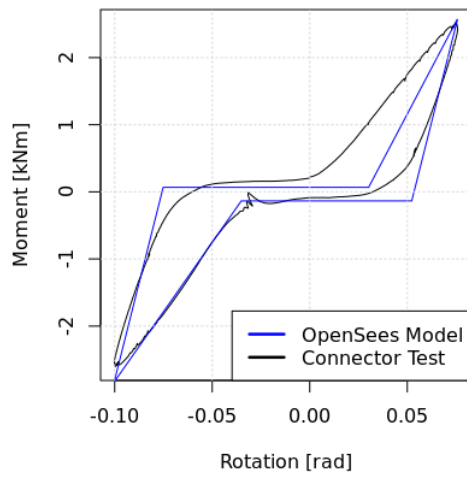
Cycle 7 Max Real Moment: 1.1437 [Nm], Min Real Moment: -2.7482 [kNm]
 Max Real Rot.: 0.0273 [rad], Min Real Rot.: -0.0999 [rad]
 vs. Max Model Moment : 1.66402 [Nm], Min Model Moment : -2.82523 [kNm]
 Max Model Rot.: 0.0272 [rad], Min Model Rot.: -0.0999 [rad]



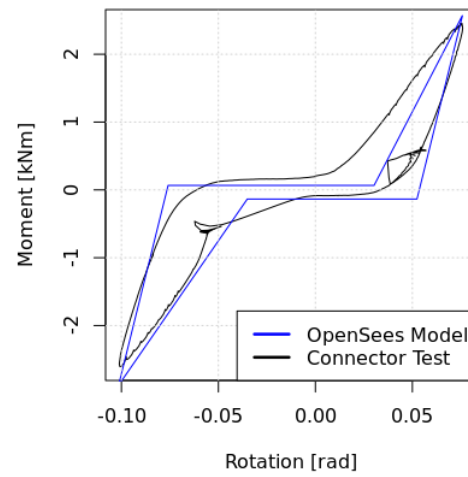
Cycle 8 Max Real Moment: 2.5742 [Nm], Min Real Moment: -2.6721 [kNm]
 Max Real Rot.: 0.0756 [rad], Min Real Rot.: -0.1001 [rad]
 vs. Max Model Moment : 2.56616 [Nm], Min Model Moment : -2.82768 [kNm]
 Max Model Rot.: 0.0755 [rad], Min Model Rot.: -0.1001 [rad]



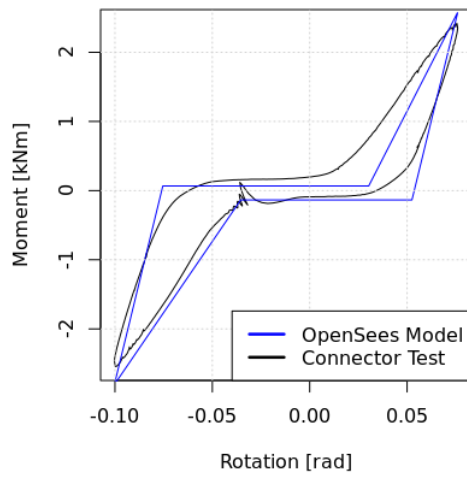
Cycle 9 Max Real Moment: 2.5113 [Nm], Min Real Moment: -2.6051 [kNm]
 Max Real Rot.: 0.0758 [rad], Min Real Rot.: -0.1002 [rad]
 vs. Max Model Moment : 2.56812 [Nm], Min Model Moment : -2.82866 [kNm]
 Max Model Rot.: 0.0757 [rad], Min Model Rot.: -0.1002 [rad]



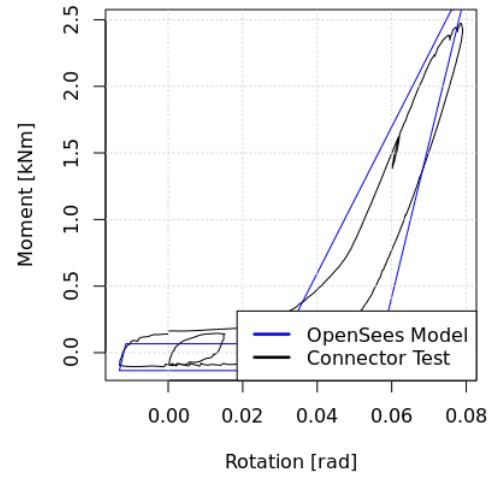
Cycle 10 Max Real Moment: 2.4567 [Nm], Min Real Moment: -2.6061 [kNm]
 Max Real Rot.: 0.0759 [rad], Min Real Rot.: -0.1011 [rad]
 vs. Max Model Moment : 2.5691 [Nm], Min Model Moment : -2.83799 [kNm]
 Max Model Rot.: 0.0758 [rad], Min Model Rot.: -0.1011 [rad]



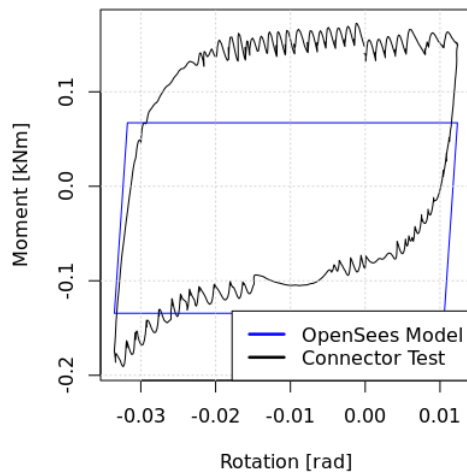
Cycle 11 Max Real Moment: 2.4192 [Nm], Min Real Moment: -2.5459 [kNm]
 Max Real Rot.: 0.076 [rad], Min Real Rot.: -0.1003 [rad]
 vs. Max Model Moment : 2.57057 [Nm], Min Model Moment : -2.8058 [kNm]
 Max Model Rot.: 0.0759 [rad], Min Model Rot.: -0.1003 [rad]



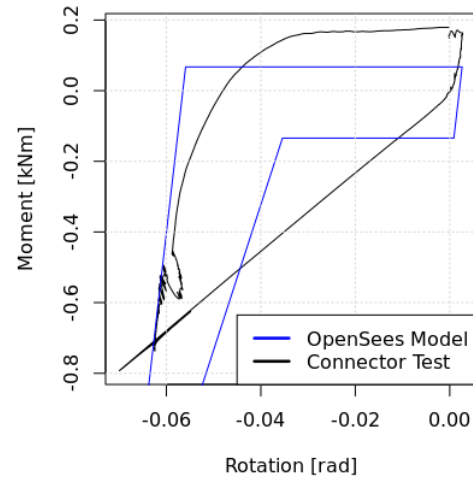
Cycle 13 Max Real Moment: 2.4732 [Nm], Min Real Moment: -0.1049 [kNm]
 Max Real Rot.: 0.079 [rad], Min Real Rot.: -0.0131 [rad]
 vs. Max Model Moment : 2.60247 [Nm], Min Model Moment : -0.1344 [kNm]
 Max Model Rot.: 0.0789 [rad], Min Model Rot.: -0.0131 [rad]



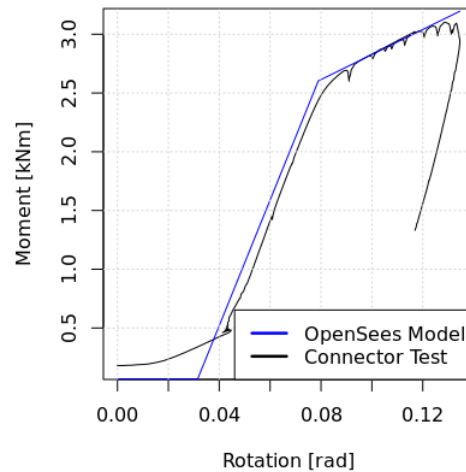
Cycle 14 Max Real Moment: 0.1725 [Nm], Min Real Moment: -0.1909 [kNm]
 Max Real Rot.: 0.0124 [rad], Min Real Rot.: -0.0335 [rad]
 vs. Max Model Moment : 0.0672 [Nm], Min Model Moment : -0.1344 [kNm]
 Max Model Rot.: 0.0123 [rad], Min Model Rot.: -0.0335 [rad]



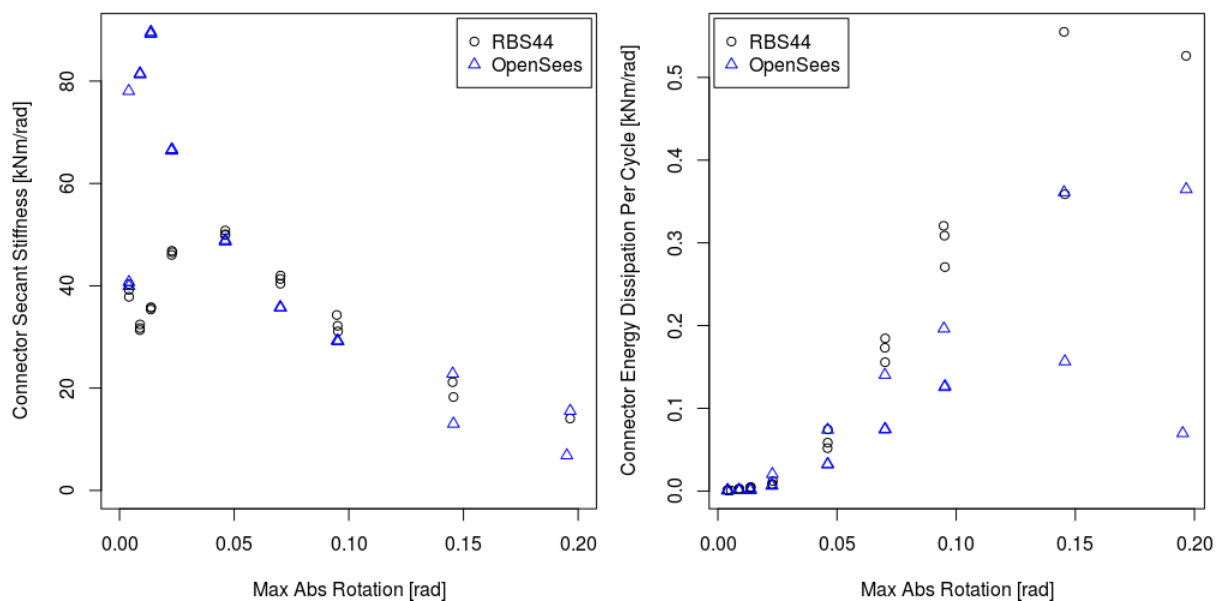
Cycle 15 Max Real Moment: 0.1793 [Nm], Min Real Moment: -0.7927 [kNm]
 Max Real Rot.: 0.0027 [rad], Min Real Rot.: -0.07 [rad]
 vs. Max Model Moment : 0.0672 [Nm], Min Model Moment : -1.55819 [kNm]
 Max Model Rot.: 0.0026 [rad], Min Model Rot.: -0.07 [rad]



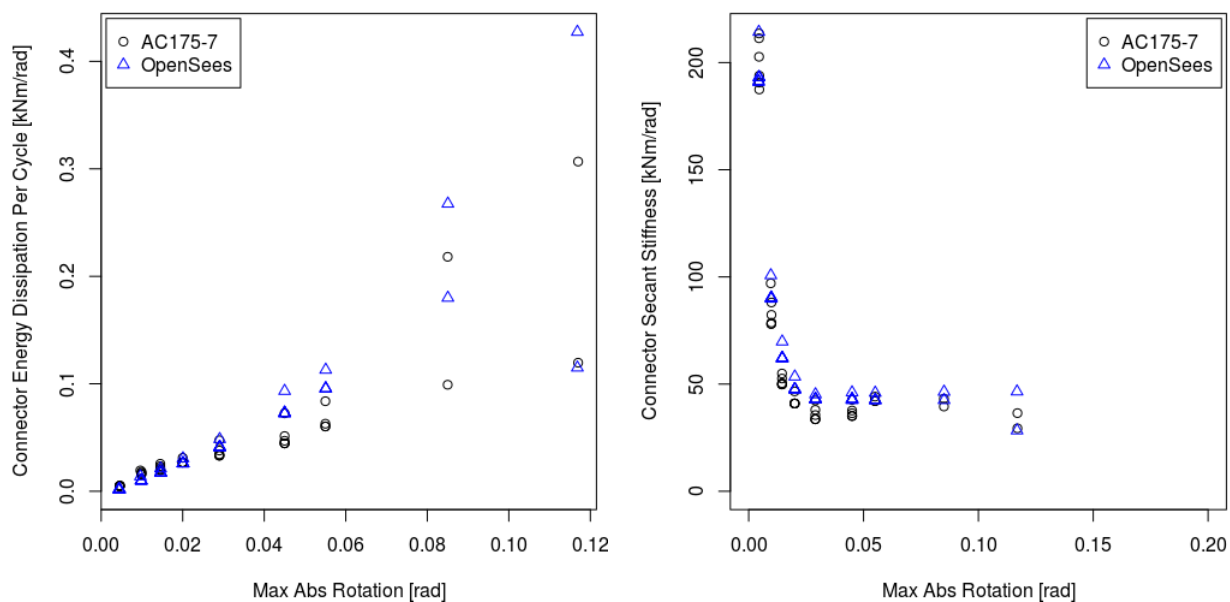
Cycle 16 Max Real Moment: 3.1014 [Nm], Min Real Moment: 0.1793 [kNm]
 Max Real Rot.: 0.1346 [rad], Min Real Rot.: -1e-04 [rad]
 vs. Max Model Moment : 3.19568 [Nm], Min Model Moment : 0.0672 [kNm]
 Max Model Rot.: 0.1345 [rad], Min Model Rot.: -2e-04 [rad]



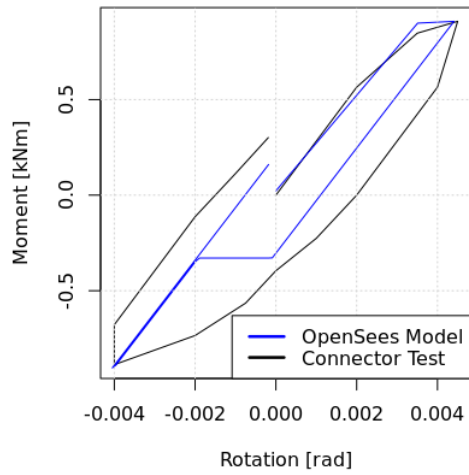
H.3. Polytechnique Connector Coldform vs. ITS data



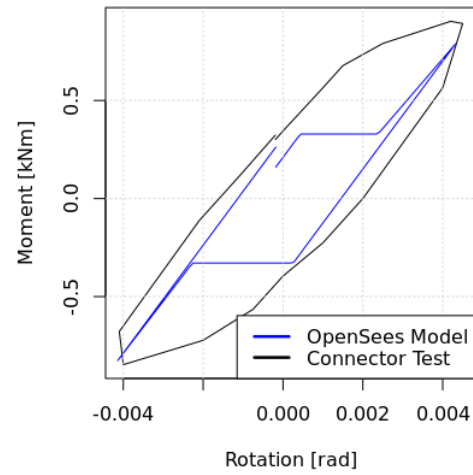
H.4. Prototype Connector 1 (Frazier AC175) vs. ITS data



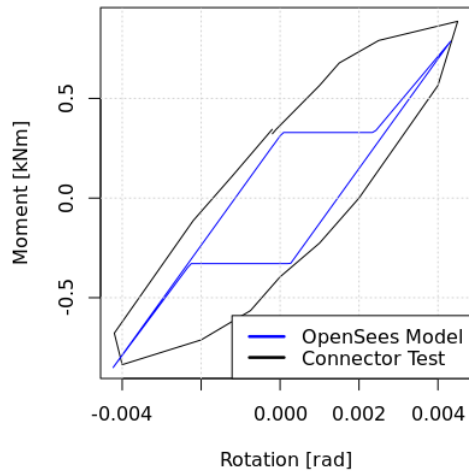
Cycle 1 Max Real Moment: 0.9095 [Nm], Min Real Moment: -0.8869 [kNm]
 Max Real Rot.: 0.0045 [rad], Min Real Rot.: -0.004 [rad]
 vs. Max Model Moment : 0.90925 [Nm], Min Model Moment : -0.903698 [kNm]
 Max Model Rot.: 0.0044 [rad], Min Model Rot.: -0.004 [rad]



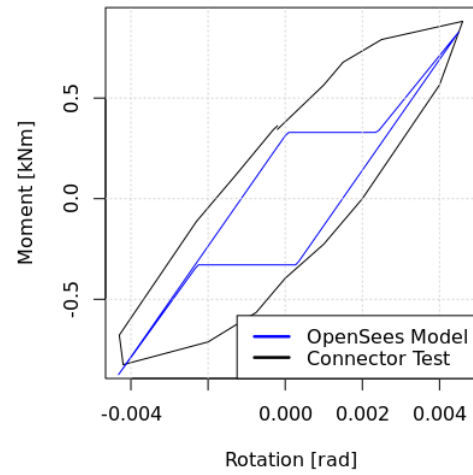
Cycle 2 Max Real Moment: 0.9039 [Nm], Min Real Moment: -0.8474 [kNm]
 Max Real Rot.: 0.0045 [rad], Min Real Rot.: -0.0041 [rad]
 vs. Max Model Moment : 0.788486 [Nm], Min Model Moment : -0.826461 [kNm]
 Max Model Rot.: 0.0043 [rad], Min Model Rot.: -0.0041 [rad]



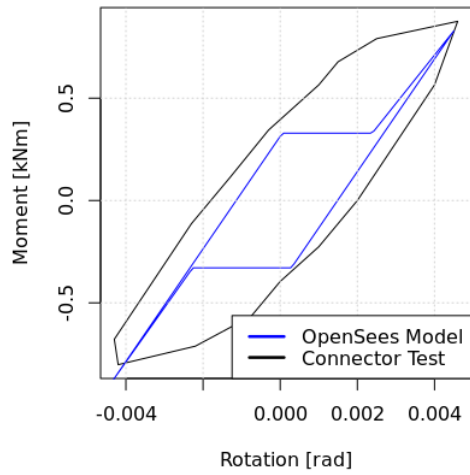
Cycle 3 Max Real Moment: 0.8869 [Nm], Min Real Moment: -0.8361 [kNm]
 Max Real Rot.: 0.0045 [rad], Min Real Rot.: -0.0042 [rad]
 vs. Max Model Moment : 0.786274 [Nm], Min Model Moment : -0.850377 [kNm]
 Max Model Rot.: 0.0043 [rad], Min Model Rot.: -0.0042 [rad]



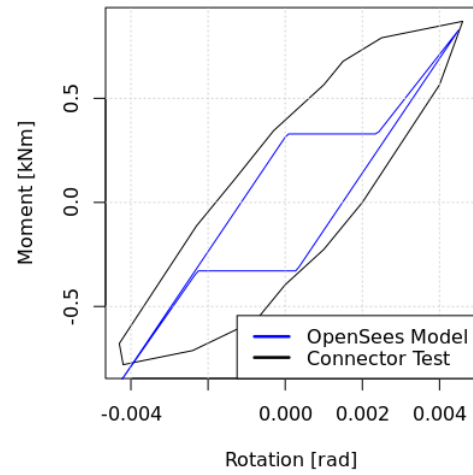
Cycle 4 Max Real Moment: 0.8813 [Nm], Min Real Moment: -0.8248 [kNm]
 Max Real Rot.: 0.0046 [rad], Min Real Rot.: -0.0043 [rad]
 vs. Max Model Moment : 0.828809 [Nm], Min Model Moment : -0.874293 [kNm]
 Max Model Rot.: 0.0045 [rad], Min Model Rot.: -0.0043 [rad]



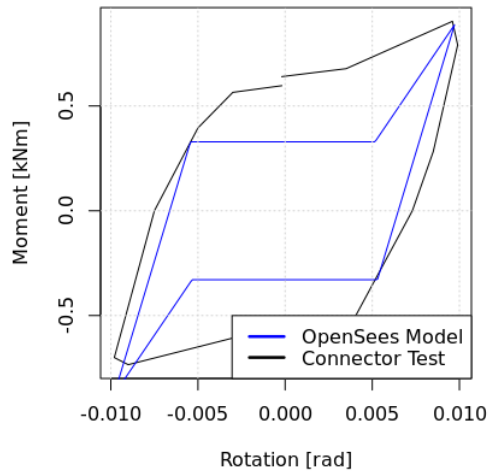
Cycle 5 Max Real Moment: 0.8756 [Nm], Min Real Moment: -0.8022 [kNm]
 Max Real Rot.: 0.0046 [rad], Min Real Rot.: -0.0043 [rad]
 vs. Max Model Moment : 0.828809 [Nm], Min Model Moment : -0.874293 [kNm]
 Max Model Rot.: 0.0045 [rad], Min Model Rot.: -0.0043 [rad]



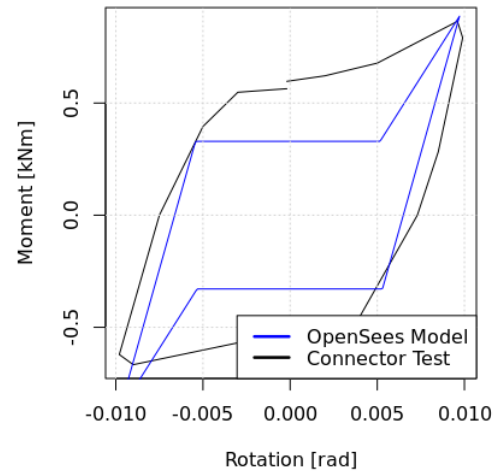
Cycle 6 Max Real Moment: 0.87 [Nm], Min Real Moment: -0.7796 [kNm]
 Max Real Rot.: 0.0046 [rad], Min Real Rot.: -0.0043 [rad]
 vs. Max Model Moment : 0.828809 [Nm], Min Model Moment : -0.874293 [kNm]
 Max Model Rot.: 0.0045 [rad], Min Model Rot.: -0.0043 [rad]



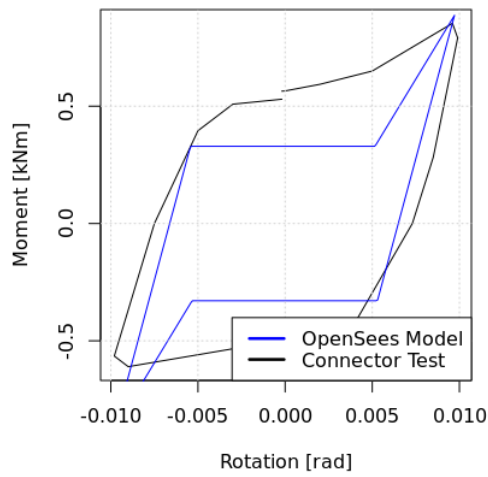
Cycle 8 Max Real Moment: 0.9039 [Nm], Min Real Moment: -0.7344 [kNm]
 Max Real Rot.: 0.0099 [rad], Min Real Rot.: -0.0098 [rad]
 vs. Max Model Moment : 0.887199 [Nm], Min Model Moment : -0.876189 [kNm]
 Max Model Rot.: 0.0097 [rad], Min Model Rot.: -0.0098 [rad]



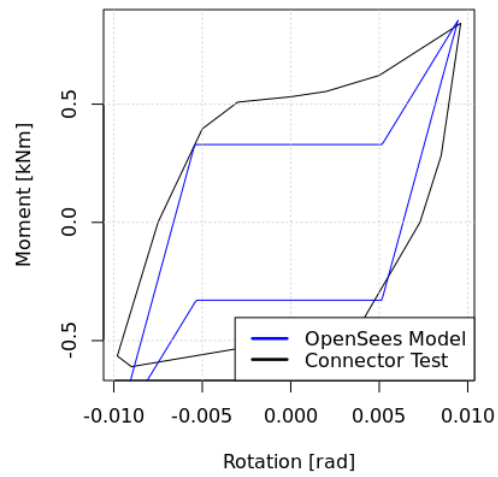
Cycle 9 Max Real Moment: 0.8643 [Nm], Min Real Moment: -0.6666 [kNm]
 Max Real Rot.: 0.0099 [rad], Min Real Rot.: -0.0098 [rad]
 vs. Max Model Moment : 0.887199 [Nm], Min Model Moment : -0.876189 [kNm]
 Max Model Rot.: 0.0097 [rad], Min Model Rot.: -0.0098 [rad]



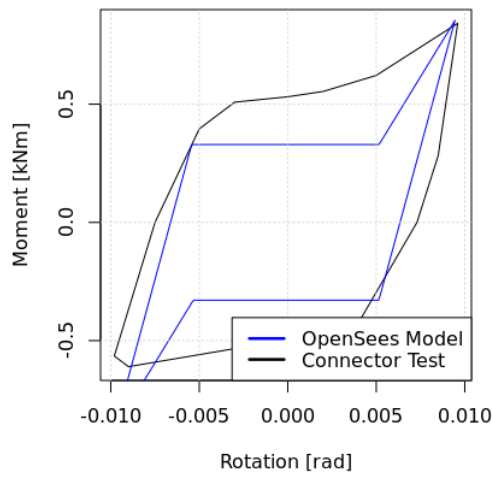
Cycle 10 Max Real Moment: 0.853 [Nm], Min Real Moment: -0.6101 [kNm]
 Max Real Rot.: 0.0099 [rad], Min Real Rot.: -0.0098 [rad]
 vs. Max Model Moment : 0.887199 [Nm], Min Model Moment : -0.876189 [kNm]
 Max Model Rot.: 0.0097 [rad], Min Model Rot.: -0.0098 [rad]



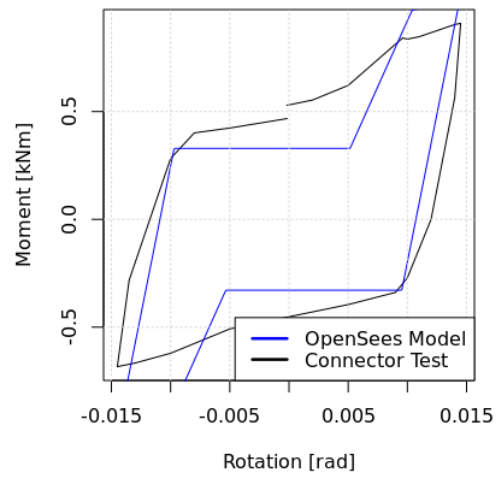
Cycle 11 Max Real Moment: 0.8417 [Nm], Min Real Moment: -0.6101 [kNm]
 Max Real Rot.: 0.0096 [rad], Min Real Rot.: -0.0098 [rad]
 vs. Max Model Moment : 0.85417 [Nm], Min Model Moment : -0.876189 [kNm]
 Max Model Rot.: 0.0094 [rad], Min Model Rot.: -0.0098 [rad]



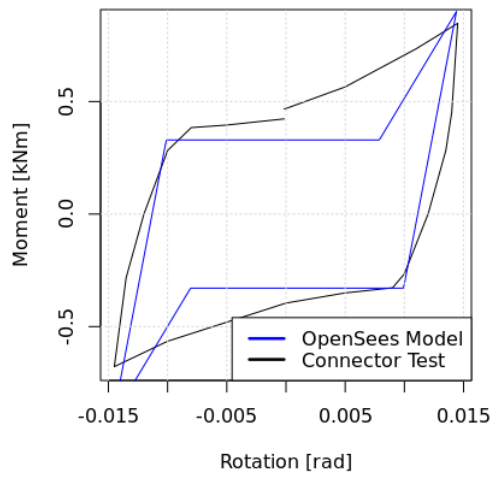
Cycle 12 Max Real Moment: 0.8417 [Nm], Min Real Moment: -0.6101 [kNm]
 Max Real Rot.: 0.0096 [rad], Min Real Rot.: -0.0098 [rad]
 vs. Max Model Moment : 0.85417 [Nm], Min Model Moment : -0.876189 [kNm]
 Max Model Rot.: 0.0094 [rad], Min Model Rot.: -0.0098 [rad]



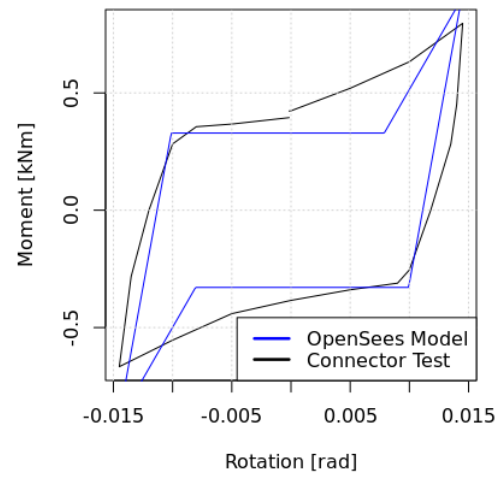
Cycle 13 Max Real Moment: 0.9095 [Nm], Min Real Moment: -0.6836 [kNm]
 Max Real Rot.: 0.0145 [rad], Min Real Rot.: -0.0145 [rad]
 vs. Max Model Moment : 1.01195 [Nm], Min Model Moment : -1.01195 [kNm]
 Max Model Rot.: 0.0144 [rad], Min Model Rot.: -0.0146 [rad]



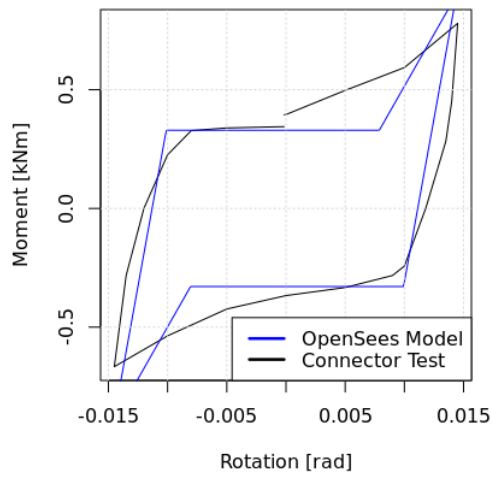
Cycle 14 Max Real Moment: 0.8474 [Nm], Min Real Moment: -0.6779 [kNm]
 Max Real Rot.: 0.0145 [rad], Min Real Rot.: -0.0145 [rad]
 vs. Max Model Moment : 0.899968 [Nm], Min Model Moment : -0.899968 [kNm]
 Max Model Rot.: 0.0144 [rad], Min Model Rot.: -0.0146 [rad]



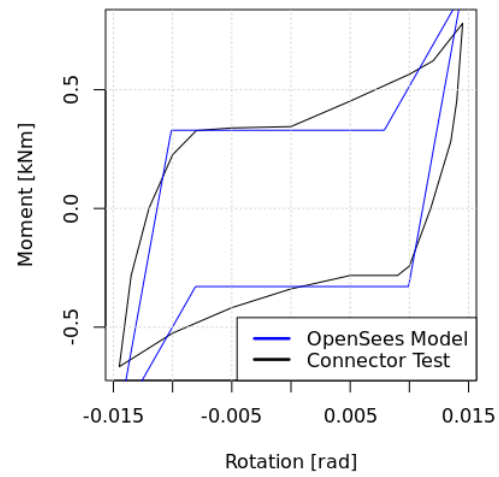
Cycle 15 Max Real Moment: 0.7965 [Nm], Min Real Moment: -0.6666 [kNm]
 Max Real Rot.: 0.0145 [rad], Min Real Rot.: -0.0145 [rad]
 vs. Max Model Moment : 0.899968 [Nm], Min Model Moment : -0.899968 [kNm]
 Max Model Rot.: 0.0144 [rad], Min Model Rot.: -0.0146 [rad]



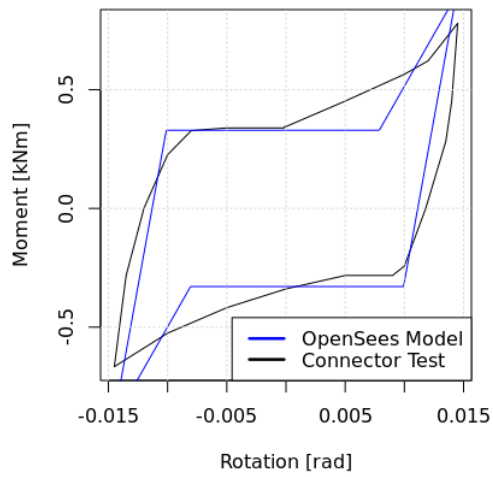
Cycle 16 Max Real Moment: 0.7796 [Nm], Min Real Moment: -0.6666 [kNm]
 Max Real Rot.: 0.0145 [rad], Min Real Rot.: -0.0145 [rad]
 vs. Max Model Moment : 0.899968 [Nm], Min Model Moment : -0.899968 [kNm]
 Max Model Rot.: 0.0144 [rad], Min Model Rot.: -0.0146 [rad]



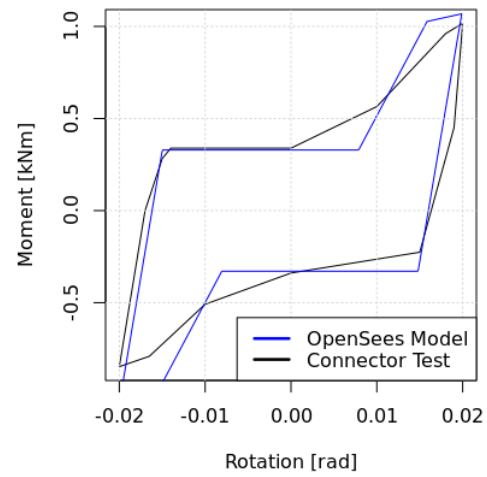
Cycle 17 Max Real Moment: 0.7796 [Nm], Min Real Moment: -0.6666 [kNm]
 Max Real Rot.: 0.0145 [rad], Min Real Rot.: -0.0145 [rad]
 vs. Max Model Moment : 0.899968 [Nm], Min Model Moment : -0.899968 [kNm]
 Max Model Rot.: 0.0144 [rad], Min Model Rot.: -0.0146 [rad]



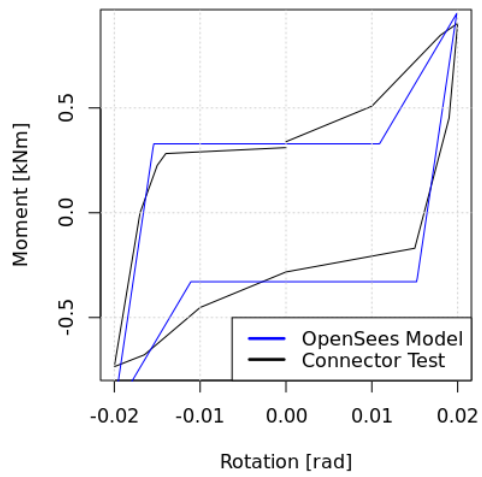
Cycle 18 Max Real Moment: 0.7796 [Nm], Min Real Moment: -0.6666 [kNm]
 Max Real Rot.: 0.0145 [rad], Min Real Rot.: -0.0145 [rad]
 vs. Max Model Moment : 0.899968 [Nm], Min Model Moment : -0.899968 [kNm]
 Max Model Rot.: 0.0144 [rad], Min Model Rot.: -0.0146 [rad]



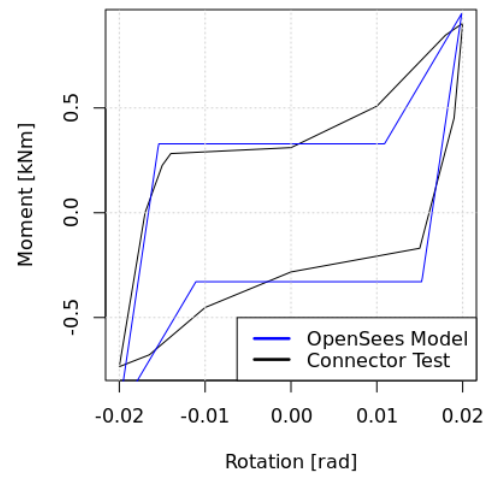
Cycle 19 Max Real Moment: 1.0169 [Nm], Min Real Moment: -0.8474 [kNm]
 Max Real Rot.: 0.02 [rad], Min Real Rot.: -0.02 [rad]
 vs. Max Model Moment : 1.06839 [Nm], Min Model Moment : -1.06839 [kNm]
 Max Model Rot.: 0.0199 [rad], Min Model Rot.: -0.0201 [rad]



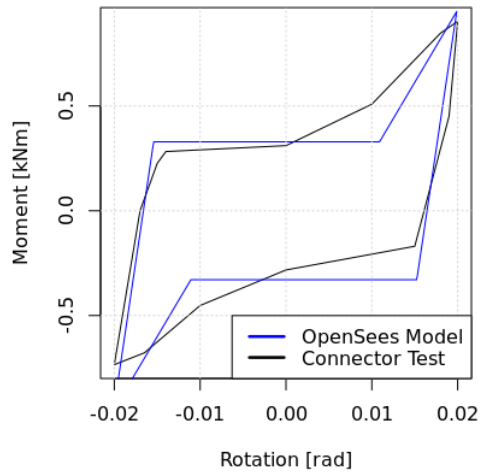
Cycle 20 Max Real Moment: 0.9039 [Nm], Min Real Moment: -0.7344 [kNm]
 Max Real Rot.: 0.02 [rad], Min Real Rot.: -0.02 [rad]
 vs. Max Model Moment : 0.950763 [Nm], Min Model Moment : -0.950762 [kNm]
 Max Model Rot.: 0.0199 [rad], Min Model Rot.: -0.0201 [rad]



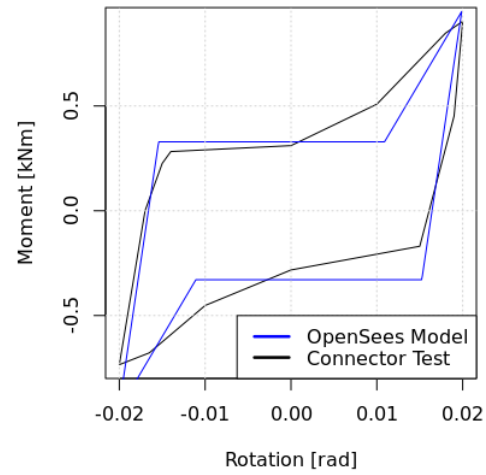
Cycle 21 Max Real Moment: 0.9039 [Nm], Min Real Moment: -0.7344 [kNm]
 Max Real Rot.: 0.02 [rad], Min Real Rot.: -0.02 [rad]
 vs. Max Model Moment : 0.950763 [Nm], Min Model Moment : -0.950762 [kNm]
 Max Model Rot.: 0.0199 [rad], Min Model Rot.: -0.0201 [rad]



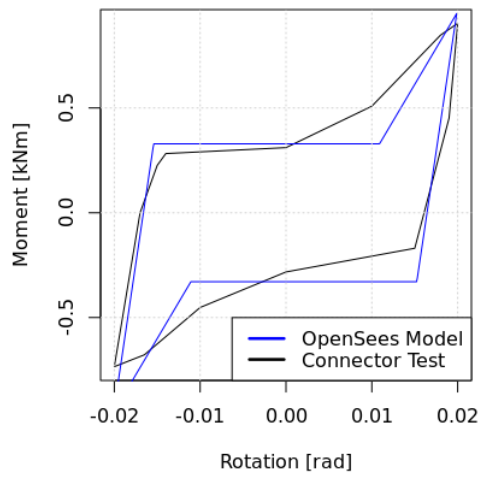
Cycle 22 Max Real Moment: 0.9039 [Nm], Min Real Moment: -0.7344 [kNm]
 Max Real Rot.: 0.02 [rad], Min Real Rot.: -0.02 [rad]
 vs. Max Model Moment : 0.950763 [Nm], Min Model Moment : -0.950762 [kNm]
 Max Model Rot.: 0.0199 [rad], Min Model Rot.: -0.0201 [rad]



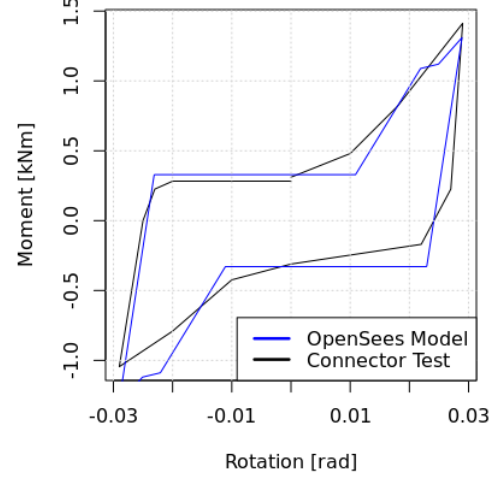
Cycle 23 Max Real Moment: 0.9039 [Nm], Min Real Moment: -0.7344 [kNm]
 Max Real Rot.: 0.02 [rad], Min Real Rot.: -0.02 [rad]
 vs. Max Model Moment : 0.950763 [Nm], Min Model Moment : -0.950762 [kNm]
 Max Model Rot.: 0.0199 [rad], Min Model Rot.: -0.0201 [rad]



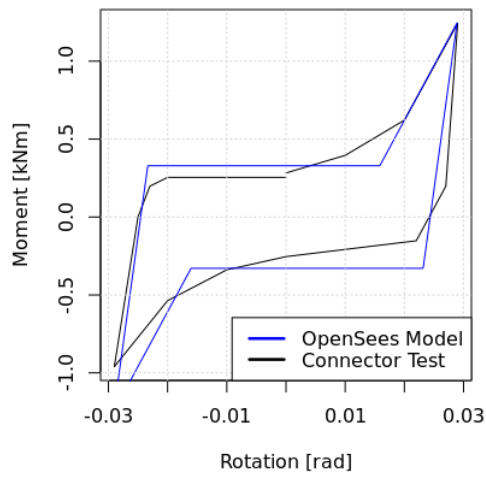
Cycle 24 Max Real Moment: 0.9039 [Nm], Min Real Moment: -0.7344 [kNm]
 Max Real Rot.: 0.02 [rad], Min Real Rot.: -0.02 [rad]
 vs. Max Model Moment : 0.950763 [Nm], Min Model Moment : -0.950762 [kNm]
 Max Model Rot.: 0.0199 [rad], Min Model Rot.: -0.0201 [rad]



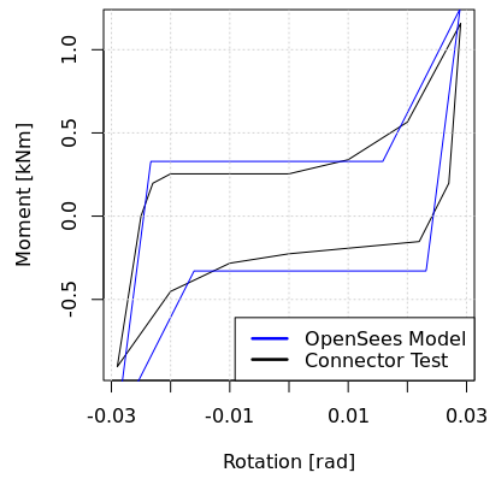
Cycle 25 Max Real Moment: 1.4123 [Nm], Min Real Moment: -1.0451 [kNm]
 Max Real Rot.: 0.029 [rad], Min Real Rot.: -0.029 [rad]
 vs. Max Model Moment : 1.30996 [Nm], Min Model Moment : -1.30996 [kNm]
 Max Model Rot.: 0.0289 [rad], Min Model Rot.: -0.0291 [rad]



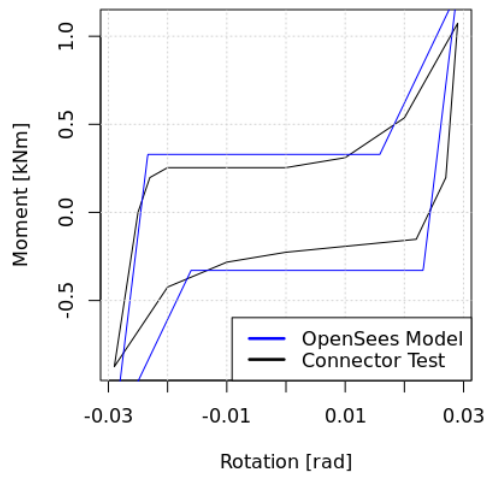
Cycle 26 Max Real Moment: 1.2428 [Nm], Min Real Moment: -0.9604 [kNm]
 Max Real Rot.: 0.029 [rad], Min Real Rot.: -0.029 [rad]
 vs. Max Model Moment : 1.24479 [Nm], Min Model Moment : -1.24478 [kNm]
 Max Model Rot.: 0.0289 [rad], Min Model Rot.: -0.0291 [rad]



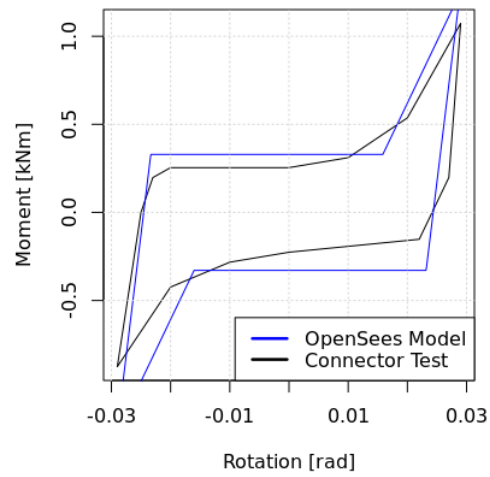
Cycle 27 Max Real Moment: 1.1581 [Nm], Min Real Moment: -0.9039 [kNm]
 Max Real Rot.: 0.029 [rad], Min Real Rot.: -0.029 [rad]
 vs. Max Model Moment : 1.24479 [Nm], Min Model Moment : -1.24478 [kNm]
 Max Model Rot.: 0.0289 [rad], Min Model Rot.: -0.0291 [rad]



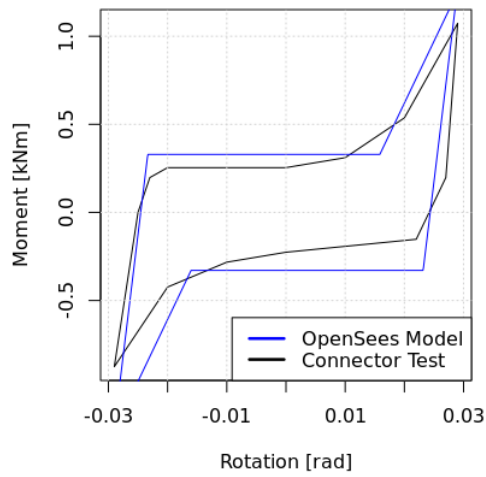
Cycle 28 Max Real Moment: 1.0734 [Nm], Min Real Moment: -0.8756 [kNm]
 Max Real Rot.: 0.029 [rad], Min Real Rot.: -0.029 [rad]
 vs. Max Model Moment : 1.24479 [Nm], Min Model Moment : -1.24478 [kNm]
 Max Model Rot.: 0.0289 [rad], Min Model Rot.: -0.0291 [rad]



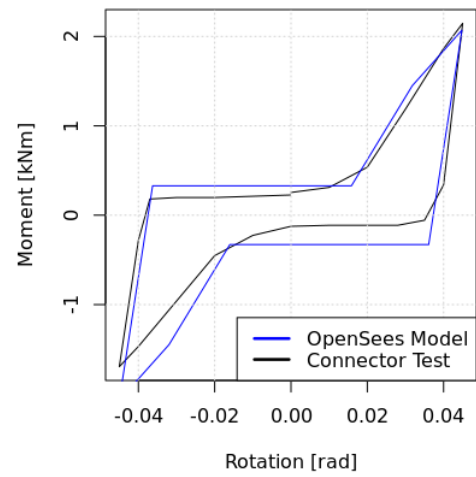
Cycle 29 Max Real Moment: 1.0734 [Nm], Min Real Moment: -0.8756 [kNm]
 Max Real Rot.: 0.029 [rad], Min Real Rot.: -0.029 [rad]
 vs. Max Model Moment : 1.24479 [Nm], Min Model Moment : -1.24478 [kNm]
 Max Model Rot.: 0.0289 [rad], Min Model Rot.: -0.0291 [rad]



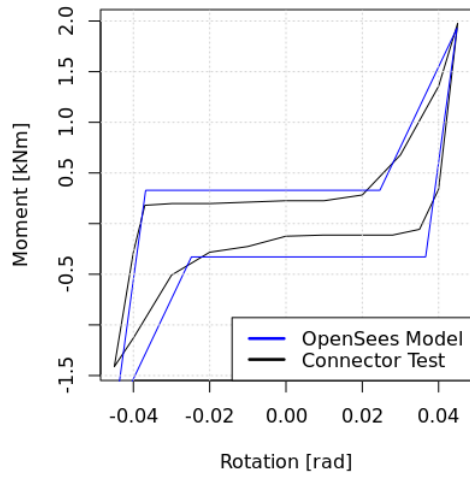
Cycle 30 Max Real Moment: 1.0734 [Nm], Min Real Moment: -0.8756 [kNm]
 Max Real Rot.: 0.029 [rad], Min Real Rot.: -0.029 [rad]
 vs. Max Model Moment : 1.24479 [Nm], Min Model Moment : -1.24478 [kNm]
 Max Model Rot.: 0.0289 [rad], Min Model Rot.: -0.0291 [rad]



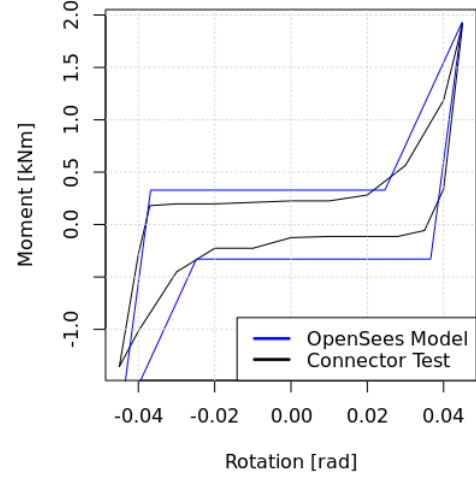
Cycle 31 Max Real Moment: 2.1467 [Nm], Min Real Moment: -1.6948 [kNm]
 Max Real Rot.: 0.045 [rad], Min Real Rot.: -0.045 [rad]
 vs. Max Model Moment : 2.07035 [Nm], Min Model Moment : -2.07034 [kNm]
 Max Model Rot.: 0.0448 [rad], Min Model Rot.: -0.045 [rad]



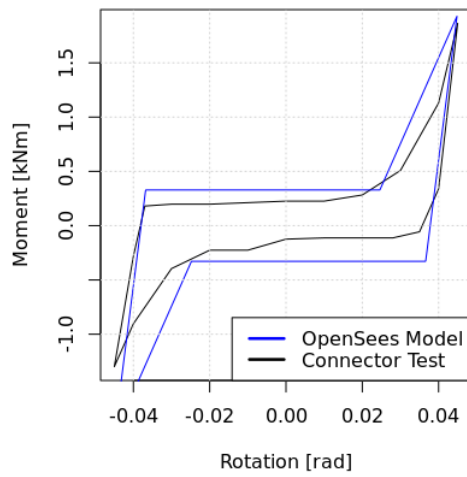
Cycle 32 Max Real Moment: 1.9772 [Nm], Min Real Moment: -1.4123 [kNm]
 Max Real Rot.: 0.045 [rad], Min Real Rot.: -0.045 [rad]
 vs. Max Model Moment : 1.92913 [Nm], Min Model Moment : -1.92913 [kNm]
 Max Model Rot.: 0.0448 [rad], Min Model Rot.: -0.045 [rad]



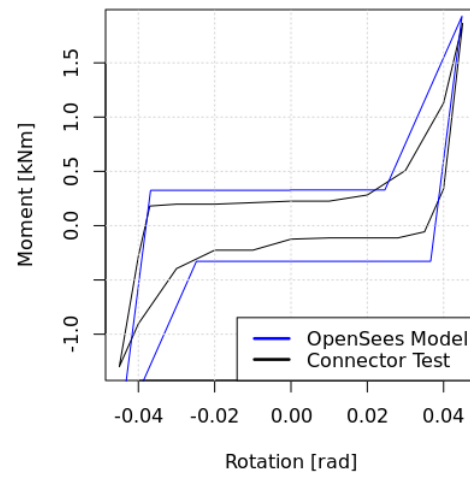
Cycle 33 Max Real Moment: 1.9207 [Nm], Min Real Moment: -1.3558 [kNm]
 Max Real Rot.: 0.045 [rad], Min Real Rot.: -0.045 [rad]
 vs. Max Model Moment : 1.92913 [Nm], Min Model Moment : -1.92913 [kNm]
 Max Model Rot.: 0.0448 [rad], Min Model Rot.: -0.045 [rad]



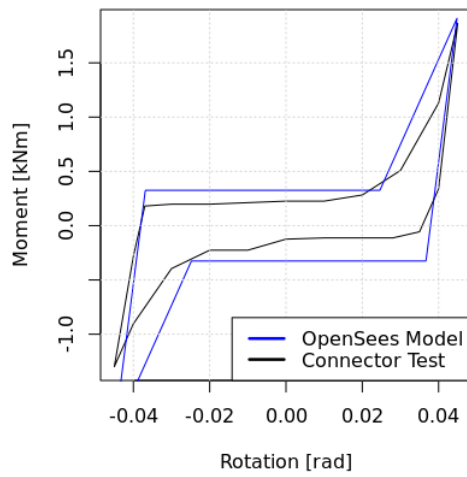
Cycle 34 Max Real Moment: 1.8642 [Nm], Min Real Moment: -1.2993 [kNm]
 Max Real Rot.: 0.045 [rad], Min Real Rot.: -0.045 [rad]
 vs. Max Model Moment : 1.92913 [Nm], Min Model Moment : -1.92913 [kNm]
 Max Model Rot.: 0.0448 [rad], Min Model Rot.: -0.045 [rad]



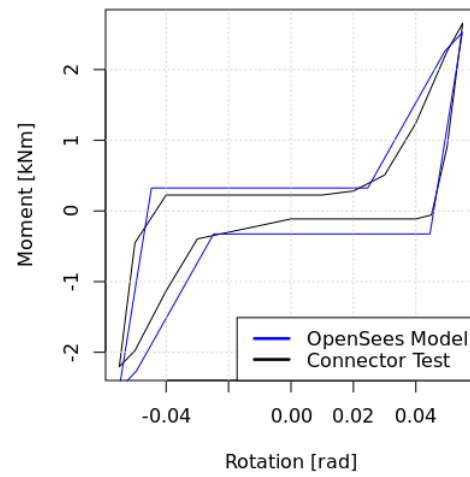
Cycle 35 Max Real Moment: 1.8642 [Nm], Min Real Moment: -1.2993 [kNm]
 Max Real Rot.: 0.045 [rad], Min Real Rot.: -0.045 [rad]
 vs. Max Model Moment : 1.92913 [Nm], Min Model Moment : -1.92913 [kNm]
 Max Model Rot.: 0.0448 [rad], Min Model Rot.: -0.045 [rad]



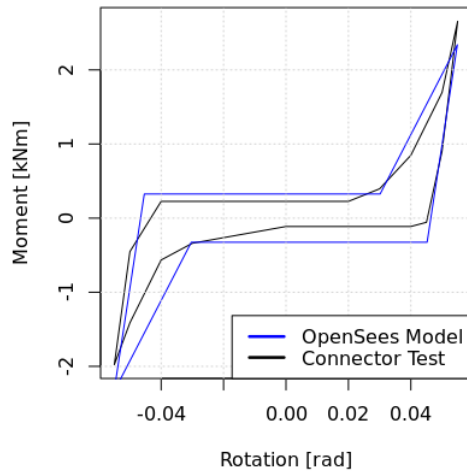
Cycle 36 Max Real Moment: 1.8642 [Nm], Min Real Moment: -1.2993 [kNm]
 Max Real Rot.: 0.045 [rad], Min Real Rot.: -0.045 [rad]
 vs. Max Model Moment : 1.90984 [Nm], Min Model Moment : -1.90984 [kNm]
 Max Model Rot.: 0.0448 [rad], Min Model Rot.: -0.045 [rad]



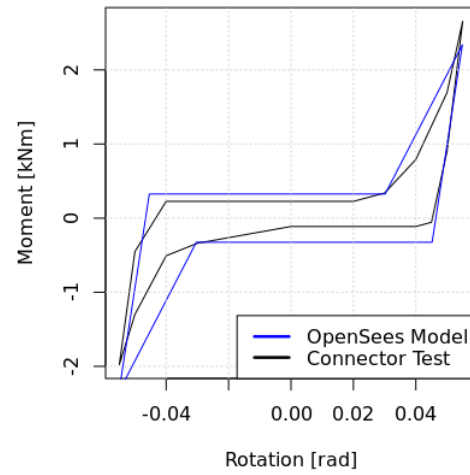
Cycle 37 Max Real Moment: 2.6551 [Nm], Min Real Moment: -2.2032 [kNm]
 Max Real Rot.: 0.055 [rad], Min Real Rot.: -0.055 [rad]
 vs. Max Model Moment : 2.52598 [Nm], Min Model Moment : -2.52597 [kNm]
 Max Model Rot.: 0.0549 [rad], Min Model Rot.: -0.0551 [rad]



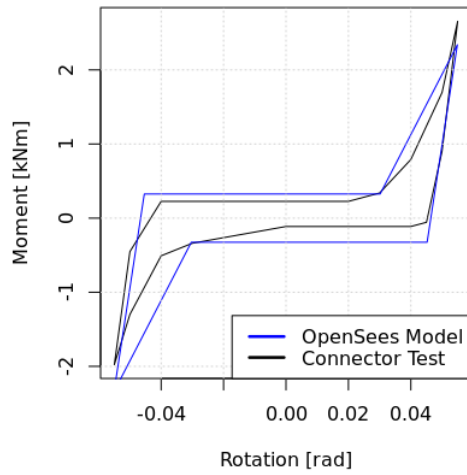
Cycle 38 Max Real Moment: 2.6551 [Nm], Min Real Moment: -1.9772 [kNm]
 Max Real Rot.: 0.055 [rad], Min Real Rot.: -0.055 [rad]
 vs. Max Model Moment : 2.33854 [Nm], Min Model Moment : -2.33854 [kNm]
 Max Model Rot.: 0.0549 [rad], Min Model Rot.: -0.0551 [rad]



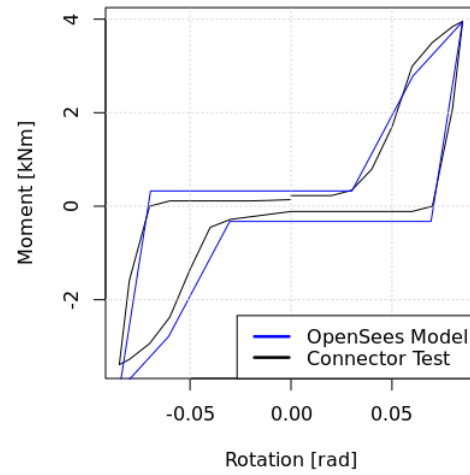
Cycle 39 Max Real Moment: 2.6551 [Nm], Min Real Moment: -1.9772 [kNm]
 Max Real Rot.: 0.055 [rad], Min Real Rot.: -0.055 [rad]
 vs. Max Model Moment : 2.33854 [Nm], Min Model Moment : -2.33854 [kNm]
 Max Model Rot.: 0.0549 [rad], Min Model Rot.: -0.0551 [rad]



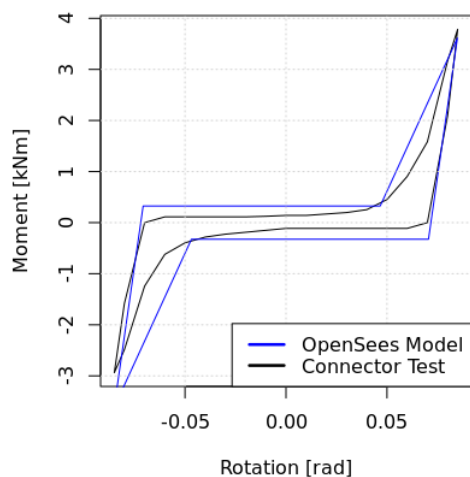
Cycle 40 Max Real Moment: 2.6551 [Nm], Min Real Moment: -1.9772 [kNm]
 Max Real Rot.: 0.055 [rad], Min Real Rot.: -0.055 [rad]
 vs. Max Model Moment : 2.33854 [Nm], Min Model Moment : -2.33854 [kNm]
 Max Model Rot.: 0.0549 [rad], Min Model Rot.: -0.0551 [rad]



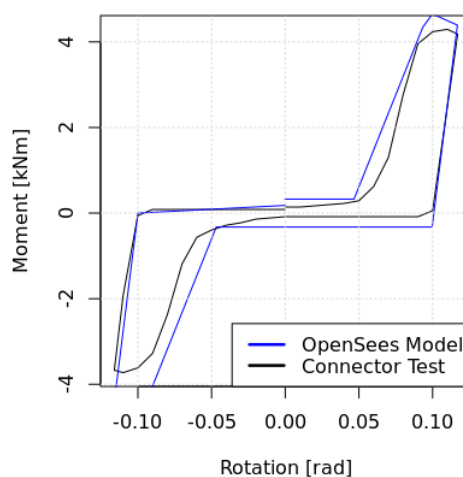
Cycle 41 Max Real Moment: 3.9545 [Nm], Min Real Moment: -3.3895 [kNm]
 Max Real Rot.: 0.085 [rad], Min Real Rot.: -0.085 [rad]
 vs. Max Model Moment : 3.94222 [Nm], Min Model Moment : -3.94222 [kNm]
 Max Model Rot.: 0.0849 [rad], Min Model Rot.: -0.085 [rad]



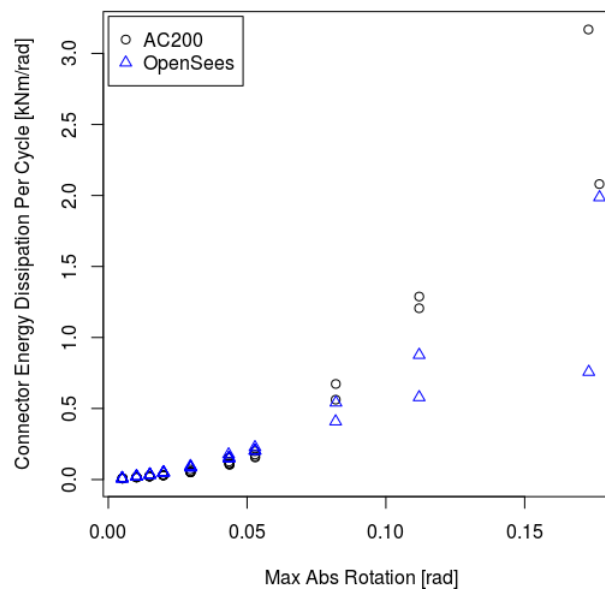
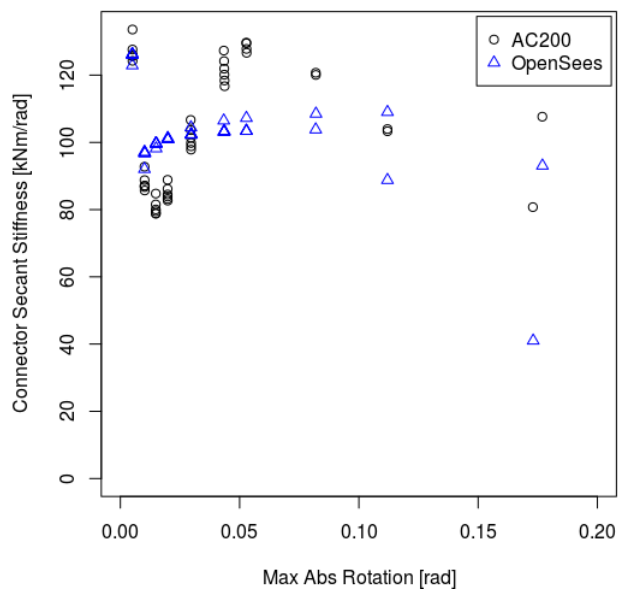
Cycle 42 Max Real Moment: 3.785 [Nm], Min Real Moment: -2.9376 [kNm]
 Max Real Rot.: 0.085 [rad], Min Real Rot.: -0.085 [rad]
 vs. Max Model Moment : 3.61317 [Nm], Min Model Moment : -3.61316 [kNm]
 Max Model Rot.: 0.0849 [rad], Min Model Rot.: -0.085 [rad]



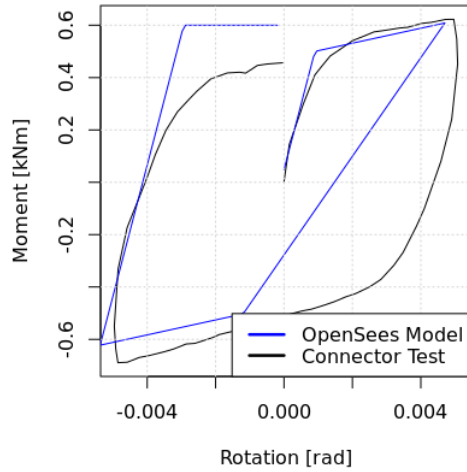
Cycle 43 Max Real Moment: 4.2934 [Nm], Min Real Moment: -3.7285 [kNm]
 Max Real Rot.: 0.117 [rad], Min Real Rot.: -0.116 [rad]
 vs. Max Model Moment : 4.65247 [Nm], Min Model Moment : -4.65247 [kNm]
 Max Model Rot.: 0.1168 [rad], Min Model Rot.: -0.116 [rad]



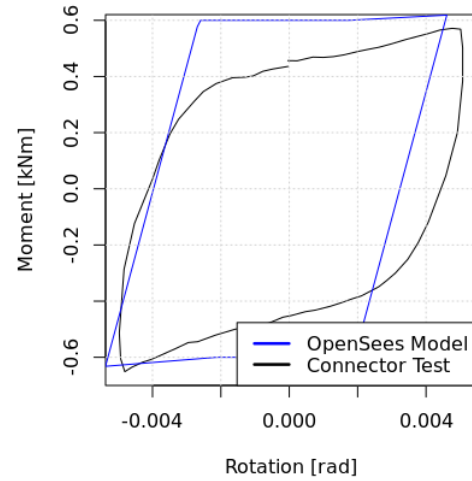
H.5. Prototype Connector 1 (Frazier AC200) vs. ITS data



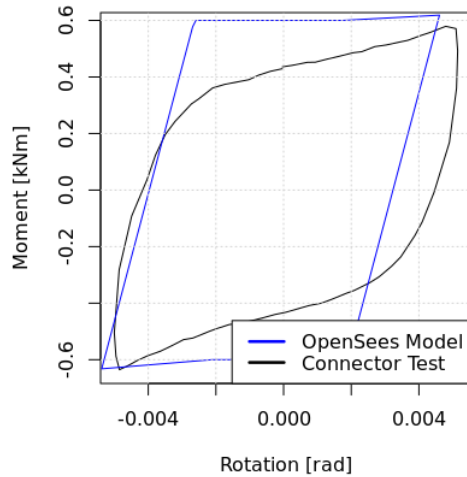
Cycle 1 Max Real Moment: 0.6226 [Nm], Min Real Moment: -0.6891 [kNm]
 Max Real Rot.: 0.0051 [rad], Min Real Rot.: -0.005 [rad]
 vs. Max Model Moment : 0.608568 [Nm], Min Model Moment : -0.62228 [kNm]
 Max Model Rot.: 0.0047 [rad], Min Model Rot.: -0.0054 [rad]



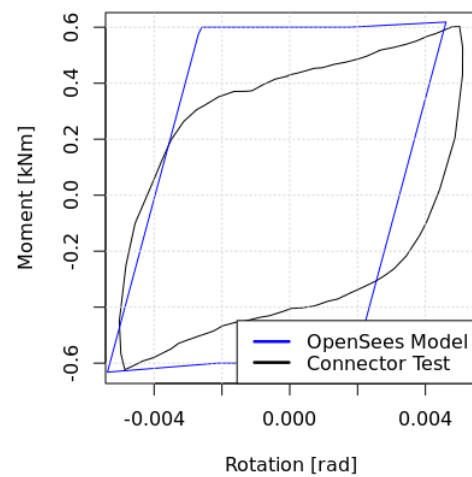
Cycle 2 Max Real Moment: 0.5715 [Nm], Min Real Moment: -0.6512 [kNm]
 Max Real Rot.: 0.0051 [rad], Min Real Rot.: -0.005 [rad]
 vs. Max Model Moment : 0.618543 [Nm], Min Model Moment : -0.632139 [kNm]
 Max Model Rot.: 0.0046 [rad], Min Model Rot.: -0.0054 [rad]



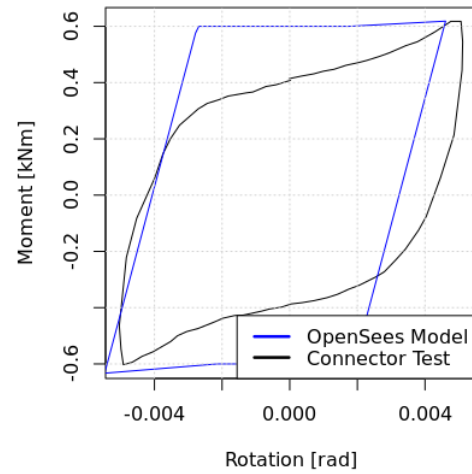
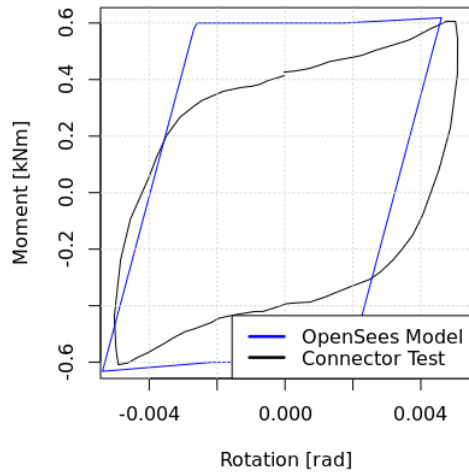
Cycle 3 Max Real Moment: 0.5791 [Nm], Min Real Moment: -0.6352 [kNm]
 Max Real Rot.: 0.0051 [rad], Min Real Rot.: -0.005 [rad]
 vs. Max Model Moment : 0.618543 [Nm], Min Model Moment : -0.632139 [kNm]
 Max Model Rot.: 0.0046 [rad], Min Model Rot.: -0.0054 [rad]



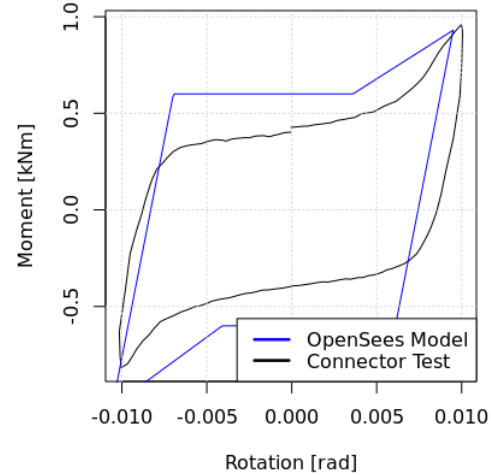
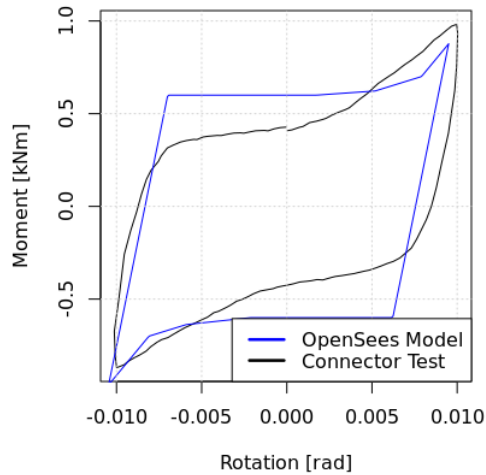
Cycle 4 Max Real Moment: 0.6033 [Nm], Min Real Moment: -0.6232 [kNm]
 Max Real Rot.: 0.0051 [rad], Min Real Rot.: -0.005 [rad]
 vs. Max Model Moment : 0.618543 [Nm], Min Model Moment : -0.632139 [kNm]
 Max Model Rot.: 0.0046 [rad], Min Model Rot.: -0.0054 [rad]



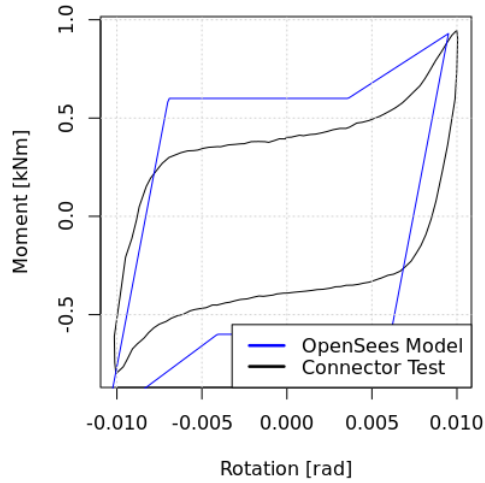
Cycle 5 Max Real Moment: 0.6061 [Nm], Min Real Moment: -0.6087 [kNm]
 Max Real Rot.: 0.0051 [rad], Min Real Rot.: -0.005 [rad]
 vs. Max Model Moment : 0.618543 [Nm], Min Model Moment : -0.632139 [kNm] vs. Max Model Moment : 0.618543 [Nm], Min Model Moment : -0.633089 [kNm]
 Max Model Rot.: 0.0046 [rad], Min Model Rot.: -0.0054 [rad]



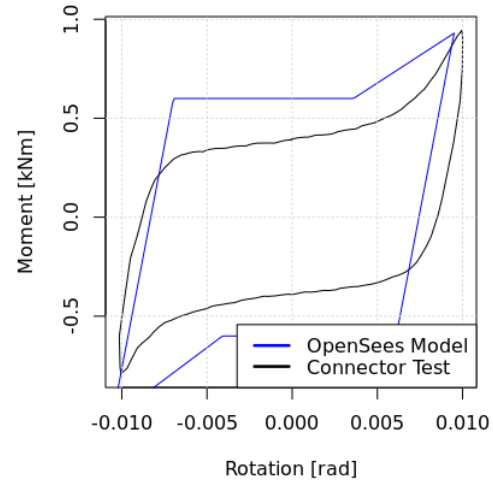
Cycle 7 Max Real Moment: 0.9818 [Nm], Min Real Moment: -0.8698 [kNm]
 Max Real Rot.: 0.01 [rad], Min Real Rot.: -0.0101 [rad]
 vs. Max Model Moment : 0.877235 [Nm], Min Model Moment : -0.962304 [kNm] vs. Max Model Moment : 0.929937 [Nm], Min Model Moment : -1.0166 [kNm]
 Max Model Rot.: 0.0095 [rad], Min Model Rot.: -0.0105 [rad]



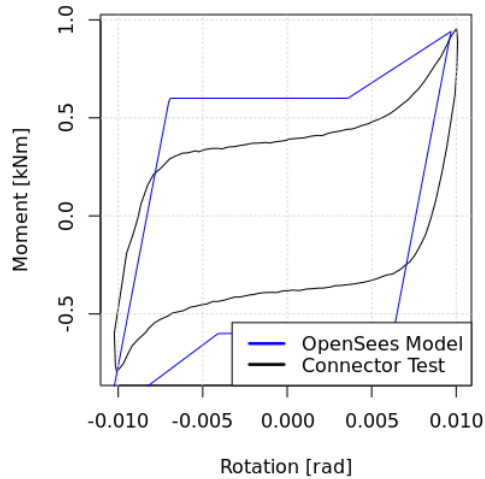
Cycle 9 Max Real Moment: 0.9464 [Nm], Min Real Moment: -0.8003 [kNm]
 Max Real Rot.: 0.01 [rad], Min Real Rot.: -0.0102 [rad]
 vs. Max Model Moment : 0.929937 [Nm], Min Model Moment : -1.0166 [kNm]
 Max Model Rot.: 0.0095 [rad], Min Model Rot.: -0.0106 [rad]



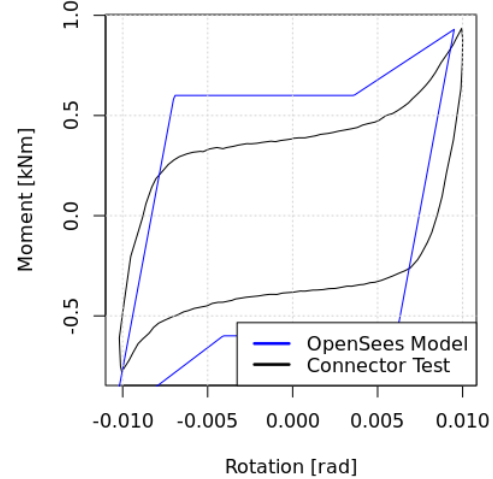
Cycle 10 Max Real Moment: 0.9442 [Nm], Min Real Moment: -0.7903 [kNm]
 Max Real Rot.: 0.01 [rad], Min Real Rot.: -0.0101 [rad]
 vs. Max Model Moment : 0.929937 [Nm], Min Model Moment : -1.0166 [kNm]
 Max Model Rot.: 0.0095 [rad], Min Model Rot.: -0.0106 [rad]



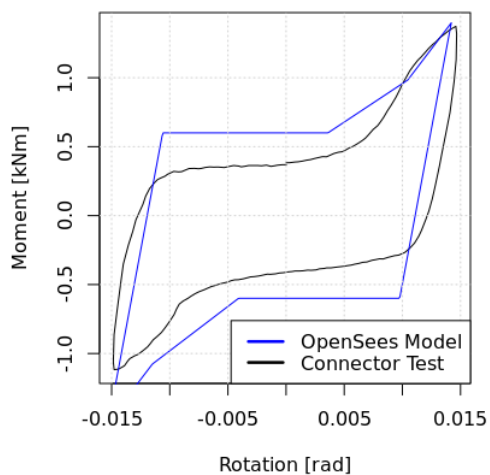
Cycle 11 Max Real Moment: 0.9566 [Nm], Min Real Moment: -0.7946 [kNm]
 Max Real Rot.: 0.0101 [rad], Min Real Rot.: -0.0102 [rad]
 vs. Max Model Moment : 0.940667 [Nm], Min Model Moment : -1.0166 [kNm]
 Max Model Rot.: 0.0097 [rad], Min Model Rot.: -0.0106 [rad]



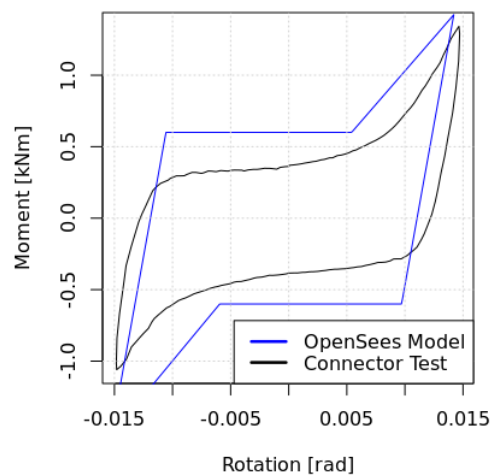
Cycle 12 Max Real Moment: 0.9353 [Nm], Min Real Moment: -0.7788 [kNm]
 Max Real Rot.: 0.01 [rad], Min Real Rot.: -0.0102 [rad]
 vs. Max Model Moment : 0.929937 [Nm], Min Model Moment : -1.0166 [kNm]
 Max Model Rot.: 0.0095 [rad], Min Model Rot.: -0.0106 [rad]



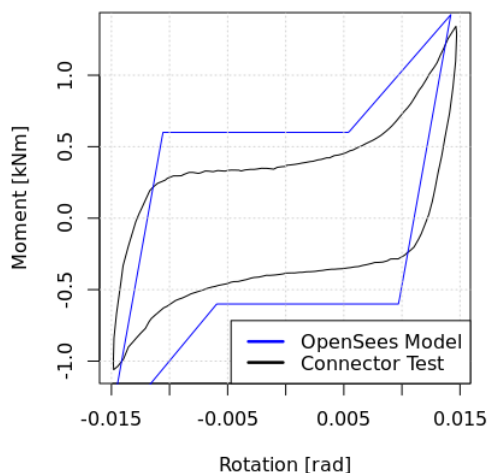
Cycle 13 Max Real Moment: 1.373 [Nm], Min Real Moment: -1.1175 [kNm]
 Max Real Rot.: 0.0147 [rad], Min Real Rot.: -0.0149 [rad]
 vs. Max Model Moment : 1.39835 [Nm], Min Model Moment : -1.49405 [kNm]
 Max Model Rot.: 0.0142 [rad], Min Model Rot.: -0.0153 [rad]



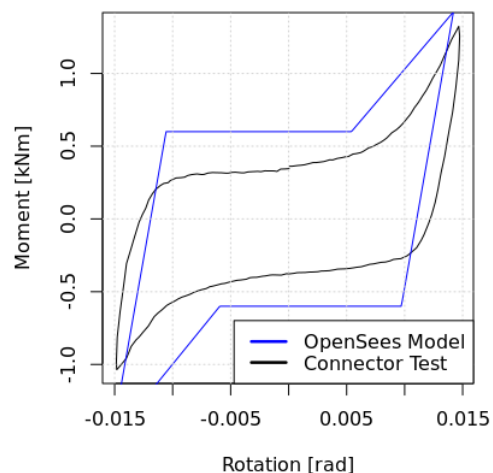
Cycle 14 Max Real Moment: 1.3419 [Nm], Min Real Moment: -1.0597 [kNm]
 Max Real Rot.: 0.0147 [rad], Min Real Rot.: -0.0148 [rad]
 vs. Max Model Moment : 1.42299 [Nm], Min Model Moment : -1.51354 [kNm]
 Max Model Rot.: 0.0142 [rad], Min Model Rot.: -0.0153 [rad]



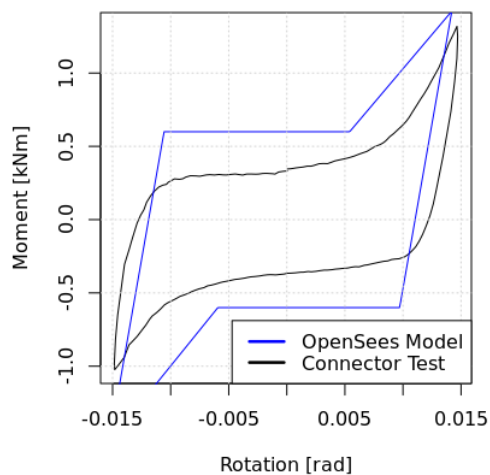
Cycle 14 Max Real Moment: 1.3419 [Nm], Min Real Moment: -1.0597 [kNm]
 Max Real Rot.: 0.0147 [rad], Min Real Rot.: -0.0148 [rad]
 vs. Max Model Moment : 1.42299 [Nm], Min Model Moment : -1.51354 [kNm]
 Max Model Rot.: 0.0142 [rad], Min Model Rot.: -0.0153 [rad]



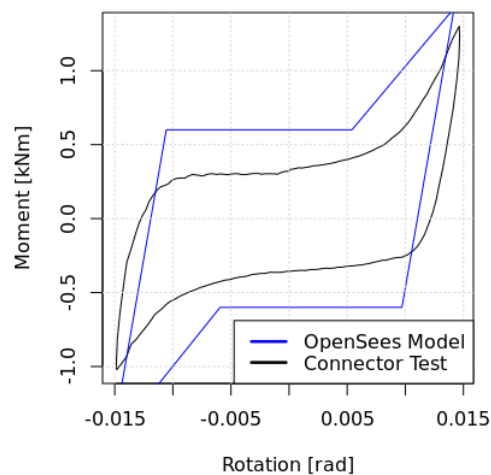
Cycle 15 Max Real Moment: 1.3239 [Nm], Min Real Moment: -1.036 [kNm]
 Max Real Rot.: 0.0147 [rad], Min Real Rot.: -0.0149 [rad]
 vs. Max Model Moment : 1.42299 [Nm], Min Model Moment : -1.51354 [kNm]
 Max Model Rot.: 0.0142 [rad], Min Model Rot.: -0.0153 [rad]



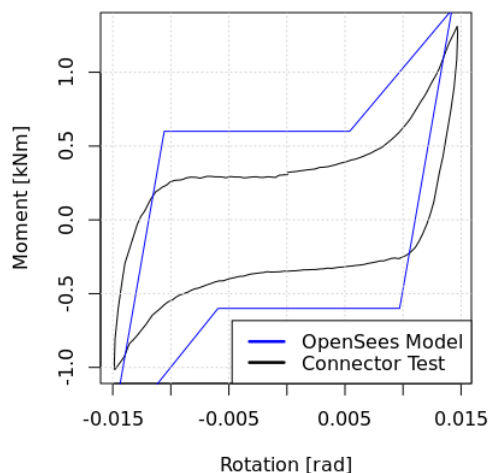
Cycle 16 Max Real Moment: 1.3192 [Nm], Min Real Moment: -1.0237 [kNm]
 Max Real Rot.: 0.0147 [rad], Min Real Rot.: -0.0149 [rad]
 vs. Max Model Moment : 1.42299 [Nm], Min Model Moment : -1.51354 [kNm]
 Max Model Rot.: 0.0142 [rad], Min Model Rot.: -0.0153 [rad]



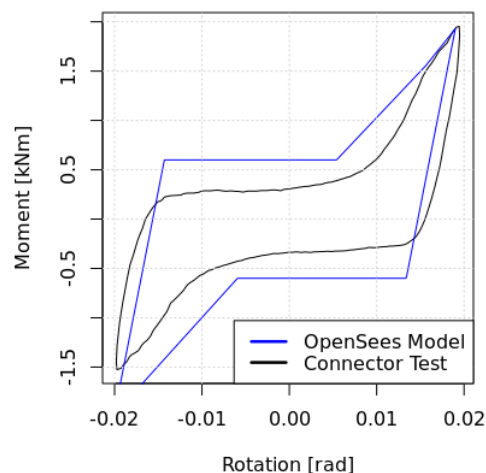
Cycle 17 Max Real Moment: 1.2997 [Nm], Min Real Moment: -1.0214 [kNm]
 Max Real Rot.: 0.0147 [rad], Min Real Rot.: -0.0149 [rad]
 vs. Max Model Moment : 1.42299 [Nm], Min Model Moment : -1.51354 [kNm]
 Max Model Rot.: 0.0142 [rad], Min Model Rot.: -0.0153 [rad]



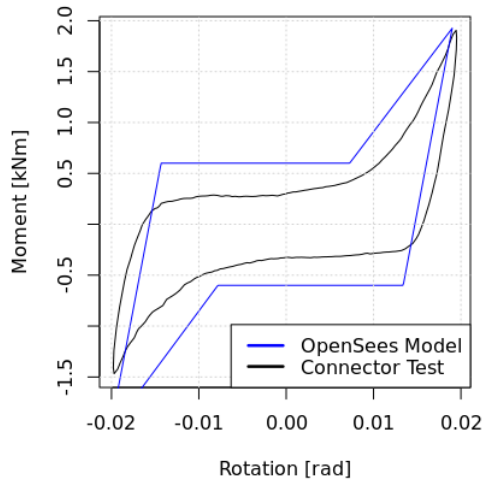
Cycle 18 Max Real Moment: 1.3114 [Nm], Min Real Moment: -1.0152 [kNm]
 Max Real Rot.: 0.0147 [rad], Min Real Rot.: -0.0149 [rad]
 vs. Max Model Moment : 1.42299 [Nm], Min Model Moment : -1.51354 [kNm]
 Max Model Rot.: 0.0142 [rad], Min Model Rot.: -0.0153 [rad]



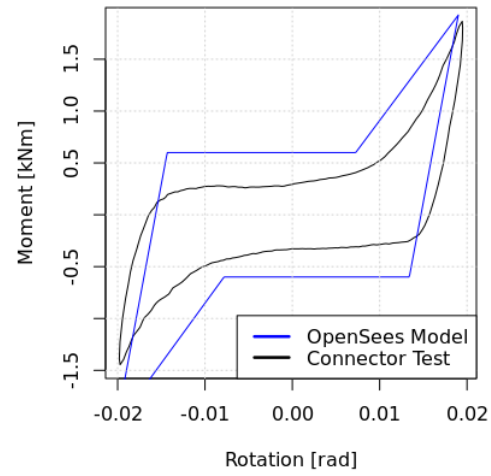
Cycle 19 Max Real Moment: 1.9539 [Nm], Min Real Moment: -1.5262 [kNm]
 Max Real Rot.: 0.0195 [rad], Min Real Rot.: -0.0198 [rad]
 vs. Max Model Moment : 1.9301 [Nm], Min Model Moment : -2.03644 [kNm]
 Max Model Rot.: 0.019 [rad], Min Model Rot.: -0.0202 [rad]



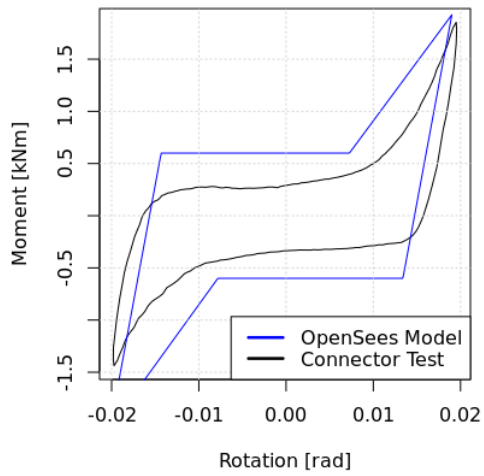
Cycle 20 Max Real Moment: 1.9056 [Nm], Min Real Moment: -1.4675 [kNm]
 Max Real Rot.: 0.0195 [rad], Min Real Rot.: -0.0198 [rad]
 vs. Max Model Moment : 1.92611 [Nm], Min Model Moment : -2.02672 [kNm]
 Max Model Rot.: 0.019 [rad], Min Model Rot.: -0.0202 [rad]



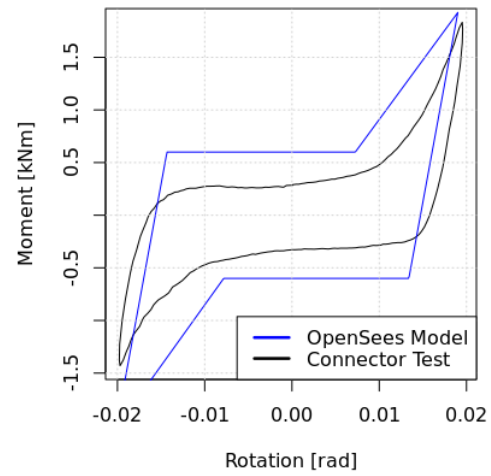
Cycle 21 Max Real Moment: 1.8653 [Nm], Min Real Moment: -1.445 [kNm]
 Max Real Rot.: 0.0195 [rad], Min Real Rot.: -0.0198 [rad]
 vs. Max Model Moment : 1.92611 [Nm], Min Model Moment : -2.02672 [kNm]
 Max Model Rot.: 0.019 [rad], Min Model Rot.: -0.0202 [rad]



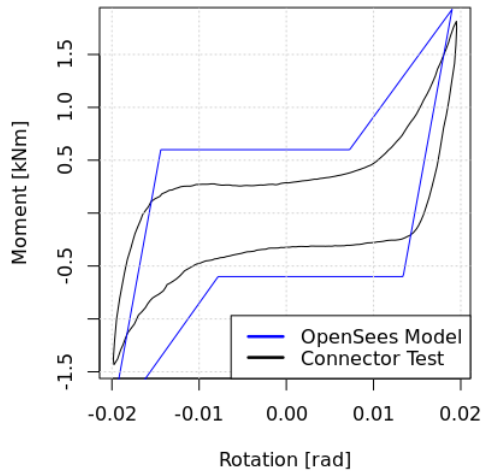
Cycle 22 Max Real Moment: 1.8536 [Nm], Min Real Moment: -1.4368 [kNm]
 Max Real Rot.: 0.0196 [rad], Min Real Rot.: -0.0198 [rad]
 vs. Max Model Moment : 1.92611 [Nm], Min Model Moment : -2.02672 [kNm]
 Max Model Rot.: 0.019 [rad], Min Model Rot.: -0.0202 [rad]



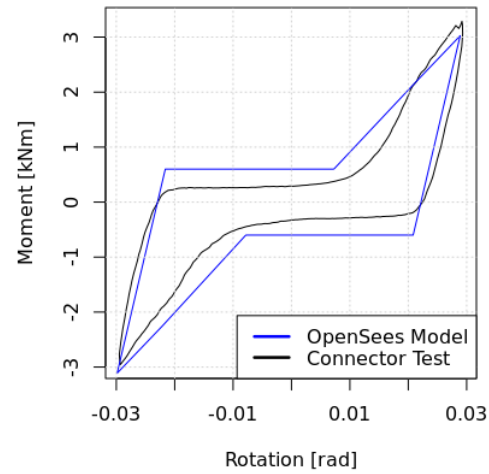
Cycle 23 Max Real Moment: 1.8327 [Nm], Min Real Moment: -1.4296 [kNm]
 Max Real Rot.: 0.0196 [rad], Min Real Rot.: -0.0198 [rad]
 vs. Max Model Moment : 1.92611 [Nm], Min Model Moment : -2.02672 [kNm]
 Max Model Rot.: 0.019 [rad], Min Model Rot.: -0.0202 [rad]



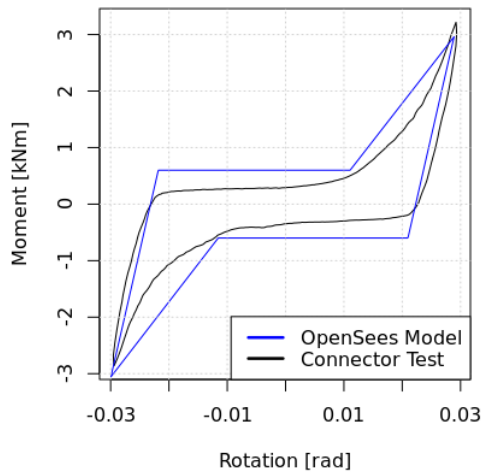
Cycle 24 Max Real Moment: 1.8134 [Nm], Min Real Moment: -1.4329 [kNm]
 Max Real Rot.: 0.0195 [rad], Min Real Rot.: -0.0198 [rad]
 vs. Max Model Moment : 1.92611 [Nm], Min Model Moment : -2.03782 [kNm]
 Max Model Rot.: 0.019 [rad], Min Model Rot.: -0.0203 [rad]



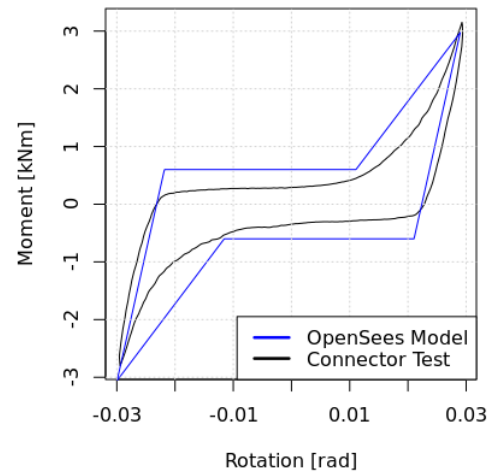
Cycle 25 Max Real Moment: 3.2872 [Nm], Min Real Moment: -2.9561 [kNm]
 Max Real Rot.: 0.0293 [rad], Min Real Rot.: -0.0295 [rad]
 vs. Max Model Moment : 3.0255 [Nm], Min Model Moment : -3.11057 [kNm]
 Max Model Rot.: 0.0289 [rad], Min Model Rot.: -0.0299 [rad]



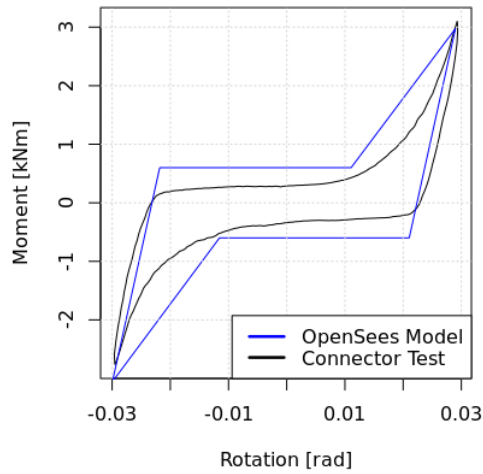
Cycle 26 Max Real Moment: 3.2168 [Nm], Min Real Moment: -2.8587 [kNm]
 Max Real Rot.: 0.0293 [rad], Min Real Rot.: -0.0295 [rad]
 vs. Max Model Moment : 2.96253 [Nm], Min Model Moment : -3.05583 [kNm]
 Max Model Rot.: 0.0289 [rad], Min Model Rot.: -0.03 [rad]



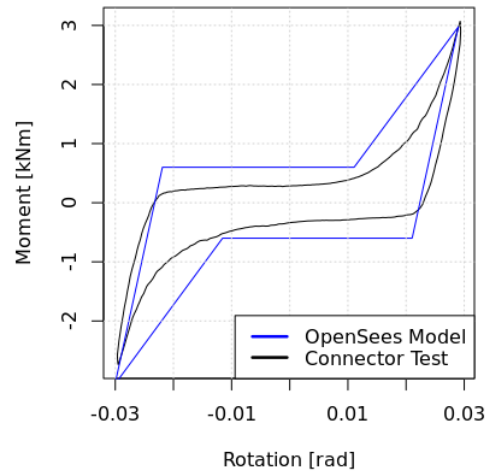
Cycle 27 Max Real Moment: 3.1527 [Nm], Min Real Moment: -2.7991 [kNm]
 Max Real Rot.: 0.0294 [rad], Min Real Rot.: -0.0296 [rad]
 vs. Max Model Moment : 2.97525 [Nm], Min Model Moment : -3.05583 [kNm]
 Max Model Rot.: 0.029 [rad], Min Model Rot.: -0.03 [rad]



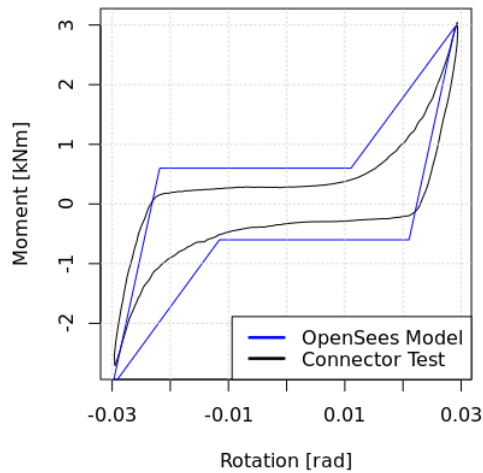
Cycle 28 Max Real Moment: 3.0997 [Nm], Min Real Moment: -2.765 [kNm]
 Max Real Rot.: 0.0294 [rad], Min Real Rot.: -0.0296 [rad]
 vs. Max Model Moment : 2.97525 [Nm], Min Model Moment : -3.05583 [kNm]
 Max Model Rot.: 0.029 [rad], Min Model Rot.: -0.03 [rad]



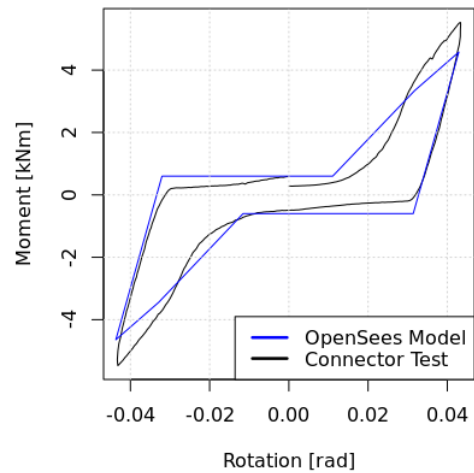
Cycle 29 Max Real Moment: 3.0693 [Nm], Min Real Moment: -2.7399 [kNm]
 Max Real Rot.: 0.0294 [rad], Min Real Rot.: -0.0297 [rad]
 vs. Max Model Moment : 2.97525 [Nm], Min Model Moment : -3.06865 [kNm]
 Max Model Rot.: 0.029 [rad], Min Model Rot.: -0.03 [rad]



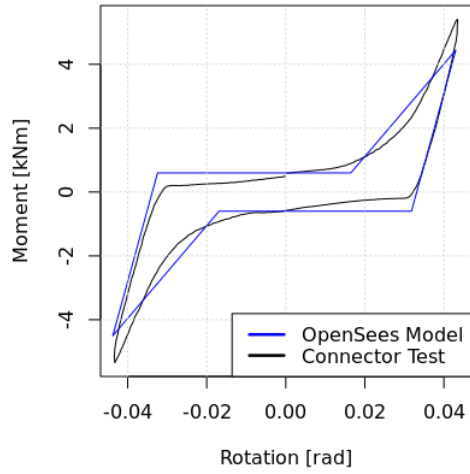
Cycle 30 Max Real Moment: 3.045 [Nm], Min Real Moment: -2.7098 [kNm]
 Max Real Rot.: 0.0294 [rad], Min Real Rot.: -0.0296 [rad]
 vs. Max Model Moment : 2.97525 [Nm], Min Model Moment : -3.05583 [kNm]
 Max Model Rot.: 0.029 [rad], Min Model Rot.: -0.03 [rad]



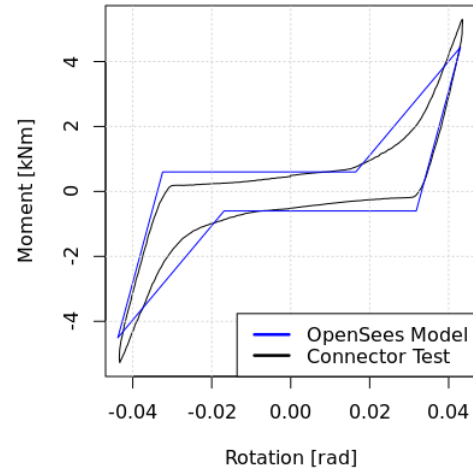
Cycle 31 Max Real Moment: 5.5315 [Nm], Min Real Moment: -5.4742 [kNm]
 Max Real Rot.: 0.0434 [rad], Min Real Rot.: -0.0433 [rad]
 vs. Max Model Moment : 4.57821 [Nm], Min Model Moment : -4.64201 [kNm]
 Max Model Rot.: 0.0429 [rad], Min Model Rot.: -0.0437 [rad]



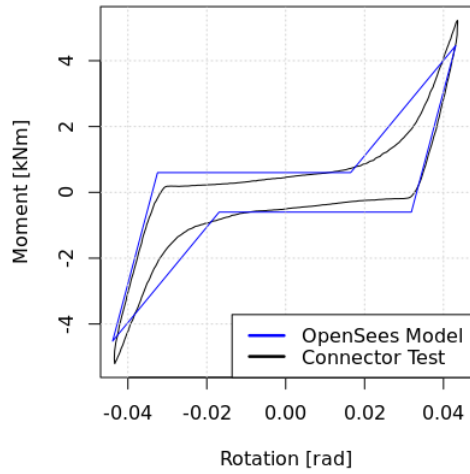
Cycle 32 Max Real Moment: 5.4097 [Nm], Min Real Moment: -5.3458 [kNm]
 Max Real Rot.: 0.0435 [rad], Min Real Rot.: -0.0434 [rad]
 vs. Max Model Moment : 4.44554 [Nm], Min Model Moment : -4.50594 [kNm]
 Max Model Rot.: 0.043 [rad], Min Model Rot.: -0.0438 [rad]



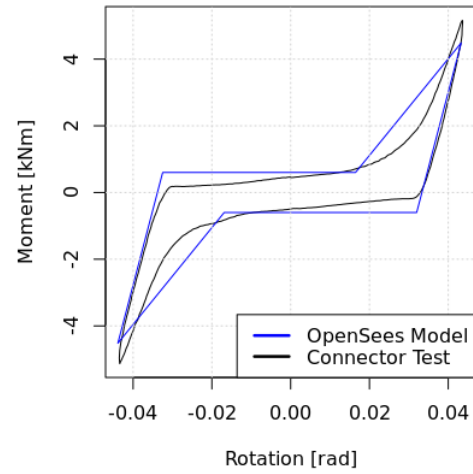
Cycle 33 Max Real Moment: 5.3013 [Nm], Min Real Moment: -5.273 [kNm]
 Max Real Rot.: 0.0435 [rad], Min Real Rot.: -0.0434 [rad]
 vs. Max Model Moment : 4.44554 [Nm], Min Model Moment : -4.50594 [kNm]
 Max Model Rot.: 0.043 [rad], Min Model Rot.: -0.0438 [rad]



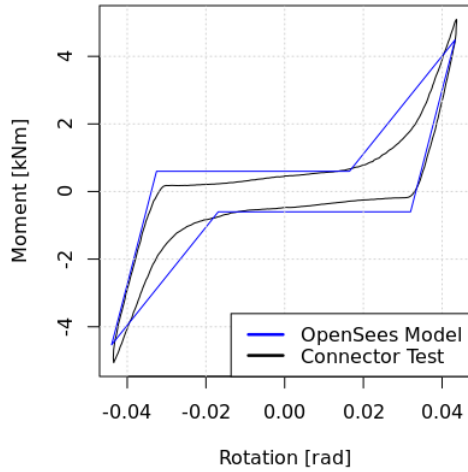
Cycle 34 Max Real Moment: 5.2276 [Nm], Min Real Moment: -5.2058 [kNm]
 Max Real Rot.: 0.0436 [rad], Min Real Rot.: -0.0434 [rad]
 vs. Max Model Moment : 4.45945 [Nm], Min Model Moment : -4.51988 [kNm]
 Max Model Rot.: 0.0431 [rad], Min Model Rot.: -0.0439 [rad]



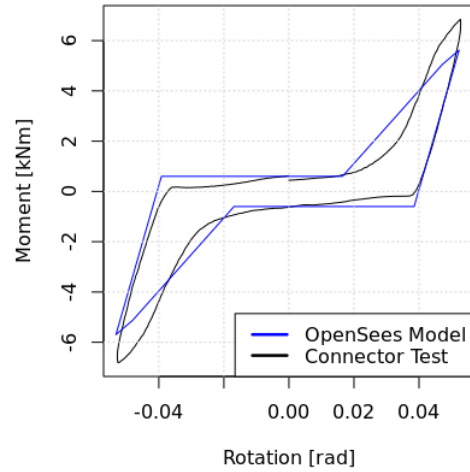
Cycle 35 Max Real Moment: 5.163 [Nm], Min Real Moment: -5.1329 [kNm]
 Max Real Rot.: 0.0437 [rad], Min Real Rot.: -0.0435 [rad]
 vs. Max Model Moment : 4.48726 [Nm], Min Model Moment : -4.51988 [kNm]
 Max Model Rot.: 0.0433 [rad], Min Model Rot.: -0.0439 [rad]



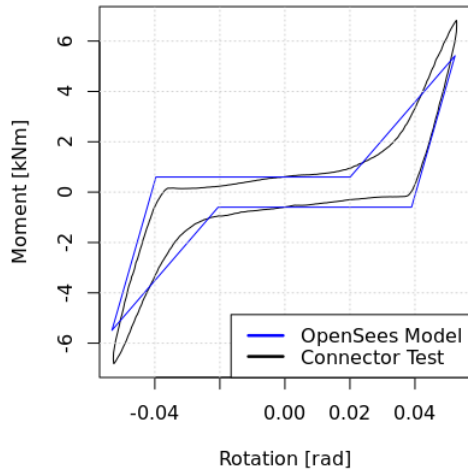
Cycle 36 Max Real Moment: 5.0961 [Nm], Min Real Moment: -5.0635 [kNm]
 Max Real Rot.: 0.0437 [rad], Min Real Rot.: -0.0435 [rad]
 vs. Max Model Moment : 4.48726 [Nm], Min Model Moment : -4.53382 [kNm]
 Max Model Rot.: 0.0433 [rad], Min Model Rot.: -0.044 [rad]



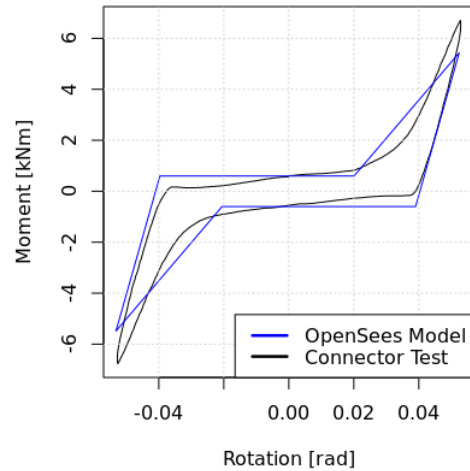
Cycle 37 Max Real Moment: 6.8459 [Nm], Min Real Moment: -6.8106 [kNm]
 Max Real Rot.: 0.0528 [rad], Min Real Rot.: -0.0528 [rad]
 vs. Max Model Moment : 5.62044 [Nm], Min Model Moment : -5.69487 [kNm]
 Max Model Rot.: 0.0523 [rad], Min Model Rot.: -0.0532 [rad]



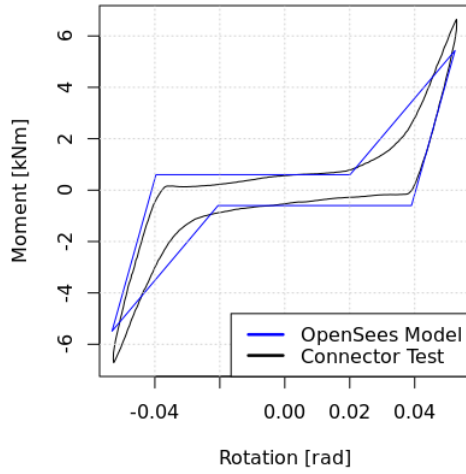
Cycle 38 Max Real Moment: 6.8251 [Nm], Min Real Moment: -6.8137 [kNm]
 Max Real Rot.: 0.0528 [rad], Min Real Rot.: -0.0528 [rad]
 vs. Max Model Moment : 5.41775 [Nm], Min Model Moment : -5.48817 [kNm]
 Max Model Rot.: 0.0523 [rad], Min Model Rot.: -0.0532 [rad]



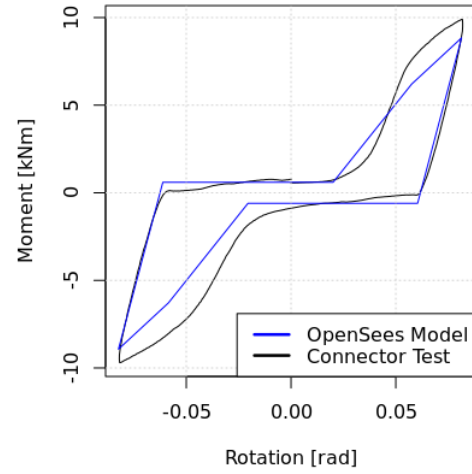
Cycle 39 Max Real Moment: 6.708 [Nm], Min Real Moment: -6.7659 [kNm]
 Max Real Rot.: 0.0529 [rad], Min Real Rot.: -0.0528 [rad]
 vs. Max Model Moment : 5.43209 [Nm], Min Model Moment : -5.48817 [kNm]
 Max Model Rot.: 0.0524 [rad], Min Model Rot.: -0.0532 [rad]



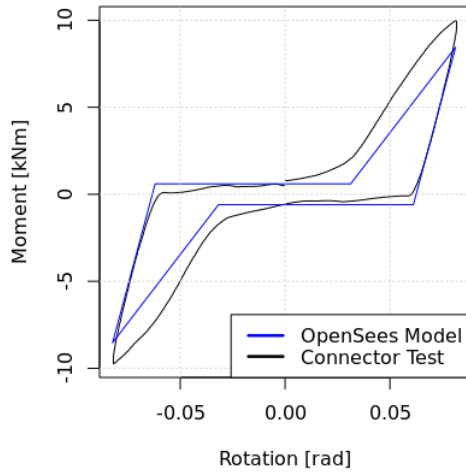
Cycle 40 Max Real Moment: 6.6471 [Nm], Min Real Moment: -6.7153 [kNm]
 Max Real Rot.: 0.0529 [rad], Min Real Rot.: -0.0528 [rad]
 vs. Max Model Moment : 5.43209 [Nm], Min Model Moment : -5.48817 [kNm]
 Max Model Rot.: 0.0524 [rad], Min Model Rot.: -0.0532 [rad]



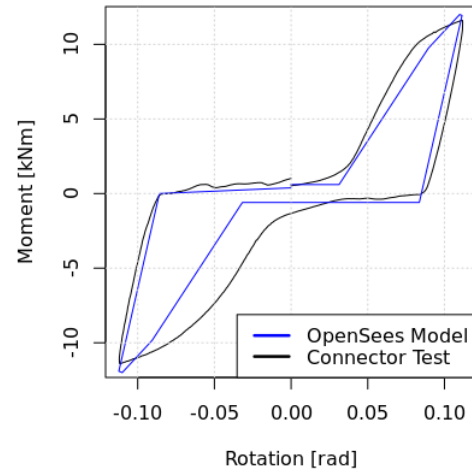
Cycle 41 Max Real Moment: 9.9007 [Nm], Min Real Moment: -9.698 [kNm]
 Max Real Rot.: 0.0819 [rad], Min Real Rot.: -0.082 [rad]
 vs. Max Model Moment : 8.84284 [Nm], Min Model Moment : -8.92791 [kNm]
 Max Model Rot.: 0.0814 [rad], Min Model Rot.: -0.0824 [rad]



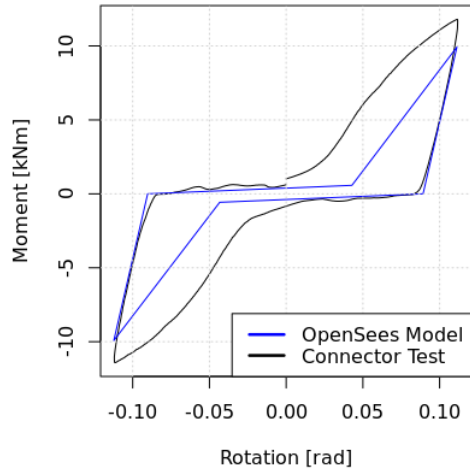
Cycle 42 Max Real Moment: 9.9955 [Nm], Min Real Moment: -9.7347 [kNm]
 Max Real Rot.: 0.0818 [rad], Min Real Rot.: -0.0819 [rad]
 vs. Max Model Moment : 8.45158 [Nm], Min Model Moment : -8.53205 [kNm]
 Max Model Rot.: 0.0813 [rad], Min Model Rot.: -0.0823 [rad]



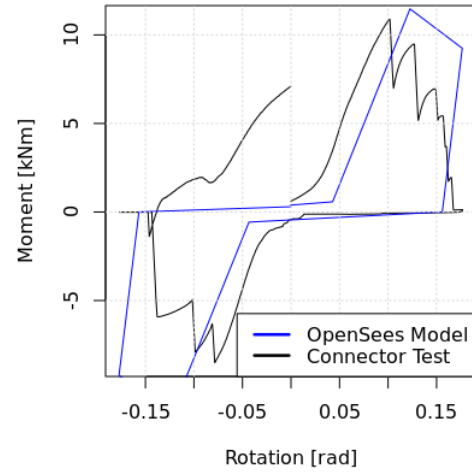
Cycle 43 Max Real Moment: 11.6117 [Nm], Min Real Moment: -11.403 [kNm]
 Max Real Rot.: 0.1119 [rad], Min Real Rot.: -0.112 [rad]
 vs. Max Model Moment : 11.9995 [Nm], Min Model Moment : -11.9995 [kNm]
 Max Model Rot.: 0.1115 [rad], Min Model Rot.: -0.1123 [rad]

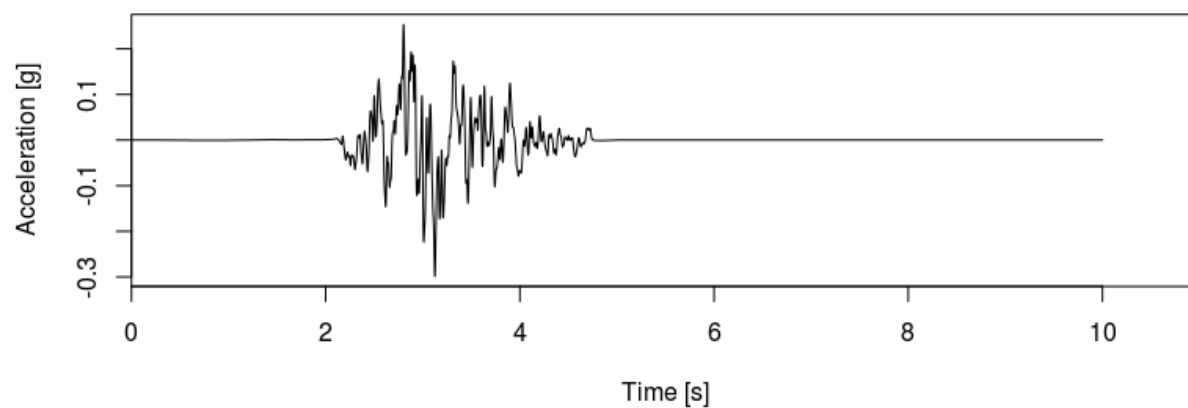
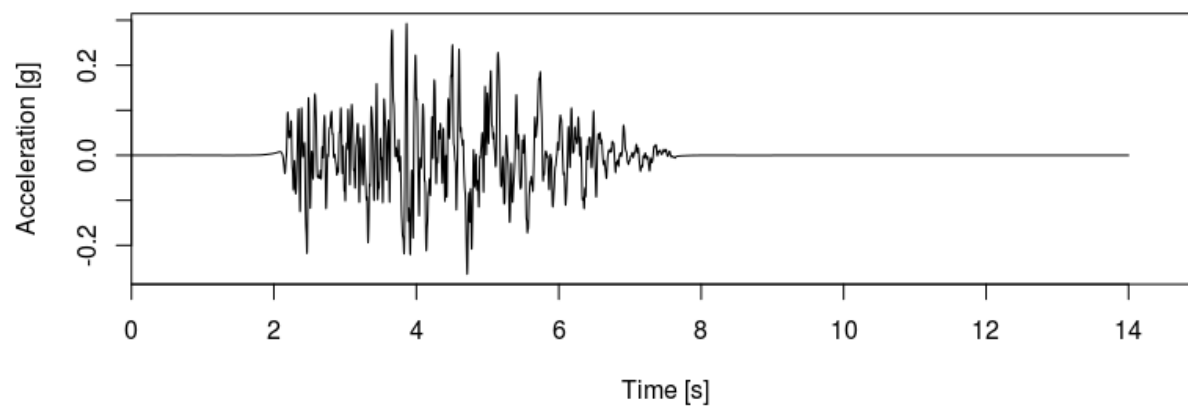


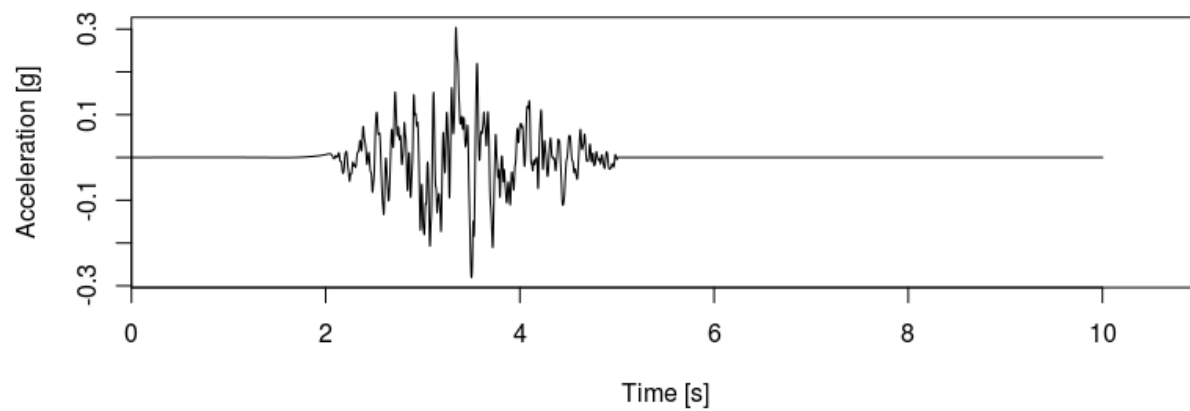
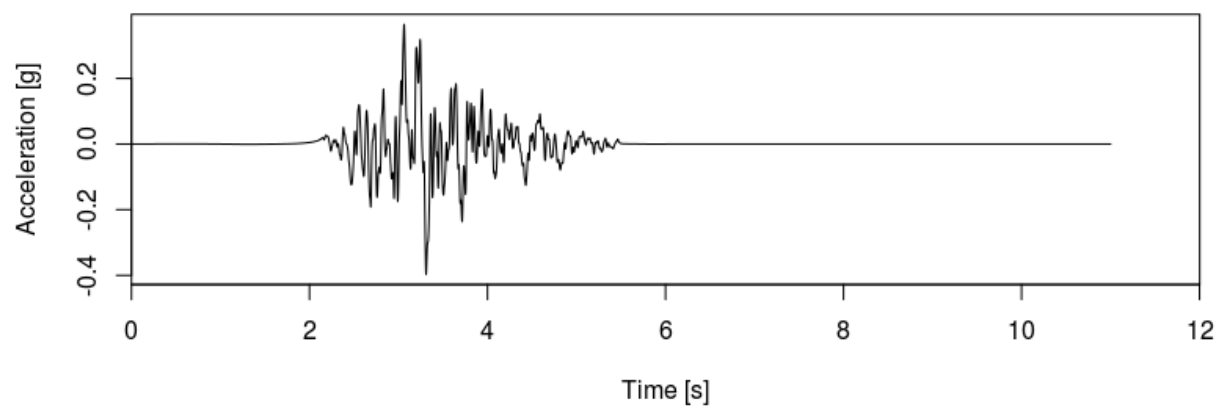
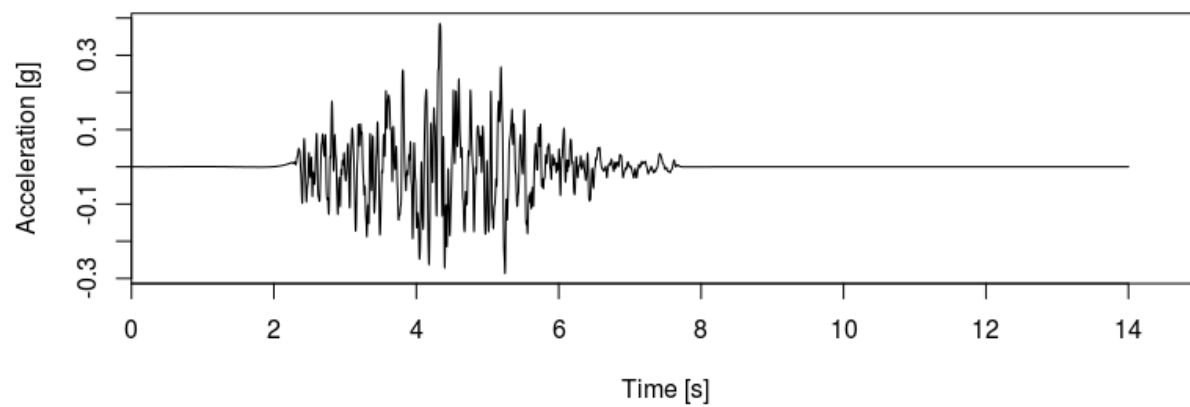
Cycle 44 Max Real Moment: 11.8002 [Nm], Min Real Moment: -11.4179 [kNm]
 Max Real Rot.: 0.1118 [rad], Min Real Rot.: -0.112 [rad]
 vs. Max Model Moment : 9.92359 [Nm], Min Model Moment : -9.92331 [kNm]
 Max Model Rot.: 0.1113 [rad], Min Model Rot.: -0.1123 [rad]

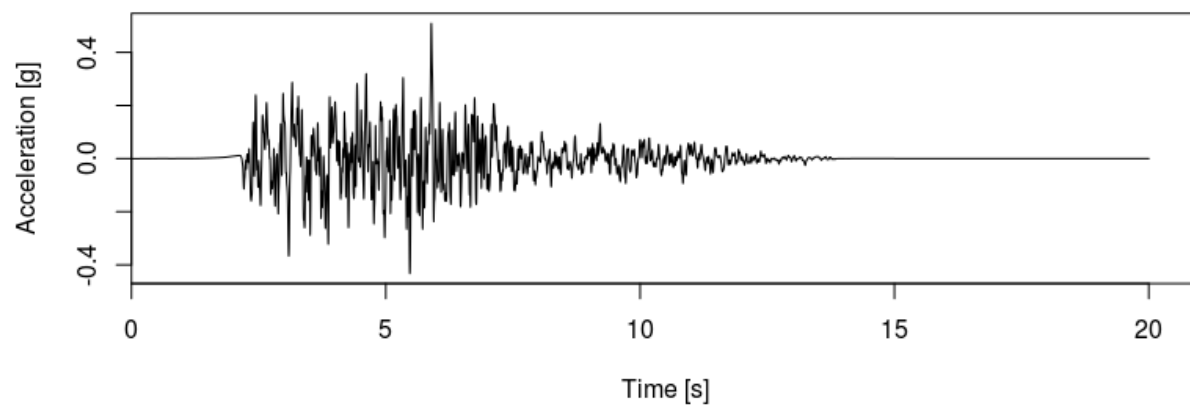
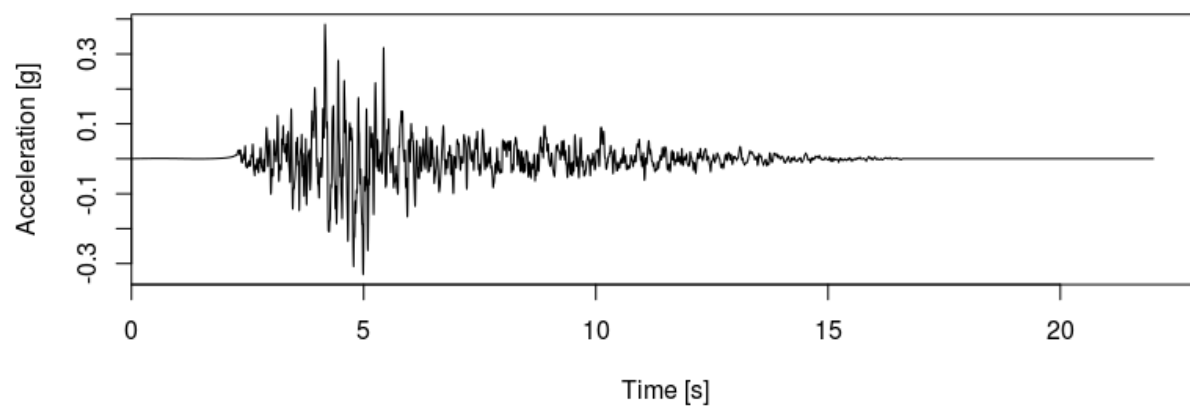
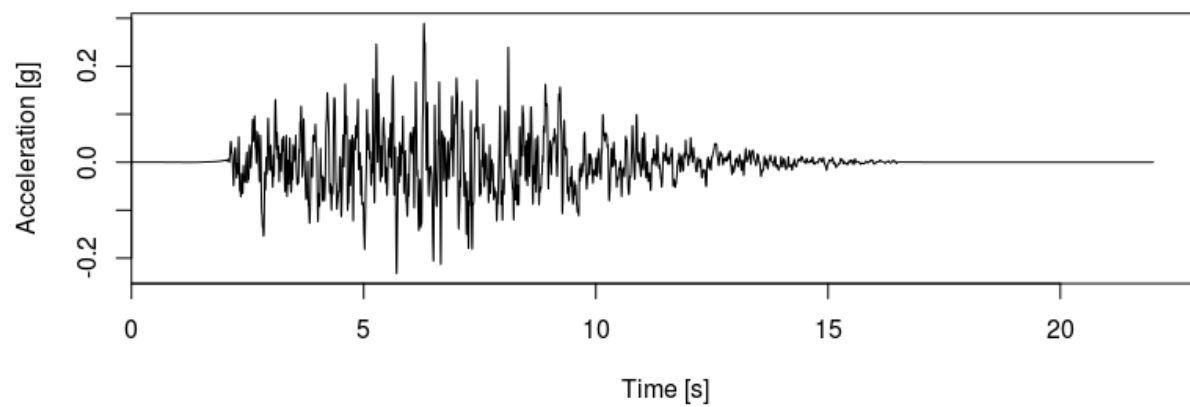


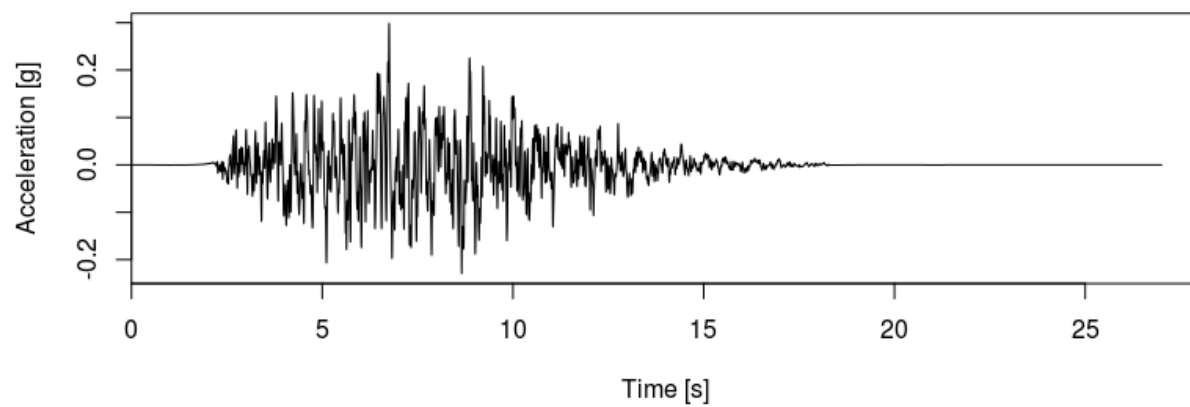
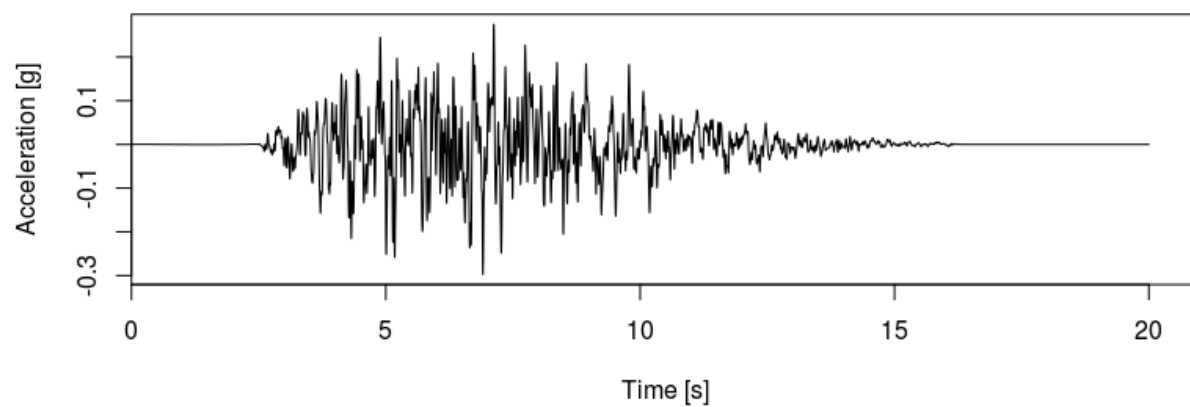
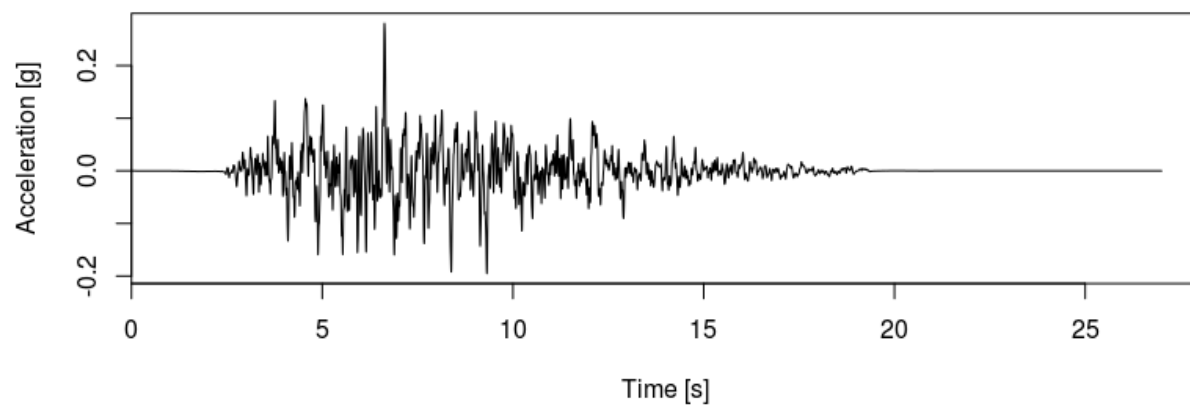
Cycle 45 Max Real Moment: 10.8816 [Nm], Min Real Moment: -8.5121 [kNm]
 Max Real Rot.: 0.1769 [rad], Min Real Rot.: -0.1769 [rad]
 vs. Max Model Moment : 11.4718 [Nm], Min Model Moment : -11.4433 [kNm]
 Max Model Rot.: 0.1764 [rad], Min Model Rot.: -0.1772 [rad]



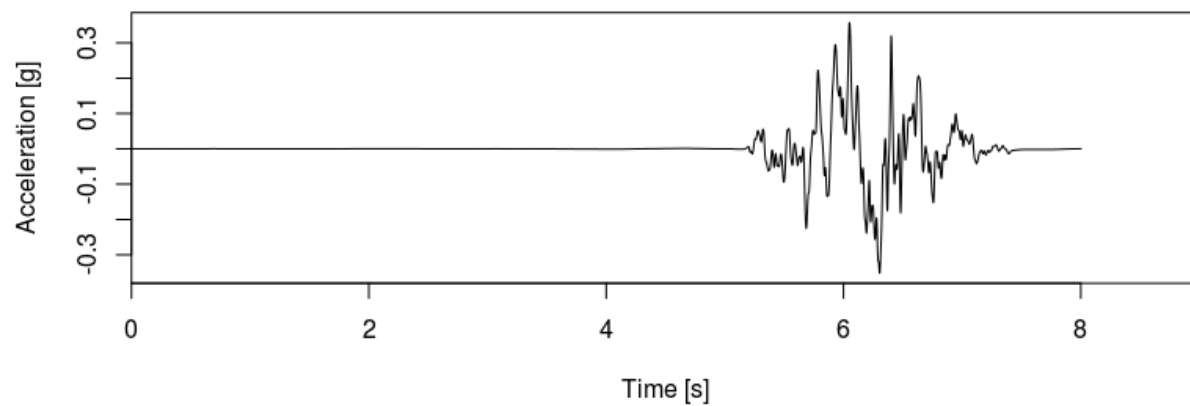
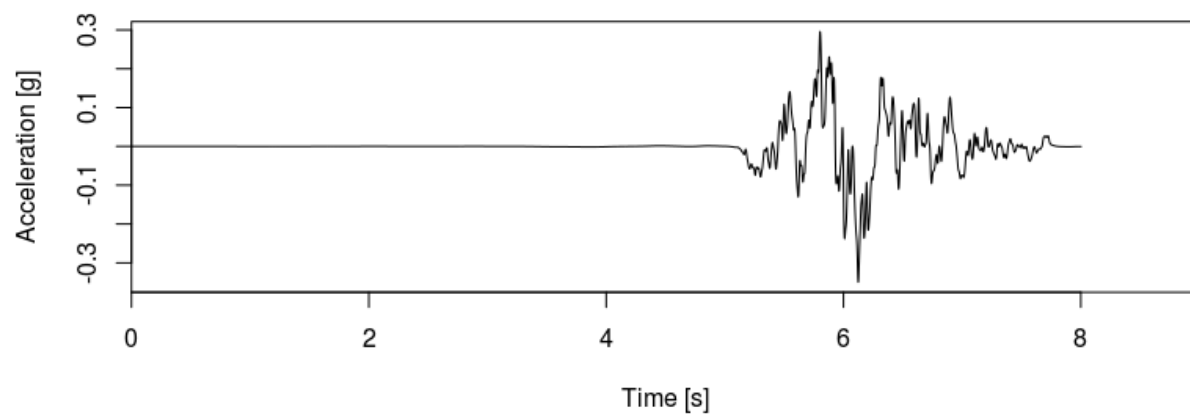
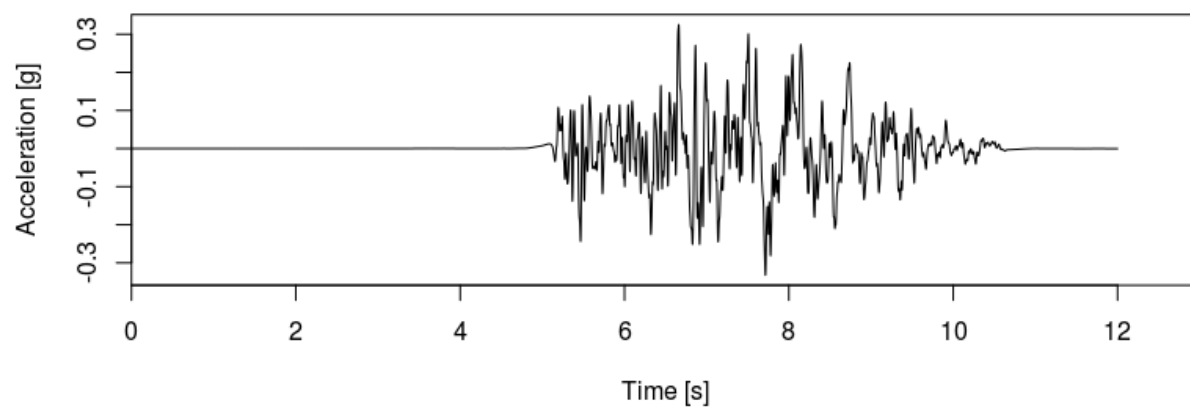
APPENDIX I GROUND MOTIONS FOR TIME HISTORY ANALYSES**CHAPTER 16****I.1. Montreal Site C Ground Motions****MC1****MC2**

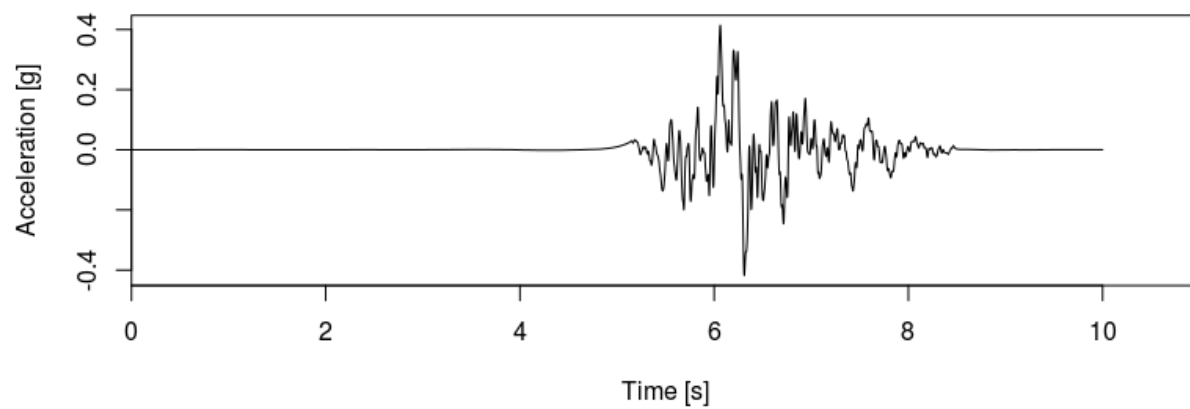
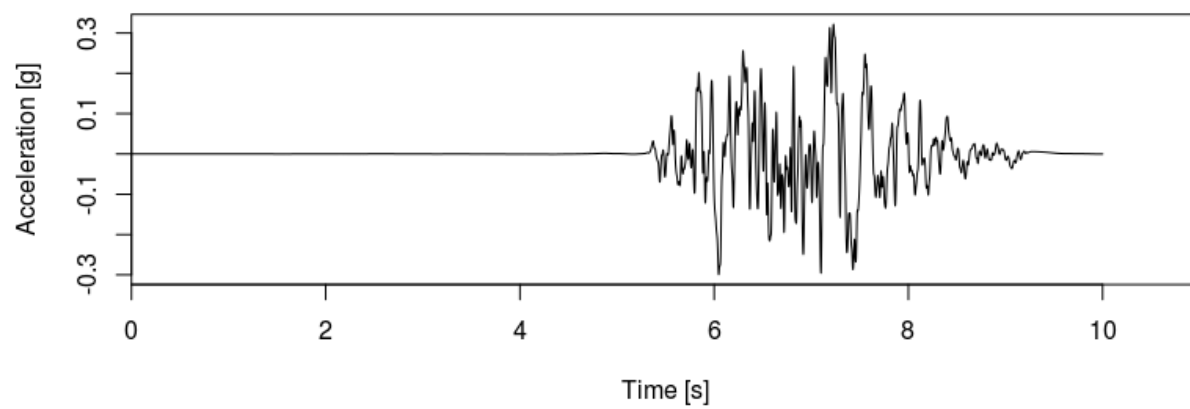
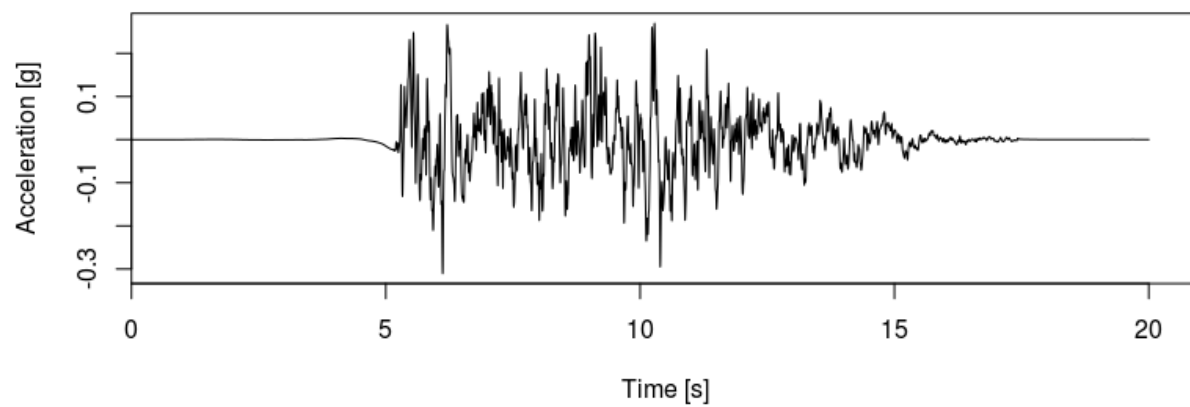
MC3**MC4****MC5**

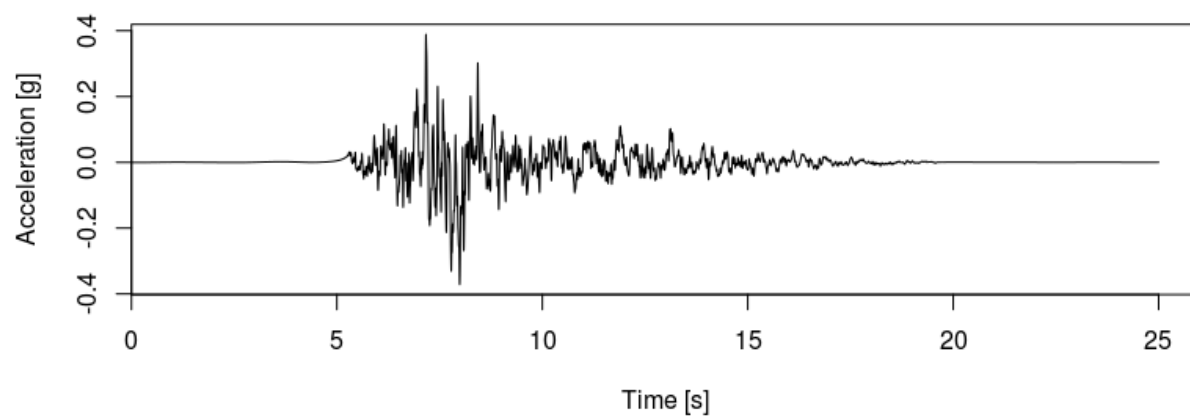
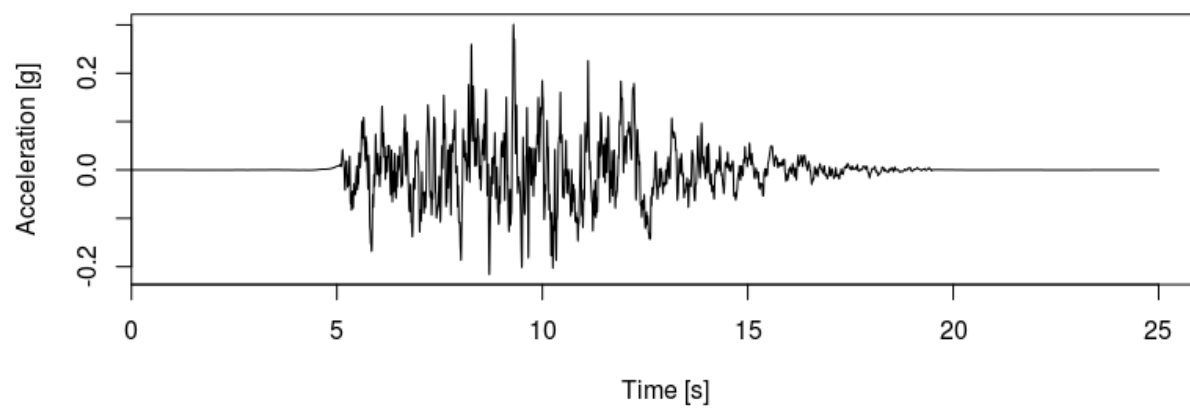
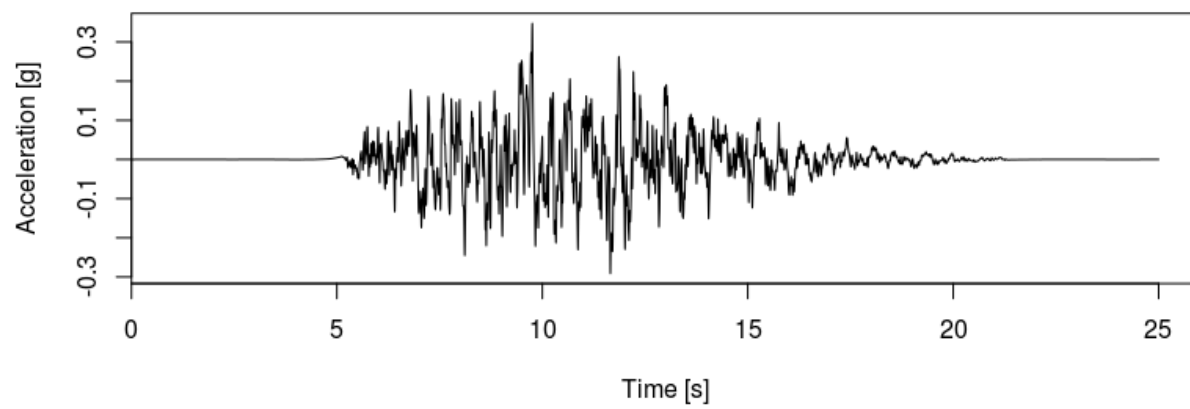
MC6**MC7****MC8**

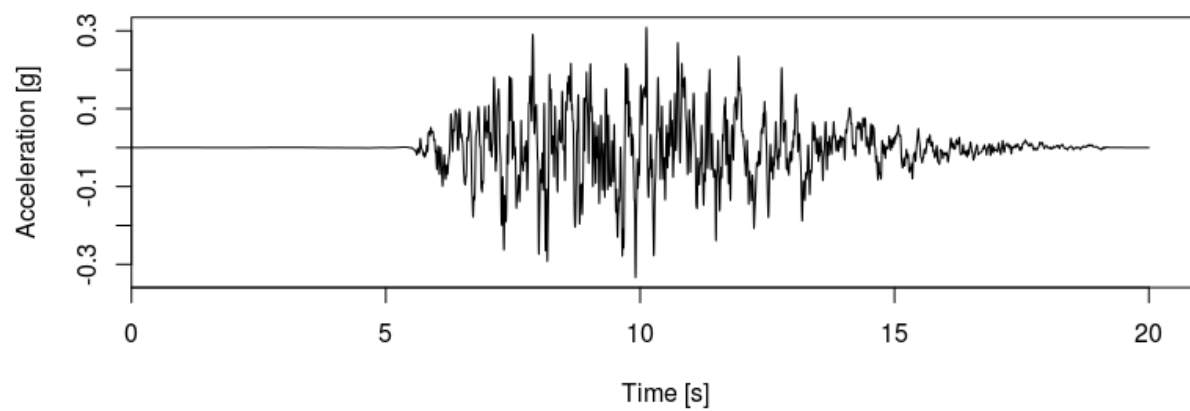
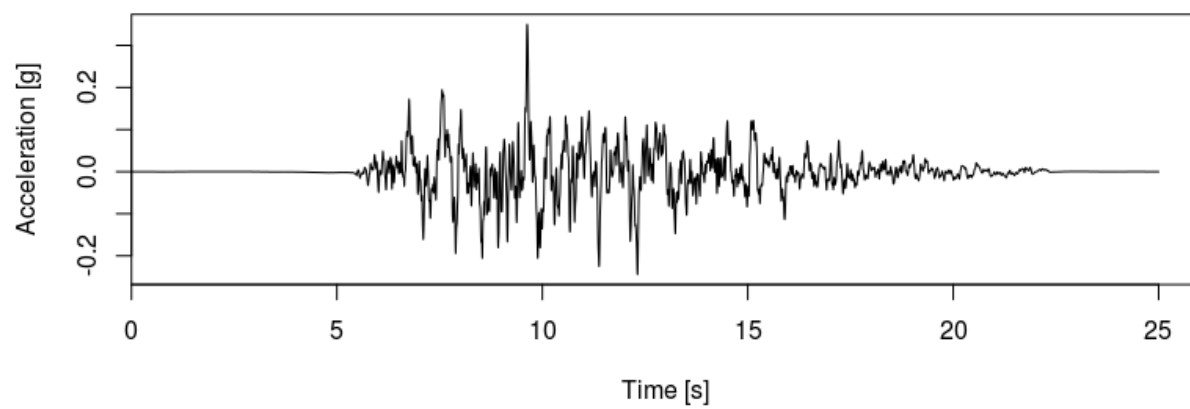
MC9**MC10****MC11**

I.2. Montreal Site E Ground Motions

ME1**ME2****ME3**

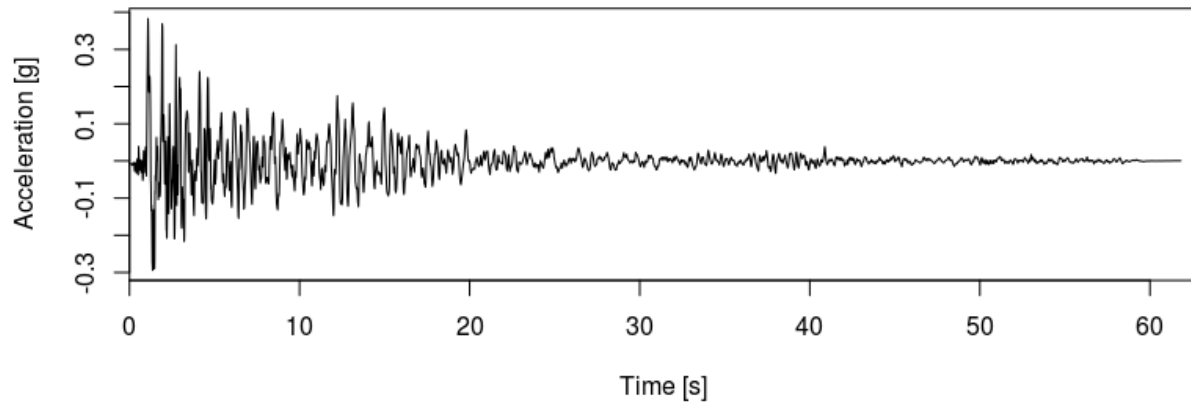
ME4**ME5****ME6**

ME7**ME8****ME9**

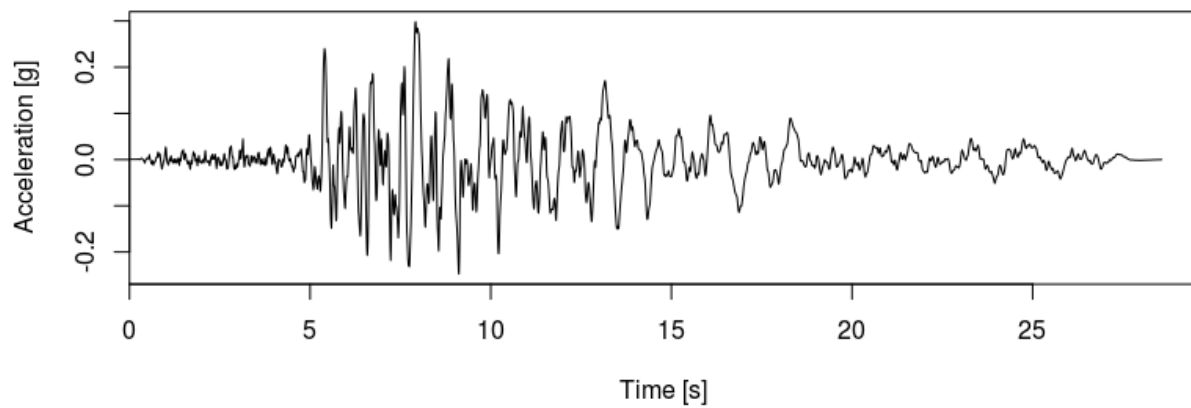
ME10**ME11**

I.3. Vancouver Site C Ground Motions

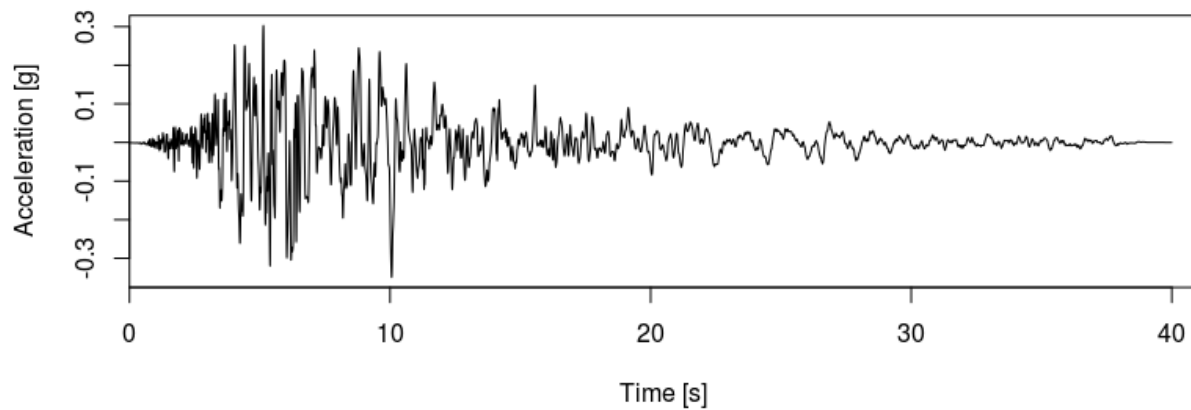
VC1

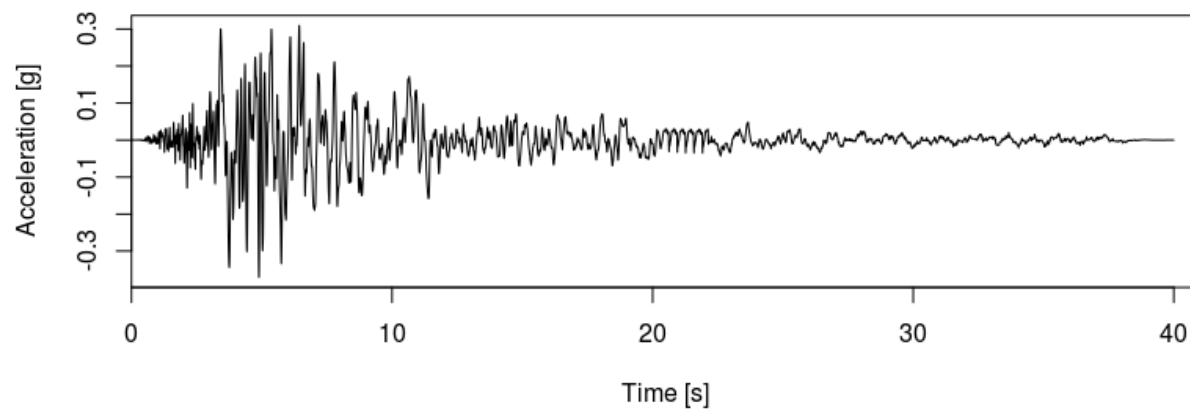
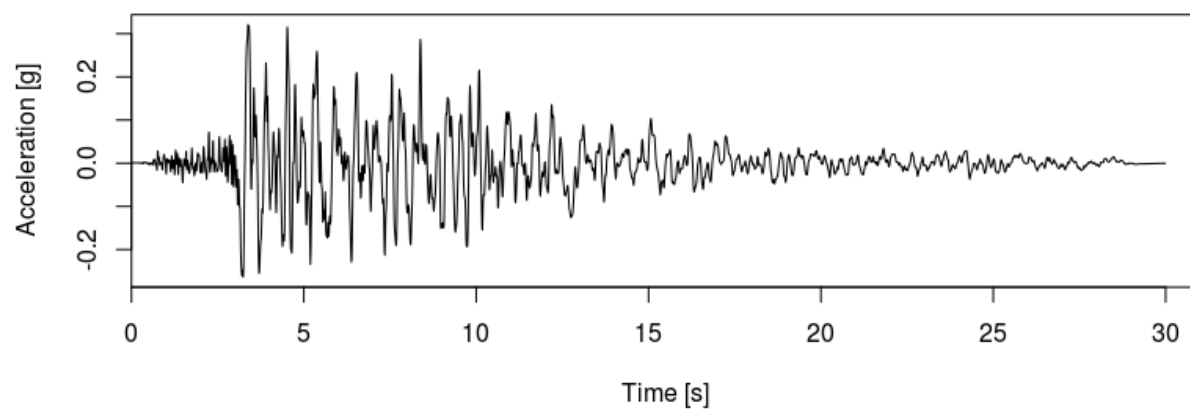
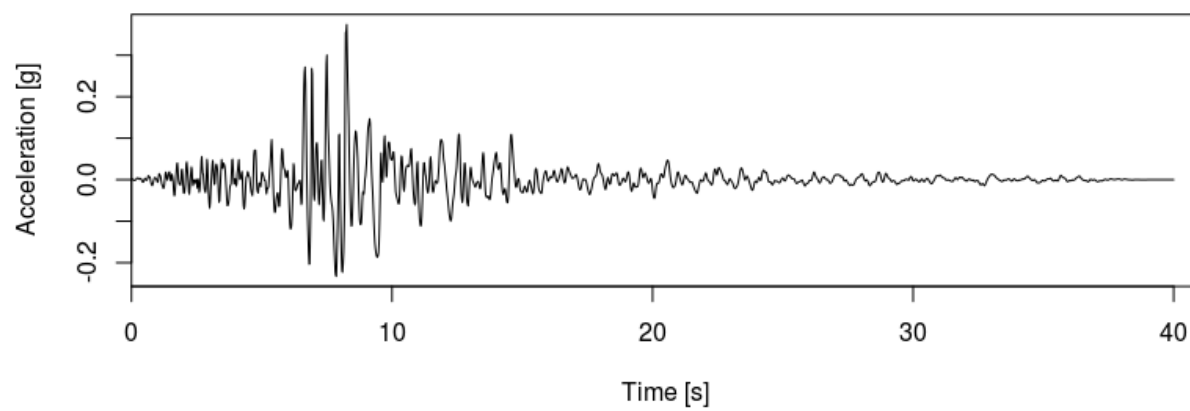


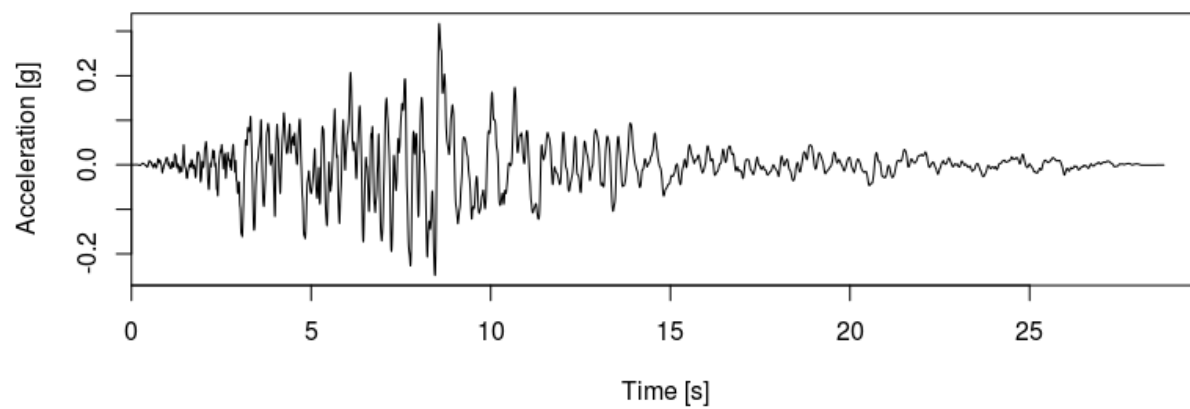
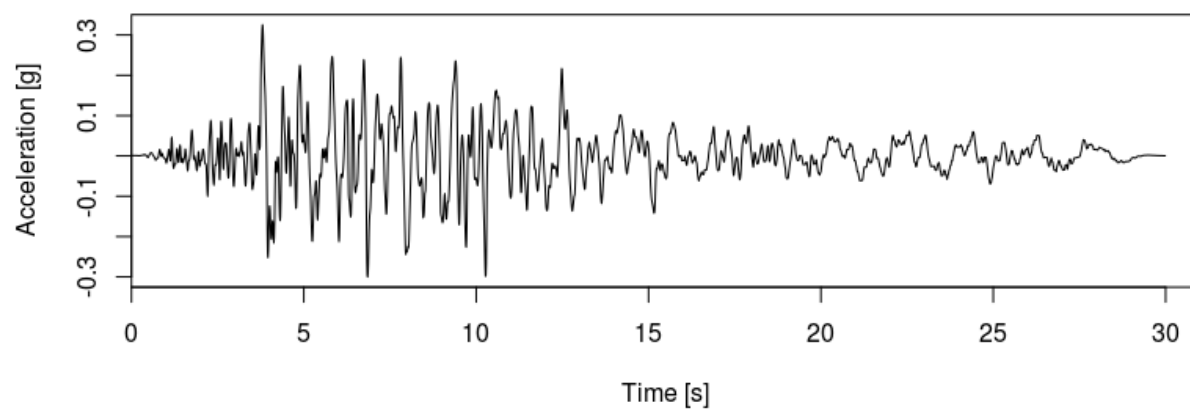
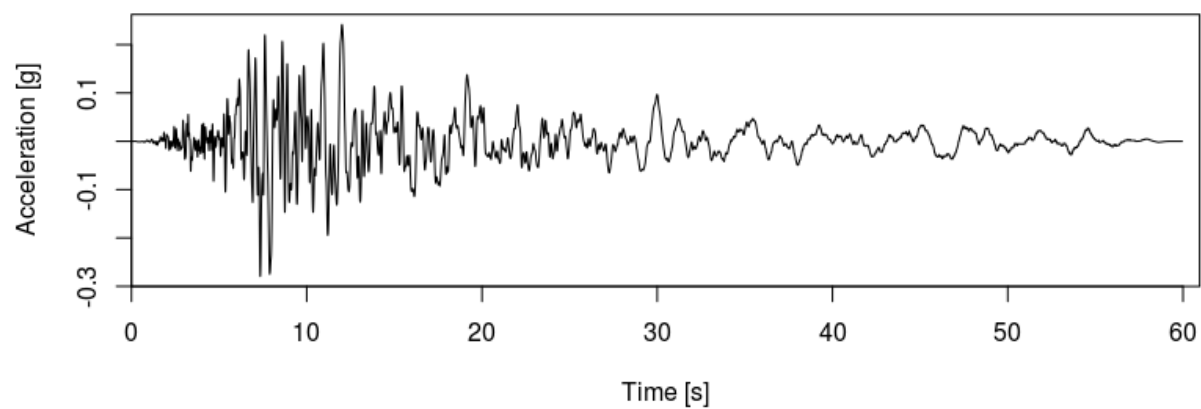
VC2

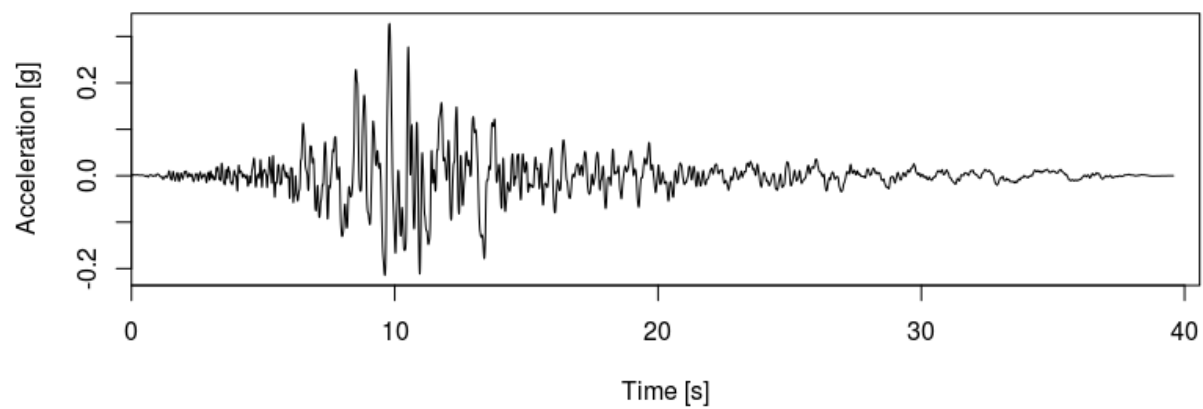
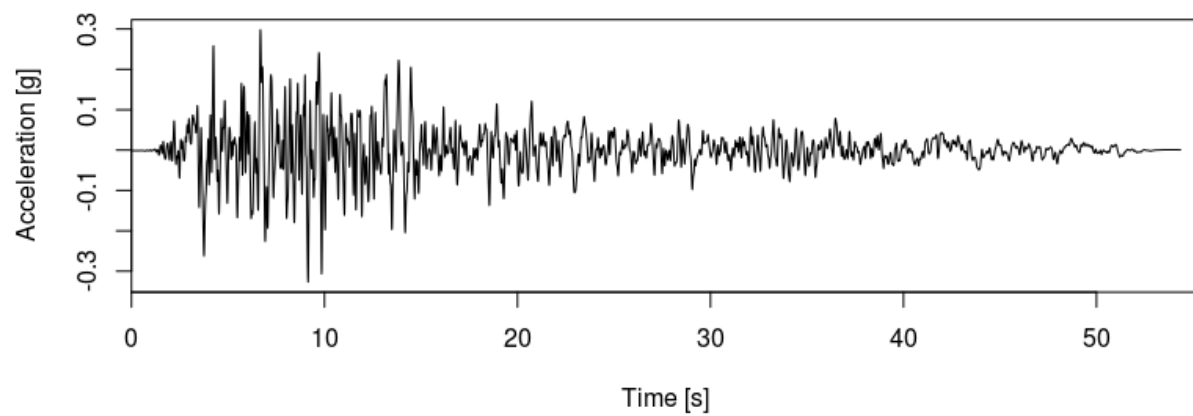
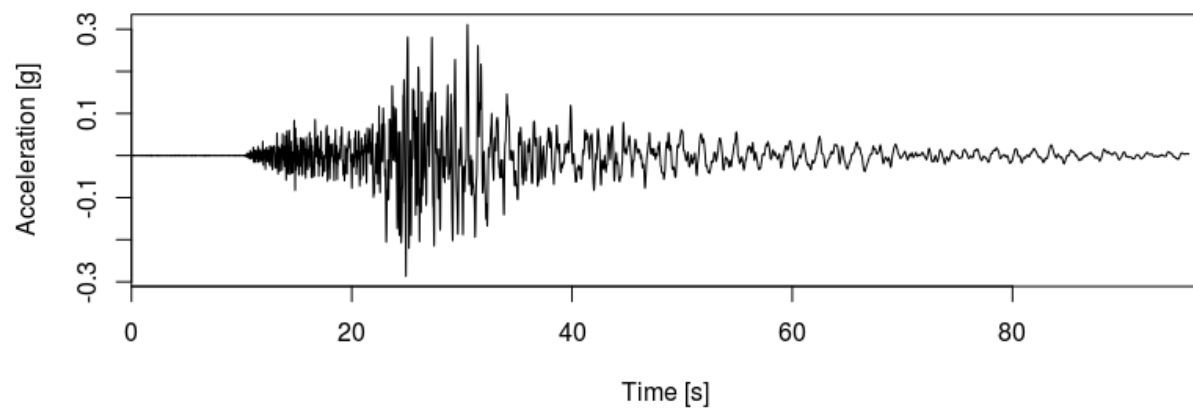


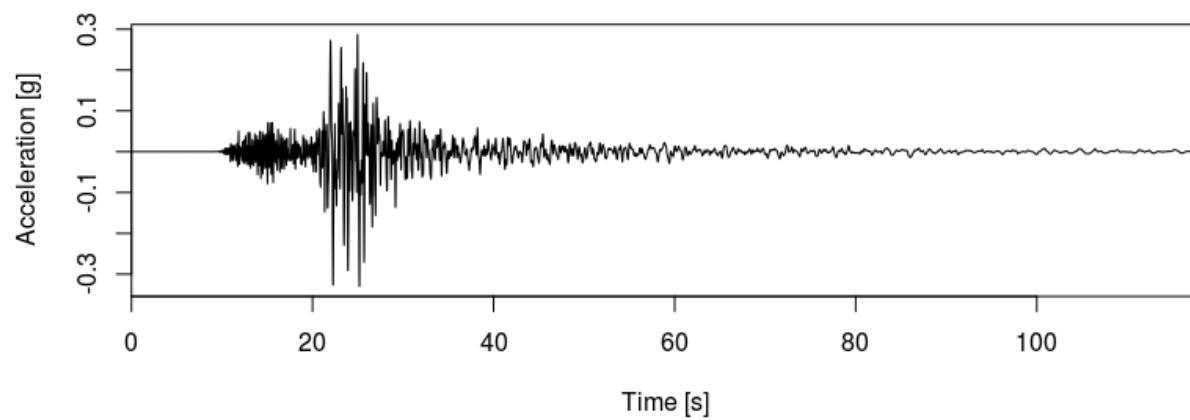
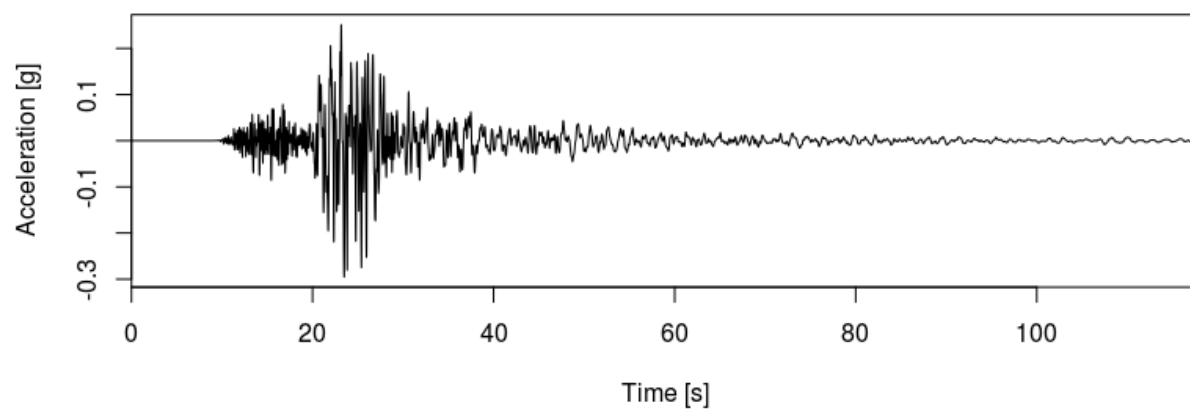
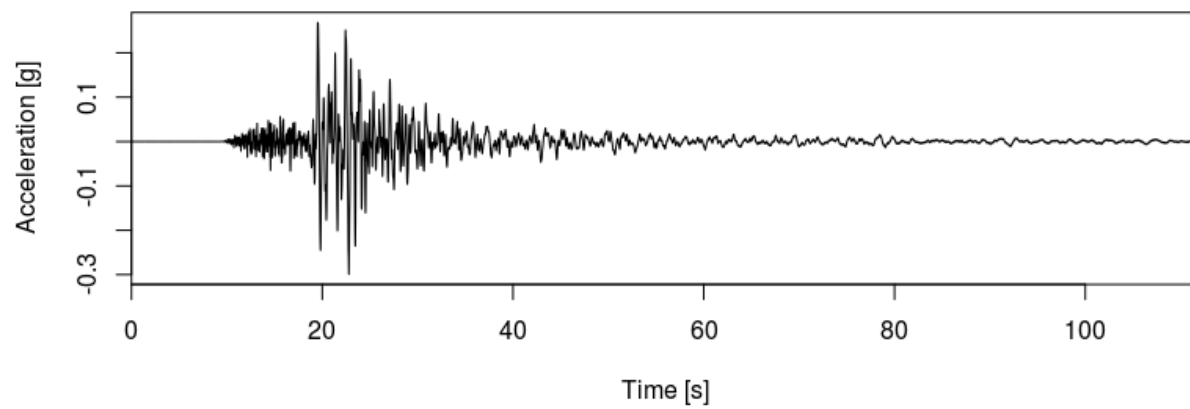
VC3

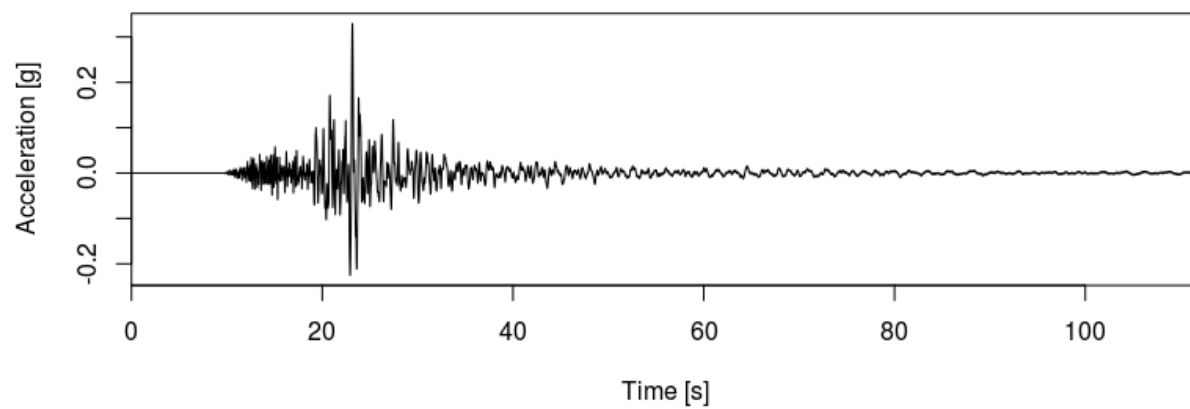
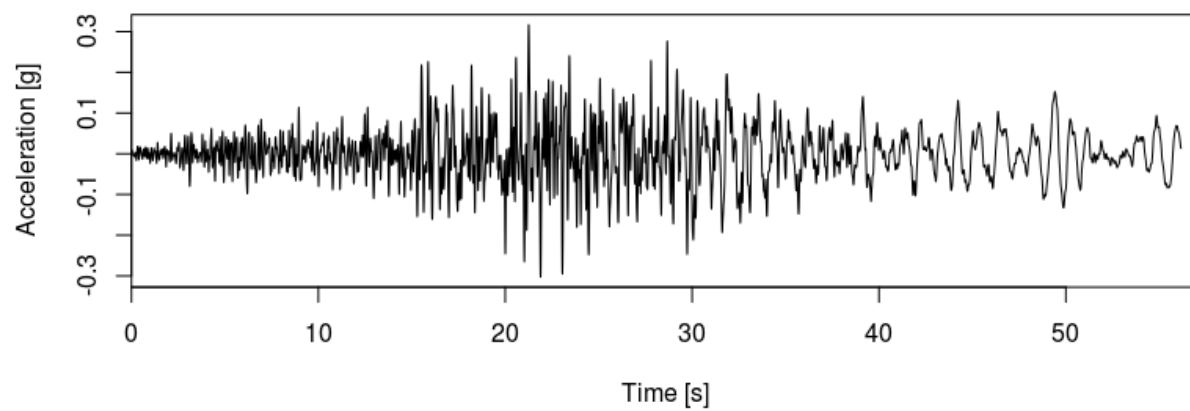
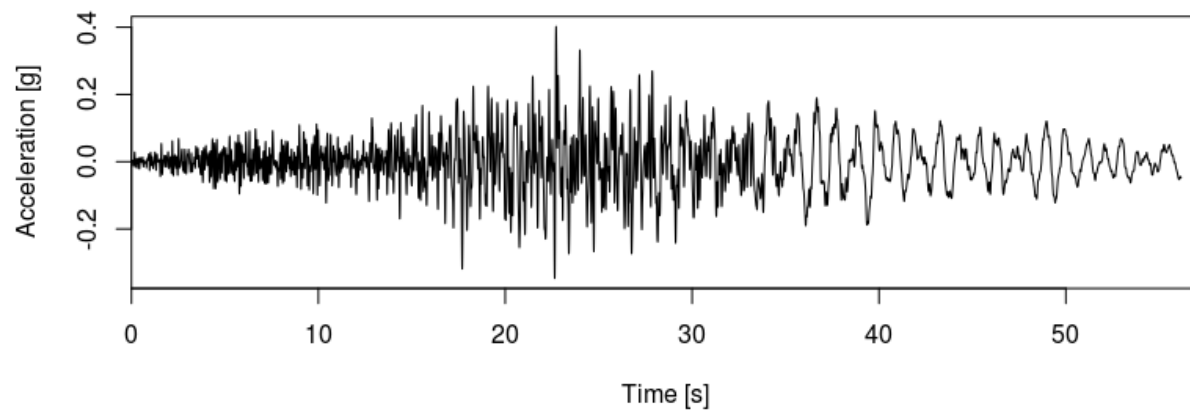


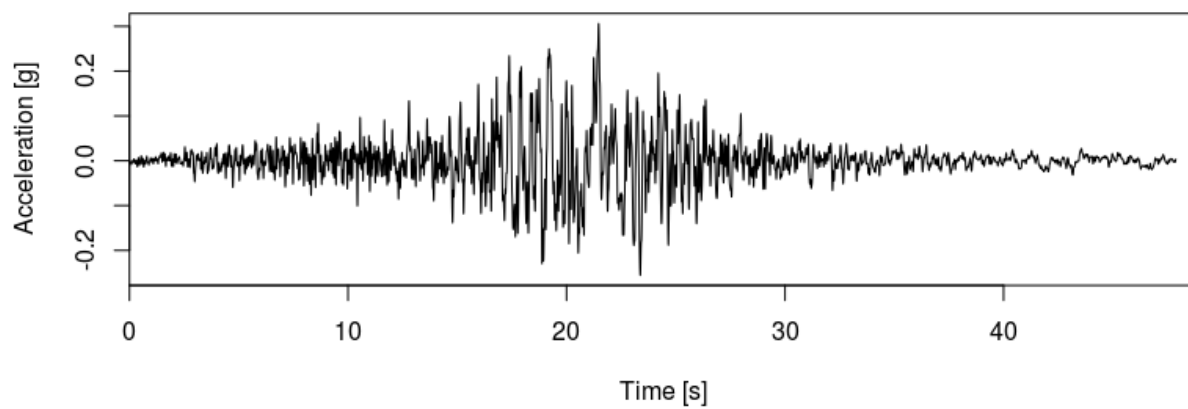
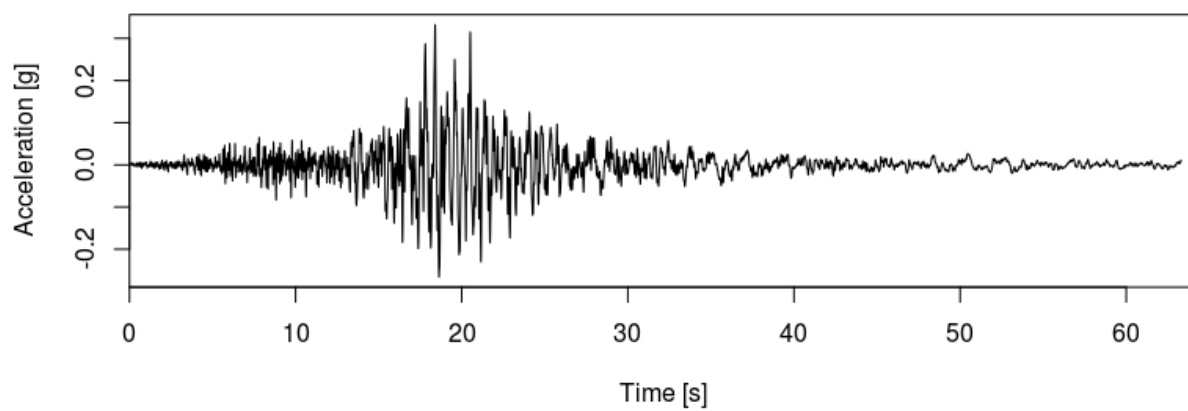
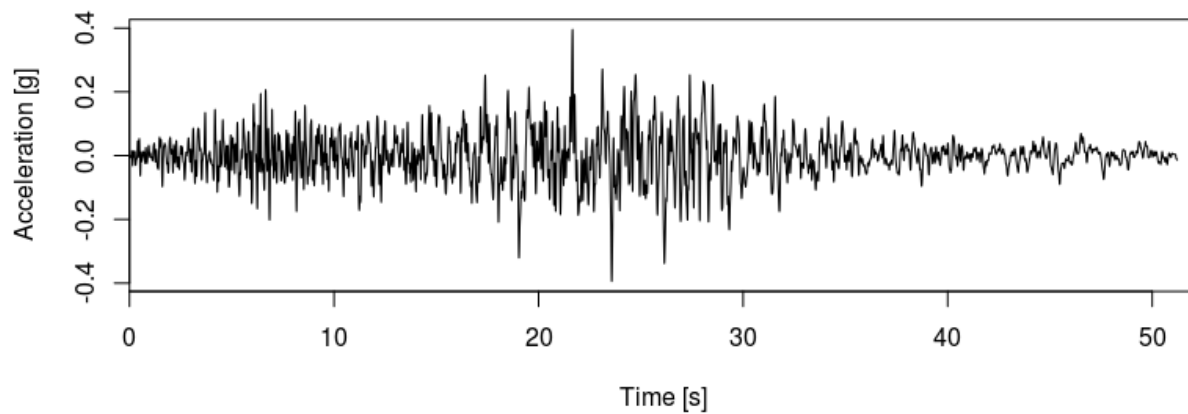
VC4**VC5****VC6**

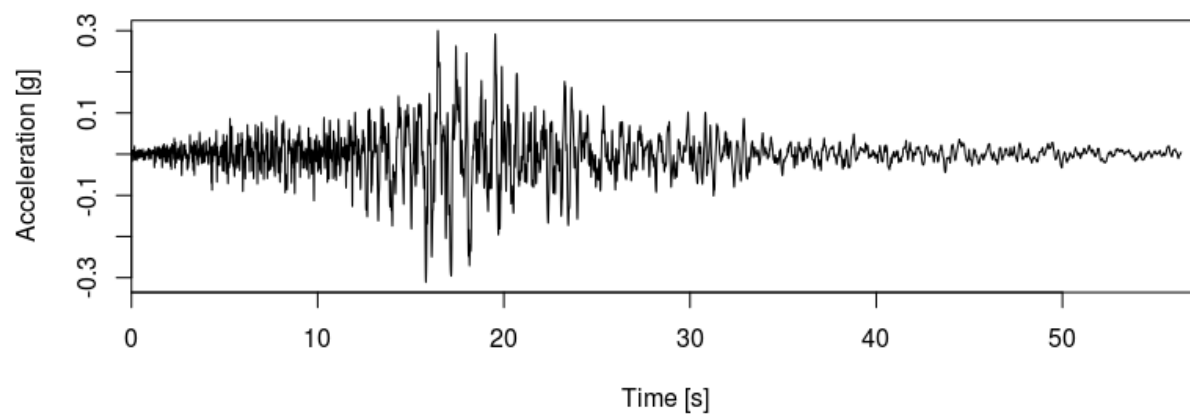
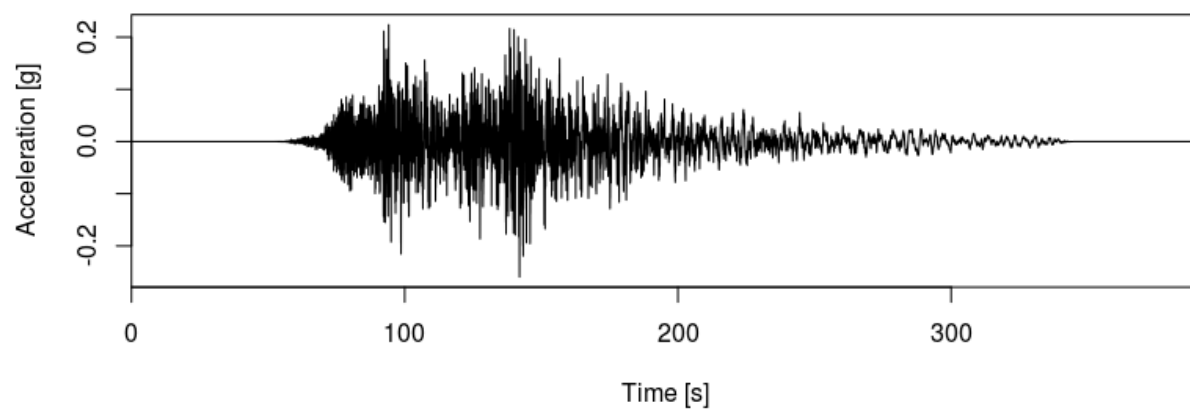
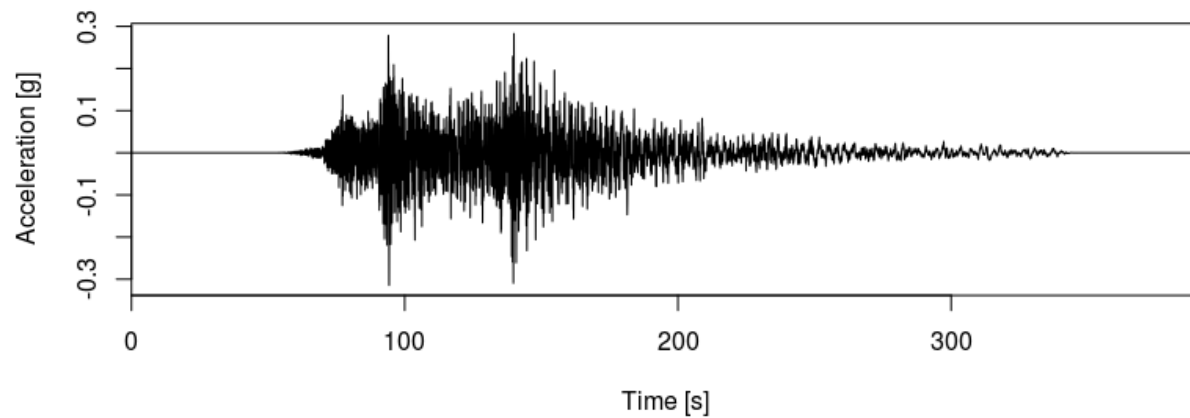
VC7**VC8****VC9**

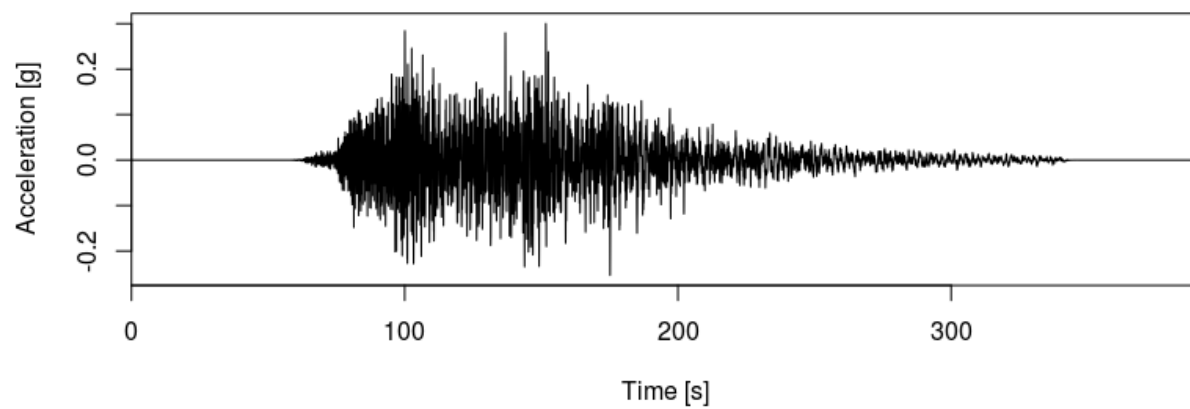
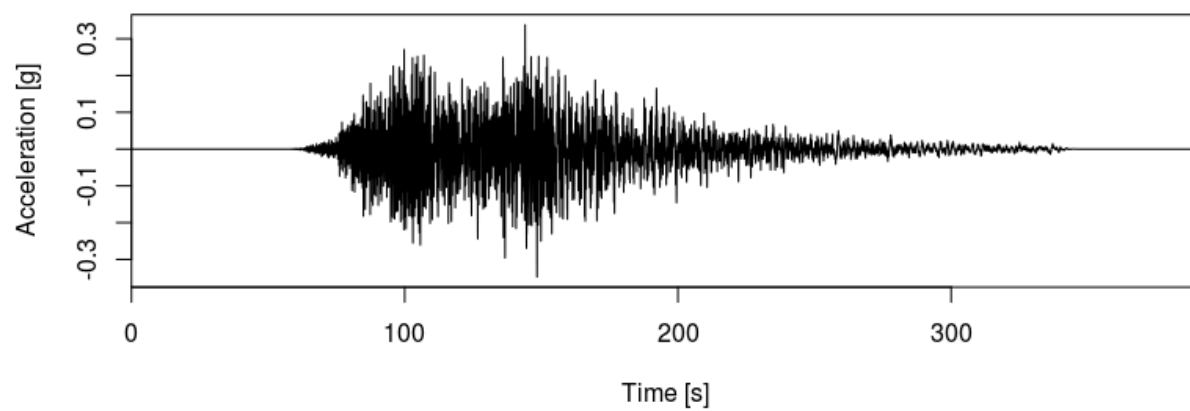
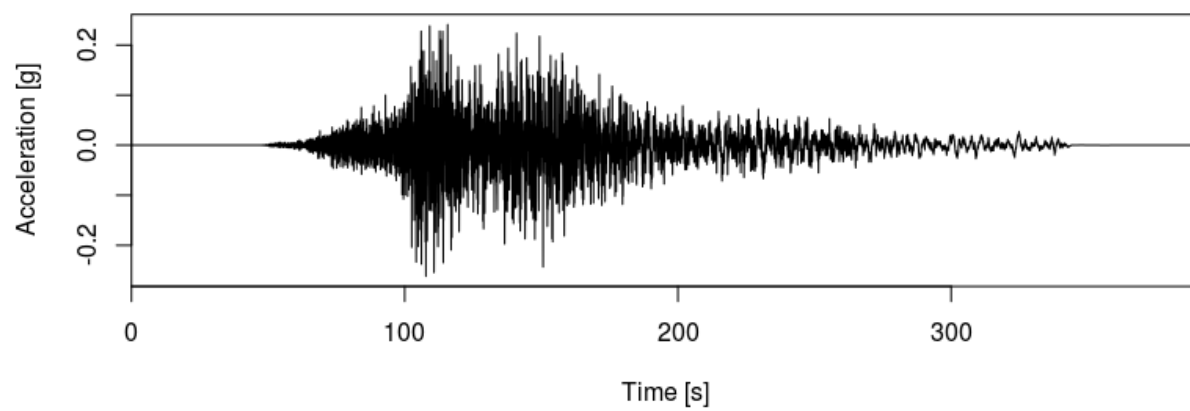
VC10**VC11****VC12**

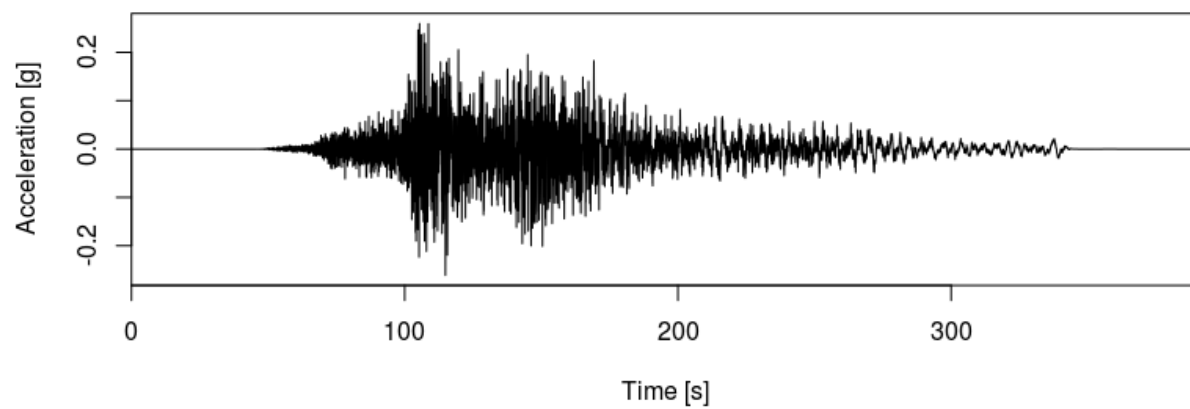
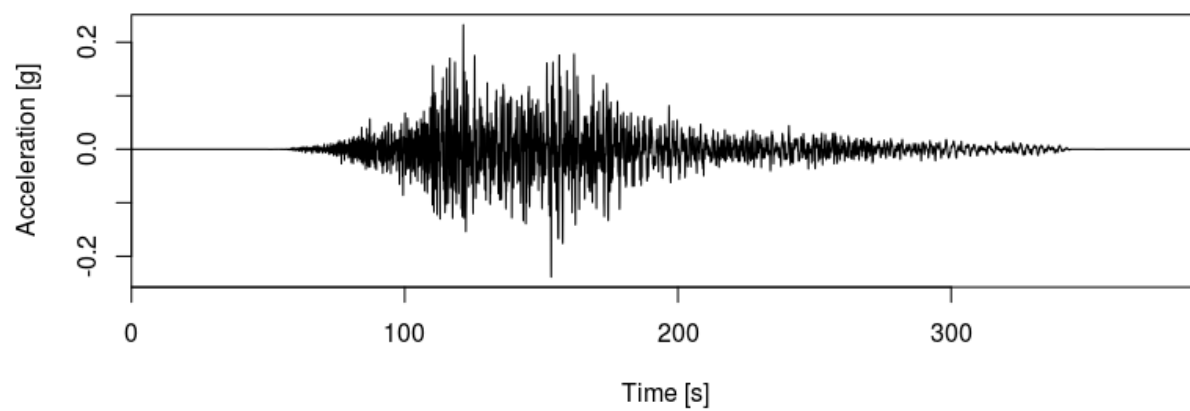
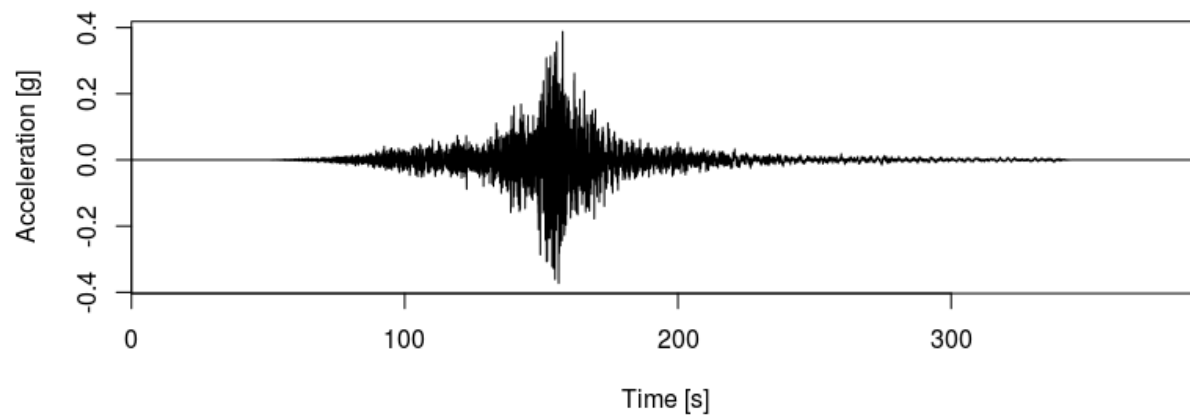
VC13**VC14****VC15**

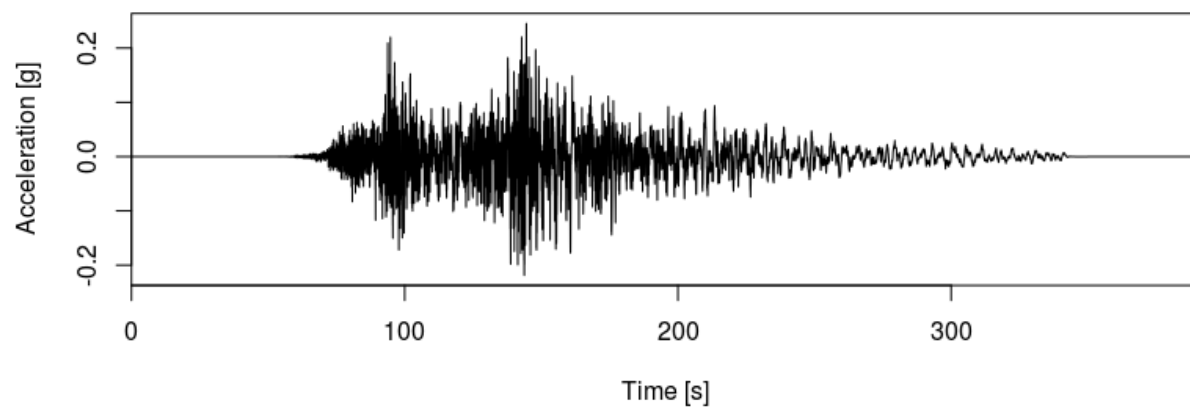
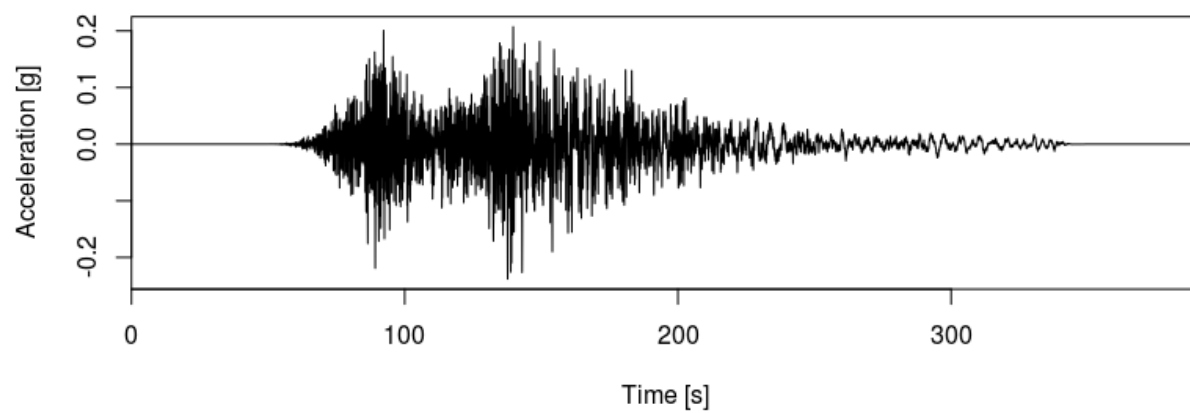
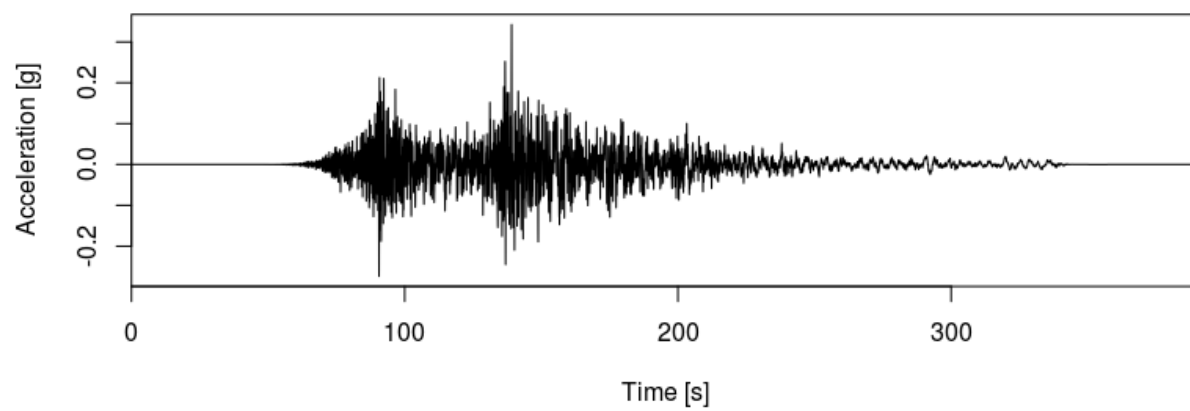
VC16**VC17****VC18**

VC19**VC20****VC21**

VC22**VC23****VC24**

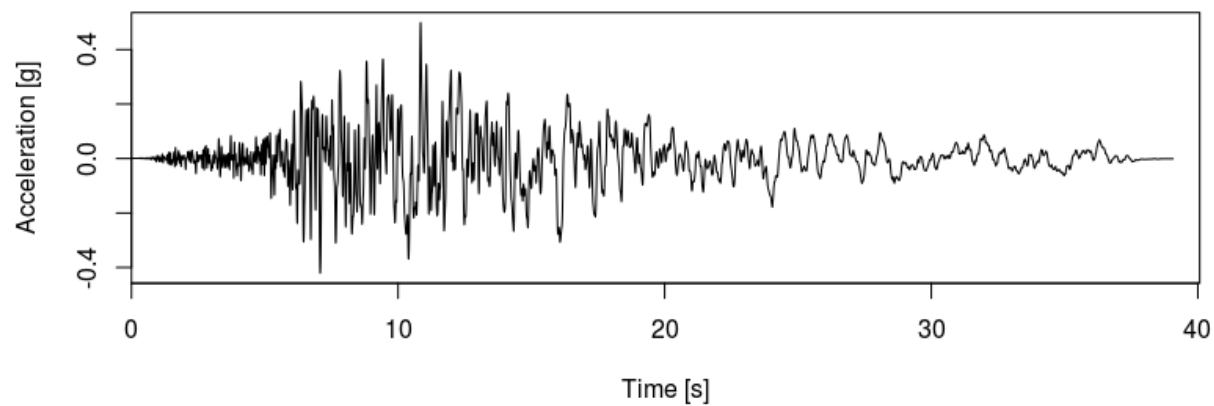
VC25**VC26****VC27**

VC28**VC29****VC30**

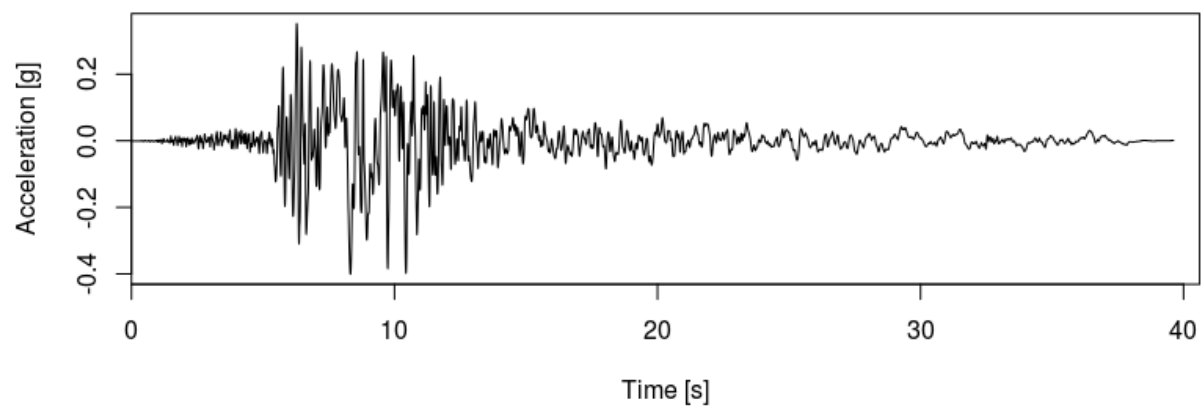
VC31**VC32****VC33**

I.4. Vancouver Site E Ground Motions

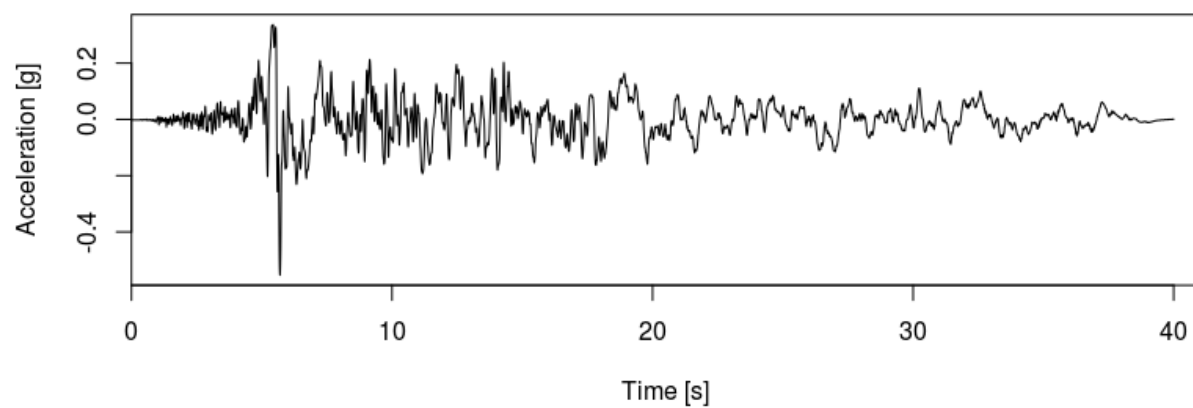
VE1

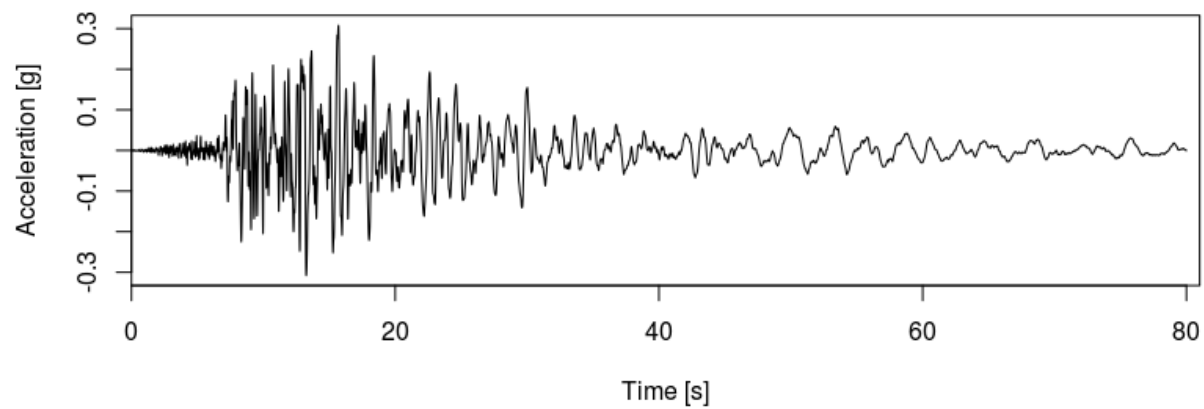
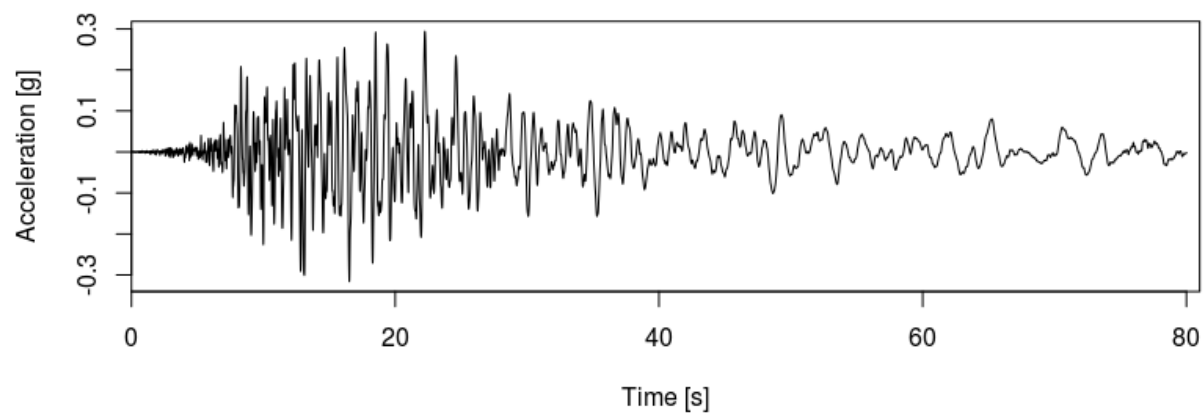
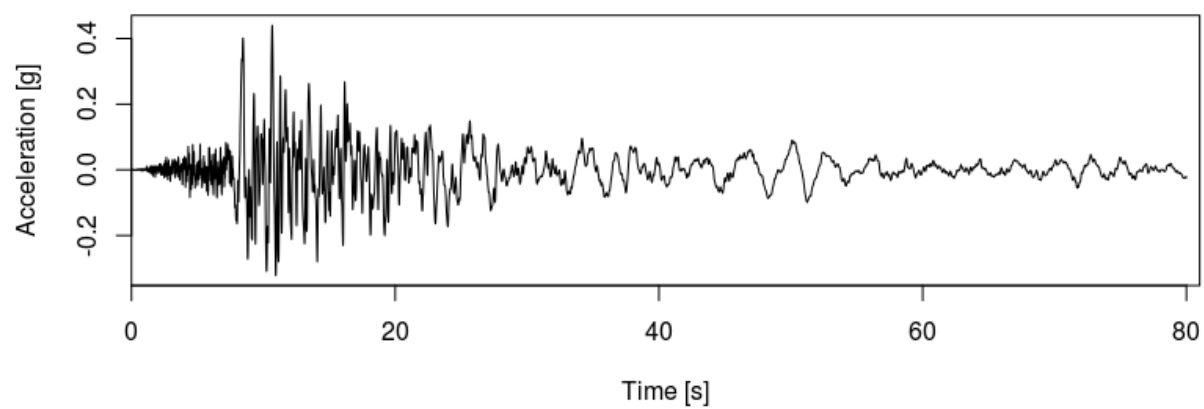


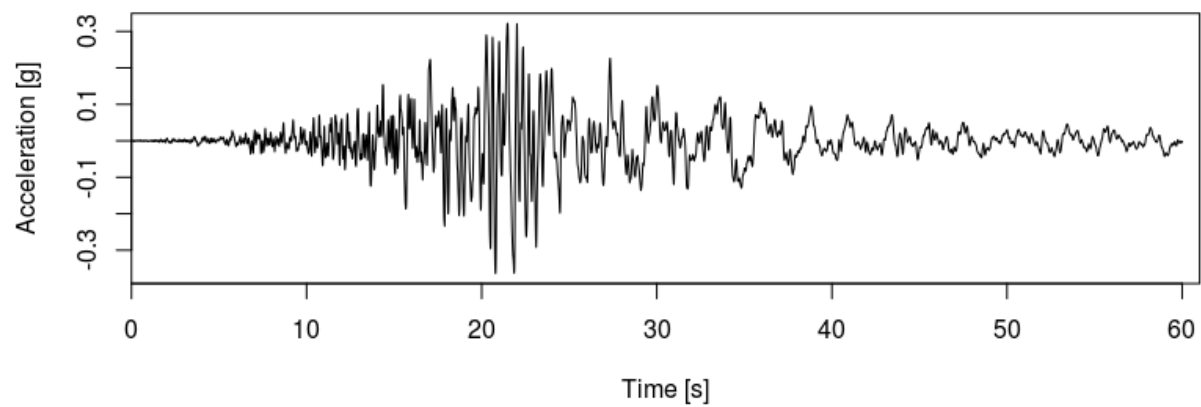
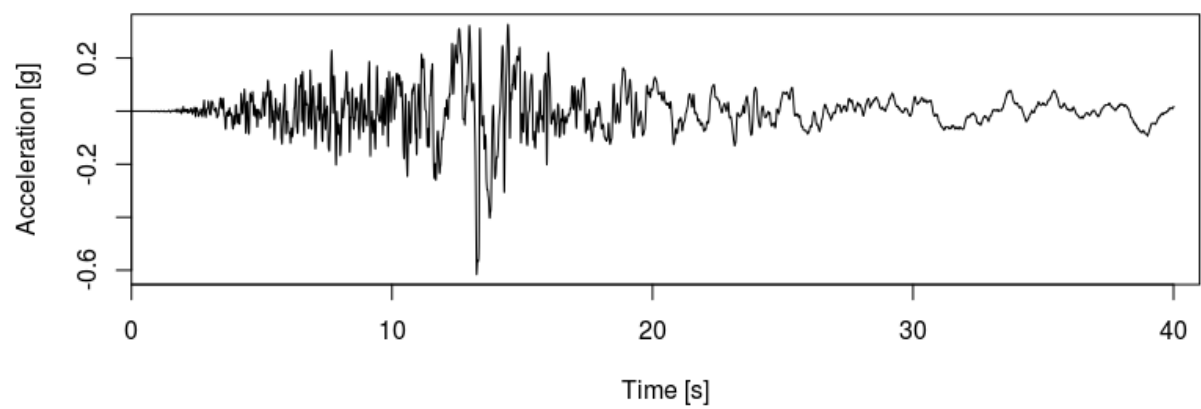
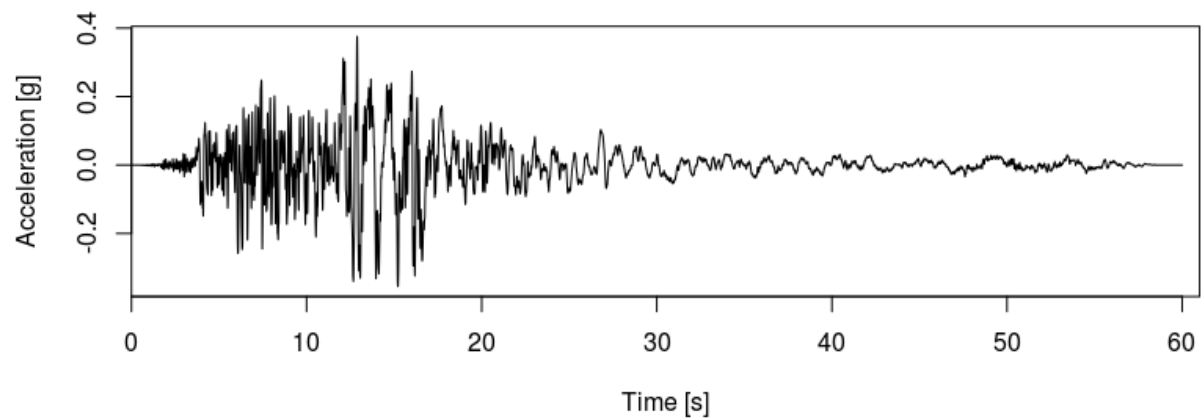
VE2

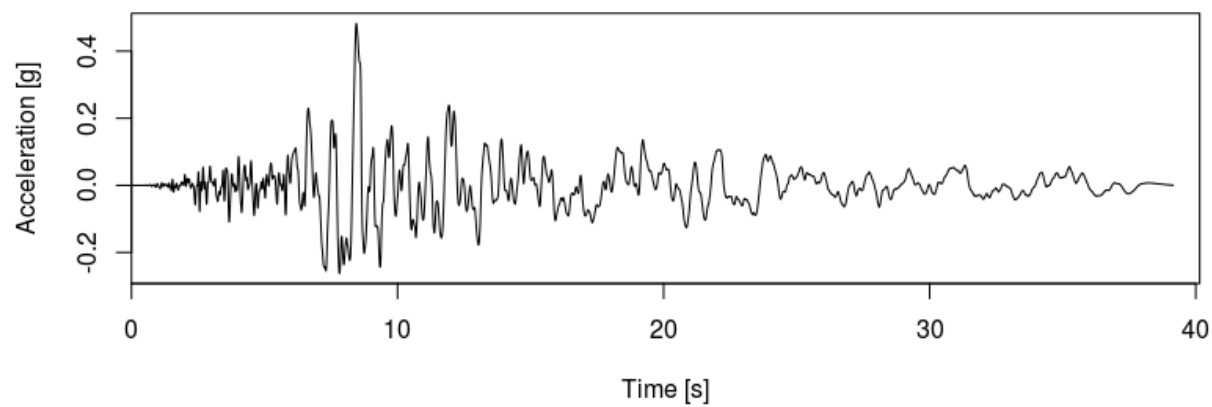
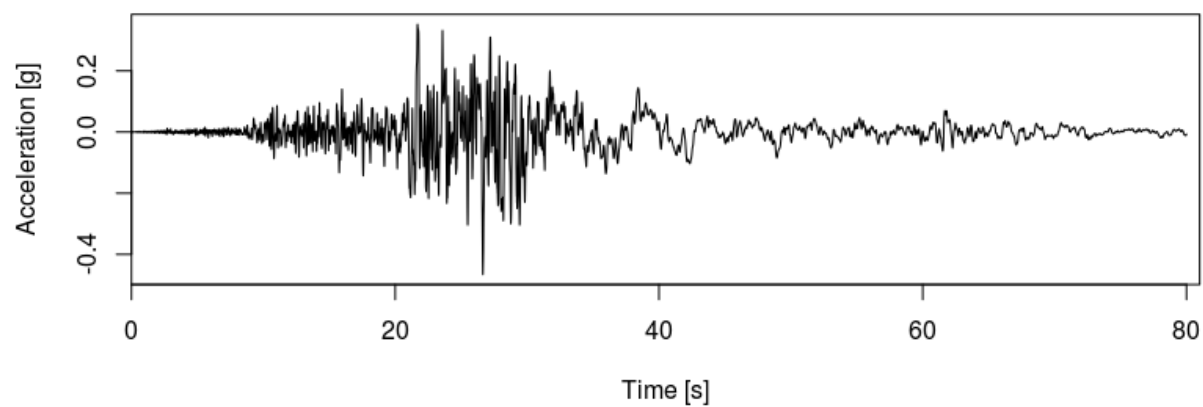
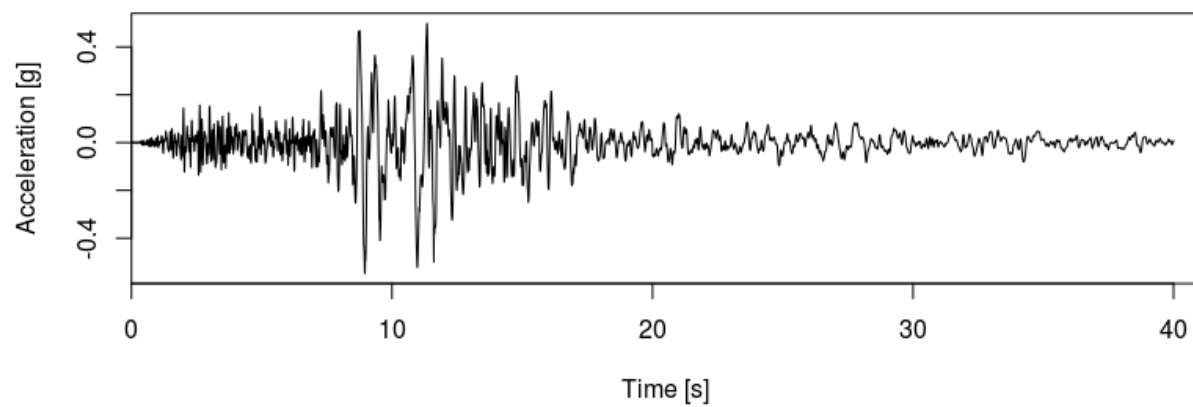


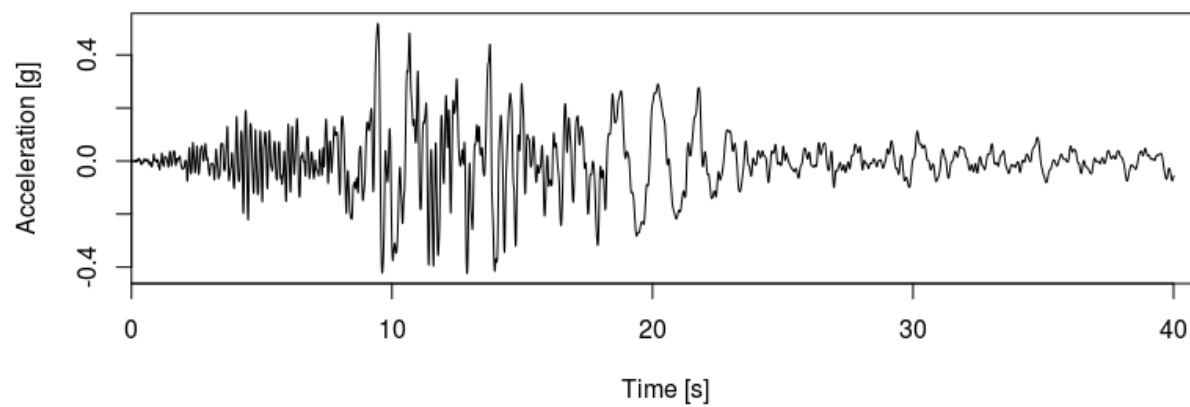
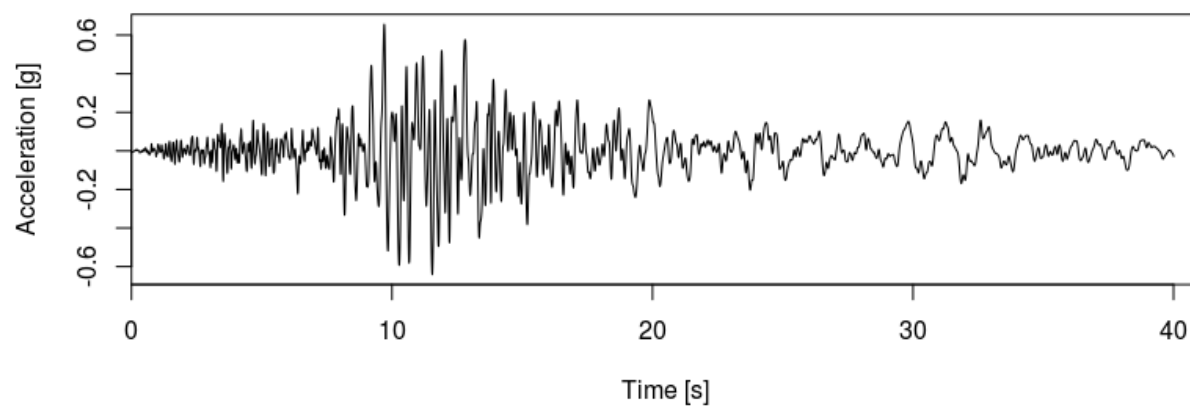
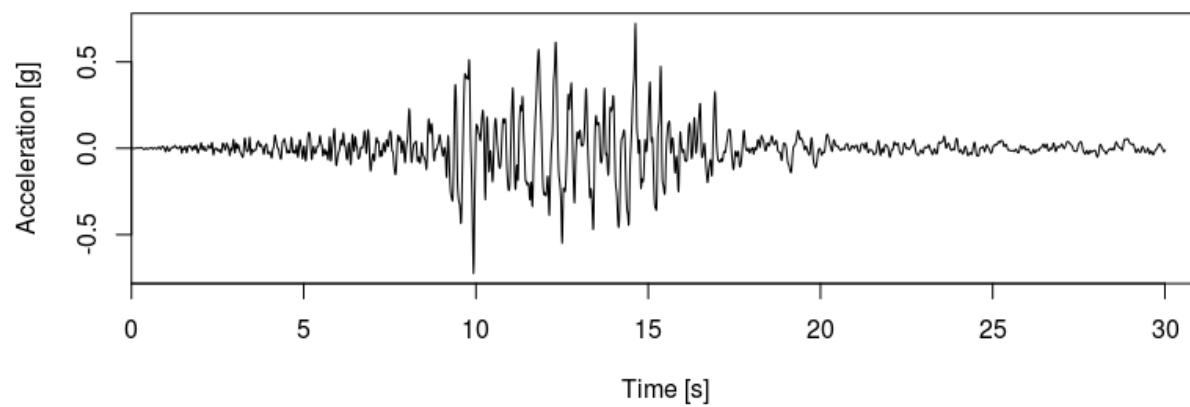
VE3

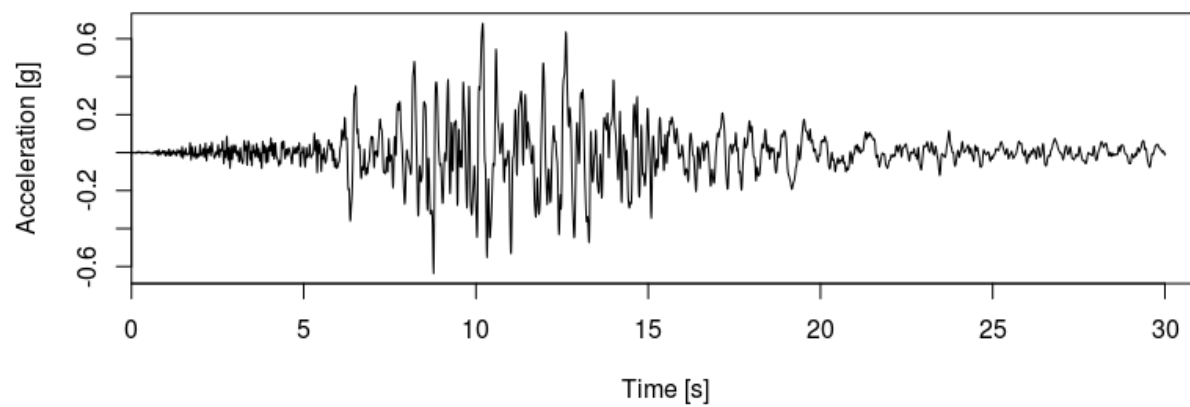
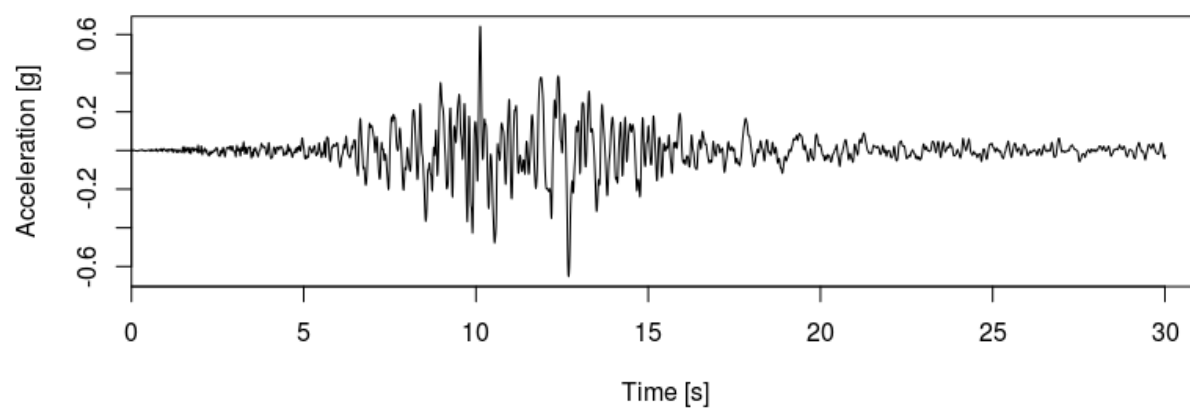
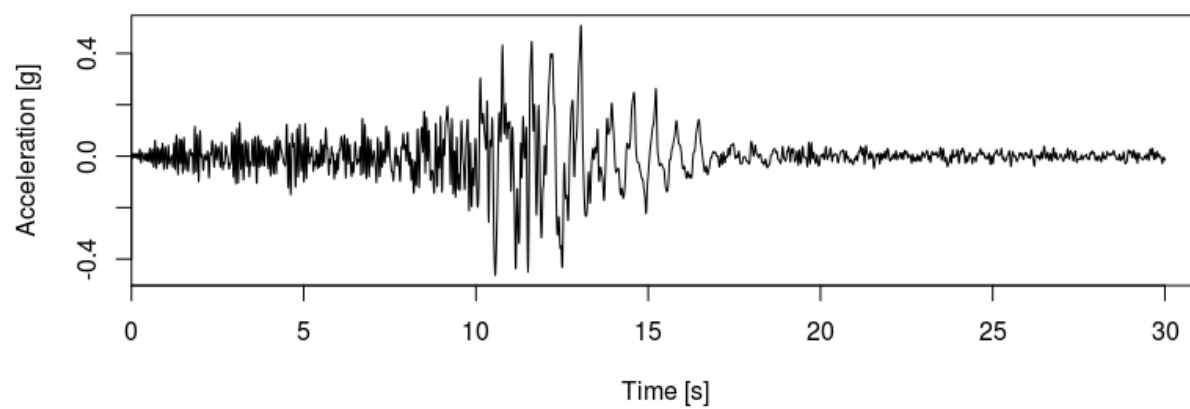


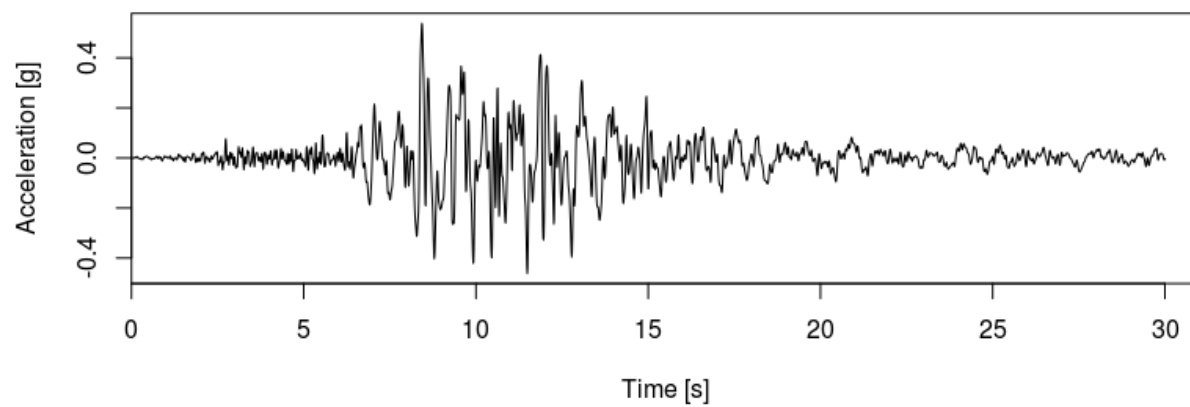
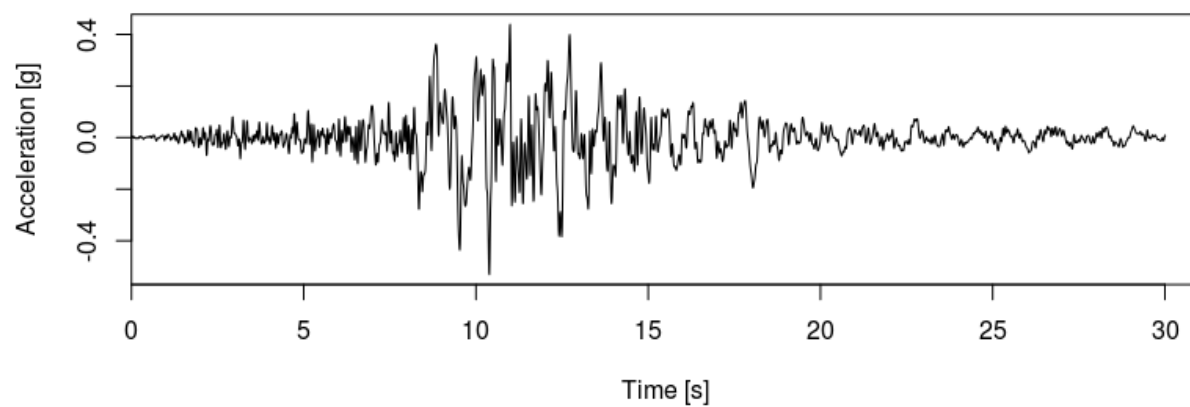
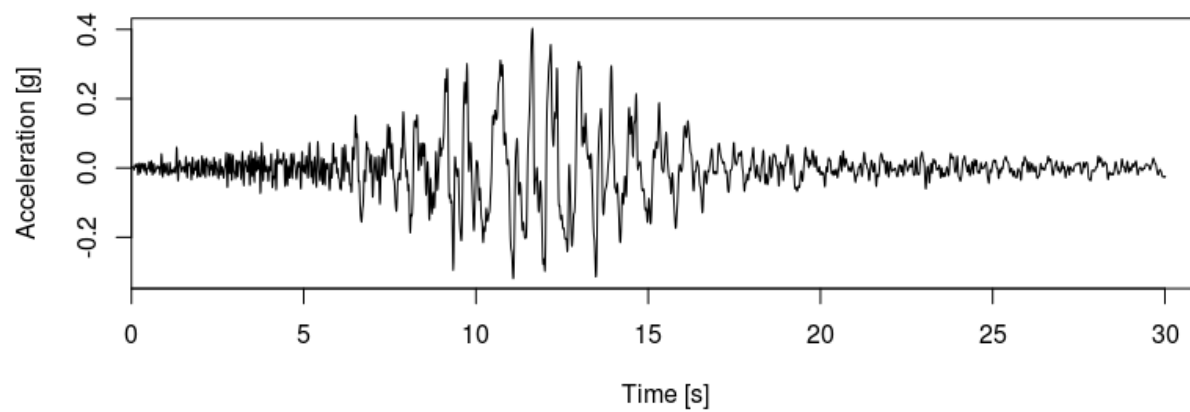
VE4**VE5****VE6**

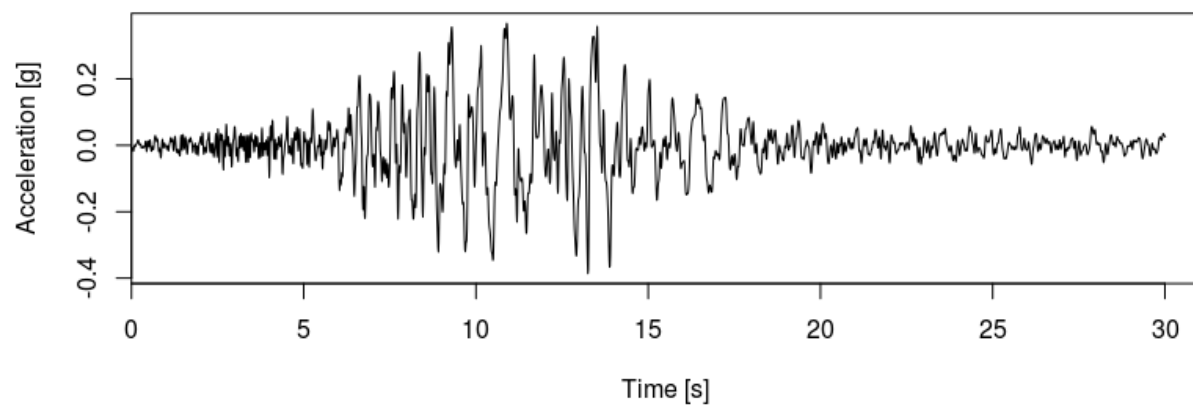
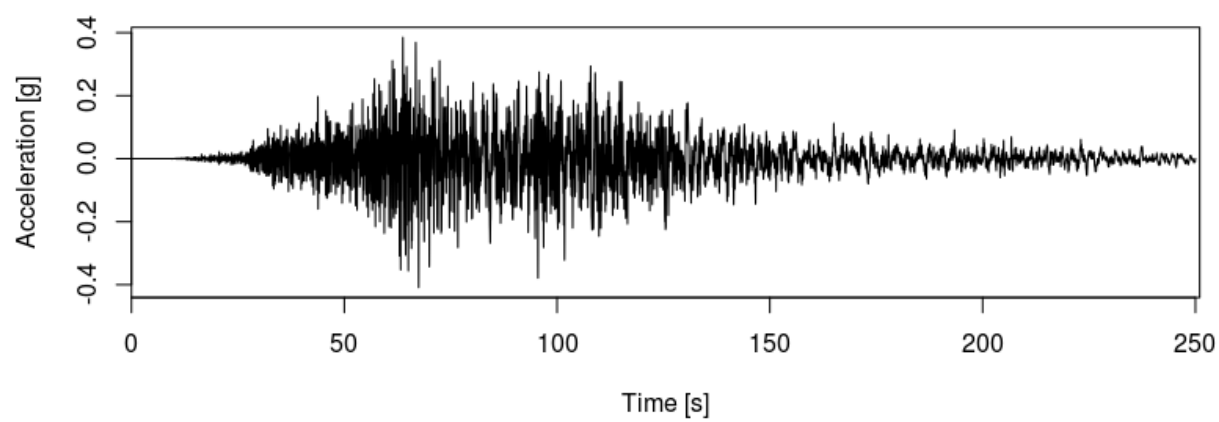
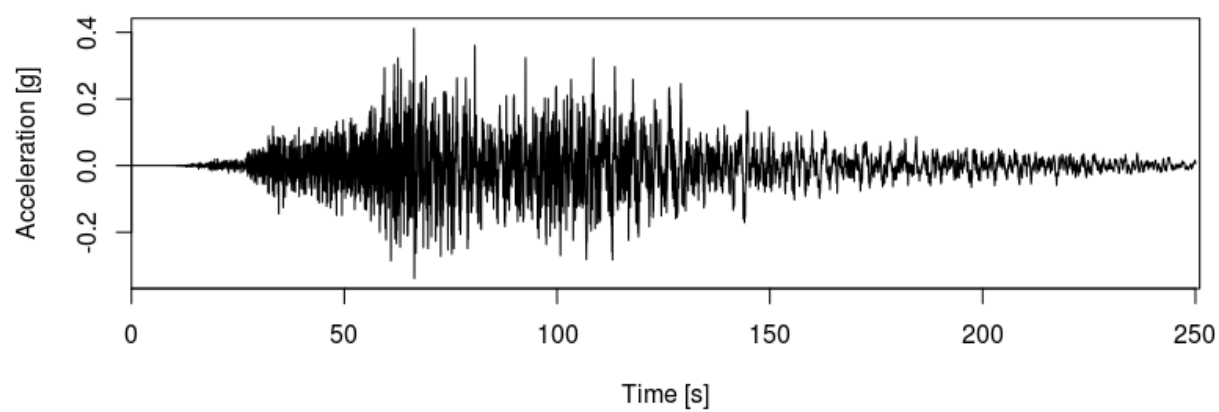
VE7**VE8****VE9**

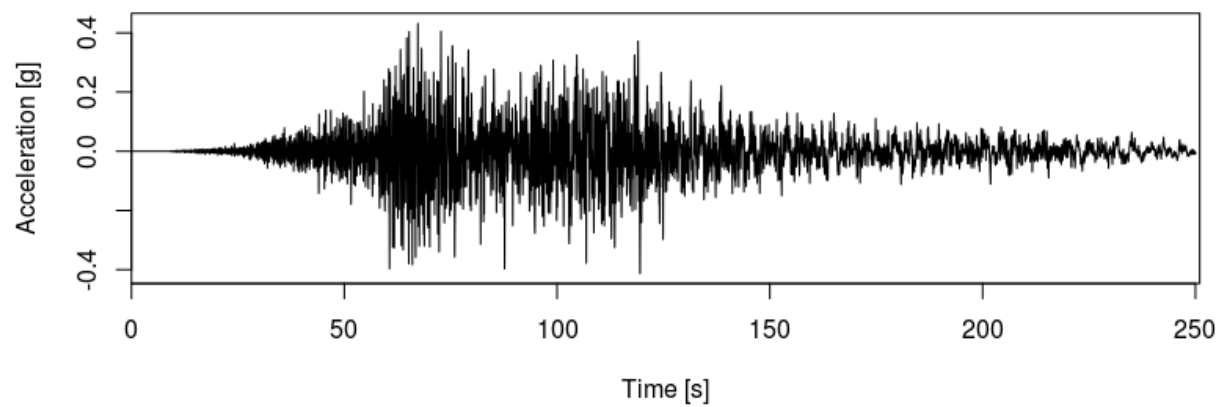
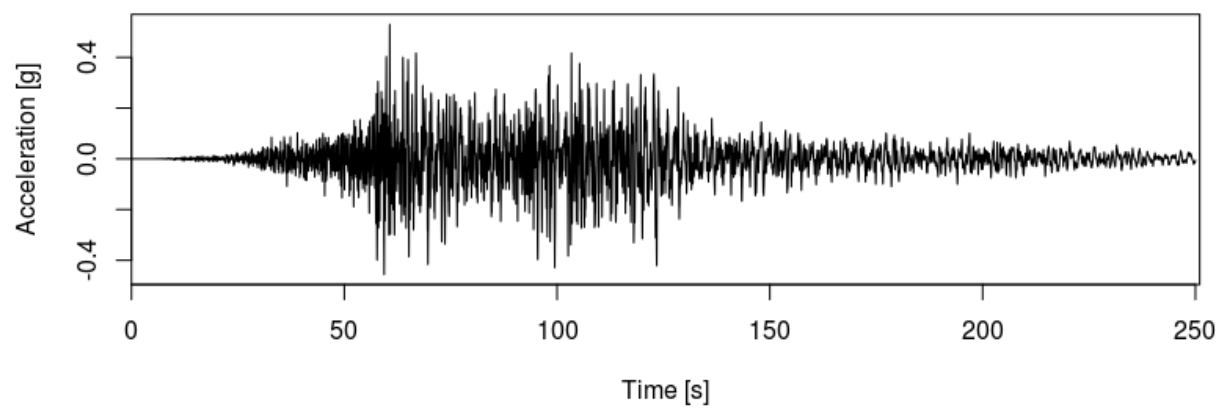
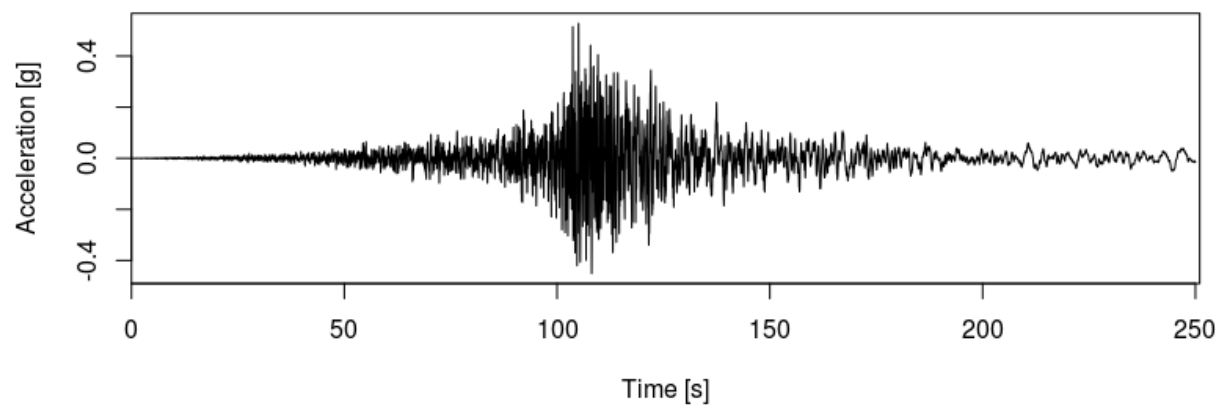
VE10**VE11****VE12**

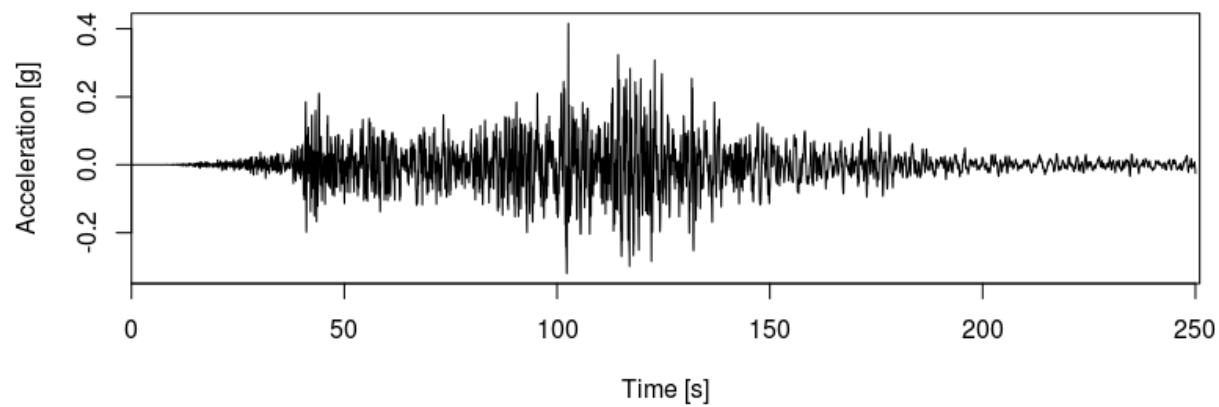
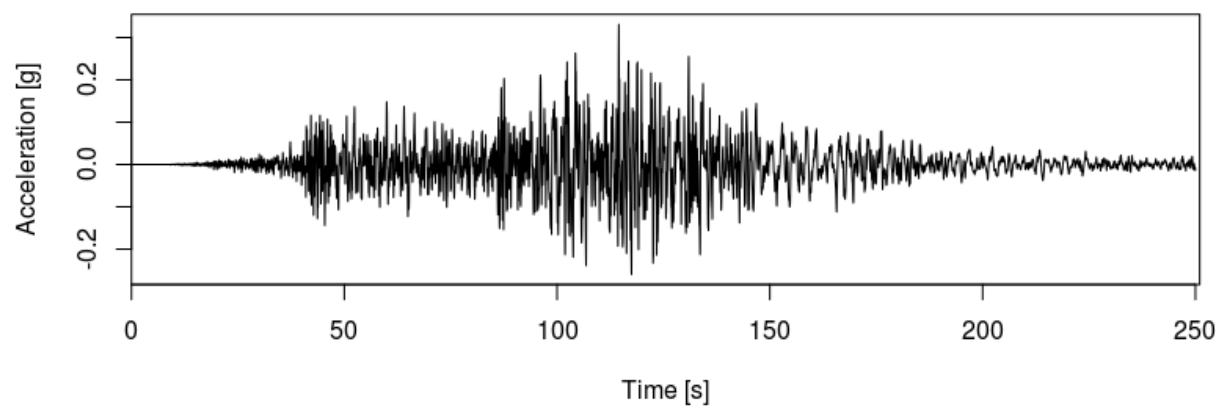
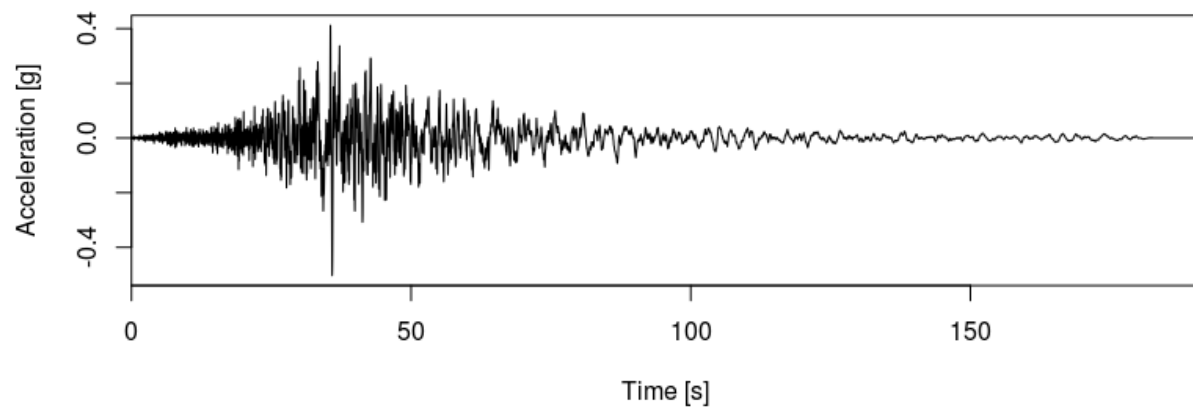
VE13**VE14****VE15**

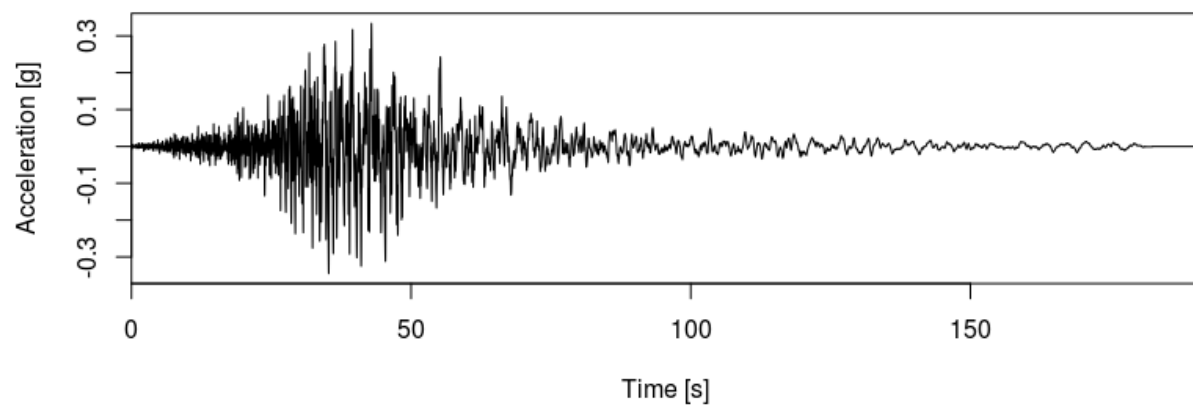
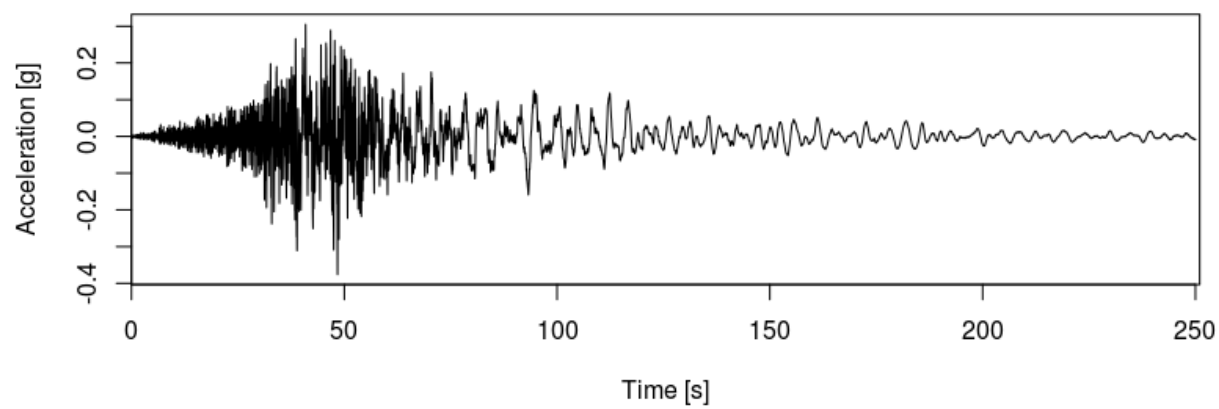
VE16**VE17****VE18**

VE19**VE20****VE21**

VE22**VE23****VE24**

VE25**VE26****VE27**

VE28**VE29****VE30**

VE31**VE32****VE33**